Site Specific Radiolabelling of Biomolecules with [99mTc(CO)3]+ and [188Re(CO)3]+ Complexes.

Williams, Jennifer Delun

Awarding institution:
King's College London

Site-Specific Radiolabelling of Biomolecules with $[^{99m}Tc(CO)_3]^+$ and $[^{188}Re(CO)_3]^+$ Complexes

A thesis submitted to King's College London for the degree of Doctor of Philosophy in Imaging Sciences and Radiation Biology

Jennifer Delun Williams

Division of Imaging Sciences and Biomedical Engineering

King's College London

September 2013

Abstract

The ability to radiolabel biomolecules for imaging purposes is imperative for the future development of molecular imaging. For the use of proteins and peptides, in order to act as optimal molecular imaging agents, the bioconjugate and the process that produces it must satisfy a number of requirements including: site-specific labelling of the biomolecule, high specific activity of the labelled product, quick and simple labelling process, greater than 95% radiochemical yield, homogeneity of the labelled product and kinetic stability *in vivo*. One of the current challenges is the potential interferences of the radiolabel at the active site and subsequent loss of affinity of the protein for its target. A controlled labelling method is necessary to direct the radiolabel to a chosen site on the biomolecule of interest. For synthetic peptides this challenge has been achieved by introducing amino acid building blocks attached to chelators. However, this approach is not applicable to proteins as they can only be produced recombinantly.

We have therefore developed a high-throughput screening methodology suitable for the identification of genetically encoded tags based on amino acid sequences. Such peptide tags will provide a site of unique reactivity to facilitate the specific labelling of biomolecules with a radioisotope of choice. The novel combination of a His-tag with adjacent Arginine (Arg) residues, LRRRLAHHHHHH (JWT-Tag), has been identified as an optimal sequence for radiolabelling with $[^{99m}Tc(CO)_3]^+$ and its analogues $[^{186}Re(CO)_3]^+$ and $[^{188}Re(CO)_3]^+$. A prostate-membrane specific antigen (PMSA) single chain antibody, J591scFv, has been engineered to contain the JWT-Tag and site-specifically radiolabelled with $[^{99m}Tc(CO)_3]^+$ for applications in the molecular imaging of prostate cancer. The J591scFvJWT protein demonstrated superior labelling efficiencies at lower protein concentrations in comparison to other proteins with a $(His)_6$-Tag alone. The $[^{99m}Tc(CO)_3$-J591scFvJWT$]^+$ conjugate was kinetically stable in human serum and has potential for use in pre-clinical and clinical applications.

The combination of $(His)_6$-Tag and Arg sequence has shown its ability to offer a fast and efficient method for the site-specific labelling of a scFv protein with $[^{99m}Tc(CO)_3]^+$. It has the

potential to become a potent tool to screen biological activities of recombinant proteins using ^{99m}Tc labelling. It can also be translational to the therapeutic $^{186/188}$Re isotope.

Acknowledgements

Over the last four years of this PhD I have experienced one of the most challenging yet rewarding times of my life. I am indebted to everyone within the department of Imaging Sciences and Biomolecular Engineering; if not for contributing towards my research project, then for waiting with me for ^{99m}Tc to arrive at 7:00am in the morning, travelling to conferences, going to the pub and most importantly for making me laugh and smile!

Firstly, I would like to take this opportunity to say a massive thank you to Phil Blower and Greg Mullen. Without them I wouldn't have been able to complete this PhD and have the opportunities that I have so much enjoyed over the past four years. Their encouragement and support throughout the project had no bounds. Without their guidance and inspirational knowledge I would not have been able to succeed over the last four years. I would especially like to say a massive thank you for all their help in reading and editing my work throughout my PhD and in particular for their work on this thesis. The speed at which it was marked was incredible and very much appreciated considering my somewhat questionable time management!

I would also like to say thanks to everyone in Imaging Sciences Department especially to those I have spent most time with or have had the pleasure of working alongside during my studies. David Thakor, Kazza, Mags and Flo, you are my heroes! This PhD would definitely not have been finished without your help. Mags I apologise now for make you do 982 TLC's within 4 hours on more than one occasion and Flo I apologise for the 7:00am starts – you always looked so happy to see me at the lifts ... Kazza you are a rock in this department, radioactivity would not exist without your involvement. Thanks for sorting out all the paperwork/ordering errors I did always with a smile (to me anyhow!). David, I'm not sure there are enough words to express how much of a lifesaver you have been. If I wanted to do something it would always happen because you made sure of it. Thanks so much (and for the veg!)

A huge thank you goes to Richard Tavare for firstly integrating me into the group and also for making a discovery during his PhD that enabled me to do my PhD. Literally without you I wouldn't be here! San Diego and Ireland were good fun too. I am very grateful to have met

and socialised with so many people over the last four years: Christoph thanks for putting up with my demanding lunchtime requests, I still can't believe you finished before me; Sabine thanks for putting up with my constant lateness and for always agreeing to go to the pub at 4:00 on a Friday; Alex, Alex, Pete, Adam, Levente thanks for all the good times in the pub and in San Diego, Miami and the Isle of Wight (!); "the 3rd floor crew" the social events wouldn't have been the same without you (especially Markus's dance); Isra you provided me with so much laughter (primarily at you!); Gavlar I feel my life was never the same after I'd done inorganic workshops with you, thanks for all your great chemistry knowledge; Katy bingefest was amazing; Puth, Maite, Max, Rafa and the rest of the Blower-Mullen-Southworth-Gee-Eykyn group, THANKS!

In particular I would like to thank Michelle, Jules, Lidl, Kazza, Erika and Fi – without you guys my time here would have been a lot less fun, more stressful and definitely not as entertaining. I feel as though I have shared some of the best times of my life with you and I very much appreciate all you have done for me, including putting up with me for 4 whole years! Jules and Kazza we were here from the beginning and shared the joys of the reject room – need I say anymore! Erika and Fi we've had some great nights out. Michelle, you arrived in a whirlwind and nothing has really changed; thanks for keeping me level headed during the hard times and providing me with a lot of chocolate (even though you didn't like to share). Lidl, where do I begin I might just mention some place names instead: Ireland, Scotland, Wales, Paris (not such fond memories) and many more to come I am sure. More importantly thanks for being there through the hardest time/night of my life ..... the thesis writing/printing.

I would also like to thank all my various housemates, Danny, Lidl, Brett and Liz for providing me with a life outside the lab! London wouldn't have been the same without you. Lastly I would like to give a big thank you to my close family and to Mamgu who have shown never ending support, encouragement and kindness. Thanks for coping with me during some of the hard times especially over the last few months! You did a tremendous job at keeping me going.

I would like to acknowledge the very generous funding provided by the EPSRC and CRUK which enabled me to do my PhD. I am very grateful.

Contents

Abbreviations

ACN – Acetonitrile

Ala/A – Alanine

Arg/R – Arginine

Asp/D - Aspartate

BFC – Bifunctional chelator

Boc – Tert-butyl carbamate

Cys/C – Cysteine

Cys/(His)-Tag – Sequence containing a cysteine in close proximity to histidine residues

C-terminus – Carboxylic acid terminal of a peptide/protein sequence

CT – Computed tomography

CO – Carbonyl

CO(g) – Carbon monoxide

DIEA – N,N-Diisopropylethylamine

DLU – Digital light units

DMF – N,N-Dimethyl formamide

DTPA – Diethylenetriamine-pentaacetic acid

EIC – Extracted ion chromatography

ESI-MS – Electrospray ionisation mass spectroscopy

Fmoc - 9-Fluorenylmethyloxycarbonyl

Glu/E – Glutamate

Gly/G – Glycine

HBTU – O-(Benzotriazol-1-yl)-N,N,N’,N’-tetramethyluronium hexafluorophosphate

HCl – Hydrochloric acid

His/H – Histidine

His-Tag – Sequence containing histidine residues

$(His)_6$-Tag – Sequence containing the generic 6 histidine residues, HHHHHH

HOBt – Hydroxybenzotriazole

Hr/Hrs – Hours

HYNIC – 6-Hydrazinonicotinic acid

ITLC – Instant thin-layer chromatography

keV – Kila electron volts

LCMS – Liquid chromatography and mass spectroscopy

Leu/L – Leucine

Lys/K – Lysine

$[M(CO)_3]^+$ - Metal tricarbonyl complex where M = Tc or Re

Min/Mins – Minutes

MRI – Magnetic resonance imaging

MSMS – Tandem mass spectroscopy

NMR – Nuclear magnetic resonance

N-terminues –Amine terminal of a peptide/protein sequence

NTA – Nitrotriacetic acid

PBS – Phosphate buffered saline

PET – Positron emission tomography

pI – Isoelectric point

P_1 – LAAALEHHHHHH

P_2 – CKLAAALEHHHHHH

^{31}P NMR – ^{31}Phosphorus nuclear magnetic resonance

Re – Rhenium

$[Re(CO)_3]^+$ - Rhenium tricarbonyl

R_f – Retention factor

RP – Radiochemical purity

rt – Retention time

RT – Room temperature

RY – Radiochemical yield

SD – Standard deviation

SPECT – Single photon emission computed tomography

SPPS – Solid phase peptide synthesis

Tc – Technetium

TFA – Trifluoroacetic acid

TIS – Triisopropylsilane

TLC – Thin-layer chromatography

Tris – Tris(hydroxymethyl)aminomethane

$t_{1/2}$ – Radioactive decay half life

UV - Ultraviolet

CHAPTER ONE

Introduction: Site-Specific Radiolabelling of Biomolecules for Molecular Imaging

1.1 Introduction: Site Specific Radiolabelling of Proteins for Molecular Imaging

1.1.1 NUCLEAR IMAGING

Nuclear imaging is an imaging modality that utilises positron or gamma emitting radionuclides to generate an image *in vivo* of the distribution of the radiopharmaceutical. As a non-invasive technique, it is dependent on the use of very small amounts of radiopharmaceuticals as tracers in the diagnosis and treatment of many diseases. This technique is able to measure the disease process at a molecular level generating images that provide information on the biochemical and physiological status of the tissue.(*1*) This is a different approach to imaging using the traditional anatomical techniques such as magnetic resonance imaging (MRI) (*2*), CT and x-ray which rely on morphological changes occurring in the later stages of the disease. Consequently, early detection and extreme sensitivity are potential aspects associated with the application of nuclear imaging in medicine.(*3*)

Modern radiopharmaceutical imaging has evolved into sub-disciplines that are distinguished according to the specific radionuclide exploited: positron-emitting radionuclides are employed by positron emission tomography (PET); gamma emitters are used in single photon emission computed tomography (SPECT); and particle-emitting radionuclides provide a therapeutic approach to nuclear medicine delivering a cytotoxic dose of radiation to the selected target tissue.(*4*)

1.1.1.1 Single Photon Emission Computed Tomography - SPECT

SPECT was the first tomographic imaging device to be developed by Edwards and Kuhl in 1963. Best known for its applications in neuroscience and cardiology, SPECT depends on the emission of single gamma photons that possess sufficient energy, > 100keV, to escape from the body and be detected by gamma cameras in three dimensions. Technetium-99m (^{99m}Tc)

generated from the ^{99m}Mo/^{99m}Tc generator has been the predominant isotope utilized with SPECT, primarily attributable to its favourable nuclear properties: 140keV energy; pure gamma-ray emitter; a decent half life $t_{1/2}$ = 6.01hrs; and it can be readily provided at low cost from generators. In addition, ^{99m}Tc is chemically analogous to ^{188}Re, a β emitter, which is an attractive therapeutic radioisotope because it too is available from a generator (^{188}W/^{188}Re) and has a relatively long half life, $t_{1/2}$ = 17hrs. Other conventional SPECT radioisotopes are also suitable such as ^{123}I ($t_{1/2}$ = 13hrs), ^{131}I (γ ray at 971keV, $t_{1/2}$ = 8.02 days), ^{67}Ga($t_{1/2}$ = 78hrs), ^{111}In ($t_{1/2}$ = 2.8days),.

1.1.1.2 Positron Emission Tomography - PET

In the early 1970's Ter-Pogossian developed the first PET which took advantage of the coincidence detection of a positron-electron annihilation.(*5*) Currently, in humans, it is possible to obtain a higher resolution with PET imaging in comparison to SPECT as is depicted in Figure 1.1-1. As a result, it is possible to visualize actual ligand-target interactions such as between neurotransmitters and brain receptors. Accordingly, it is an excellent technique used to monitor drug distribution and analyse the associated pharmacodynamics and pharmacokinetics.(*6*)

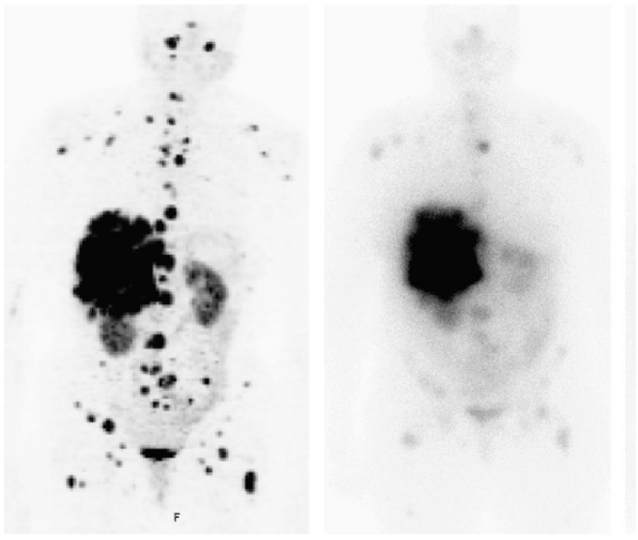

Figure 1.1-1 Images of a woman with multiple liver and lymph node metastases. **Left:** PET image with ^{68}Ga-DOTA-TOC. **Right:** SPECT image with ^{111}In-DOTA-TOC. Additional bone metastases were detected in the PET image but absent when using conventional scintigraphy.(*7*)

Positron-emitting radionuclides are produced by cyclotrons in which the target material is bombarded with accelerated protons. “Organic” radionuclides have been historically renowned for their use in PET imaging such as ^{11}C, ^{13}N, ^{15}O, ^{18}F, whereas radionuclides of metals and heavier non metals are gaining in importance e.g. ^{64}Cu, ^{68}Ga, ^{89}Zr and ^{76}Br. The organic isotopes are advantageous to PET imaging in that they are responsible for the ability to image naturally occurring physiological molecules with radionuclides that are identical or nearly identical to the atoms in the unlabelled compounds. In this respect, ^{18}F and ^{11}C are the radionuclides most used for the synthesis of natural substances as tracers. ^{11}C has been used for the labelling of Methionine whereas the labelling of glucose with ^{18}F, ^{18}Fluorodeoxyglucose, has been highly influential in the acceptance of PET as a recognised diagnostic technique. Chemically known as 2-deoxy-2-(^{18}F)fluoro-D-glucose, ^{18}FDG, is a glucose analogue with the positron-emitting ^{18}F substituted for the normal hydroxyl group at the 2’ position. Malignancies are associated with an elevated glucose metabolism and therefore glucose analogues such as ^{18}FDG localise within the tumour providing a mechanism for its detection. (Figure 1.1-2) Another example is the (18F)-3’-fluoro-3’-deoxy-L-Thymidine (FLT) tracer used for the imaging of tumour cell proliferation.(*8*) In this instance, 18F replaces the normal hydroxyl group at the 3’ position of a thymidine molecule.

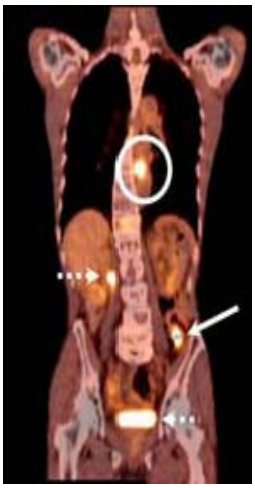

Figure 1.1-2 A coronal PET/CT colonography image. ^{18}FDG uptake can be detected in the: (**solid arrow**) colon cancer; (**circle**) esophageal tumor; and, (**broken arrows**) normal glucose uptake. (*9*)

1.1.2 DESIGN OF BIOMOLECULAR CONJUGATES

The design of a radiopharmaceutical requires the incorporation of the radionuclide into a molecule that can be systemically injected and localised in the target tissue. Using gamma and positron emitters, a SPECT or PET image can be generated as a result of the external detection of the emitted radiation. Therapeutically, the radiation from α and β particles or secondary electrons are absorbed locally at the site of action and consequently induce cell death. Often radiopharmaceuticals involve the use of a biomolecular vehicle to which the radionuclide is attached. This could be a protein, small peptide, monoclonal antibody, antibody fragment or signalling protein. The biomolecular vehicle should have specific affinity for a receptor, transporter or other molecular target and be able to localise at the site of interest providing a method of targeting. As a result, the radionuclide itself should have little influence on the targeting mechanism. (Figure 1.1-3)

In some instances the chemistry of the radioactive element provides the necessary properties for the targeting and localisation of the probe at the diseased tissue. Copper bis(thiosemicarbazone) complexes, labelled with ^{64}Cu, are an apt example as it is the redox activity of the copper that is essential for the targeting properties of the imaging probe. These complexes are PET tracers used for the imaging of blood flow and hypoxia, that is, oxygen deficiency.

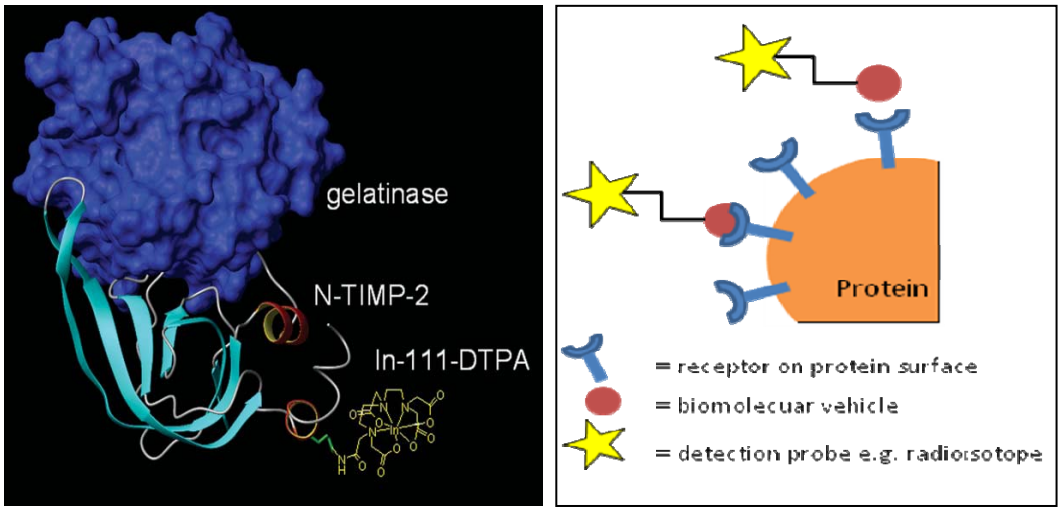

Figure 1.1-3. Models that demonstrate the targeting of a radiolabelled biomolecular vehicle to a site of interest. **Left)** A radionuclide-chelator-protein bioconjugate. The protein N-TIMP is conjugated with DTPA, the chelator, via a Lys residue and then labelled with In-111. N-TIMP binds to the gelatinase target in vivo.(*10*) **Right)** A schematic representation of the radionuclide-chelator-protein bioconjugate.

1.1.2.1 Requirements for the Radiolabelling of Biomolecules

To be used as a molecular imaging agent, the biomolecular vehicles must be modified in order to incorporate a suitable radionuclide. There are several approaches to the modification of biomolecules including indirect labelling, which involves the use of synthetic binding sites in the form of bifunctional chelators, and direct labelling that exploits the affinity of reactive side chains within the protein structure. Bifunctional chelators are molecules that comprise two functional components: a metal-binding moiety that is designed to bind efficiently to the radionuclide and maintain a sufficient kinetic stability, and a functionality that can covalently bind to the target biomolecule. In both methods of labelling the efficient conjugation of the radioactive probe to the biomolecule is a requirement and improvements would contribute significantly to clinical advancements within critical areas of disease.

For peptides and proteins, to act as an optimal molecular imaging agent, the radiolabelled bioconjugate and the process that produces it must satisfy a number of requirements.

Firstly, the labelling process must be as quick and simple as possible in order to reduce losses of radioactivity by decay, reduce the opportunity for introduction of microbial contamination and reduce the radiation exposure to the operator. The conjugation itself must be biologically compatible and the molecular recognition function of the protein or peptide preserved. This means that the modification should be site-specific and remote from the target-binding site. Labelling should occur with a radiochemical yield of > 95% to avoid the necessity of incorporating an additional time consuming purification step. It is essential that the labelled product is stable *in vivo* for the requisite period to perform the imaging procedure. To reduce the chances of producing a toxic or undesired physiological effect in vivo, it is preferable that the minimum amount of biomolecular vehicle is labelled with sufficient radioactivity for the imaging procedure i.e. keeping the specific activity of the labelled product as high as possible. Finally, it would be ideal if the bioconjugate could be as homogenous as possible and that every radiolabelled molecule has the same structure, stability and affinity for the target.

Combining the attributes required for an optimal molecular imaging agent is difficult because design features that increase the rate of complex formation with the radiometal, by lowering the free energy of activation of the labelling reaction, also increases the rate of dissociation. Other issues involve achieving fast, high yield and high purity labelling with low concentrations of radionuclide whilst minimising the concentration of the biomolecule. It is critical that the highest possible fraction of encounters between radionuclide and biomolecule lead to binding. To achieve this, a well-designed binding site for the radionuclide must be incorporated into the biomolecule. An efficient binding site will have a much higher affinity than any other part of the biomolecule for the radionuclide, leading to optimal homogeneity and site-specific labelling. If the site is remote from the biological recognition site of the biomolecule then it would ensure that the biological activity is preserved.

1.1.3 NON-SITE SPECIFIC LABELLING

The initial approach to the labelling of biomolecules has primarily been non-site selective in that the modifications to the biomolecular surface have been uncontrolled leading to the formation of a heterogeneous mixture of products. In the context of labelling proteins, the

most general approach has involved the targeting of functionalities already present in the side chain of the native amino acids. This encompasses the use of simple second-order reactions; with an electrophilic reagent targeting the nucleophilic groups present on the biomolecule surface. As a labelling strategy this has been applied to all biomolecules that contain amino acids including: proteins, small functional peptides and antibodies.

1.1.3.1 Targeting Lys and Cys Residues

Due to their nucleophilicity, Cys and Lys are the residues most commonly targeted for modification. The thiol side-chain associated with Cys can undergo numerous modifications: disulfides are formed as a result of disulfide exchange; and thioethers are synthesised during Michael additions with α, β-unsaturated carbonyl compounds and alkylations with alkyl halide reagents. (*11*) (Figure 1.1-4). Lys residues are popular due to the many methods available for the alteration of primary amine functionalities. For instance, activated esters, sulfonyl chlorides, isocyanates and isothiocyanates are all electrophilic synthons capable of reacting with primary amino groups to afford amides, sulphonamides, ureas and thioureas respectively (*12*) (Figure 1.1-4). Another conventional reaction is the reductive amination of Lys with aldehydes. It is important to consider that the primary amine functionality is also present at the N-termini of the protein in addition to the side chain of all the Lys residues.

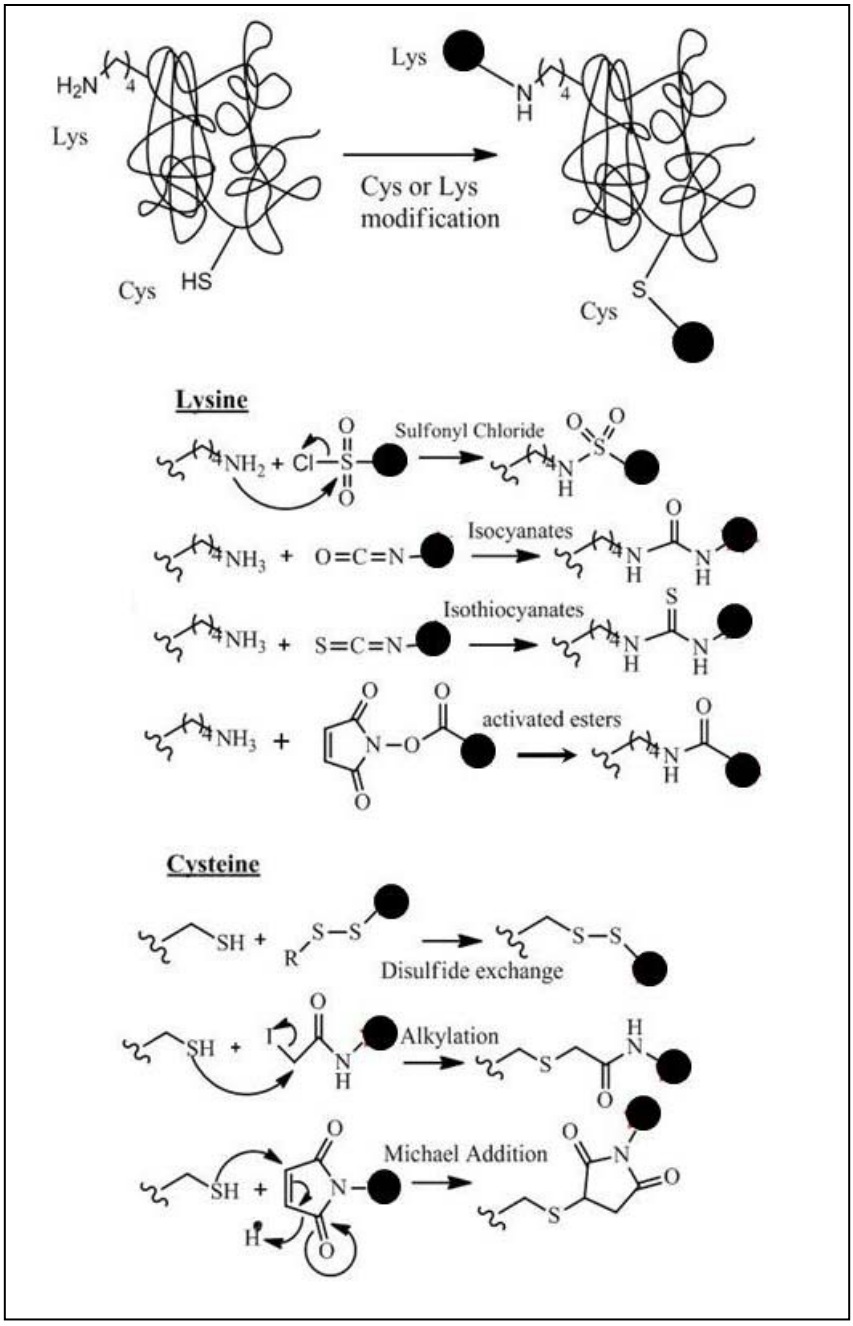

Figure 1.1-4. Classic bioconjugation methods for the non-site specific labelling of Cys and Lys residues on the protein surface.(*11*) ● = radioactive isotope

In comparison, minimal research has been executed in the exploitation of the remaining 18 proteogenic amino acids as potential sites for modifications. Of these, the nucleophilic Glu and Asp residues are possibly the most suitable targets for bioconjugation. This is attributable to the presence of the carboxylic acid side chain which can undergo coupling with amines via carbodiimide formation.(*13*)

This approach to the labelling of proteogenic amino acids can only be referred to as non-selective predominately due to the sheer abundance of nucleophilic groups on the surface of a biomolecule. Approximately 70% of all electrophilic reagents are reactive towards the Lys and Cys residues.(*14*) Consequently, it is difficult or impossible to control the bioconjugation conditions and achieve modifications at only one chosen site within the protein structure which may contain many Lys residues.

1.1.3.2 Example: Non-Site Specific Labelling of Annexin V

The non-site-specific labelling of the biomolecule Annexin V highlighted the magnitude of problems associated with this conventional approach.(*15*) Annexin V is an important protein when considering its potential application as an imaging agent for apoptosis.(*16-17*) It is a relatively small cytoplasmic protein with a high affinity for phosphatidylserine, which is exposed extracellularly in apoptopic cells increasing accessible binding sites from 10^2-10^3 to 10^7.(*18-19*) Due to the 21 available Lys residues, amine-directed conjugation was considered most appropriate.(*20*) However, observations concluded that there were adverse modifications to the biological activity of Annexin V and a substantial reduction in its membrane affinity as a consequence of the conjugation sites (Lys) situated near the active site. Investigations were pursued in the labelling of an engineered form of the Annexin V protein, Annexin V-128, which contains a Cys residue.(*21*) Thiol reactive reagents such as iodoacetamide and N-substituted maleimides were used to conjugate the ^{99m}Tc radionuclide to the Cys residue. Consequently, the site specific labelled Annexin V-128 demonstrated twice the amount of uptake in apoptopic cells in a rat liver model than did the Lys conjugated Annexin V.(*15*) Many proteins do not contain a unique binding site such as a single Cys residue which would limit the possibility of a site-specific labelling methodgy. Another important consideration is that Cys residues can introduce problems such as undesirable disulfide bond formation which can alter the protein fold or cause dimerisation, and are not always suitable for the purpose of bioconjugation.

1.1.4 SITE-SPECIFIC LABELLING OF PEPTIDES

The labelling of small peptides that contain only one nucleophilic functionality can be easily achieved site-specifically with bioconjugates that target that particular site of reactivity. Chemotactic peptide analogs comprising of 3 or 4 amino acid building blocks have been radiolabelled site-specifically with ^{99m}Tc.(*22*) The peptides contain only one free amino functionality at the N-terminus and were consequently derivatized with a bifunctional chelator, hydrazinonicotinic acid (HYNIC), through the formation of an amide bond with the activated ester on the HYNIC molecule.

1.1.4.1 N-Terminus Radiolabelling of Peptide Sequences

Due to the abundance of the Lys residue, many small peptides contain more than one reactive amine functionality and consequently the site-specific labelling of such peptides becomes more problematic. Initially, protecting groups were used to shield the amine side chain of the Lys residues, affording conjugation at the N-termini. The preparations of two ^{99m}Tc-labelled somatostatin analogues were subjected to such a modification.(*23-25*) (Figure 1.1-5) HYNIC and two N_3S compounds were used as BFC conjugating site-specifically to the N-terminal of the peptide chains in the presence of a Boc (tert-butyl carbamate) protected Lys residue. Subsequent addition of the ^{99m}Tc yields a site-specifically radiolabelled somatostatin analogue. However, this strategy would become complex in the presence of other nucleophilic functionalities and also limits the location of the imaging probe to the N-terminal.

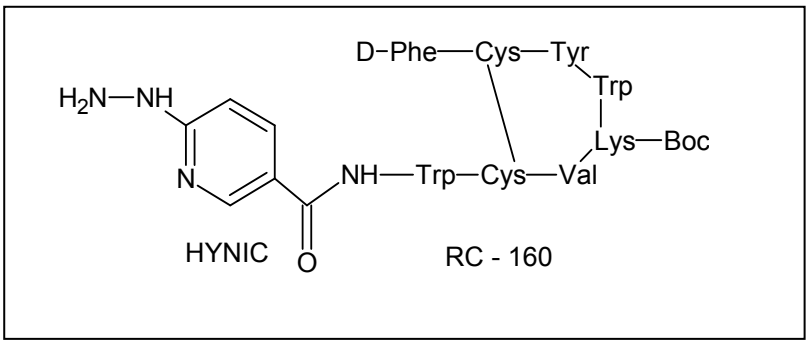

Figure 1.1-5. Structure of HYNIC bound to the RC-160 somatostatin analogue. The Lys residue is protected with Boc.

1.1.4.2 Site-Specific Labelling with Non-Natural Synthetic Amino Acid Building Blocks

Another development to overcome the non-unique reactivity of the amino acid side chains, has been the site-specific labelling of peptides through the use of non-natural synthetic amino acid building blocks with side chains containing chelators.(*26-27*) Peptides can be made synthetically through solid phase peptide synthesis (SPPS). Therefore the incorporation of an amino acid, already conjugated to a prosthetic probe, as a building block during the peptide synthesis is a possibility. This is beneficial as it allows the flexibility to integrate the chelator with total site specificity at any chosen point in the peptide amino acid sequence. In addition, it can be used for the labelling of peptides with any metal radioisotope since any specifically designed synthetic chelator can be included in the sequence during solid phase synthesis.

A HYNIC conjugate of salmon calcitonin, a 32 amino acid neuropeptide, was prepared with the use of solid phase synthesis and a HYNIC derivatized Lys as a building block. The presence of another 2 reactive amino groups in the structure of salmon calcitonin did not hinder its site-specific modification and subsequent labelling with ^{99m}Technetium.(*28*) Similarly, a novel single amino acid chelate (SAAC) has been designed for the binding of Tc(I) and Re(I).(*29*) This chelator, based on the Lys residue, has been incorporated as a building block into an urea derived MLF(SAAC)G (Met-Leu-Phe-single amino acid chelate-Gly) peptide sequence. This was then used for the imaging of infection and inflammation with ^{99m}Tc. (Figure 1.1-6)

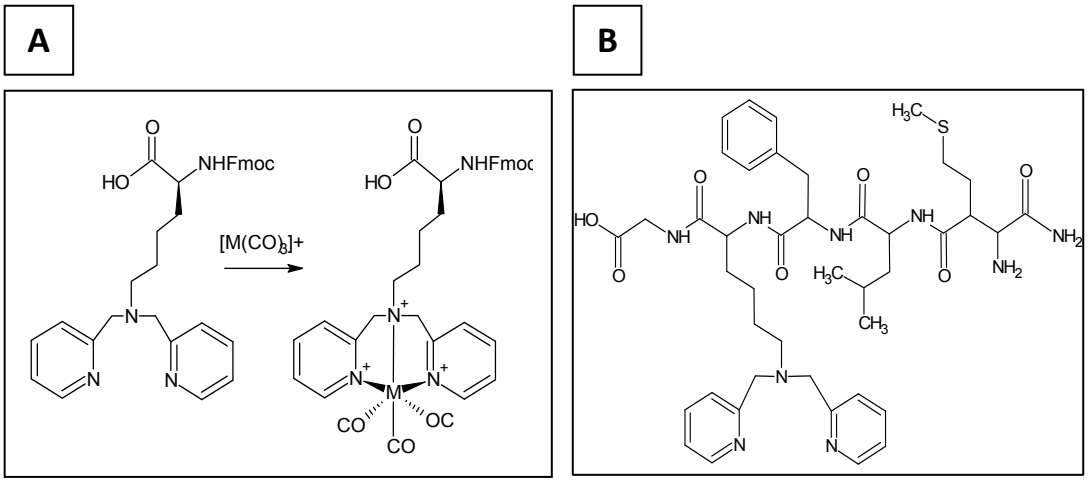

Figure 1.1-6. A. Structure of the single amino acid chelate (SAAC) and its complex with the $[M(CO)_3]^+$ CORE. **B.** MLF(SAAC)G peptide sequence structure.

Further developments into the design of other amino acid building blocks containing chelators would provide a greater scope for the labelling of peptide biomolecules with various metal radioisotopes. Unfortunately, this approach is not applicable to biologically produced large peptides and recombinant proteins as they cannot be synthetically produced via SPPS procedures. The cellular translational apparatus cannot handle the synthetic amino acid building blocks and therefore it is only possible to use the twenty proteogenic amino acids during their assembly. As a result, the exploitation of derivatised amino acid residues is prohibited.

1.1.5 SITE-SPECIFIC LABELLING OF PROTEINS

The development of a straightforward site-specific labelling procedure could enable the use of a wider range of biomolecules that may have enhanced capabilities within the field of diagnostic imaging and therapy. This would be achievable with a single site modification method in which an imaging probe can be conjugated to a specific location on the biomolecule without interfering with the biologically active site. Theoretically labelling could then be accomplished more efficiently and quickly.

Progress in the development of site-specific labelling methods for biomolecules is not only beneficial in the imaging context; it is also applicable to the isolation and purification of proteins via chromatographic techniques; anchoring of proteins to solid surfaces and nanoparticles; structural analysis of peptides and proteins via NMR studies; and, the synthesis of vaccines.(*30-32*) The bioconjugation of proteins and biomacromolecules to the surface of artificial receptor scaffolds known as nanoparticles is essential for their application as targeted intracellular delivery systems for genes, antibodies and protein therapies. Multiple efforts have focused on the engineering of the nanoparticle-protein interaction including the construction of the protein and nanoparticle complex within aqueous media and the formulation of a nanoparticle protein sensor.(*33*) Improvements in such bioconjugation methods could potentially lead to the development of a new approach to medicine known as nanomedicine.(*34*)

Currently, there have been several approaches to the development of a site-specific labelling methodology for protein biomolecules.(*11*) These have included the use of N-

terminal amines, a bioorthogonal reaction strategy, genetically encoded tags and enzymatic modifications. The following sub-sections will discuss such methods of bioconjugation and evaluate their effectiveness as a strategy for the labelling of proteins site-specifically.

1.1.5.1 N-terminal Modifications

The amino group at the N-terminus of a protein has a unique pH-dependant reactivity and is therefore an attractive target for single-site modification.(*35*) In comparison to the amino groups of the Lys it has a decreased pKa and is therefore more reactive as a nucleophile within acylation or alkylation procedures. However, selective bioconjugations to the N-terminus of the protein are often more difficult than expected due to the large number of competing Lys (approximately 10^{-40} in most proteins) which poses a limitation. A transamination reaction at the N-terminus has been particularly successful in accomplishing a site-specific modification within a protein.

1.1.5.1A Transamination

A biomimetic transamination has been designed that can proceed under physiological conditions without the addition of metals or bases.(*36*) This method involves the condensation of the N-terminal amine with pyridoxal-5-phosphate (P5P) and the subsequent hydrolysis to yield a pyruvamide. The newly formed ketone of the pyruvamide can undergo conjugation with aminooxy or hydrazine functionalised probes. (Figure 1.1-7) Characterisations concluded that the presence of an Ala, Gly, Asp, Glu or Asn residue at the N-terminal position optimised the reaction. A site-specific modification to the N-terminal of horse heart myoglobin was achieved with P5P at 37^{o}C with a 75% conversion from the amine to the ketone product.

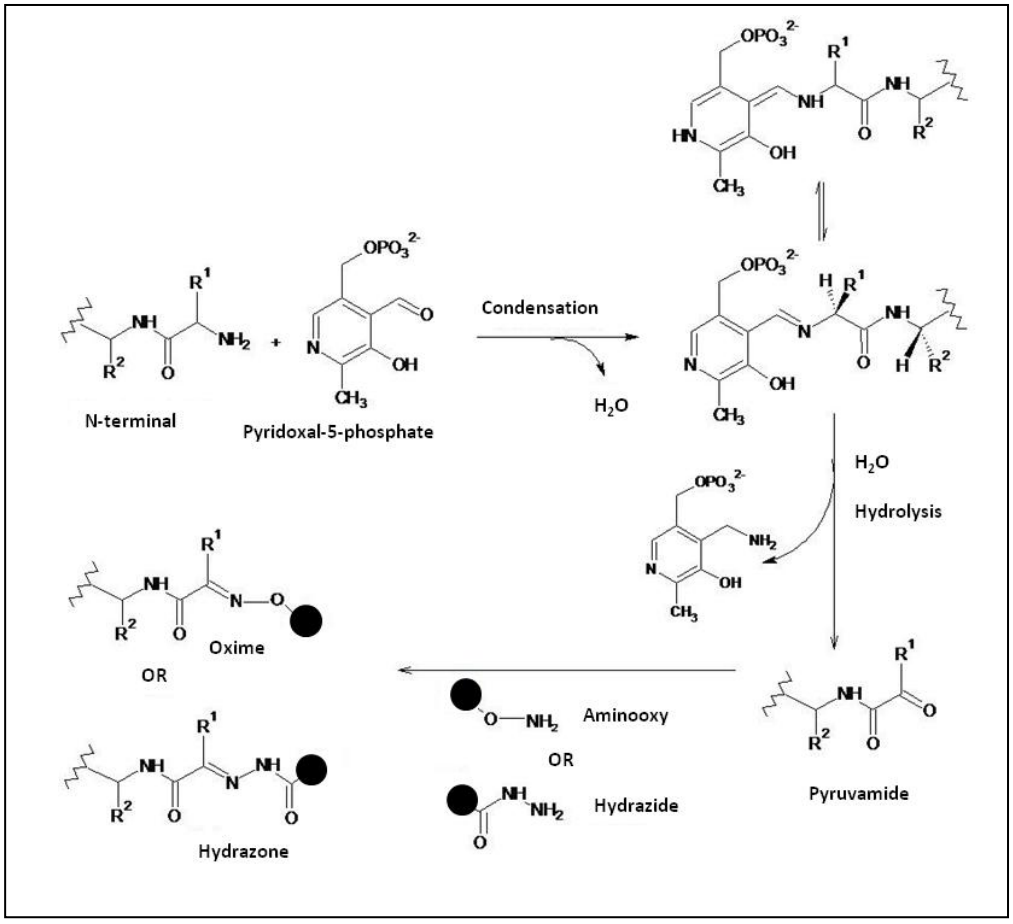

Figure 1.1-7. Transamination reaction scheme for the N-terminal Asp, Gly, Asn, Glu or Ala amino acid residue. Initial site specific labelling with pyridoxal-5-phosphate and a subsequent labelling with an aminooxy or hydrazide functionalised imaging probe. ● = radioactive isotope

1.1.5.1B Specific Amino Acid Side Chains at N-terminal Position

Alternative strategies for the targeting of the amino N-terminus rely on the presence of specific amino acid side chains at the N-terminal position. Reactive aldehydes, such as glyoxylamide, can be formed through the periodate oxidation of N-terminal serine and threonine residues.(*37*) Glyoxylamide can be conjugated to aminooxy or hydrazine functionalised probes. (Figure 1.1-11) N-terminal Trp residues can be selectively modified with an aldehyde probe through a Pictet-Spengler reaction. (Figure 1.1-8) This is beneficial due to the formation of a strong carbon-carbon bond between the protein and synthetic probe in a one step procedure, whereas the hydrazine and aminooxy based probes do not form irreversible linkers.

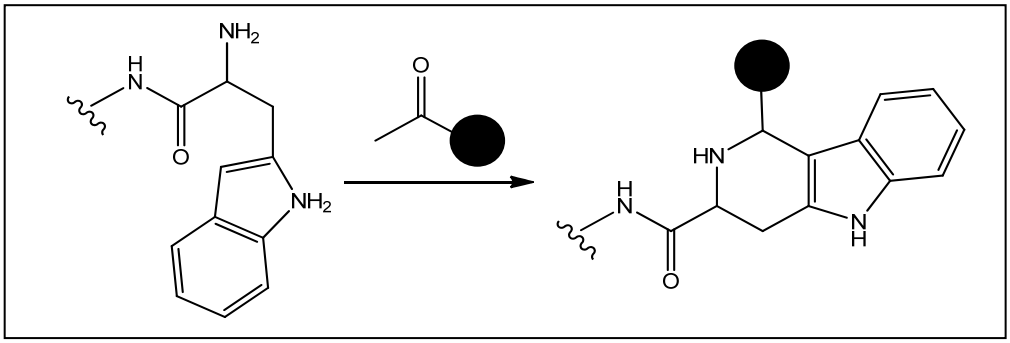

Figure 1.1-8. Pictet-Spengler reaction with an N-terminal Trp residue and an aldehyde probe. ● = radioactive isotope

1.1.5.1C Native Chemical Ligation (NCL)

The reaction between thioesters and N-terminal Cys has been of particular interest and affords protein fusion through native chemical ligation.(*38*) NCL forms an amide bond between two peptide sequences that is biologically stable. Mechanistically, an NCL transformation is a two step reaction that firstly involves a thioesterification between the thiol side chain of the Cys and the thioester. This step is in rapid equilibrium and is interrupted by an irreversible intramolecular reaction with the amino N-terminal (S-N acyl transfer) ultimately producing an amide bond. (Figure 1.1-9)

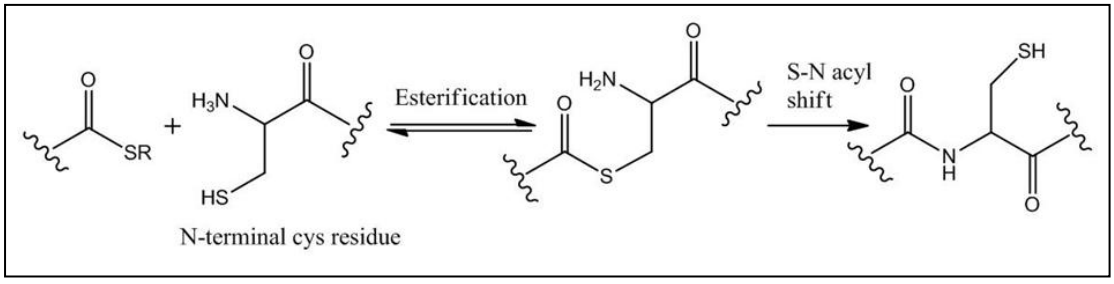

Figure 1.1-9. Schematic representation of NCL between two peptide sequences. One of the sequences has an N-terminal Cys and the other a C-terminal thioester.

The NCL technique has been used for the selective conjugation of unprotected peptides that have an N-terminal Cys residue and a C-terminal thioester in the synthesis of complex

polypeptides or protein biomolecules. (*39-40*) An example is the total chemical synthesis of a 68 amino acid potent anti-HIV molecule referred to as AOP-RANTES.(*41*) In addition, the N-terminal Cys provides a reactivity site for conjugation to thioester functionalised fluorophores or chelators for radioisotope labelling.(*42*)

The selective modification of proteins at the N-terminal is restricting due to limitations in the possible location of the imaging probe. The N-terminal may not always be accessible to the conjugation probe and the labelling of such a protein would not be possible. Furthermore, the selective labelling of N-terminal amines in proteins that have an abundance of Lys residues will be problematic due to the considerable amount of competition present.

1.1.5.2 Bioorthogonal Chemical Reporter Strategy (BCR)

An alternative method for the labelling of biomolecules, including proteins, glycans, lipids, nucleic acids and various metabolites, incorporates the use of BCRs. In a prototypical experiment this involves the labelling of biomolecules with unique chemical functionalities (chemical reporters) that possess orthogonal reactivity to that of natural biomolecules. It is a necessity that the chemical reactions designed are inert to the vast range of functionalities found in vivo and that the reagents react rapidly and selectively with each other under physiological conditions. Tagging of a biomolecule with a chemical reporter is achieved through the use of the cell's own biosynthetic pathway in a method referred to as metabolic labelling. An exogenously delivered probe that contains a complimentary chemical moiety can then conjugate to the chemical reporter through a chemoselective ligation. (Figure 1.1-10)

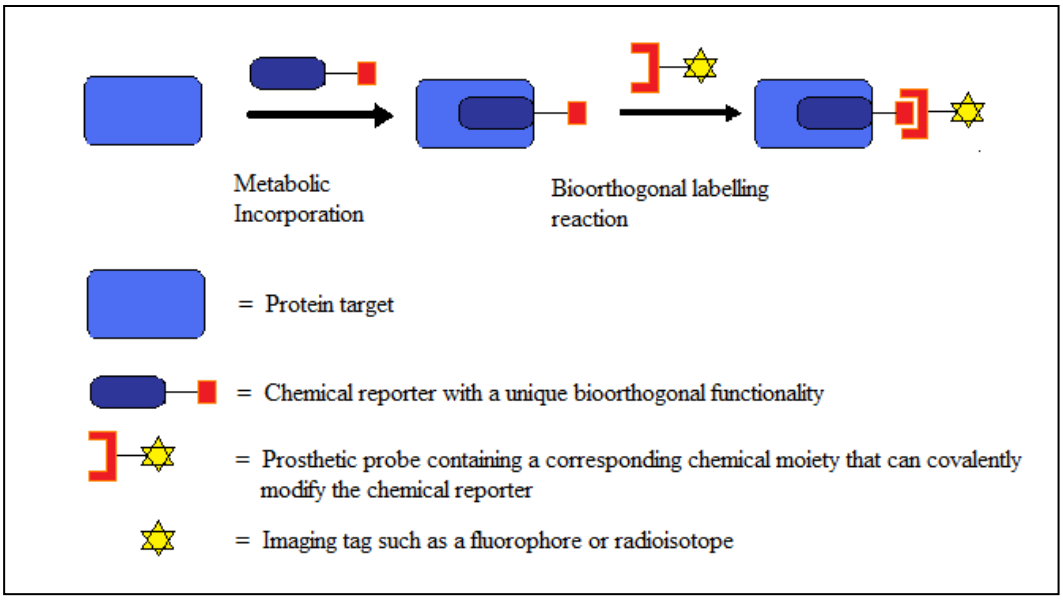

Figure 1.1-10. A schematic diagram representing the labelling of biomolecules with the BCR strategy.

Advances in biocompatible synthetic organic chemistry have afforded new opportunities within this field and as a result a diverse assortment of two-step labelling strategies have been developed.(*43*) In particular emphasis has been on the Staudinger ligation of azides and triarylphosphines (figure 1.1-12); the condensation of carbonyl moieties with aminooxy and hydrazine functionalized probes (figure 1.1-11); a click chemistry procedure for the Cu catalysed conjugation of azides and alkynes (figure 1.1-14); and, the cycloaddition reaction of alkenes with dienes. These reactions will be discussed further in the next section.

1.1.5.2A Condensation Reaction of Ketones and Aldehydes

The introduction of carbonyl moieties into the protein structure are a possibility: the transamination or oxidation of the N-terminal amine functionality and some of the enzymatic (and hence, site-specific) post-translational modifications yield aldehyde or ketone functionalities at selective sites within a protein. Ketones and aldehydes are capable of reacting with amine nucleophiles that have an enhanced reactivity due to an α-effect; that is, the presence of an adjacent atom with a lone pair of electrons. In a prototypical labelling experiment, hydrazine and aminooxy functionalised probes are used, and form

hydrazone and oxime linkages respectively with the carbonyl moiety under physiological conditions (Figure 1.1-11). Other biological nucleophiles such as amines, alcohols and thiols can also react with the hydrazine and oxime functionalities however, under aqueous conditions an equilibrium is formed which favours the carbonyl compound.(*44*) Many fluorophores have been functionalised with hydrazine and aminooxy moieties for the labelling of biomolecules and subsequent tracking through optical imaging modalities.(*45*)

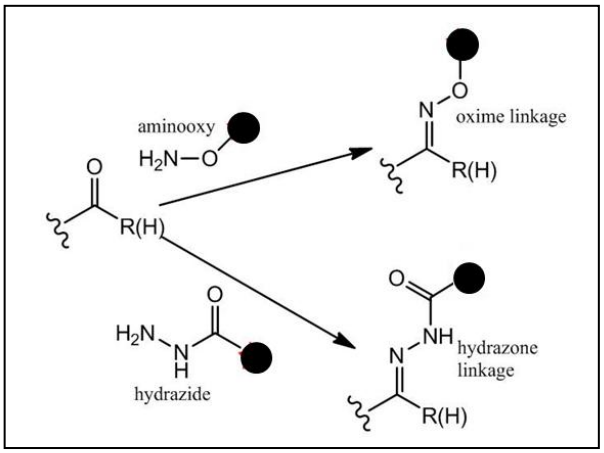

Figure 1.1-11. Schematic diagram for the condensation of ketones and aldehydes with aminooxy and hydrazide functionalised probes. This is a common method used for labelling unique sites of carbonyl reactivity in the protein. ● = radioisotope

1.1.5.2B The Staudinger Ligation

Azides have proven to be particularly viable as chemical reporters for the labelling of all classes of biomolecules. They possess orthogonal reactivity to the majority of the biological functionalities and are completely absent from all biological systems. Additionally, the azide group is small and therefore its incorporation into the biomolecular structure should not interfere with the structure or activity of the host molecule in question. Azides are mild electrophiles similar to the aldehyde and ketone moieties. However, they are more reactive towards “soft” nucleophiles, such as phosphines, than the “hard” nucleophiles abundant within biological systems such as amines.

A modification of the Staudinger reaction, termed Staudinger ligation, was developed for the conjugation of triphenylphosphines with azide chemical reporters in live cells.(*46*)

Mechanistically, this involves the initial formation of an aza-ylide intermediate that can undergo an intramolecular reaction to form an amide bond; initiated as a result of the strategically placed ester group on one of the phosphine aryl substituents. A hydrolysis then takes place to produce a stable ligation product that includes a phosphine oxide functionality. (Figure 1.1-12)

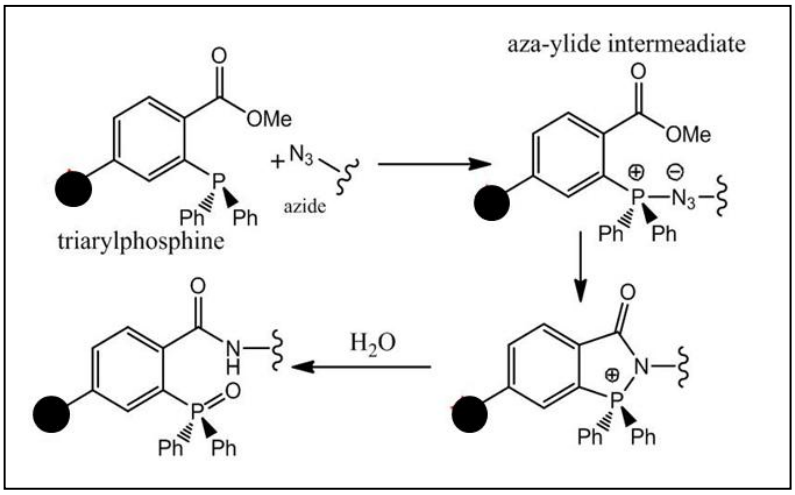

Figure 1.1-12. Schematic representation of the mechanism for the Staudinger Ligation.
● = radioisotope

The bioorthogonality of the Staudinger ligation reagents are questionable due to possible cross-reactivities between the azide and phosphine substrates with the thiols and disulfides respectively. Thiols have a potential to reduce alkyl and aryl azides, which despite being slow at physiological pH, is apparent within the glutathione reduction of 3'-azidothymidine.(*47*) Furthermore, phosphines are also recognised as reducing agents for disulfide bonds. However, the use of triarylphosphines significantly reduces the production of free sulfhydryl groups due to the bulky substituents present in their structure.

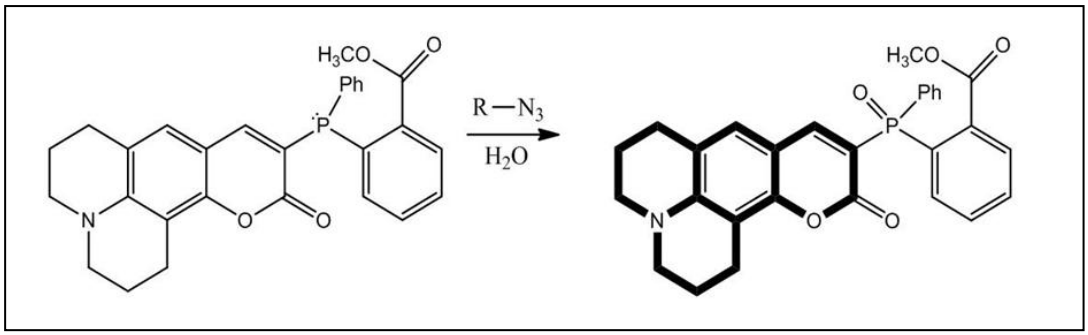

Figure 1.1-13. Coumarin-based fluorogenic phosphines that fluoresce upon phosphine oxidation during the Staudinger Ligation. The bold lines represent the fluorescent molecule.

The impact of the Staudinger Ligation is particularly noticeable in the labelling of biomolecules with fluorogenic reagents for real-time optical imaging. The lone pair of electrons on the phosphorus atom can quench the fluorescence of the coumarin dye. After oxidation, during the Staudinger ligation, the quenching effect is suspended which produces a highly fluorescent biomolecule (Figure 1.1-13). The fluorescence visualisation of the active Cys protease, cathepsin, in living cells has been accomplished through the incorporation of an azide and reaction with phosphine functionalised p-biotin.(*48*)

1.1.5.2C Cu Catalysed and Cu-Free Click Chemistry

Another method of reactivity for the azide functionality is its 1,3-dipole that is useful in the [3+2] dipolar azide-alkyne cycloaddition. This [3+2] cycloaddition involves the production of a stable triazole adduct through reactions with substrates such as terminal alkenes or alkynes. In addition to the orthogonal reactivity of the azide, π systems are also extremely rare and inert within biological systems. Sharpless presented the Cu(I) catalysed cycloaddition that could proceed at room temperature, known as the copper-catalysed azide-alkyne 1,3-dipolar cycloaddition (CuAAC).(*49*) This reaction involves the cycloaddition of azides to terminal alkynes with the formation of a regiospecific 1,4-disubstituted 1,2,3-triazole (Figure1.1-14).

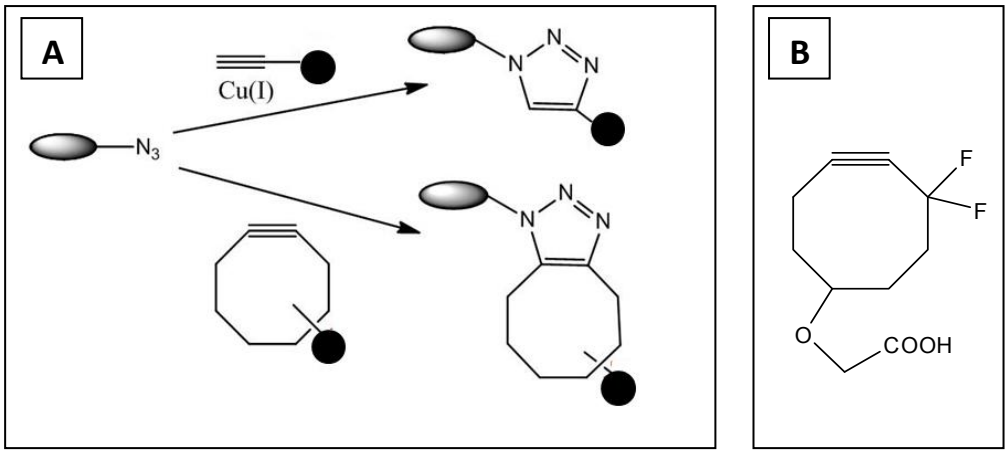

Figure 1.1-14. Bioorthogonal [$_3^+$2] cycloaddition. **A) Top**: CuAAC- alkynes are activated with a Cu(I) catalyst and then react with azides. **Bottom**: Cyclooctynes react with azides through a ring strain promotion cycloaddition. **B)** Structure of DIFO

It appeared that the Cu(I) catalyst takes advantage of the copper acetylide formation in order to activate the terminal alkynes. In addition the presence of the catalyst increased the reaction rate in comparison to that of the Staudinger Ligation. As a consequence of its favourable properties, including efficiency, simplicity and selectivity, CuAAC is now simply referred to as "click chemistry".(*50*)

Applications of CuAAC in living systems were limited due to the problem encountered as a result of the toxicity of the Cu(I) catalyst. Improving the biocompatibility involved the development of methods that activated the alkynes without resorting to metal catalysis, such as the use of ring strain (Figure 1.1-14 A). Cyclooctynes had been previously reported as the smallest stable cycloalkyne and would react vigorously with phenylazide. A difluorinated cyclooctyne (Figure 1.1-14 B) was established as a suitable reagent due to its comparable kinetic properties with the CuAAC reaction and nontoxicity.(*51*) Subsequently its conjugation with azides was referred to as "copper-free click chemistry".

Azides and alkynes are similar in size and therefore in a cycloaddition reaction it is also possible to utilize the alkyne as a chemical reporter. The site-specific labelling of azido functionalised sialic acid residues on the surface glycans of ovarian cells has been accomplished with biotinylated and Alexa Fluor 488 derivatives of DIFO.(*52*) A set of azide and alkyne derivatised fluorophores that virtually covered the entire visible spectrum were

synthesised and their suitability for the fluorescent labelling of biomolecules analysed through copper free-click chemistry.(*53*)

1.1.5.2D [3+2]-Cycloaddition of Alkenes with Dienes

Dienes and alkenes with 1,3-dipoles can also undergo cycloaddition reactions, promoted by ring strain or light, to produce a triazoline which is relatively unstable.(*54*) Aromatic triazoles are more stable and consequently oxanobornadienes, containing an electron-deficient olefin, underwent a [3+2]-cycloaddition procedure with an azide and a subsequent diels-Alder reaction to yield an aromatic triazole product.(*55*) Despite increased stability, the reaction kinetics were relatively slow. Improvements in the reaction kinetics were observed in a reverse-electron demand Diels-Alder reaction of tetrazines with strained alkenes which proceeded rapidly under aqueous conditions.(*56*)

A photochemical 1,3-diploar cycloaddition has also been reported between alkenes and tetrazoles to produce a pyrazoline. Modifications to the aryl groups on the tetrazole meant that the reaction could occur with irradiation at 365nm, avoiding photodamage to the living systems. Labelling of alkene-containing proteins in E-coli with diaryl tetrazole functionalised fluorophores has been achieved.(*57*)

Ruthenium-catalysed cross-metathesis has been employed as another method for the chemoselective modification of alkenes.(Figure 1.1-15) Preliminary results have shown the use of the Hoveyda-Grubbs ruthenium catalyst for the modification of allyl sulfide functionalised proteins through cross-metathesis.(*58*) A tert-butanol/H_2O solution was used which is not biologically compatible.

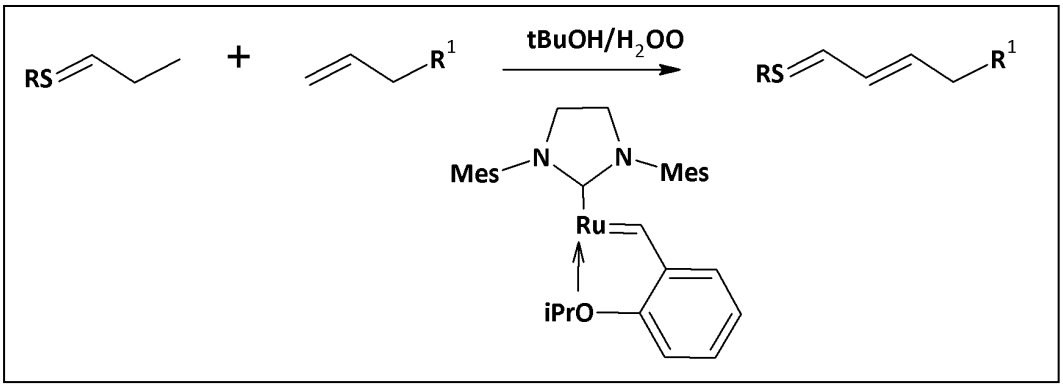

Figure 1.1-15. Schematic diagram of the ruthenium-catalysed cross-metathesis between two alkenes.

1.1.5.2E Limitations in the BCR Strategy

There are two major limitations relating to the use of the bioorthogonal chemical reporter strategy in the selective labelling of proteins. These include the reaction kinetics between the chemical reporter and prosthetic probe, and the incorporation of the chemical reporter into the target biomolecule. The majority of the bioorthogonal reactions follow second-order kinetics and therefore the rate of reaction is dependent on the concentration of the two reactive species. In an in vitro context this is not such a problem as the concentration of the labelled species can be controlled however; in vivo the labelled biomolecule is often at low concentrations. The rate constants of the bioorthogonal reactions listed above range from approximately 10^{-4} to 10^{3} $M^{-1}s^{-1}$ whereas biological labelling agents such as monoclonal antibodies binding to their antigens have rate constants at 10^{9} $M^{-1}s^{-1}$.(*59*) Consequently, high concentrations of the complimentary labelling components are required to improve the rate. This can cause issues in terms of toxicity and solubility when designing the labelling probe. Optimisation of reaction kinetics in a bioorthogonal reaction is essential in order to reduce the concentrations required of the reagents.(*56*)

Incorporation of the chemical reporter functionality into the target biomolecule is also a problem. The azide, ketone and alkyne functionalities of the chemical reporters are not present in the side chains of the 20 proteogenic amino acids and therefore are not recognised by the cell's translational machinery during protein synthesis. A straightforward method of introducing the chemical reporters involves a metabolic labelling approach in

which the cells are subjected to the unnatural amino acids that are tolerated by the translational machinery.(*60*) Met tRNA-synthetase can accept unnatural Met substrates which replace all the Met residues within the protein with either an azide, alkene or alkyne functionality.(*61*) Modification of Met side chains with chemical reporters is not site-specific and increases the toxicity within the biomolecule. In addition, some of the unnatural amino acids are far too dissimilar to the native residue and cannot be incorporated into the protein through metabolic labelling.

A site-specific method for the incorporation of unique bioorthogonal functionalities is possible and has been achieved using the amber nonsense stop codon (UAG codon). The gene that encodes the protein is mutated to contain an UAG codon at the desired site of modification, whilst all other stop codons are removed from the sequence. An artificial tRNA is synthesised which contains a complementary anticodon and the unnatural amino acid. The addition of the synthetic tRNA and the mutated gene to an E.coli transcription/translation system will yield a selectively modified protein(*62*) (Figure 1.1-10). Many problems are associated with this technique including the considerable effort involved with the synthesising of amino-acylated tRNA and the disappointingly low yields obtained of the modified protein. Despite limitations, unnatural amino acids have been incorporated site-specifically into proteins such as the replacement of specific residues within α-helices and β-sheets with ester analogues for the analysis of backbone amide bonds.(*63*)

1.1.5.3 Enzymatic Modifications to Peptide Sequences

The challenge for achieving site-specific attachment of radioisotopes is that often there is no single site of unique reactivity within a biomolecular structure suitable for selective conjugation with imaging probes. Many enzymes posses the ability to recognise short peptide sequences within the biomolecular structure. Enzymes can covalently modify a single amino acid within a specific peptide sequence with a small molecular co-factor. A site of unique reactivity is therefore established within the protein structure. The specific peptide sequences can be inserted into proteins for enzyme modification providing opportunities for the selective targeting of different biomolecules in live cells.(*64*)

Enzyme catalysed protein modifications are somewhat advantageous in comparison to non-enzymatic methods as they occur naturally within a biological context. In addition to fast reaction kinetics, enzyme catalyzed reactions allow for the site-specific labelling of proteins with functionalised imaging probes without the need to synthetically incorporate unnatural amino acids into the biomolecular structure.(*65*) There are a variety of methods available for the enzymatic modifications of proteins including:

I) the labelling of proteins catalyzed by posttranslational modification enzymes;

II) the labelling of proteins by posttranslational modifications with "swinging arms". Here, the transfer of the prosthetic "swinging arms" to small protein domains occurs within large mutli-enzyme complexes

III) the labelling of proteins via enzyme self-modification.

Each modification will provide different functionalities on the surface of a protein molecule that can be targeted with functionalised imaging probes.

In particular, the enzymatic posttranslational modifications purposefully equip proteins with bioorthogonal functionalities that are not present in the 20 proteogenic amino acids.(*66*) The formylglycine generating enzyme (FGE) can covalently modify a Cys residue within a 13 amino acid sequence to produce an aldehyde bearing Cα-formylglycine catalytic residue. This provides an aldehyde functionality within the active site of many sulfatase proteins. Aldehydes can be targeted with aminooxy or hydrazine functionalised imaging probes. (Figure 1.1-11)

1.1.5.4 Chemical Modifications to Genetically Encoded Peptide Tags

To mimic the behaviour of enzymes in nature, research was pursued to exploit combinations of amino acids to provide new functionalities within a protein for selective chemical modifications. These amino acid combinations are often referred to as peptide tags and their reactivity is dependent on the proximity and the side chains of the amino acids within a specific sequence. The peptide tags only contain natural amino acids and can easily be genetically encoded into a specific protein of interest.

1.1.5.4 A Fluorescent Conjugations of Peptide Tags

Fluorescent imaging has become an essential tool for the analysis of cellular processes, yet it is limited by the large size of the fluorescent proteins that often hinders the biological activity of the targeted protein. Small peptide tag sequences embedded in the protein structure have enabled the direct labelling of proteins with small molecular fluorophores. A novel fluorescent labelling strategy was designed in which a short peptide sequence containing a tetraCys motif demonstrated selective reactivity with biarsenicals.(*67*) The CCXXCC tetraCys motif, where XX can be any two amino acids but optimally proline and glycine, reacts selectively with bisarsenical fluorescent dyes such as FlAsH and ReAsH when situated in a hairpin structure.(*68*) This is shown in Figure 1.1-15 where FlAsH and ReAsH reagents are bis(ethanedithiol) (EDT_2) adducts.

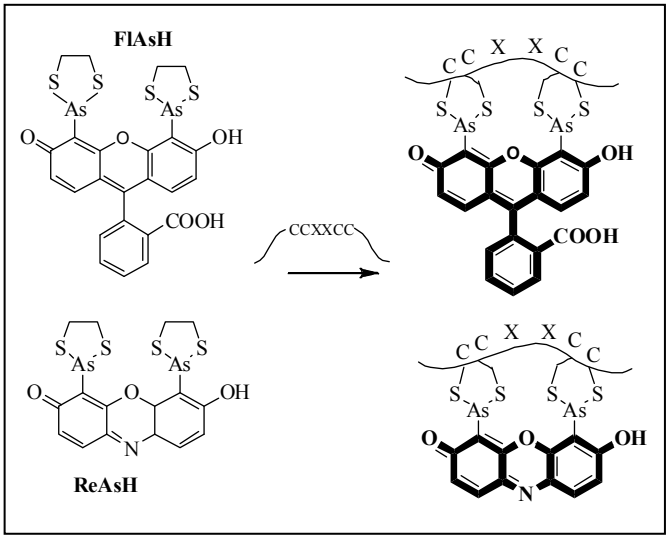

Figure 1.1-15. Bisarsenical fluorescent tags, FlAsH and ReAsH, binding to the CCXXCC motif. Binding increases the fluorescence intensity (bold lines).

The CCXXCC sequence can be genetically encoded into target proteins and then covalently labelled with the biarsenical probes in living cells. Additionally, the bisarsenical fluorescent conjugates are only mildly fluorescent when free in solution but undergo a dramatic increase in fluorescence when they bind to the CCXXCC sequence. In an imaging context, this reduces background fluorescence and enables real-time imaging. A combination of FlAsH and ReAsH agents have been used in the real-time trafficking of protein targets

including studies of mRNA translations(*69*), the analysis of G-protein-coupled receptor activation(*70*), and the transport of HIV-1 complexes within the body(*71*).

Another approach utilises bisboronic acid rhodamine dyes (RhoBo) as a selective method for the binding of tetraserine motifs also situated in a hairpin structure.(*72*) (Figure 1.1-16) RhoBos have demonstrated similar fluorogenic properties and cell-permeability to the FlAsH and ReAsH reagents, with the added advantage of eliminating the use of the cytotoxic element, arsenic. Initially RhoBo was designed for the detection of monosaccharides. However, binding affinities to peptides with an SSPGSS recognition sequence appeared to be higher, thus allowing the selective modification of proteins to occur in the presence of carbohydrates. Unfortunately, the SSXXSS recognition sequence is also present in some endogenous proteins which can often lead to the off-target conjugation of RhoBo dyes in living systems.

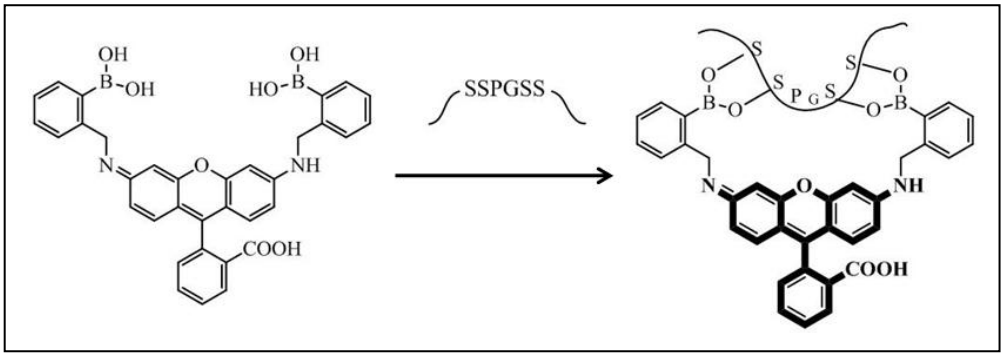

Figure 1.1-16. RhoBo dyes binding to a SSPGSS recognition motif.

1.1.5.4B $^{188}Re/^{99m}TcO_3^+$ Complexes Conjugation Peptide Tags

For many imaging applications the radioisotope ^{99m}Tc is preferred due to its favourable properties as mentioned in section 1.1.1-A. Its periodic congener Re can be used analogously by virtue of the availability of beta-emitting radioisotopes, ^{186}Re and ^{188}Re. These radiometals have complex chemistry with a variety of ligand preferences and structures in different metal oxidation states. The MO^{3+} core, where M equals ^{99m}Tc or Re in their n+3 oxidation state, is a particularly stable complex which has been widely used due to its synthetic accessibility from $^{99m}TcO_4^-$ and $^{188}ReO_4^-$, the forms in which the radiometals are most readily available.(*73*) MO^{3+} can be coordinated by various BFCs, such as chelator-

derivatised amino acids, for the labelling of a protein. Initially it was used as a method of forming oxo-technetium complexes with chelators that typically formed the base of a square pyramidal complex to incorporate the MO_3^+ core. Primary examples include tetradentate chelators such as triamidethiols (N3S), diamidedithiols (N2S2) and propylene amine oxime (N4).

In addition, MO^{3+} has demonstrated an ability to be bound by sequences of amino acids. MO^{3+} has been particularly effective in the context of coordinating amino acid sequences containing a Cys thiol. Investigations have been carried out into the use of several small peptides such as GGC, KGC and CGC as BFCs for the MO^{3+} complex.(*74-75*) Like the tetradentate BFCs, these peptides also form square pyramidal complexes to encompass the $^{99m}TcO^{3+}$ core. The coordinating atoms comprise typically of the thiolate sulfur and three sequential anionic, deprotonated amide nitrogens of the peptide backbone. Recently, it was found that binding of $^{99m}TcO^{3+}$, generated in situ by the reduction of pertechnetate with stannous compounds, to peptides is enhanced by the presence of a series of Arg residues.(*76*) The mechanism behind this enhancement is unclear. One might suggest that the Arg residue may assist in lowering the pKa of the nearby amide backbone enabling more efficient formation of the anionic, deprotonated amide nitrogens.

Other ^{99m}Tc/Re metal complexes have been investigated for coordination to peptide tags. Of note is the $[M(CO)_3]^+$ complex in which the metal centre, ^{99m}Tc or Re, is in its +1 oxidation state. $[M(CO)_3]^+$ complexes are well established for effective coordination to Hexahistidine peptide tags ($(His)_6$-Tag), that is, a sequence comprising of 6 consecutive His residues. The coordination of $[M(CO)_3]^+$ to $(His)_6$-Tagged proteins is discussed in detail in the next section, 1.2.

REFERENCES

1. Phelps, M. E. (2000) PET: the merging of biology and imaging into molecular imaging, *J Nucl Med 41*, 661-681.
2. Padhani, A. R., Gapinski, C. J., Macvicar, D. A., Parker, G. J., Suckling, J., Revell, P. B., Leach, M. O., Dearnaley, D. P., and Husband, J. E. (2000) Dynamic contrast

enhanced MRI of prostate cancer: correlation with morphology and tumour stage, histological grade and PSA, *Clin Radiol 55*, 99-109.
3. Adams, S., Baum, R. P., Stuckensen, T., Bitter, K., and Hor, G. (1998) Prospective comparison of 18F-FDG PET with conventional imaging modalities (CT, MRI, US) in lymph node staging of head and neck cancer, *Eur J Nucl Med 25*, 1255-1260.
4. Torres Martin de Rosales, R., Arstad, E., and Blower, P. J. (2009) Nuclear imaging of molecular processes in cancer, *Target Oncol 4*, 183-197.
5. Nutt, R. (2002) 1999 ICP Distinguished Scientist Award. The history of positron emission tomography, *Mol Imaging Biol 4*, 11-26.
6. Schubiger, P. A. (2007) Molecular imaging with PET--open questions?, *Ernst Schering Res Found Workshop*, 1-13.
7. Gabriel, M., Decristoforo, C., Kendler, D., Dobrozemsky, G., Heute, D., Uprimny, C., Kovacs, P., Von Guggenberg, E., Bale, R., and Virgolini, I. J. (2007) 68Ga-DOTA-Tyr3-octreotide PET in neuroendocrine tumors: comparison with somatostatin receptor scintigraphy and CT, *J Nucl Med 48*, 508-518.
8. Been, L. B., Suurmeijer, A. J., Cobben, D. C., Jager, P. L., Hoekstra, H. J., and Elsinga, P. H. (2004) [18F]FLT-PET in oncology: current status and opportunities, *Eur J Nucl Med Mol Imaging 31*, 1659-1672.
9. Nagata, K., Ota, Y., Okawa, T., Endo, S., and Kudo, S. E. (2008) PET/CT colonography for the preoperative evaluation of the colon proximal to the obstructive colorectal cancer, *Dis Colon Rectum 51*, 882-890.
10. Blower, P. (2006) Towards molecular imaging and treatment of disease with radionuclides: the role of inorganic chemistry, *Dalton Trans*, 1705-1711.
11. Sletten, E. M., and Bertozzi, C. R. (2009) Bioorthogonal Chemistry: Fishing for Selectivity in a Sea of Functionality, *Angew Chem Int Edit 48*, 6974-6998.
12. Fichna, J., and Janecka, A. (2003) Synthesis of target-specific radiolabeled peptides for diagnostic Imaging, *Bioconjugate Chemistry 14*, 3-17.
13. Glazer, A. N. (1970) Specific chemical modification of proteins, *Annu Rev Biochem 39*, 101-130.
14. Molecular ProbesTM and Pierce Biotechnology
15. Tait, J. F., Smith, C., Levashova, Z., Patel, B., Blankenberg, F. G., and Vanderheyden, J. L. (2006) Improved detection of cell death in vivo with annexin V radiolabeled by site-specific methods, *J Nucl Med 47*, 1546-1553.
16. Lahorte, C. M., Vanderheyden, J. L., Steinmetz, N., Van de Wiele, C., Dierckx, R. A., and Slegers, G. (2004) Apoptosis-detecting radioligands: current state of the art and future perspectives, *Eur J Nucl Med Mol Imaging 31*, 887-919.
17. Vermeersch, H., Loose, D., Lahorte, C., Mervillie, K., Dierckx, R., Steinmetz, N., Vanderheyden, J. L., Cuvelier, C., Slegers, G., and Van de Wiele, C. (2004) 99mTc-HYNIC Annexin-V imaging of primary head and neck carcinoma, *Nucl Med Commun 25*, 259-263.
18. Thiagarajan, P., and Tait, J. F. (1990) Binding of annexin V/placental anticoagulant protein I to platelets. Evidence for phosphatidylserine exposure in the procoagulant response of activated platelets, *J Biol Chem 265*, 17420-17423.
19. Fadok, V. A., Voelker, D. R., Campbell, P. A., Cohen, J. J., Bratton, D. L., and Henson, P. M. (1992) Exposure of phosphatidylserine on the surface of apoptotic lymphocytes triggers specific recognition and removal by macrophages, *J Immunol 148*, 2207-2216.
20. Fonge, H., de Saint Hubert, M., Vunckx, K., Rattat, D., Nuyts, J., Bormans, G., Ni, Y., Reutelingsperger, C., and Verbruggen, A. (2008) Preliminary in vivo evaluation of a

novel 99mTc-labeled HYNIC-cys-annexin A5 as an apoptosis imaging agent, *Bioorg Med Chem Lett 18*, 3794-3798.
21. Li, X., Link, J. M., Stekhova, S., Yagle, K. J., Smith, C., Krohn, K. A., and Tait, J. F. (2008) Site-specific labeling of annexin V with F-18 for apoptosis imaging, *Bioconjug Chem 19*, 1684-1688.
22. Babich, J. W., Solomon, H., Pike, M. C., Kroon, D., Graham, W., Abrams, M. J., Tompkins, R. G., Rubin, R. H., and Fischman, A. J. (1993) Technetium-99m-labeled hydrazino nicotinamide derivatized chemotactic peptide analogs for imaging focal sites of bacterial infection, *J Nucl Med 34*, 1964-1974.
23. Decristoforo, C., and Mather, S. J. (1999) Preparation, (99m)Tc-labeling, and in vitro characterization of hynic and N(3)S modified RC-160 and, *Bioconjug Chem 10*, 701-702.
24. Decristoforo, C., and Mather, S. J. (1999) Technetium-99m somatostatin analogues: effect of labelling methods and peptide sequence, *Eur J Nucl Med 26*, 869-876.
25. Decristoforo, C., and Mather, S. J. (1999) 99m-Technetium-labelled peptide-HYNIC conjugates: effects of lipophilicity and stability on biodistribution, *Nucl Med Biol 26*, 389-396.
26. King, R., Surfraz, M. B., Finucane, C., Biagini, S. C., Blower, P. J., and Mather, S. J. (2009) 99mTc-HYNIC-Gastrin Peptides: Assisted Coordination of 99mTc by Amino Acid Side Chains Results in Improved Performance Both In Vitro and In Vivo, *J Nucl Med 50*, 591-598.
27. Meszaros, L. K., Dose, A., Biagini, S. C., and Blower, P. J. (2011) Synthesis and evaluation of analogues of HYNIC as bifunctional chelators for technetium, *Dalton Trans 40*, 6260-6267.
28. Greenland, W. E., Howland, K., Hardy, J., Fogelman, I., and Blower, P. J. (2003) Solid-phase synthesis of peptide radiopharmaceuticals using Fmoc-N-epsilon-(hynic-Boc)-lysine, a technetium-binding amino acid: application to Tc-99m-labeled salmon calcitonin, *J Med Chem 46*, 1751-1757.
29. Stephenson, K. A., Banerjee, S. R., Sogbein, O. O., Levadala, M. K., McFarlane, N., Boreham, D. R., Maresca, K. P., Babich, J. W., Zubieta, J., and Valliant, J. F. (2005) A new strategy for the preparation of peptide-targeted technetium and rhenium radiopharmaceuticals. The automated solid-phase synthesis, characterization, labeling, and screening of a peptide-ligand library targeted at the formyl peptide receptor, *Bioconjug Chem 16*, 1189-1195.
30. Deiters, A., Geierstanger, B. H., and Schultz, P. G. (2005) Site-specific in vivo labeling of proteins for NMR studies, *Chembiochem 6*, 55-58.
31. Duckworth, B. P., Xu, J., Taton, T. A., Guo, A., and Distefano, M. D. (2006) Site-specific, covalent attachment of proteins to a solid surface, *Bioconjug Chem 17*, 967-974.
32. Whitney, C. G., Farley, M. M., Hadler, J., Harrison, L. H., Bennett, N. M., Lynfield, R., Reingold, A., Cieslak, P. R., Pilishvili, T., Jackson, D., Facklam, R. R., Jorgensen, J. H., and Schuchat, A. (2003) Decline in invasive pneumococcal disease after the introduction of protein-polysaccharide conjugate vaccine, *N Engl J Med 348*, 1737-1746.
33. You, C. C., De, M., and Rotello, V. M. (2005) Monolayer-protected nanoparticle-protein interactions, *Curr Opin Chem Biol 9*, 639-646.
34. Klein, J. (2007) Probing the interactions of proteins and nanoparticles, *Proc Natl Acad Sci U S A 104*, 2029-2030.
35. Dixon, H. B. F. (1984) N-Terminal Modification of Proteins - a Review, *J Protein Chem 3*, 99-108.

36. Gilmore, J. M., Scheck, R. A., Esser-Kahn, A. P., Joshi, N. S., and Francis, M. B. (2006) N-terminal protein modification through a biomimetic transamination reaction, *Angew Chem Int Ed Engl 45*, 5307-5311.
37. Geoghegan, K. F., and Stroh, J. G. (1992) Site-directed conjugation of nonpeptide groups to peptides and proteins via periodate oxidation of a 2-amino alcohol. Application to modification at N-terminal serine, *Bioconjug Chem 3*, 138-146.
38. Hackenberger, Christian P. R., and Schwarzer, D. (2008) Chemoselective Ligation and Modification Strategies for Peptides and Proteins, *Angewandte Chemie International Edition 47*, 10030-10074.
39. Dawson, P. E., and Kent, S. B. (2000) Synthesis of native proteins by chemical ligation, *Annu Rev Biochem 69*, 923-960.
40. Dawson, P. E., Muir, T. W., Clark-Lewis, I., and Kent, S. B. (1994) Synthesis of proteins by native chemical ligation, *Science 266*, 776-779.
41. Wilken, J., Hoover, D., Thompson, D. A., Barlow, P. N., McSparron, H., Picard, L., Wlodawer, A., Lubkowski, J., and Kent, S. B. (1999) Total chemical synthesis and high-resolution crystal structure of the potent anti-HIV protein AOP-RANTES, *Chem Biol 6*, 43-51.
42. Schwarzer, D., and Cole, P. A. (2005) Protein semisynthesis and expressed protein ligation: chasing a protein's tail, *Curr Opin Chem Biol 9*, 561-569.
43. Raghavan, A. S., and Hang, H. C. (2009) Seeing small molecules in action with bioorthogonal chemistry, *Drug Discov Today 14*, 178-184.
44. Jencks, W. P. (1959) Studies on the Mechanism of Oxime and Semicarbazone Formation, *Journal of the American Chemical Society 81*, 475-481.
45. Sadamoto, R., Niikura, K., Ueda, T., Monde, K., Fukuhara, N., and Nishimura, S. (2004) Control of bacteria adhesion by cell-wall engineering, *J Am Chem Soc 126*, 3755-3761.
46. Kohn, M., and Breinbauer, R. (2004) The Staudinger ligation-a gift to chemical biology, *Angew Chem Int Ed Engl 43*, 3106-3116.
47. Handlon, A. L., and Oppenheimer, N. J. (1988) Thiol reduction of 3'-azidothymidine to 3'-aminothymidine: kinetics and biomedical implications, *Pharm Res 5*, 297-299.
48. Hang, H. C., Loureiro, J., Spooner, E., van der Velden, A. W., Kim, Y. M., Pollington, A. M., Maehr, R., Starnbach, M. N., and Ploegh, H. L. (2006) Mechanism-based probe for the analysis of cathepsin cysteine proteases in living cells, *ACS Chem Biol 1*, 713-723.
49. Rostovtsev, V. V., Green, L. G., Fokin, V. V., and Sharpless, K. B. (2002) A stepwise huisgen cycloaddition process: copper(I)-catalyzed regioselective "ligation" of azides and terminal alkynes, *Angew Chem Int Ed Engl 41*, 2596-2599.
50. Kolb, H. C., Finn, M. G., and Sharpless, K. B. (2001) Click Chemistry: Diverse Chemical Function from a Few Good Reactions, *Angew Chem Int Ed Engl 40*, 2004-2021.
51. Agard, N. J., Baskin, J. M., Prescher, J. A., Lo, A., and Bertozzi, C. R. (2006) A comparative study of bioorthogonal reactions with azides, *ACS Chem Biol 1*, 644-648.
52. Baskin, J. M., Prescher, J. A., Laughlin, S. T., Agard, N. J., Chang, P. V., Miller, I. A., Lo, A., Codelli, J. A., and Bertozzi, C. R. (2007) Copper-free click chemistry for dynamic in vivo imaging, *Proc Natl Acad Sci U S A 104*, 16793-16797.
53. Kele, P., Li, X., Link, M., Nagy, K., Herner, A., Lorincz, K., Beni, S., and Wolfbeis, O. S. (2009) Clickable fluorophores for biological labeling--with or without copper, *Org Biomol Chem 7*, 3486-3490.

54. Lin, F. L., Hoyt, H. M., van Halbeek, H., Bergman, R. G., and Bertozzi, C. R. (2005) Mechanistic investigation of the staudinger ligation, *J Am Chem Soc 127*, 2686-2695.
55. van Berkel, S. S., Dirks, A., Meeuwissen, S. A., Pingen, D. L., Boerman, O. C., Laverman, P., van Delft, F. L., Cornelissen, J. J., and Rutjes, F. P. (2008) Application of metal-free triazole formation in the synthesis of cyclic RGD-DTPA conjugates, *Chembiochem 9*, 1805-1815.
56. Blackman, M. L., Royzen, M., and Fox, J. M. (2008) Tetrazine ligation: fast bioconjugation based on inverse-electron-demand Diels-Alder reactivity, *J Am Chem Soc 130*, 13518-13519.
57. Song, W., Wang, Y., Qu, J., and Lin, Q. (2008) Selective functionalization of a genetically encoded alkene-containing protein via "photoclick chemistry" in bacterial cells, *J Am Chem Soc 130*, 9654-9655.
58. Lin, Y. A., Chalker, J. M., Floyd, N., Bernardes, G. J., and Davis, B. G. (2008) Allyl sulfides are privileged substrates in aqueous cross-metathesis: application to site-selective protein modification, *J Am Chem Soc 130*, 9642-9643.
59. Voss, E. W., Jr. (1993) Kinetic measurements of molecular interactions by spectrofluorometry, *J Mol Recognit 6*, 51-58.
60. Link, A. J., Mock, M. L., and Tirrell, D. A. (2003) Non-canonical amino acids in protein engineering, *Curr Opin Biotechnol 14*, 603-609.
61. Kiick, K. L., Saxon, E., Tirrell, D. A., and Bertozzi, C. R. (2002) Incorporation of azides into recombinant proteins for chemoselective modification by the Staudinger ligation, *Proc Natl Acad Sci U S A 99*, 19-24.
62. Noren, C. J., Anthony-Cahill, S. J., Griffith, M. C., and Schultz, P. G. (1989) A general method for site-specific incorporation of unnatural amino acids into proteins, *Science 244*, 182-188.
63. Koh, J. T., Cornish, V. W., and Schultz, P. G. (1997) An experimental approach to evaluating the role of backbone interactions in proteins using unnatural amino acid mutagenesis, *Biochemistry 36*, 11314-11322.
64. Chen, I., and Ting, A. Y. (2005) Site-specific labeling of proteins with small molecules in live cells, *Curr Opin Biotechnol 16*, 35-40.
65. Foley, T. L., and Burkart, M. D. (2007) Site-specific protein modification: advances and applications, *Curr Opin Chem Biol 11*, 12-19.
66. Sunbul, M., and Yin, J. (2009) Site specific protein labeling by enzymatic posttranslational modification, *Org Biomol Chem 7*, 3361-3371.
67. Griffin, B. A., Adams, S. R., and Tsien, R. Y. (1998) Specific covalent labeling of recombinant protein molecules inside live cells, *Science 281*, 269-272.
68. Cao, H., Xiong, Y., Wang, T., Chen, B., Squier, T. C., and Mayer, M. U. (2007) A red cy3-based biarsenical fluorescent probe targeted to a complementary binding peptide, *J Am Chem Soc 129*, 8672-8673.
69. Rodriguez, A. J., Shenoy, S. M., Singer, R. H., and Condeelis, J. (2006) Visualization of mRNA translation in living cells, *J Cell Biol 175*, 67-76.
70. Hoffmann, C., Gaietta, G., Bunemann, M., Adams, S. R., Oberdorff-Maass, S., Behr, B., Vilardaga, J. P., Tsien, R. Y., Ellisman, M. H., and Lohse, M. J. (2005) A FlAsH-based FRET approach to determine G protein-coupled receptor activation in living cells, *Nat Methods 2*, 171-176.
71. Arhel, N., Genovesio, A., Kim, K. A., Miko, S., Perret, E., Olivo-Marin, J. C., Shorte, S., and Charneau, P. (2006) Quantitative four-dimensional tracking of cytoplasmic and nuclear HIV-1 complexes, *Nat Methods 3*, 817-824.

72. Halo, T. L., Appelbaum, J., Hobert, E. M., Balkin, D. M., and Schepartz, A. (2009) Selective recognition of protein tetraserine motifs with a cell-permeable, pro-fluorescent bis-boronic acid, *J Am Chem Soc 131*, 438-439.
73. Liu, S., and Edwards, D. S. (1999) 99mTc-Labeled Small Peptides as Diagnostic Radiopharmaceuticals, *Chem Rev 99*, 2235-2268.
74. Tait, J. F., Smith, C., and Blankenberg, F. G. (2005) Structural requirements for in vivo detection of cell death with 99mTc-annexin V, *J Nucl Med 46*, 807-815.
75. Tait, J. F., Brown, D. S., Gibson, D. F., Blankenberg, F. G., and Strauss, H. W. (2000) Development and characterization of annexin V mutants with endogenous chelation sites for (99m)Tc, *Bioconjug Chem 11*, 918-925.
76. Le Clainche, L., LeCoq, A., Zinn-Justin, S., Thai, R., Masella, M., Cuniasse, P. . (2010) Cysteine-Free Technetium (Tc) or Rhenium (Re) Chelating Peptide Tags and Their Use, In *France:* , p WO2010/076654

1.2 Introduction: The His-Tag and its Conjugation with Metal Complexes

1.2.1 EARLY USE OF THE HIS-TAG

1.2.1.1 His-Tag as a Method of Protein Purification

Perhaps the most versatile and commonly used genetically encoded peptide tag within protein research is the His-Tag. Typically, this polyHis tag consists of 6 consecutive His residues and was originally developed to be incorporated at the N or C-terminus of a recombinant protein and facilitate downstream purification via immobilised metal-affinity chromatography.(*1*) Immobilisation was accomplished through the coordination of two or more of the His residues to a metal ion. An incompletely coordinated Ni(II) metal ion is often utilised due to its high binding affinity with the imidazole side chain of the His residue. The Ni(II) ion is attached to a chelating substrate such as nitriotriacetic acid, NTA, forming an Ni:NTA complex.(*2*) Recently the immobilisation of His tag proteins has been accomplished with the use of nickel-chelated nanolipoprotein particles.(*3*) The nanolipoprotein particles were model membrane mimetics for the stabilisation and analysis of membrane proteins.

1.2.1.2 His-Tag as a Method of Fluorescent Labelling

Further work identified the possibility of extending the application of genetically encoded His-Tags into an imaging context. Fluorescent probes including rhodamine derivatives, fluorescein and cyanine dyes, were conjugated to the Ni:NTA coordination system and processes.(*4*) Examples have included labelling to both $(His)_6$ and $(His)_{10}$ sequences. However, the binding between His and Ni(II) is noncovalent and conjugation is therefore not robust. The development of the His-Tag as a target for covalent surface attachments would be invaluable in the design of suitable imaging agents.

A trifunctional labelling reagent has proven to be successful in the covalent labelling of recombinant proteins selectively through the recognition of His-tags.(*5*) This strategy involves the initial noncovalent coordination of the Ni:NTA substrate to the His-tag on the proteins surface. The juxtaposed photoreactive group is then activated with the use of a long-wavelength UV light and creates a covalent bond to the protein surface. A fluorescent probe or affinity tag is also conjugated to the trifunctional reagent and is consequently site specifically covalently attached to the protein following light activation. (Figure 1.2-1).

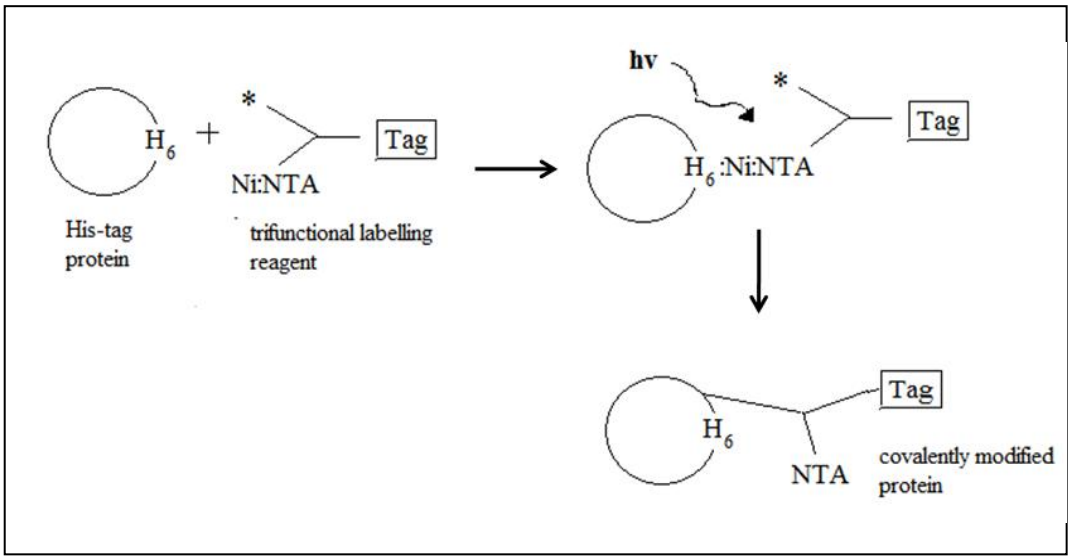

Figure 1.2-1. Trifunctional labelling reagents with a photoreactive group (*) and a Ni:NTA substrate that bind to His-tags covalently upon photoactivation

Affinity-driven coordination of the trifunctional labelling reagent through its Ni:NTA functionality ensures that the formation of the covalent bond is proximal to the His-tag sequence. Studies were commenced utilizing two trifunctional labelling reagents; NAB containing an azide photoreactive group and a biotin functional group; and NBzM with a benzophenone photoconjugating group and a maleimide functionality. The principal reaction products were, as predicted, monofunctionalised proteins that retained their biological activity and were selectively modified.

Further improvements to this technique have involved the development of a Zn(II) metal ion for conjugation with polyHis sequence in order to overcome the toxicity issues

associated with nickel. The HisZiFit fluorescent tag has demonstrated binding to $(His)_6$, mediated by the Zn(II) ion, in the study of the STIM1 stromal interaction molecule.(*6*)

1.2.2 $[M(CO)_3]^+$ CONJUGATION TO HIS-TAG

1.2.2.1 $[M(CO)_3]^+$ Complex (M = ^{99m}Tc/Re)

An elegant method was developed by Waibel et al. for the radiolabelling of proteins engineered with the His-Tag.(*7*) Radiolabelling was achieved using the $[^{99m}Tc(CO)_3(H_2O)_3]^+$ complex with ^{99m}Tc in its stable +1 oxidation state. This complex is especially attractive for several reasons. The CO-Tc bond is particularly inert towards ligand substitution and complex oxidation which renders it useful for in vivo experimentation. In addition it utilises the His-Tag as a means by which to coordinate and this is a very common motif in recombinant proteins because of its value in protein purification as mentioned earlier. ^{99m}Tc itself is analogous to ^{188}Re and consequently the molecular imaging of processes with $[^{99m}Tc(CO)_3]^+$ can also be adapted for therapy with the $[^{186/188}Re(CO)_3]^+$ complex. Both $[M(CO)_3]^+$ synthons are easily prepared by reduction from the generator eluted MO_4^- radioisotopes by a simple one-step kit based method.(*8-10*)

1.2.2.2 $[M(CO)_3]^+$ Coordination to His-Tags

It has been proposed that $[^{99m}Tc(CO)_3(OH_2)_3]^+$ coordinate to the His-Tag through the His imidazole groups which are believed to coordinate directly to the Tc(I) by displacement of water.(*7, 11-12*) A stable complex forms when the H_2O ligands are exchanged for the sp^2 nitrogen of the imidazole group. The soft Tc(I) centre binds strongly to the easily polarisable imidazole ligands and once bound, competition by ligand exchange is kinetically very slow in this d^6 system. (*13*)

The binding mode of the His-Tag to Tc center and the structure of the formed complex has not been determined experimentally. A model proposed by Schibli et al. has suggested that coordinating ligands are believed to comprise of two alternate His imidazole side chains and a third ligand possibly a H_2O molecule.(*12*) However, the actual identity of the supposed third ligand remains ambiguous. (Figure 1.2-2)

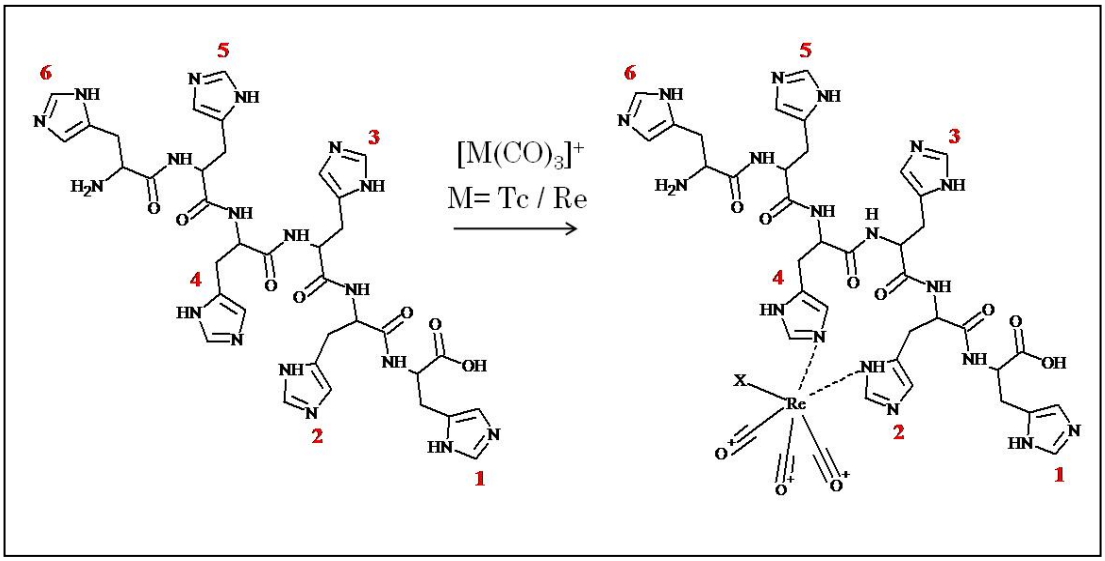

Figure 1.2-2. Schematic diagram representing the proposed binding of $[M(CO)_3]^+$ to a $(His)_6$-Tag via two alternate His residues. X represents the third ligand which is proposed as H_2O but is currently still experimentally unidentified.(*12*)

1.2.2.4 Radiolabelling of His-Tagged Proteins with $[M(CO)_3]^+$

Proteins are often engineered to contain a "generic" His-Tag consisting of 6 consecutive His residues which are commonly used as a method of purification via Ni^{2+} column and adopted as a method for the site-specific labelling of proteins with $[M(CO)_3]^+$ complexes. Examples include the direct radiolabelling of Herceptin for breast cancer imaging and Annexin V for apoptosis imaging.(*14-15*) With a $(His)_6$-Tag there are 6 possible sites of coordination for $[M(CO)_3]^+$ which increases the entropy of the reaction but at the same time increases the chances of isomer formation and inhomogeneity for the labelled product.

In the absence of a $(His)_6$-Tag some proteins can still be labelled although with reduced efficiency, therefore it is not certain that the use of the $(His)_6$-Tag guarantees site-specificity. Tavare et al. demonstrated that without a His-Tag within the C2A recombinant protein, phosphatidylserine (PS)-domain of rat synaptotagmin I, the construct radiolabelled with a 15% radiochemical yield in comparison to the His-Tag containing C2AcH which had a 96% radiochemical yield after the same 30 mins incubation.(*12, 16*)

For the $(His)_6$-Tagged C2A recombinant protein C2AcH, which also contains a cysteine close to the His tag, site-specificity was achieved for the $[M(CO)_3]^+$ coordination. In order to map

the $[M(CO)_3]^+$ binding specifically to the C-terminus $(His)_6$-Tag, the $[Re(CO)_3]^+$ labelled and unlabelled C2AcH were subjected to trypsin digest and the fragments analysed by LCMS.(*17*) Mass Spectrometry demonstrated that for the labelled C2AcH, the major ion had an *m/z* corresponding to $[C2AcH + Re(CO)_3]^+$ = 16787.320 (Expected *m/z* = 16787.166) which confirmed that the addition of only one $[Re(CO)_3]^+$ had been made to the protein and no other exogenous ligands were present in the coordination sphere according to the mass spectrum. UV chromatograms of the tryptic digested C2AcH and $[C2AcH\text{-}Re(CO)_3]^+$ revealed that a single peak, rt = 25mins, in the C2AcH chromatogram (Figure 1.2-3 A, bold arrow) was substantially decreased post complexation with $[Re(CO)_3]^+$, according to the $[C2AcH\text{-}Re(CO)_3]^+$ chromatogram (Figure 1.2-3 B, bold arrow). It was confirmed by MS that this peak corresponded to the peptide fragment containing the $(His)_6$-Tag, LAAALEHHHHHH, at the C-terminal of the protein (*m/z* = 705.348 for $[LAAALEHHHHHH + 2H]^{2+}$). All other peaks remained unaffected post addition of $[Re(CO)_3]^+$. In the tryptic digested chromatogram of $[C2AcH\text{-}Re(CO)_3]^+$ new peaks appeared at rt = 32-35 mins (Figure 1.2-3 B, open arrow). From MS, these peaks were associated with the $[LAAALEHHHHHH\text{-}Re(CO)_3]^+$ fragmented ion (*m/z* = 840.307) and contained the characteristic $^{185/187}$Re isotope pattern. Evidently, from this data the $[Re(CO)_3]^+$ binding site is confirmed as the $(His)_6$-Tag region.

Multiple new peaks with identical mass numbers (m/z = 840.307) appear in the UV chromatogram of $[C2AcH\text{-}Re(CO)_3]^+$ at rt = 32-35 mins. The mass number corresponds to the $[LAAALEHHHHHH\text{-}Re(CO)_3]^+$ fragmented ion and the presence of multiple peaks indicates that the $[LAAALEHHHHHH\text{-}Re(CO)_3]^+$ complex has formed different isomers. In figure 1.2-3 C the extracted ion chromatogram (EIC) of $[LAAALEHHHHHH\text{-}Re(CO)_3]^+$ (*m/z* = 840.307) verifies that multiple peaks exist. Due to the availability of the 6 imidazole in the $(His)_6$-Tag it is probable that regio- and stereoisomers have been formed on coordination between $[Re(CO)_3]^+$ and the $(His)_6$-Tag, since it has been indicated that $[Re(CO)_3]^+$ requires only 2 imidazoles for its coordination. Further discussions on the formation of isomers will be addressed in Chapter 2.

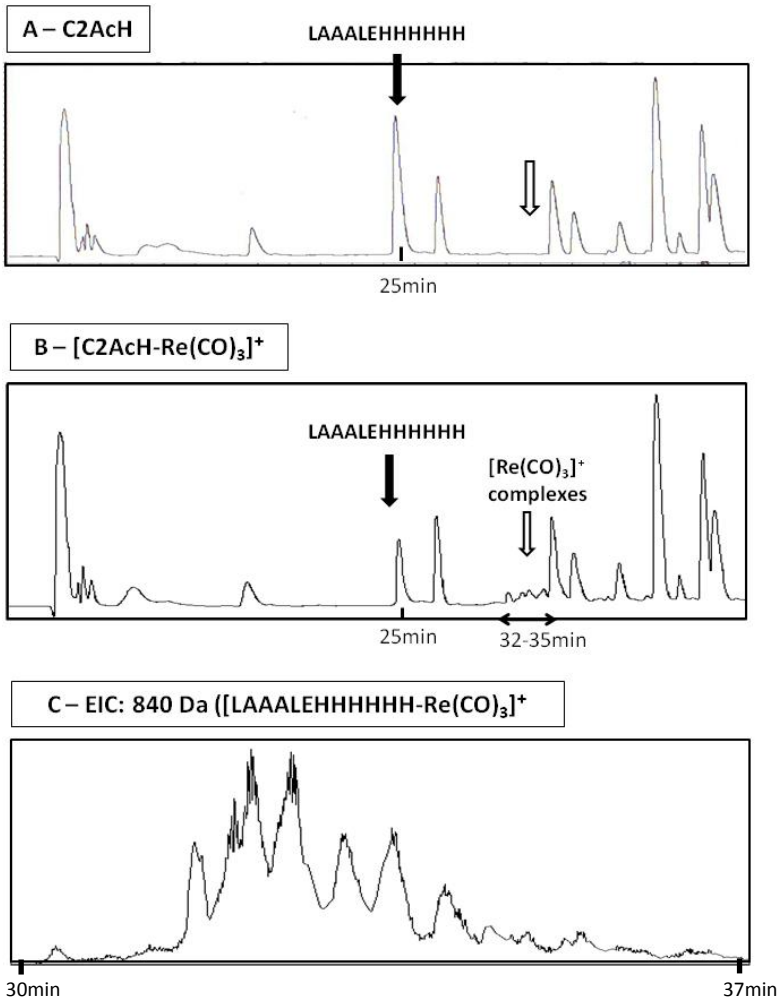

Figure 1.2-3. UV chromatograms post trypsin digest of C2AcH and $[C2AcH\text{-}Re(CO)_3]^+$. **A)** UV chromatogram of C2AcH. **B)** UV chromatogram of $[C2AcH\text{-}Re(CO)_3]^+$. Bold arrows correspond to the peptide peak LAAALEHHHHHH. Open arrows highlight the presence of new peaks appearing post incubation with $[Re(CO)_3]^+$. **C)** EIC of *m/z* = 840.307 corresponding to $[LAAALEHHHHHH\text{-}Re(CO)_3 + 1H]^{2+}$. (*17*)

Another study was performed to visualise the specificity of the His-Tag for $[M(CO)_3]^+$ complexes.(*18*) A competitive binding assay was carried out by co-incubating equimolar amounts of $(His)_6$-Tagged (C2A) and non-$(His)_6$-Tagged (CD33) containing proteins with $[^{99m}Tc(CO)_3]^+$.(*16, 19*) It was demonstrated that a significant 98% of the $[^{99m}Tc(CO)_3]^+$ preferentially bound to the His-Tagged protein after 1hr.(Figure 1.2-4) Less than 2% of $[^{99m}Tc(CO)_3]^+$ was 'non-specifically' coordinated to non His-Tagged protein. From these results, it is clear that of all the amino acids, His is the most reactive towards $[M(CO)_3]^+$ complexes and it is most likely that in the presence of a $(His)_6$-Tag proteins label site-specifically with $[M(CO)_3]^+$ complexes.

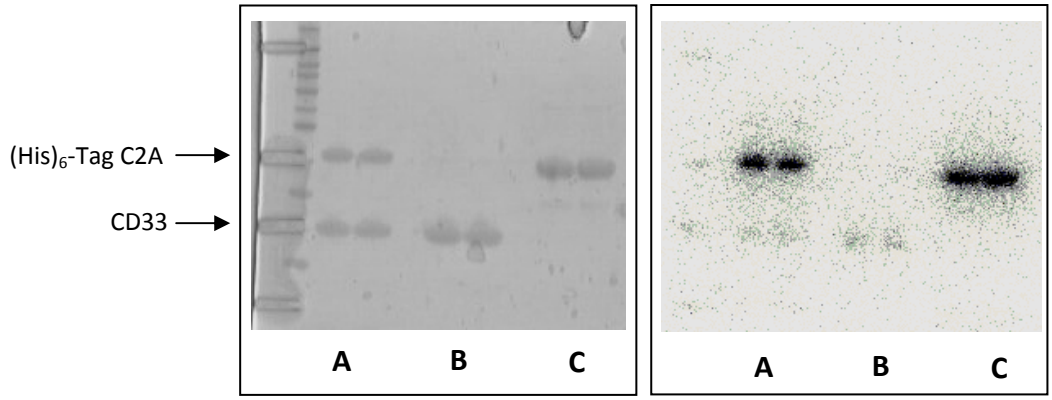

Lane	Protein
A	$(His)_6$-Tagged C2A protein (*16*)
B	Non $(His)_6$-Tagged CD33 protein (*19*)
C	Competition: $(His)_6$-Tagged C2A and non $(His)_6$-TagCD33 protein

Figure 1.2-4. Competition experiment demonstrating specificity of $[^{99m}Tc(CO)_3]^+$ binding to $(His)_6$-Tagged proteins. **A)** $[^{99m}Tc(CO)_3]^+$ labelled $(His)_6$-Tagged C2A protein. **B)** $[^{99m}Tc(CO)_3]^+$ labelled CD33 protein with no $(His)_6$-Tag. **C)** Co-incubation of $(His)_6$-Tagged C2A and non $(His)_6$-Tag C2A with $[^{99m}Tc(CO)_3]^+$ in a competition radiolabelling experiment. **Left image)** SDS-PAGE separation of the proteins. **Right)** Phosphor image giving a visual image of the location of the $[^{99m}Tc(CO)_3]^+$ complex.(*18*)

In many His-Tagged proteins the radiolabelling works well and satisfies to a variable extent the requirements discussed in Chapter 1.1 for the design of an optimal molecular imaging agent.(*16, 20*) A summary of the conditions used and yields obtained post labelling of $(His)_6$-Tagged proteins with $[^{99m}Tc(CO)_3]^+$ has been presented in figure 1.2-5. Here, some His-Tagged proteins label efficiently at reasonably low concentrations and gave high radiochemical yields. (*16, 20*) Other His-Tagged proteins require higher protein concentration (*21*), higher temperature labelling conditions (*22-23*) and a longer incubation time.(*14, 24*). To be used in pre-clinical studies, radiochemical purity must be > 90%-95% for a His-Tagged protein. In table 1.2-1 it is revealed that often a radiochemical yield less than 90% is achieved and consequently a subsequent purification step is required prior to pre-clinical or clinical use.(*25-27*) This is not advantageous as it results in the loss of costly protein and can be time consuming.

Ref.	Labelling Conditions	Labelling time	RY (%)	Purification	RP (%) post purification	Specific Activity
Mees et al. 2012 (*27*)	37°C, blown dry with N_2	1-1.5hr	40-50%	Yes	>95%	8.9-10.4 MBq/μg
Shah et al. 2012 (*24*)	37°C, PBS at pH 7.4	2hr	98%			
Cortez-Retamozo et al. 2008 (*23*)	52°C, carbonate buffer at pH 8 and PBS at	1hr		Often purification step was necessary	98%	
Teran et al. 2011 (*28*)	50°C, H_2O for protein	50min	95%			0.7MBq/μg
Orlova et al. 2006 (*29*)	50°C, PBS buffer	40min	60%			
Deyev et al. 2003 (*20*)			95%			2MBq/μg
Tait et al. 2002 (*26*)	37°C, 0.5/0.1M HEPES-Na pH 7.4	1hr	80%	Yes	98%	
Chen et al. 2008 (*14*)	37°C	3hr	90%	Yes	90%	
Tavare et al. 2009 (*16*)	37°C, PBS buffer at pH 7.4	30min	95%	Yes	100%	
Zahnd et al. 2010 (*30*)	37°C, 0.6M phosphate buffer at pH 7	1hr				
Tolmachev et al. 2010 (*22*)	50°C, PBS Buffer	1hr	80%	Yes	95%	2 MBq/μg

Bidlingmaier et al. 2009 (*21*)	37°C, PBS buffer	1hr		Yes		
Berndorff et al. 2006 (*25*)	37°C, 0.1M HEPES and PBS buffer	1hr	54%	Yes	91%	2.1MBq/μg

Figure 1.2-1. Radiolabelling conditions and the radiochemical yield (RY) and radiochemical purity (RP) of $(His)_6$-Tagged proteins with $[^{99m}Tc(CO)_3]^+$.

It remains uncertain as to why some His-Tagged proteins are able to demonstrate characteristics that comply with the requirements specified for an imaging agent, while others do not. Clearly, the incorporation of a $(His)_6$-Tag into a protein sequence is not in itself sufficient to guarantee efficient labelling and to provide the desirable attribute that the radiolabelling efficiency should be fundamentally independent of the protein type. Currently, radiolabelling of each new individual protein must be optimised before it can be biologically and clinically evaluated as a molecular imaging agent. This is an inefficient and unpredictable way of assessing large libraries of trial recombinant proteins for applications in imaging.

1.2.2.5 The Cys/$(His)_6$-Tag – A Combination of a $(His)_6$-Tag and an Adjacent Cys

The factors responsible for the labelling efficiency of the proteins are unknown. However, the amino acids that surround the $(His)_6$-Tag are likely to be an important factor influencing its reactivity. Progress towards the optimisation of the $(His)_6$-Tag design, to improve its utility as an imaging agent, has been reported by Tavare et al. A Cys within close proximity to the $(His)_6$-Tag (Cys/$(His)_6$-Tag), 8 amino acids away, produced a significant improvement in the radiolabelling efficiency of the C2A protein biomolecule; the phosphatidylserine (PS)-domain of rat synaptotagmin I. The C2A fragment was initially designed to include the C-terminus sequence CKLAAALEHHHHHH (C2AcH) for versatility, allowing both the incorporation of a single cysteine residue for covalent modification and a $(His)_6$-Tag for conjugation with $[M(CO)_3]^+$. The unexpected benefit of the additional Cys residue adjacent to the $(His)_6$-Tag seen in the labelling efficiency of C2AcH clearly reveals how amino acids surrounding the $(His)_6$-Tag can substantially influence the coordination of $[M(CO)_3]^+$.

It has been proposed that the increase in labelling efficiency in the presence of a free Cys is attributable to the presence of the thiol functionality and its involvement in the formation of a protein-metal complex. Firstly it has been suggested that the Cys is involved in an initial coordination with the $[M(CO)_3]^+$ complex. Cys-thiol groups have been established as key nucleophilic catalysts in many enzymes, and therefore it is conceivable that an intermediate M-S bond can be formed between the thiolate anions forms and the $[M(CO)_3]^+$. Thus, in this hypothesis it is acting as a local catalyst by performing an initial nucleophilic attack on the positively charged metal. The preliminary binding between the Cys and metal complex increases the proximity of the $[M(CO)_3]^+$ to the His residues and enables a more efficient coordination to occur. In this instance, the metal-thiolate bond is temporary and in the presence of the His residues, is displaced from metal coordination sphere. Another possibility is the direct permanent involvement of the Cys in coordination to the metal and that the binding of $[Re(CO)_3]^+$ to a His-Tagged sequence involves three coordination sites including two imidazoles functionalities from the His residues and the thiol from the reduced Cys. During my studies further investigations are pursued into the influence of the Cys residue, including its role in the coordination sphere of the protein-$[M(CO)_3]^+$ complex. These investigations are described in Chapter 2.

1.2.3 RATIONALE AND AIMS OF THE PROJECT

None of the currently available site-specific protein labelling methods fully satisfy the requirements discussed in Chapter 1.1 for the production of an optimal biomolecular imaging agent in a reliable and predictable way. The $(His)_6$-Tag is perhaps one of the most promising methods for applications in molecular SPECT imaging and therapy. Proteins containing $(His)_6$-Tags have demonstrated site-specific labelling whilst maintaining the molecular recognition function of the protein. His residues are biologically compatible and can easily be engineered into a recombinant protein without increasing the toxicity of the imaging agent. In addition, the $(His)_6$-Tag labelling mechanism is common to both ^{99m}Tc, the preferred γ radioisotope for imaging, and the analogous $^{186}/^{188}Re$, which are β-emitter suitable for therapeutic applications. Despite some favourable properties of the $(His)_6$-Tag, the unpredictability and inefficiency associated with the radiolabelling of $(His)_6$-Tagged proteins needs to be addressed if widespread use of this system can be employed.

The purpose of my study is to provide a solution to the problems related to the use of the $(His)_6$-Tag for radiolabelling biomolecules with $[^{99m}Tc(CO)_3]^+$ and $[^{186}/^{188}Re(CO)_3]^+$ cores. This will be achieved through optimisation of a sequence of proteogenic amino acids that can be incorporated into recombinant proteins and provide a binding site that offers highly efficient and site-specific labelling under biological conditions, regardless of the nature of the proteins used. Focus will primarily be on the influence of surrounding amino acids on the coordination of the His residues with $[M(CO)_3]^+$ complexes. Initially investigations will pursue the use of an adjacent Cys residue in improving the labelling and attempt to clarify the reasons behind this observation. A longer term aim is the development of a high throughput screening mechanism that will identify, on a large scale, novel genetically encoded tags that may be more suitable for coordination with $[M(CO)_3]^+$ complexes.

Ultimately it is desirable to produce a sequence of proteogenic amino acids that can be easily incorporate into a protein and will render them amenable to site-specific radiolabelling in a simple kit-based procedure. This should occur at low protein concentrations to give a very high specific activity and high radiochemical yield which will avoid the need for additional purification steps. A radiopharmaceutical should be produced with high structural homogeneity and excellent kinetic stability of the radiolabelled biomolecule in vivo whilst keeping intact the biological recognition activity.

REFERENCES

1. Skerra, A., Pfitzinger, I., and Pluckthun, A. (1991) The functional expression of antibody Fv fragments in Escherichia coli: improved vectors and a generally applicable purification technique, *Biotechnology (N Y) 9*, 273-278.
2. Terpe, K. (2003) Overview of tag protein fusions: from molecular and biochemical fundamentals to commercial systems, *Appl Microbiol Biotechnol 60*, 523-533.
3. Fischer, N. O., Blanchette, C. D., Chromy, B. A., Kuhn, E. A., Segelke, B. W., Corzett, M., Bench, G., Mason, P. W., and Hoeprich, P. D. (2009) Immobilization of His-tagged proteins on nickel-chelating nanolipoprotein particles, *Bioconjug Chem 20*, 460-465.
4. Kapanidis, A. N., Ebright, Y. W., and Ebright, R. H. (2001) Site-specific incorporation of fluorescent probes into protein: hexahistidine-tag-mediated fluorescent labeling with (Ni(2+):nitrilotriacetic Acid (n)-fluorochrome conjugates, *J Am Chem Soc 123*, 12123-12125.

5. Meredith, G. D., Wu, H. Y., and Allbritton, N. L. (2004) Targeted protein functionalization using His-tags, *Bioconjug Chem 15*, 969-982.
6. Hauser, C. T., and Tsien, R. Y. (2007) A hexahistidine-Zn2+-dye label reveals STIM1 surface exposure, *Proc Natl Acad Sci U S A 104*, 3693-3697.
7. Waibel, R., Alberto, R., Willuda, J., Finnern, R., Schibli, R., Stichelberger, A., Egli, A., Abram, U., Mach, J. P., Pluckthun, A., and Schubiger, P. A. (1999) Stable one-step technetium-99m labeling of His-tagged recombinant proteins with a novel Tc(I)-carbonyl complex, *Nat Biotechnol 17*, 897-901.
8. Roger Alberto, R. S., Andre Egli, August P. Schubiger. (1998) A Novel Organometallic Aqua Complex of Technetium for the Labeling of Biomolecules: Synthesis of $[^{99m}Tc(OH_2)_3(CO)_3]^+$ from $[^{99m}TcO_4]^-$ in Aqueous Solution and Its Reaction with a Bifunctional Ligand, *J. Am. Chem. Soc. 120*, 7987-7988.
9. Torres Martin de Rosales, R., Finucane, C., Foster, J., Mather, S. J., and Blower, P. J. (2010) $^{188}Re(CO)_3$-dipicolylamine-alendronate: a new bisphosphonate conjugate for the radiotherapy of bone metastases, *Bioconjug Chem 21*, 811-815.
10. Schibli, R., and Schubiger, P. A. (2002) Current use and future potential of organometallic radiopharmaceuticals, *European Journal of Nuclear Medince 29*.
11. Egli, A., Alberto, R., Tannahill, L., Schibli, R., Abram, U., Schaffland, A., Waibel, R., Tourwe, D., Jeannin, L., Iterbeke, K., and Schubiger, P. A. (1999) Organometallic 99mTc-aquaion labels peptide to an unprecedented high specific activity, *J Nucl Med 40*, 1913-1917.
12. Schibli, R., and Schubiger, P. A. (2002) Current use and future potential of organometallic radiopharmaceuticals, *Eur J Nucl Med Mol Imaging 29*, 1529-1542.
13. Zamora, P. O., and Rhodes, B. A. (1992) Imidazoles as well as thiolates in proteins bind technetium-99m, *Bioconjug Chem 3*, 493-498.
14. Chen, W. J., Yen, C. L., Lo, S. T., Chen, K. T., and Lo, J. M. (2008) Direct 99m Tc labeling of Herceptin (trastuzumab) by 99m Tc(I) tricarbonyl ion, *Appl Radiat Isot 66*, 340-345.
15. Chen, Y. L., Wu, C. C., Lin, Y. C., Pan, Y. H., Lee, T. W., and Lo, J. M. (2009) 99mTc(I)-tricarbonyl Labeled Histidine-tagged Annexin V for Apoptosis Imaging., *ICBME 2008, Proceedings 23*, 1393-1396.
16. Tavare, R., Torres Martin De Rosales, R., Blower, P. J., and Mullen, G. E. (2009) Efficient site-specific radiolabeling of a modified C2A domain of synaptotagmin I with [99mTc(CO)3]+: a new radiopharmaceutical for imaging cell death, *Bioconjug Chem 20*, 2071-2081.
17. Tavare, R., Williams, J., Howland, K., Blower, P. J., and Mullen, G. E. (2012) $[Re(CO)_3]^+$ labelling of a novel cysteine/hexahistidine tag: insights into binding mode by liquid chromatography-mass spectrometry, *J Inorg Biochem 114*, 24-27.
18. Badar, A. (2012) Investigating site specific binding of $[^{99m}Tc(CO)_3]^+$ to the Hexahistidine Tag. (*Unpublished*), King's College London.
19. Emberson, L. M., Trivett, A. J., Blower, P. J., and Nicholls, P. J. (2005) Expression of an anti-CD33 single-chain antibody by Pichia pastoris, *J Immunol Methods 305*, 135-151.
20. Deyev, S. M., Waibel, R., Lebedenko, E. N., Schubiger, A. P., and Pluckthun, A. (2003) Design of multivalent complexes using the barnase*barstar module, *Nat Biotechnol 21*, 1486-1492.
21. Bidlingmaier, S., He, J., Wang, Y., An, F., Feng, J., Barbone, D., Gao, D., Franc, B., Broaddus, V. C., and Liu, B. (2009) Identification of MCAM/CD146 as the target antigen of a human monoclonal antibody that recognizes both epithelioid and sarcomatoid types of mesothelioma, *Cancer Res 69*, 1570-1577.

22. Tolmachev, V., Hofstrom, C., Malmberg, J., Ahlgren, S., Hosseinimehr, S. J., Sandstrom, M., Abrahmsen, L., Orlova, A., and Graslund, T. (2010) HEHEHE-tagged affibody molecule may be purified by IMAC, is conveniently labeled with $[^{99m}Tc(CO)_3]^+$, and shows improved biodistribution with reduced hepatic radioactivity accumulation, *Bioconjug Chem 21*, 2013-2022.
23. Virna Cortez-Retamozo, T. L., Vicky Caveliers, Lea Olive Tchoute Gainkam, Sophie Hernot, Ann Packeu, Filip De Vos, Chris Vanhove, Serge Muyldermans, Patrick De Baetselier, Hilde Revets. (2008) 99mTc-Labeled Nanobodies: A New Type of Targeted Probes for Imaging Antigen Expression, *Current Radiopharmaceuticals 1*, 37-41.
24. Shah, S. Q., Khan, A. U., and Khan, M. R. (2012) (99m)Tc(CO)(3)-Ibritumomab tiuxetan; a novel radioimmunoimaging (RII) agent of B cell non-Hodgkin's lymphoma (NHL), *Biol Chem 393*, 71-75.
25. Berndorff, D., Borkowski, S., Moosmayer, D., Viti, F., Muller-Tiemann, B., Sieger, S., Friebe, M., Hilger, C. S., Zardi, L., Neri, D., and Dinkelborg, L. M. (2006) Imaging of tumor angiogenesis using 99mTc-labeled human recombinant anti-ED-B fibronectin antibody fragments, *J Nucl Med 47*, 1707-1716.
26. Tait, J. F., Smith, C., and Gibson, D. F. (2002) Development of annexin V mutants suitable for labeling with Tc(i)-carbonyl complex, *Bioconjug Chem 13*, 1119-1123.
27. Mees, G., Dierckx, R., Mertens, K., Vermeire, S., Van Steenkiste, M., Reutelingsperger, C., D'Asseler, Y., Peremans, K., Van Damme, N., and Van de Wiele, C. (2012) 99mTc-labeled tricarbonyl his-CNA35 as an imaging agent for the detection of tumor vasculature, *J Nucl Med 53*, 464-471.
28. Teran, M. A., Martinez, E., Reyes, A. L., Paolino, A., Vital, M., Esperon, P., Pacheco, J. P., and Savio, E. (2011) Biological studies in animal models using $[^{99m}Tc(CO)_3]^+$ recombinant annexin V as diagnostic agent of apoptotic processes, *Nucl Med Biol 38*, 279-285.
29. Orlova, A., Nilsson, F. Y., Wikman, M., Widstrom, C., Stahl, S., Carlsson, J., and Tolmachev, V. (2006) Comparative in vivo evaluation of technetium and iodine labels on an anti-HER2 affibody for single-photon imaging of HER2 expression in tumors, *J Nucl Med 47*, 512-519.
30. Zahnd, C., Kawe, M., Stumpp, M. T., de Pasquale, C., Tamaskovic, R., Nagy-Davidescu, G., Dreier, B., Schibli, R., Binz, H. K., Waibel, R., and Pluckthun, A. (2010) Efficient tumor targeting with high-affinity designed ankyrin repeat proteins: effects of affinity and molecular size, *Cancer Res 70*, 1595-1605.

CHAPTER TWO

$[M(CO)_3]^+$ Labelling of His-Tagged Peptides with Adjacent Cys Residues

2 Influence of a Cys in Combination with the His-Tag on the Labelling Efficiency of Peptide Sequences with $[M(CO)_3]^+$

2.1 INTRODUCTION

2.1.1 Aims and Objectives

As previously mentioned in Chapter 1.2, it has been reported that a Cys residue in combination with the $(His)_6$-Tag is kinetically more favourable in terms of its labelling with $[M(CO)_3]^+$ than the $(His)_6$-Tag alone.(*1*) This observation was made based on data obtained from the labelling of a single recombinant protein with and without a Cys residue adjacent to the His-Tag. Consequently, the objectives within this chapter are to fully investigate the effect of a nearby Cys residue on the labelling efficiency of the His-Tag with the aim to improve and optimise the His-Tag labelling method and to provide answers to questions that should help gain an understanding behind the mechanism of coordination between $[M(CO)_3]^+$ and His-Tag peptide sequences. Specific questions addressed during this chapter are:

i) Does the Cys/His-Tag significantly improve the labelling efficiency incomparison to a His-Tag alone?

ii) How does Cys improve labelling? Is it involved in direct coordination to the $[M(CO)_3]^+$ complex or does it behave as a catalyst?

iii) Are multiple isomers formed when $[M(CO)_3]^+$ binds to the $(His)_6$-Tag and can these isomers be reduced?

iv) What is the preferred coordination between His-Tags and $[M(CO)_3]^+$? Is a 1-3 (HXHX) or 1-4 (HXXH) arrangement of His residues preferred?

To accomplish this, ten individual peptide sequences were synthesised that were variants on the C-terminal sequence of C2Ac, CKLAAALEHHHHHH. The Cys/$(His)_6$-Tag sequence at the C-terminal of C2Ac recombinant protein had shown superior labelling kinetics in comparison to an equivalent sequence without the Cys residues e.g. CKLAAALEHHHHHH

had a higher labelling efficiency than LAAALEHHHHHH. (see Chapter 1.2 for more detail) (*1*) The 10 peptides were synthesised in pairs with and without the CysLys motif. Each pair had a different arrangement and number of His residues in the sequence.

2.2 MATERIALS

Peptides were synthesised in the Biomolecular Analysis Laboratory, University of Kent using a PSSM-8 Multiple Peptide Synthesiser (Shimadzu). All analytical LC-ESMS was performed on a system comprising an Agilent 1200 Series Liquid Chromatography and an Agilent 6520 Accurate Mass Q-TOF mass spectrometer with a dual ESI ion source. Data analysis was carried out using the corresponding Agilent MassHunter Workstation Qualitative Analysis Software (Agilent Technologies, Cheshire, UK). A Vydac 218TP C-18 column (250mm x 2.1mm) was used (Agilent Technologies, Berkshire, UK). Preparative HPLC was carried out using a LKB Bromma 2152 LC Controller Liquid Chromatography system (Rollabiotech, UK). $^{99m}TcO_4^-$ was kindly provided by the Radiopharmacy Department at Guy's and St. Thomas' NHS Trust, London, eluted in saline from a Drytec generator (GE Healthcare, Amersham, UK). The Isolink kits were generously provided by Covidien, Petten, The Netherlands. Chemicals and reagents were obtained from Sigma-Aldrich unless otherwise specified and sterile water was used for buffer preparation. For the TLC analysis, the glass backed silica gel 60 TLC plates were obtained from Merck Millipore (Darmstadt, Germany) and the iTLC-SA paper purchased from Varian Medical Systems UK, Ltd (Crawley, UK). TLC analysis was achieved using a radio-TLC scanner (Lablogic, UK) or a γ-counter (LKB Wallac, 1282 COMPUGAMMA).

2.3 EXPERIMENTAL METHODS

2.3.1 Synthesis of Cys/His-Tag Peptides

The 10 Cys/His-Tag peptide analogues were synthesised on an automated peptide synthesiser using standard solid-state 9-fluorenylmethyloxycarbonyl (Fmoc) chemistry on a

20μmol scale.(Table 1-2) Resin, NovaSyn TGT resin 0.2mmol/g substitution, (Novabiochem) in dimethylformamide (DMF) was used . The Fmoc amino acids (NovaBioChem) were added in 8 fold excess. A combination of HBTU, HOBt +H_2O and DIEA were used as the coupling reagents in a 1:1, 1:1, and 1:2 stoichiometric ratio to the amino acids (amino acid-reagent) respectively. Fmoc deprotection occurred in a 30% piperidine solution in DMF. Peptide sequences were removed from the resin using 2ml of a cleavage cocktail containing TFA:H_2O:EDT:TIS in a 94:2.5:2.5:1 ratio. Incubation in the cleavage cocktail was carried out for 2 hours and precipitation of the peptide was then induced by addition of 3 x 20ml of ice cold diethyl ether. The peptide precipitate was dried using a lyophiliser. Peptide purification was carried out by preparative RP HPLC LC-ESMS and a Vydac 218TP C-18 column using a 15 ml/min flow rate and the following gradient: (time(min):%B) 0:10, 5:10, 10:25, 40:75, 45:100, 50:100, 51:10, 70:10, 71:10 where A was H_2O with 0.1%TFA and B was H_2O with 70%ACN and 0.09%TFA. The purified fraction was lyophilised to provide a white solid that was stored at 180^oC. The 10 peptides synthesised are listed below:

Peptide Sequence	**His-Tag Region**
LAAALEHHHHHH	Generic $(His)_6$-Tag – HHHHHH
CKLAAALEHHHHHH	Generic $(His)_6$-Tag – HHHHHH
LAAALEHAHAHA	HXHXHX
CKLAAALEHAHAHA	HXHXHX
LAAALEHHHH	Abbreviated His-Tag
CKLAAALEHHHH	Abbreviated His-Tag
LAAALEHAHA	HXHX
CKLAAALEHAHA	HXHX
LAAALEHAAH	HXXH
CKLAAALEHAAH	HXXH

Table 2-1. A summary of the 10 Cys/His-Tag peptide sequences synthesised. Each peptide was one of a pair with and without a CysLys dipeptide. For every pair a different number and arrangement of His residues was present.

2.3.2 Conversion of $^{99m}TcO_4^-$ to $[^{99m}Tc(CO)_3]^+$

Preparation of the $[^{99m}Tc(CO)_3]^+$ was achieved using the conventional IsoLink kit that contains 4.5mg sodium-boranocarbonate, 2.85 mg sodium tetraborate•$10H_2O$, 8.5 mg sodium tartrate•$2H_2O$ and 7.15 mg sodium carbonate. (The IsoLink™ kit provided is suitable for1ml of $^{99m}TcO_4^-$ and 3700MBq). 2200-2500MBq of $^{99m}TcO_4^-$ (^{99m}Tc pertechnetate) in 400µl of saline was added to the Isolink kit which was then heated to 97°C for 30min. The kit pH was adjusted with 1M HCl (approximately 160 µl) to pH 7.5 and quality control performed by thin layer chromatrography (TLC) to verify the conversion rate of $^{99m}TcO_4^-$ to $[^{99m}Tc(CO)_3]^+$. Glass backed silica gel 60 TLC plates (3 cm x 7.5 cm) were used with a mobile phase of 1% HCl in methanol for the quality control.

2.3.3 Radiolabelling Cys/(His)-Tag Peptides with $[^{99m}Tc(CO)_3]^+$

Development of a TLC Method for Percentage Labelling Analysis:
LAAALEHHHHHH was dissolved in 10% ACN in PBS at pH 7.4 to an approximate 1mg/ml concentration. 20µl (approximately 20MBq) $[^{99m}Tc(CO)_3]^+$ kit solution was added to 20µL of LAAALEHHHHHH peptide and the mixture incubated at 37°C for 60 mins. Aliquots of the labelling solution were taken and analysed by 16 different TLC methods in order to identify a method with a suitable separation between the $[^{99m}Tc(CO)_3$-peptide$]^+$ complex, unreacted $[^{99m}Tc(CO)_3]^+$ and unreduced $^{99m}TcO_4^-$. Table 2-2 contains details of all the TLC methods used.

TLC plate	Mobile Phase		TLC plate	Mobile Phase
ITLC-SG (coated in BSA)	H_2O:ethanol:ammonia (5:2:1)		Reverse Phase	70%ACN, 30% H_2O
Whatman Paper (coated in BSA)	H_2O:ethanol:ammonia (5:2:1)		Reverse Phase	50% ACN, 50% H_2O

Whatman Paper	H_2O:ethanol:ammonia (5:2:1)		Reverse Phase	75% TEAP (triethylammonium phosphate), 25% methanol
Whatman Paper	Saline		Normal Phase (Aluminium backed silica plates)	PBS
Whatman Paper	Acetone		Normal Phase (Aluminium backed silica plates)	Saline
ITLC-SA	Citrate Buffer		Normal Phase (Aluminium backed silica plates)	Acetone
ITLC-SA	H_2O/ACN/acetic acid (1:1:2)		Normal Phase (Aluminium backed silica plates)	H_2O
ITLC-SA	Saline		Normal Phase (Aluminium backed silica plates)	TFA:methanol:saline (2:68:30)

Table 2-2. A table containing details of the different TLC methods used to analyse the radiochemical yield of the Cys/His-Tag peptides with $[^{99m}Tc(CO)_3]^+$. Information in the table includes the type of TLC plate used and the mobile phase

Radiolabelling Efficiency Analysis of Peptides at Different Concentrations

All peptides were dissolved in 10% ACN in PBS buffer at pH 7.4 at a concentration of 250μM. A 5:1 dilution series was performed to give 4 different concentrations of each peptide: 250 μM, 50 μM, 10 μM and 2 μM. To 20 μL of each peptide, 20 μL (approximately 40 MBq) of $[^{99m}Tc(CO)_3]^+$ was added and the solutions incubated at 37°C for up to 90mins. Aliquots were taken at 5, 15, 30, 60 and 90 mins and percentage radiochemical yield measured using TLC.

iTLC-silicic acid paper (ITLC-SA, 0.75 x 9 cm) was used with the origin at 1cm from the bottom of the strip and solvent front at 8 cm. 2μl of the labelled peptide solutions were spotted at the origin and the strip allowed to air-dry before development in a mobile phase of 0.1 M citrate buffer at pH 5. The iTLC-SA strips were cut in half and the radioactivity in

each half recorded using a gamma counter as counts per minute (cpm). Through visualisation using the PhosphorImager and the TLC reader it had previously been determined that the $[^{99m}Tc(CO)_3]^+$ conjugated proteins had an Rf = 0 (remained at the baseline) whereas unbound $[^{99m}Tc(CO)_3]^+$ or unreduced $^{99m}TcO_4^-$ would move to the solvent front (Rf = 1). The percentage radiochemical yield was calculated by dividing the cpm recorded from the lower half of the strip by the total cpm for the whole strip

$$\text{Radiochemical yield (\%)} = \left(\frac{\text{Cpm from lower half of TLC strip}}{\text{Total cpm from TLC strip}} \right) \text{X } 100$$

2.3.4 Peptide Competition Experiment: CKLAAALEHHHHHH VS LAAALEHHHHHH for $[Re(CO)_3]^+$ coordination.

Rhenium tricarbonyl (fac-$[(H_2O)_3Re(CO)_3]Br$) was prepared and characterised as previously reported by Lazarova et al.(*2*) Briefly, $[Re(CO)_5]Br$ was refluxed in distilled H_2O for 24h. The crude mixture was filtered and the solution concentrated under vacuum to give fac-$[(H_2O)_3Re(CO)_3]Br$ as a light green powder in nearly quantitative yield. Solid fac--$[(H_2O)_3Re(CO)_3]Br$ was collected by filtration and air dried. The final product was characterised by ESI-MS and IR.

Equimolar amounts of the LAAALEHHHHHH and CKLAAALEHHHHHH peptides were prepared to approximately 0.5 mg/ml by dissolving a mixture of both peptides, in the same eppendorf, in 10%ACN in PBS buffer at pH 7.4. The peptide solution was incubated with 1 molar equivalence of $[Re(CO)_3(H_2O)_3]Br$ and heated at 37^{o}C for a total time of 30mins. The competition between the peptides for $[Re(CO)_3(H_2O)_3]Br$ coordination was monitored by LC-ESMS and a C-18 column using the following gradient: (time/%B) 0:5, 5:5, 10:50, 45:100, 50:100, 55:5, 60:5 where A was H_2O with 0.05% TFA and B wash H_2O with 70%ACN and 0.0425% TFA. A flow rate of 0.2 ml/min was used. LC-ESMS analysis on the peptide labelling solution was carried out before addition of $[Re(CO)_3(H_2O)_3]Br$ (at 0 mins) and 5mins and 30mins post incubation.

2.3.5 LC-ESMS Analysis of Trypsin Digested [C2AcH-Re(CO)$_3$]$^+$ Protein.

C2AcH and C2AcH-A, a C2AcH construct with an alkylated C-terminal Cys residue (where in this notation C2A is the protein designation, C refers to the presence of Cys and A means the Cys is alkylated) were previously engineered and labelled with [Re(CO)$_3$]$^+$ by Richard Tavare et al.(*1, 3*) Briefly, for the [Re(CO)$_3$]$^+$ labelling, C2AcH and C2AcH-A were incubated with 10-fold molar excess [Re(CO)$_3$(H$_2$O)$_3$]Br for 30 mins at 37^{o}C and purified with a PD-10 column (Sephadex G-25, GE Healthcare). Tryptic digest was performed through the incubation of the labelled and unlabelled proteins in a 0.5 mg/ml solution of modified sequence grade trypsin solution (Promega, Southampton, UK) for 3 hrs at RT.(*1, 3*)

Immediately after digestion the fragments were analysed by LC-ESMS using A Vydac 218TP C-18 column (250 mm x 2.1 mm) and the following gradient: (time (min):%B) 0:5, 5:5, 50:50, 75:100, 80:100, 81:5, 95:5 where buffer A was H$_2$O with 0.05% TFA and B was H$_2$O with 70% ACN and 0.045 %TFA. A flow rate of 0.2 ml/min was used. Analysis of the ESI-MS data was performed using Agilent MassHunter Workstation Qualitative Analysis Software.

2.3.6 LC-ESMS and MS-MS Analysis of [Re(CO)$_3$-Peptide]$^+$ Complex

[Re(CO)$_3$(H$_2$O)$_3$]$^+$ was prepared as previously mentioned in Chapter 2.3.4 following the protocol reported by Lazarova et al.(*2*) 100 μg of the Cys/His-Tag peptide analogues were dissolved in a 100μl solution of 10% ACN in PBS to give a 1 mg/ml concentration. A one molar equivalence or 3-fold molar excess of the [Re(CO)$_3$(H$_2$O)$_3$]$^+$ was added to the peptides and the labelling reaction heated at 37^{o}C for 1 hr. After cooling a 10μl sample was taken for LCMS analysis.

LCMS analysis was performed using a Vydac 218TP C-18 column with a 2.1mm internal diameter and a flow rate of 0.2 ml/min. Buffer A was H$_2$O and 0.05% TFA and buffer B was 70% ACN in H$_2$O with 0.045% TFA. The following gradient was used: (time(mins):%B) 0:5, 5:5, 10:50, 45:100, 50:100, 55:5, 60:5. A 2 μl sample of the peptides was injected. Positive mode ESI-MS was carried out with a fragmentor voltage of 175V and a wavelength of 214 nm for the UV chromatogram.

MS-MS was carried on the $[Re(CO)_3]^+$ conjugated CKLAAALEHHHHHH (P_1) and LAAALEHHHHHH (P_2) peptide sequences. Labelling of the P_1 and P_2 sequences for MS-MS was carried out with a one molar equivalent of $[Re(CO)_3]^+$. The method used was identical to that of the LCMS analysis. For $[Re(CO)_3\text{-}P_1]^+$, MS-MS was performed on the *m/z* = 560.5000 parent ion and for $[Re(CO)_3\text{-}P_2]^+$, the targeted parent ion had a *m/z* = 637.6000 where z = 3 for both parent ions. A CID voltage of 15V, 17V and 20V was used.

Data analysis for the LC and ESI-MS was carried out using the Agilent MassHunter Software.

2.4 RESULTS

2.4.1 Synthesis of Cys/His-Tag Peptide Analogues

The hexahistidine peptide sequence analogues were synthesised successfully using Fmoc chemistry on an automated peptide synthesiser. The peptides were synthesised with and without a CysLys motif as it mimicked the sequences at the C-terminal of the C2Ac protein. Electrospray mass spectroscopy (ESI-MS) analysis confirmed the correct molecular weight of each peptide as is shown in Table 2-3. The peptides were purified via HPLC purification and approximately 10 mg of the pure products were obtained in each case.

Peptide	Peptide Sequence	Expected MW (g/mol)	Obtained MW (g/mol)
1	LAAALEHHHHHH	1408.69	1408.72
2	CKLAAALEHHHHHH	1639.79	1639.31
3	LAAALEHAHAHA	1210.62	1210.58
4	CKLAAALEHAHAHA	1441.72	1441.72
5	LAAALEHHHH	1134.57	1134.59
6	CKLAAALEHHHH	1365.67	1365.42
7	LAAALEHAHA	1139.58	1139.38
8	CKLAAALEHAHA	1370.69	1370.66
9	LAAALEHAAH	1139.58	1139.60
10	CKLAAALEHAAH	1370.69	1370.71

Table 2-3. Summary of the ESI-MS data for the 10 synthesised Cys/His-Tag peptide sequences.

2.4.2 Conversion of $^{99m}TcO_4^-$ to $[^{99m}Tc(CO)_3]^+$

^{99m}Tc is obtained in the form of $^{99m}TcO_4^-$, and it is therefore necessary to perform a reduction using the standard Isolink kit to produce $[^{99m}Tc(CO)_3]^+$. The reverse phase silica TLC method with a 1% HCl in methanol mobile phase successfully separates the components of the reduction reaction and is a suitable quality control to monitor the rate of conversion. On the TLC plate, $^{99m}TcO_4^-$ migrates to the solvent front and has an Rf of 0.9, whilst ^{99m}Tc colloids remain at the baseline with an Rf of 0 and $[^{99m}Tc(CO)_3]^+$ appears as a broad peak with an Rf between 0.2 and 0.8 (Figure 2-1). The area under the peak provides the abundance of each complex present within the sample. For all the radiolabelling experiments, $[^{99m}Tc(CO)_3(H_2O)_3]^+$ was successfully produced with at least a > 95% rate of conversion from $^{99m}TcO_4^-$. No further purification was required before use of the complex in the radiolabelling of the Cys/His-Tag peptides.

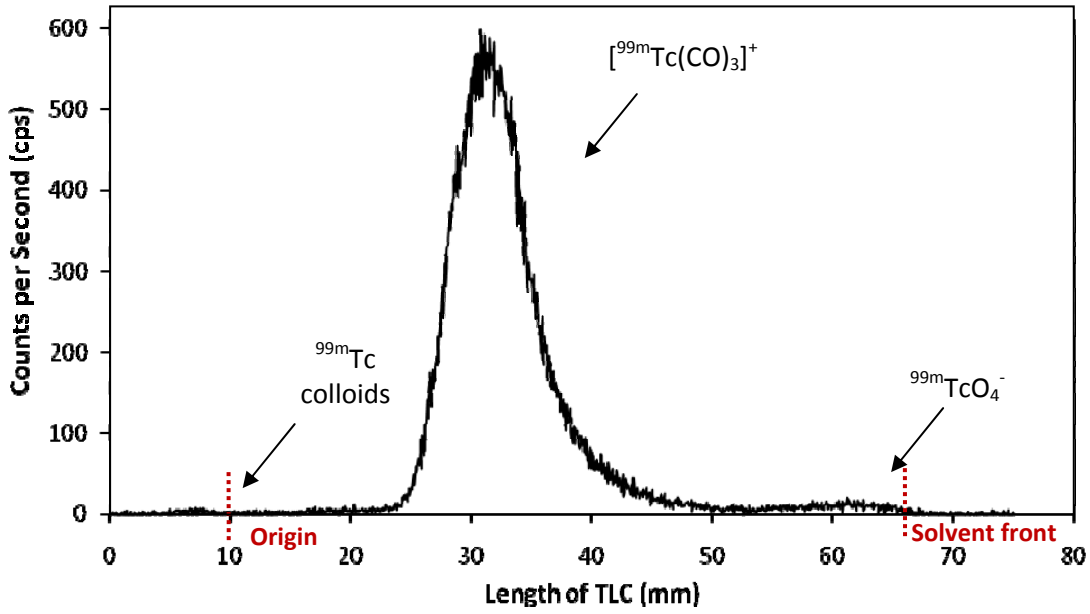

Figure 2-1. TLC quality control of $^{99m}TcO_4^-$ reduction to $[^{99m}Tc(CO)_3]^+$ for use in the radiolabelling of the scFv fragments: **Rf = 0.9** for $^{99m}TcO_4^-$, **Rf = 0** for ^{99m}Tc colloids and **Rf = 0.2-0.8** for $[^{99m}Tc(CO)_3(H_2O)_3]^+$.

2.4.3 TLC Method for Analysing Labelling Efficiency of Cys/His-Tag Peptide Analogues

The development of a radio-TLC method suitable for analysing the labelling efficiencies of the Cys/His-Tag peptides for $[^{99m}Tc(CO)_3]^+$ coordination was the initial priority. Sixteen different TLC systems were chosen for evaluation based on the most popular methods currently used in the literature. For each method TLCs of both the $[^{99m}Tc(CO)_3]^+$-peptide labelling solution and the stock $[^{99m}Tc(CO)_3(H_2O)_3]^+$ solution were performed in order to compare the retention times of the unbound and bound $[^{99m}Tc(CO)_3]^+$. An efficient TLC system should have excellent separation between the individual components within the labelling solution; a peak at the baseline (Rf = 0-0.1) and a peak at the solvent front (Rf = 0.9-1). Table 2-4 summarises the results obtained during the development process of the TLC method.

TLC plate	Solvent system	Rf $Tc(CO)_3$	Rf Labelled Peptide	Success
ITLC-SG (coated in BSA)	H_2O:ethanol:ammonia (5:2:1)	1	1	✗
Whatman Paper (coated in BSA)	H_2O:ethanol:ammonia (5:2:1)	1	1	✗
Whatman Paper	H_2O:ethanol:ammonia (5:2:1)	0 = 6% 1 = 94% (streaking)	1	✗
Whatman Paper	Saline	0 = 17% 1 = 83% (streaking)	0	✗
Whatman Paper	Acetone	0	0	✗
ITLC-SA	Citrate Buffer	0 = 7% 1 = 93%	0 = 95% 1 = 5%	✓
ITLC-SA	H_2O/ACN/acetic acid (1:1:2)	1	0 = 91% 1 = 9%	✓

ITLC-SA	Saline	0 = 27% 1 = 73% (streaking)	0	✗
Reverse Phase (	70%ACN, 30% H_2O	0 = 6% 1 = 94% (streaking)	Streaking throughout plate	✗
Reverse Phase	50% ACN, 50% H_2O	<u>4 peaks</u> near 0 = 63% near 1 = 37% (streaking)		✗
Reverse Phase	75% TEAP (triethylaminephosphate), 25% methanol	0 = majority (streaking)	0	✗
Normal Phase (Aluminium backed silica plates)	PBS	0 = 88% 1 = 12%	0	✗
Normal Phase (Aluminium backed silica plates)	Saline	0 = 88% 1 = 12%	0	✗
Normal Phase (Aluminium backed silica plates)	Acetone	<u>3 peaks</u> 0 = majority	0	✗
Normal Phase (Aluminium backed silica plates)	H_2O	Silica disintegrates from the glass	Silica disintegrates from the glass	✗
Normal Phase (Aluminium backed silica plates)	TFA:methanol:saline (2:68:30)	0.5 = 80% 0.9 = 20%	0.5 = 94% 0.9 = 6%	✗

Table 2-4. A summary of the results obtained from the TLC analysis of the LAAALEHHHHHH-$[^{99m}Tc(CO)_3]^+$ labelling solution using sixteen different methods. In the table information is shown with regards to the TLC plate used, mobile phase, Rf values of the $[^{99m}Tc(CO)_3]^+$ and

[LAAALEHHHHHH-^{99m}Tc(CO)$_3$]$^+$ peaks and the suitability of the method for calculating the radiochemical yield of the Cys/His-Tag peptides. The percentages represent the ratio of the compound that is bound at each Rf point in situations where multiple peaks can be seen on the TLC for a single compound. **X** = a non-successful separation method, ✓ = a successful separation method

Results revealed that ITLC-SA paper with either a 0.1 M citrate buffer at pH 5.1 or H_2O:ACN:glacical acetic acid (1:1:2) as the mobile phase provided the best TLC method for the labelling efficiency analysis of the Cys/His-Tag peptides. It was decided that 0.1 M citrate buffer at pH 5.1 would be used. This system provided a definitive separation between the unbound [^{99m}Tc(CO)$_3$]$^+$, unreduced ^{99m}TcO$_4^-$ (both migrating towards the solvent front with an Rf = 1), and the [^{99m}Tc(CO)$_3$]$^+$ labelled peptide, which remained at the baseline with an Rf = 0. The large separation between the peaks is advantageous and enables analysis of the iTLC-SA strips by gamma-counter. The strips can be cut in the middle without compromising the radioactive peaks. Images of the iTLC-SA for the individual components of the labelling solution can be seen in Figure 2-2.

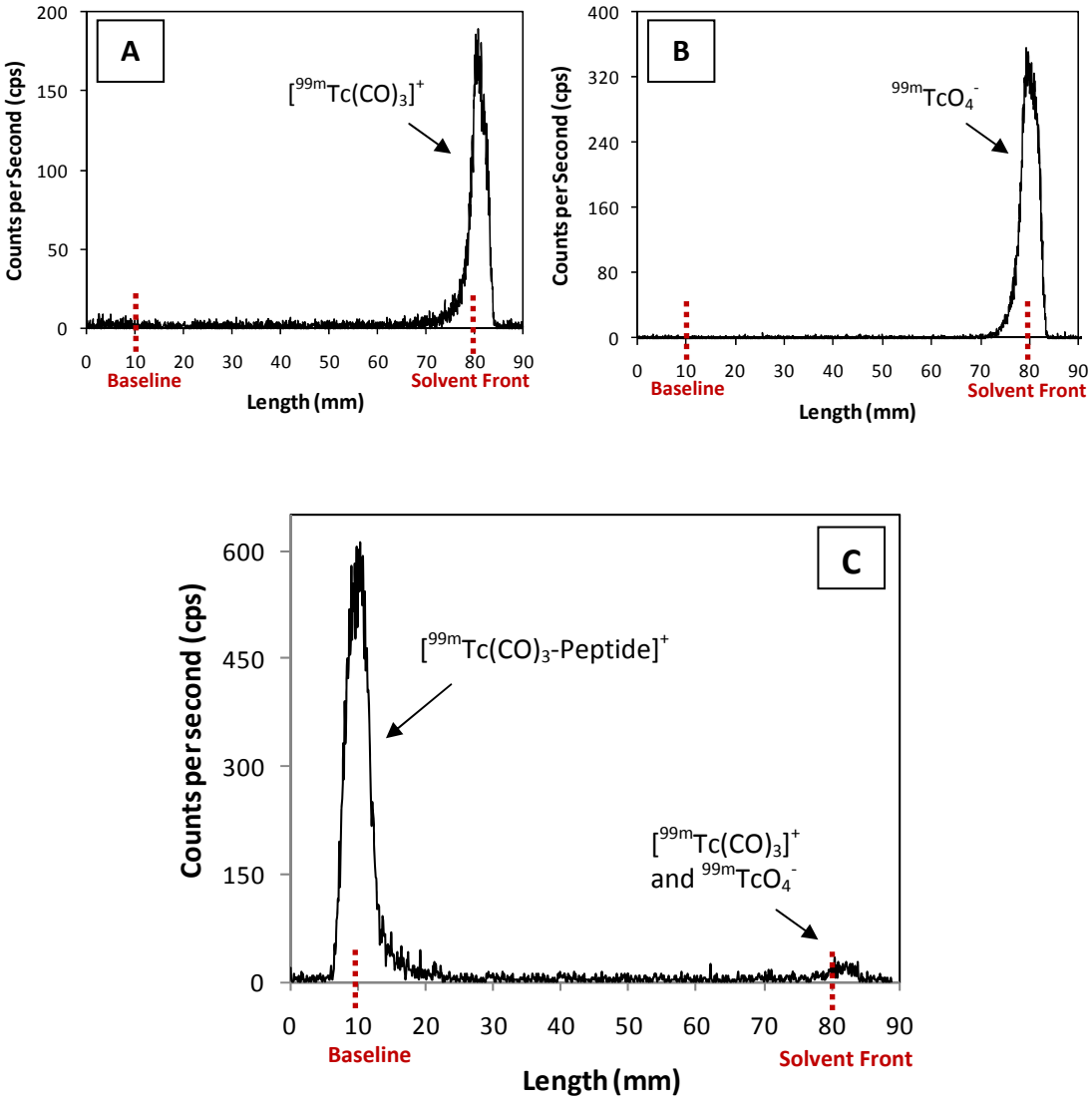

Figure 2-2. iTLC-SA images of the individual components present in the labelling reaction. The strips (7.5 x 90 mm) had an origin at 10 mm and a solvent front at 80 mm. A mobile phase of citrate buffer at pH 5.5 was used. **A)** Unbound $[^{99m}Tc(CO)_3]^+$ with an Rf = 1, **B)** Unreduced $^{99m}TcO_4^-$ with an Rf = 1 and **C)** Cys/His-Tag labelling reaction with $[^{99m}Tc(CO)_3]^+$. The $[^{99m}Tc(CO)_3$-peptide$]^+$ conjugate appears at the baseline with an Rf = 0 whereas the $[^{99m}Tc(CO)_3]^+$ and $^{99m}TcO_4^-$ migrate to the solvent front.

One disadvantage associated with the iTLC-SA and citrate buffer method is its inability to separate the ^{99m}Tc colloids from the $[^{99m}Tc(CO)_3]^+$ labelled Cys/His-Tag peptides. Therefore information regarding the abundance of ^{99m}Tc colloids in the labelling solution must be extracted from the TLC performed as a quality control for the $[^{99m}Tc(CO)_3]^+$ production or from an iTLC-SA obtained of the labelling solution without the presence of the Cys/His-Tag peptides. For the $[^{99m}Tc(CO_3]^+$ labelling of the Cys-His-Tag peptide experiments, the quantity

of ^{99m}Tc-colloids present was negligible. Another drawback is the incapability to separate the $[^{99m}Tc(CO)_3]^+$ and unreduced $^{99m}TcO_4^-$ in the iTLC-SA; both migrate to the solvent front. The percentage of unreduced $^{99m}TcO_4^-$ in the labelling solution must be calculated from the quality control TLC of the $[^{99m}Tc(CO)_3]^+$ production. In a situation where there is more than 10% $^{99m}TcO_4^-$ present, further purification would be carried out prior to labelling.

2.4.4 Does the Cys/His-Tag significantly improve the labelling kinetics and efficiency in comparison to a His-Tag alone?

The $[^{99m}Tc(CO)_3]^+$ labelling of the 10 Cys/His-Tag peptide analogues was successfully carried out at 4 different concentrations and the radiochemical yield of the peptides monitored over time by the iTLC-SA method. Cys/His-Tag peptide sequence analogues were synthesised with and without CysLys residues and therefore comparisons between the relative labelling efficiencies provided information with respect to the influence of the CysLys dipeptide Radiochemical yields were plotted against protein concentration (log[protein]) for all time points (5, 15, 60, 90 and 120 mins) and the results are displayed in Figure 2-3.

The data reveal that at all time points, a His-Tag in combination with a CysLys residue demonstrates superior labelling efficiency in comparison to sequences containing a His-Tag alone (Figure 2-3, A-E). This trend is independent of the number of His residues or arrangement of His residues present in the sequences. With the exception of the CKLAAALEHAHAHA sequence, there is a distinct separation between the labelling efficiency curves of the Cys/His-Tag sequences and the non-Cys containing sequences at all time points. This emphasises the kinetically preferential coordination of $[^{99m}Tc(CO)_3]^+$ to sequences with a Cys/His-Tag combination.

For identical sequences with and without the CysLys residue, the $[^{99m}Tc(CO)_3]^+$ labelling efficiency of the CysLys-containing His-Tag sequence is always significantly higher than that of the standard His-Tag sequence at all concentrations and time points e.g. CKLAAALEHHHH at a 250 μM concentration can achieve a 95% radiochemical yield after 15 mins incubation with $[^{99m}Tc(CO)_3]^+$, however the non-CysLys equivalent, LAAALEHHHH, requires at least

60mins incubation before reaching a 95% radiochemical yield (Figure 2-3, B and D for the 15 min and 60 min graphs respectively).

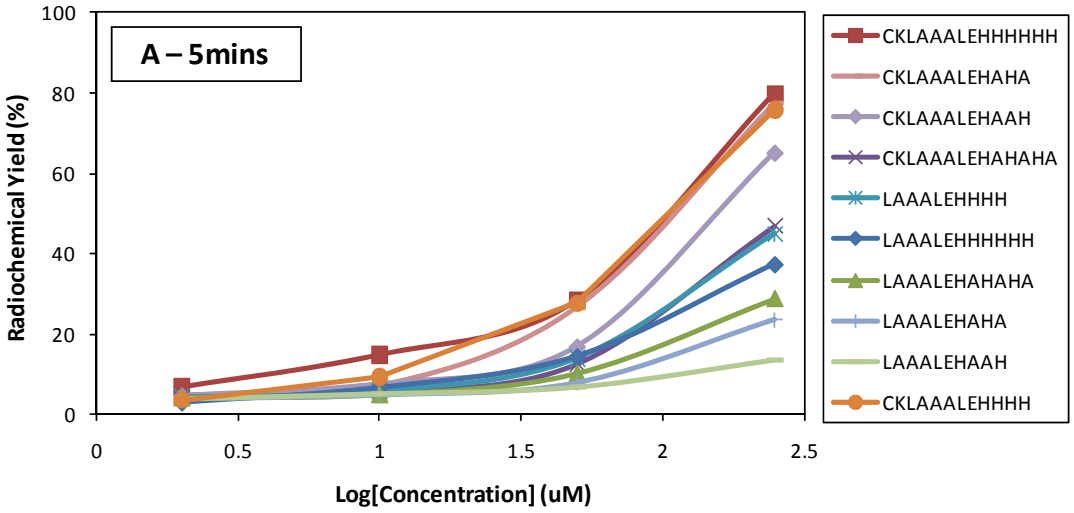

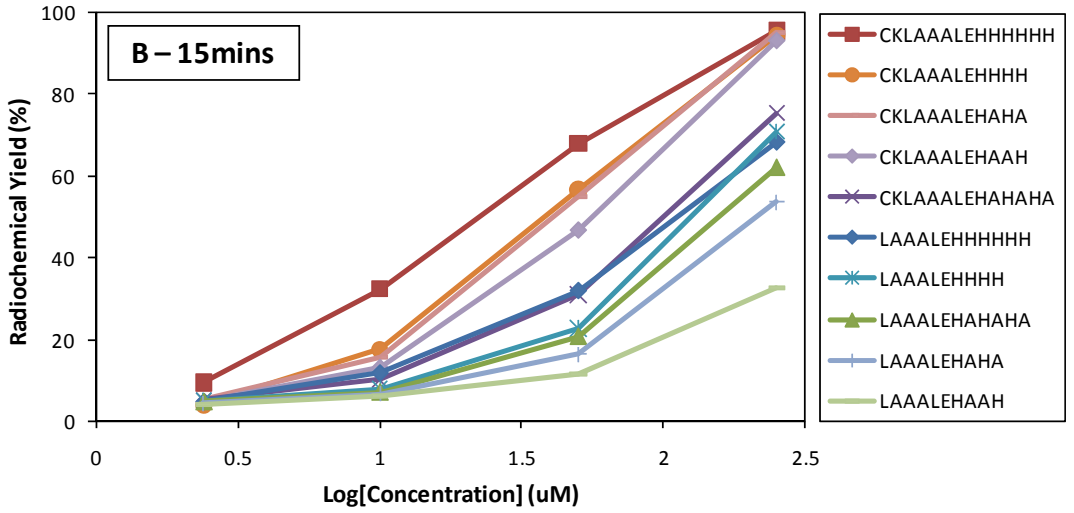

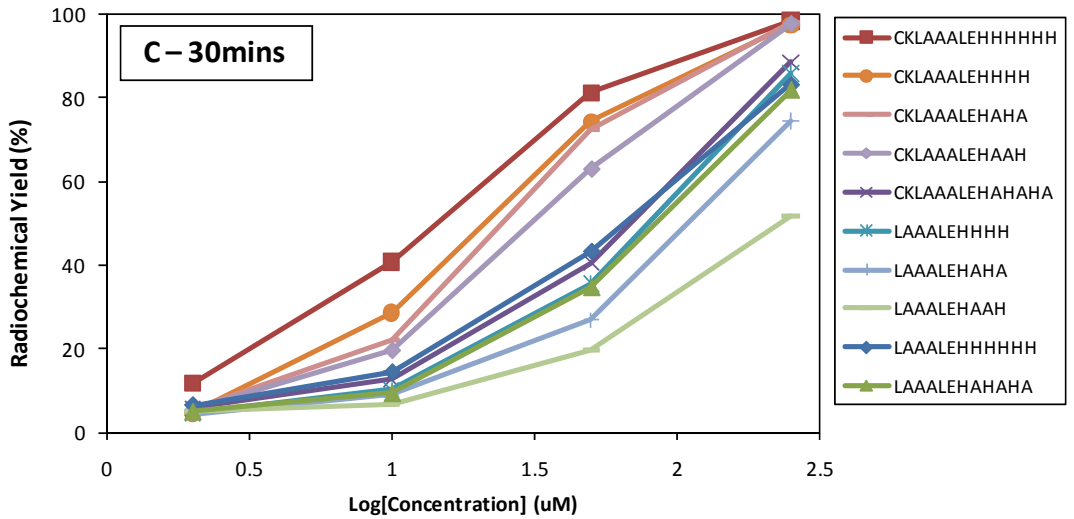

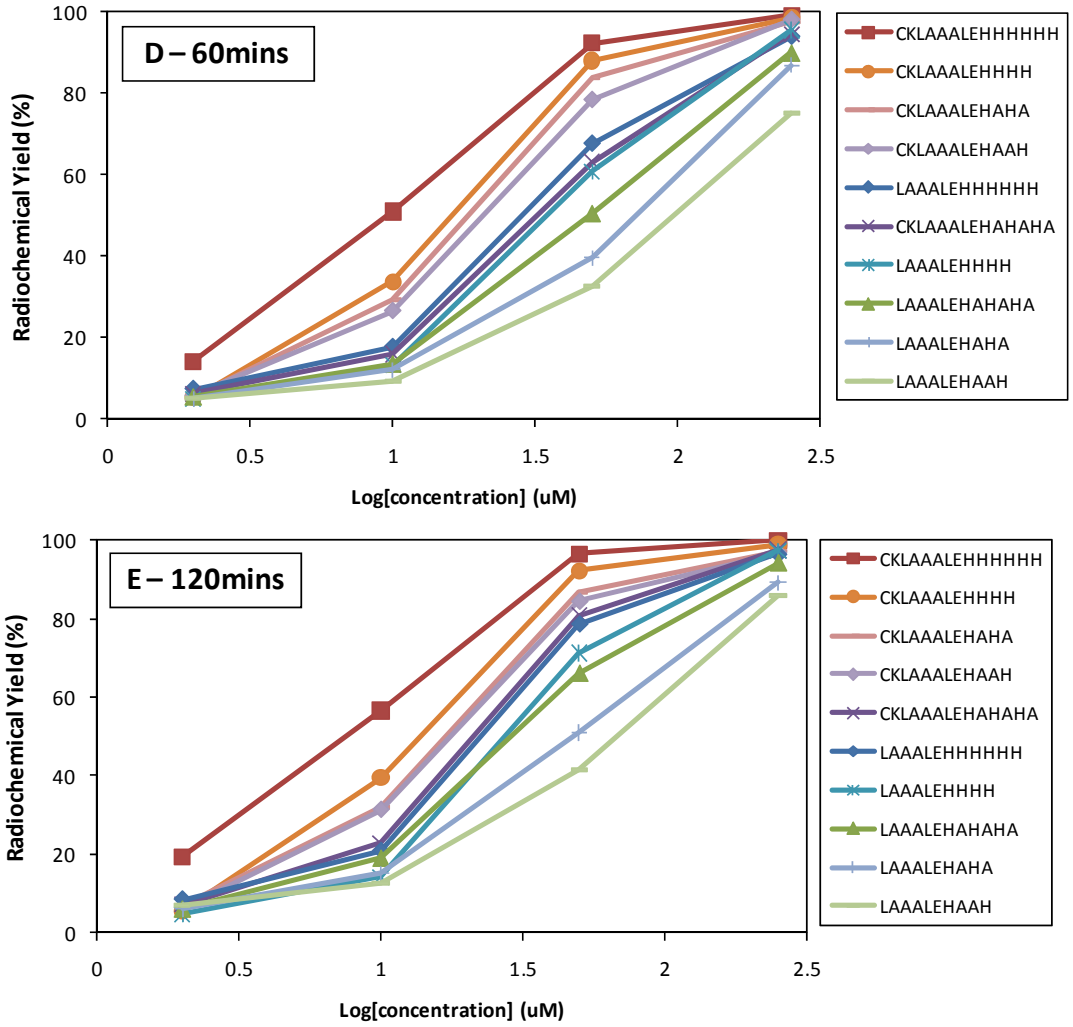

Figure 2-3. Radiolabelling efficiencies of the Cys/His-Tag peptide analogues at 4 different concentrations: 250 μM, 50 μM, 2 μM and 0.4 μM. The radiochemical yields of the peptides were analysed after different incubation times with $[^{99m}Tc(CO)_3]^+$. **A)** 5 mins, **B)** 15 mins, **C)** 30 mins, **D)** 60 mins and **E)** 120 mins. The radiochemical yield data plotted on the graphs was obtained as an average of 3 experiments (n=3) and the maximum percentage error observed is ± 4.4%.

Another trend observed from the radiolabelling efficiency data is the correlation between radiochemical yield and the number of His residues within the sequence. A decrease in His residues coincides with a decrease in radiochemical yield (Figure 2-3). The $(His)_6$-Tag, HHHHHH, has been established as the preferred His combination within a labelling sequence. Interruption of the His residues with other amino acids is not favourable especially for the CKLAAALEHAHAHA which demonstrated an unexpectedly lower radiochemical yield than all other Cys containing sequences. A decrease in labelling efficiency for sequences with alternate His residues, separated by Ala, could be attributed

to the consequent decrease in the number of His residues e.g. a reduction in His residues from 6, HHHHHH, to 3, HAHAHA, when His is arranged in an alternate pattern. For both the CysLys and non-CysLys containing sequences, labelling efficiency was greater for His residues arranged in a 1,3 (alternate configuration, HAHA), in comparison to His residues arranged in a 1,4 (HAAH) configuration. This suggests that preferential coordination of $[^{99m}Tc(CO)_3]^+$ is for a 1, 3 rather than 1, 4 arrangement of His residues. A general trend was observed in which the preferred His-Tag was as follows: $(His)_6$-Tag (HHHHHH)>HHHH>HAHAHA>HAHA>HAAH. For the Cys containing HAHAHA sequence, labelling to $[^{99m}Tc(CO)_3]^+$ was surprisingly unfavourable when compared to the CysLys containing HAHA and HAAH sequences.

CKLAAALEHHHHHH is the sequence that evidently shows the most favourable coordination to $[^{99m}Tc(CO)_3]^+$ as it constantly achieves the highest radiochemical yield at all concentrations and time points. At a 250 μM concentration it demonstrates a 95% radiochemical yield after 15 mins incubation whereas the non CysLys containing equivalent, LAAALEHHHHHH takes an additional 75 min to achieve a comparable radiochemical yield (Figure 2-3, B and E for the 15 min and 120 min graphs respectively). The CKLAAALEHHHHHH combines both the CysLys residue and a $(His)_6$-Tag which, in comparison to the other sequences analysed, was the optimal sequence for radiolabelling with $[^{99m}Tc(CO)_3]^+$. The results obtained in this study confirmed that CysLys combination has a positive influence on the labelling efficiency of a His-Tagged sequence with $[^{99m}Tc(CO)_3]^+$.

To further support these data an LC-ESMS competition experiment was performed between the two $(His)_6$-Tagged sequences, CKLAAALEHHHHHH and LAAALEHHHHHH.(*3*) This was performed using non-radioactive $[Re(CO)_3]^+$ as the labelling complex. $[Re(CO)_3]^+$ is analogous to $[^{99m}Tc(CO)_3]^+$ and has, on many occasions, been utilised as a method of labelling His residues for structural analysis and modelling.(*4-5*) The ESI-MS spectrum of the synthesised $[Re(CO)_3(H_2O)_3]^+$ is shown in Figure 2-4 in which the three peaks at *m/z* = 311.9677, 352.9936 and 394.0192 correspond to $[Re(CO)_3 + CH_3CN]^+$, $[Re(CO)_3 + 2(CH_3CN)]^+$ and $[Re(CO)_3 + 3(CH_3CN)]^+$.

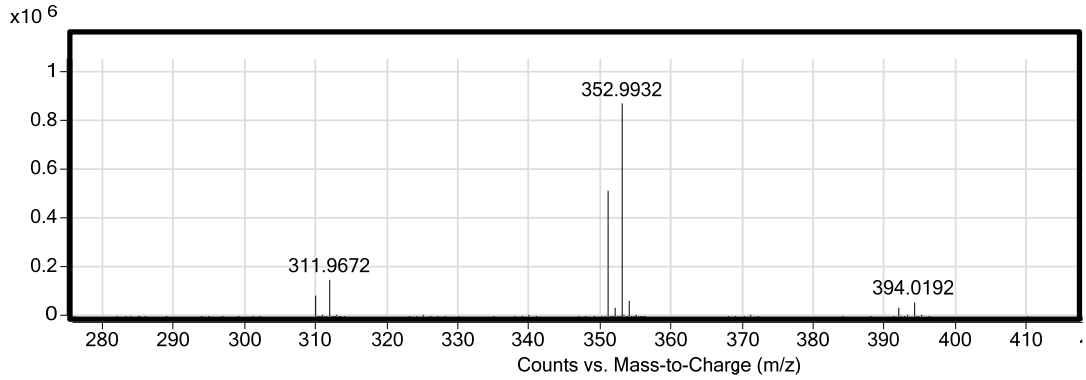

Figure 2-4. $[Re(CO)_3(H_2O)_3]^+$ ESI-MS positive mode spectra. Peaks at *m/z* = 311.9677, 352.9936 and 394.0192 correspond to $[Re(CO)_3 + CH_3CN]^+$, $[Re(CO)_3 + 2(CH_3CN)]^+$ and $[Re(CO)_3 + 3(CH_3CN)]^+$.

In the competition experiment a mixture of 0.5 mol equivalents of both peptides were incubated with 1 molar equivalent of $[Re(CO)_3]^+$.(*3*) LC-ESMS analysis was performed before the addition of $[Re(CO)_3]^+$, and at 0 , 5 and 30 mins after incubation with $[Re(CO)_3]^+$. The UV chromatogram results are revealed in Figure 2-5 and the superiority of the Cys/$(His)_6$-Tag sequence is clearly evident. In the UV chromatogram obtained at 0 mins (Figure 2-5, A), the peak representing the peptides was identified by ESI-MS; Peak 1 corresponded to LAAALEHHHHHH, *m/z* = 705.345 for $[P_1 + 2H]^{2+}$, and Peak 2 corresponded to CKLAAALEHHHHHH, *m/z* = 820.892 ($[P_2 + 2H]^{2+}$ where P_1 and P_2 represent LAAALEHHHHHH and CKLAAALEHHHHHH respectively (Figure 2-6, A and B, ESI-MS of P_1 and P_2 respectively). UV chromatograms at 5 and 30mins demonstrated that $[Re(CO)_3]^+$ complexes were formed at a much faster rate with CKLAAALEHHHHHH (Figure 2-5, dotted line) than with LAAALEHHHHHH (Figure 2-5, straight line). A significant reduction in the abundance of the peak representing unbound CKLAAALEHHHHHH in comparison to LAAALEHHHHHH was observed. After 30mins incubation time 92% of CKLAAALEHHHHHH (Figure 2-5, C, dotted line) was coordinated by $[Re(CO)_3]^+$ whereas in contrast, only 9% of LAAALEHHHHHH was coordinated. Coordination of $[Re(CO)_3]^+$ to CKLAAALEHHHHHH coincided with the emergence of multiple new peaks (Figure 2-5, B and C). According to ESI-MS, these peaks appear to all have the same mass where *m/z* = 637.57 representing $[P_2\text{-}Re(CO)_3 + 2H]^{3+}$ (Figure 2-6, C). This competition experiment provided direct evidence that the presence of CysLys residue combination dramatically improves the labelling of His-Tagged sequences with $[M(CO)_3]^+$ complexes.

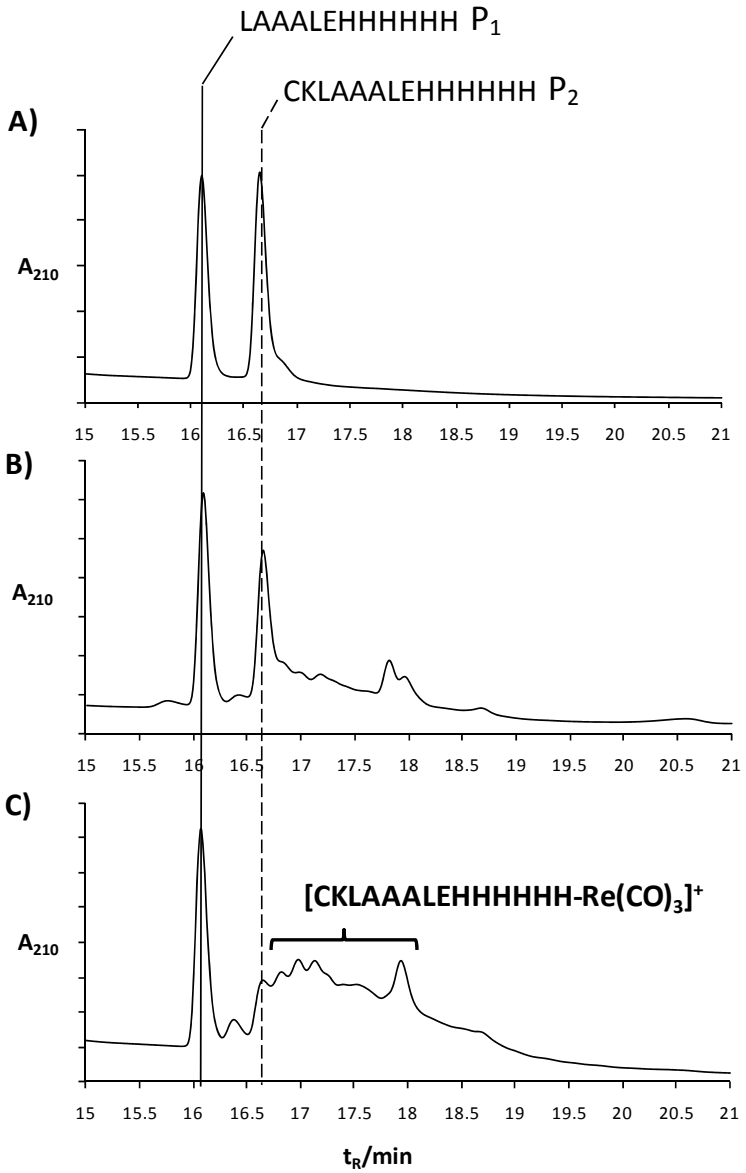

Figure 2-5. A competition study between the labelling efficiency of CKLAAALEHHHHHH and LAAALEHHHHHH for $[Re(CO)_3]^+$. LC-ESMS was used to monitor experiment. **A)** UV chromatogram of equimolar mixtures of P_1 and P_2, **B)** UV chromatogram after 5 min incubation time with 1 molar equivalent of $[Re(CO)_3]^+$, **C)** UV chromatogram 30 mins post incubation with 1 molar equivalent of $[Re(CO)_3]^+$.(*3*)

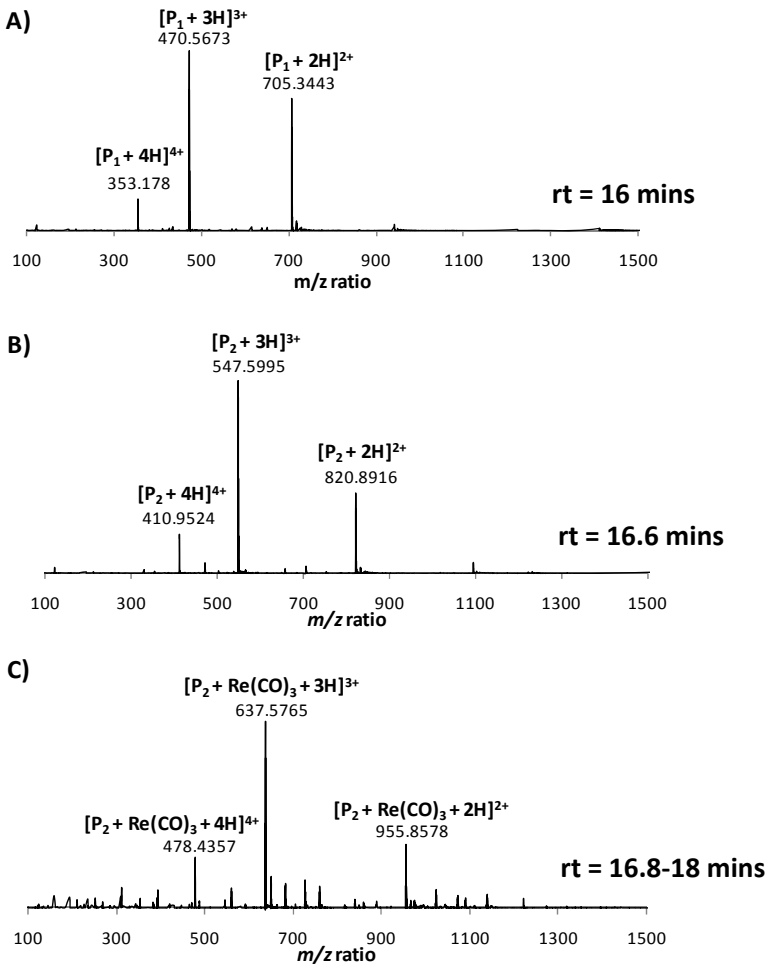

Figure 2-6. ESI-MS spectra obtained for individual components of the competition experiment: **A)** ESI-MS spectra of P_1**, B)** ESI-MS spectra of P_2 and **C)** ESI-MS spectra of $[P_2\text{-}Re(CO)_3]^+$ conjugate.(*3*)

2.4.5 How does CysLys improve labelling; is it involved in direct coordination to the $[M(CO)_3]^+$ complex or does it behave as a catalyst?

2.4.5A LCMS Analysis of Trypsin Digested $[C2AcH\text{-}Re(CO)_3]^+$ Protein

In Chapter 1.2, it was reported that a trypsin digest had been performed on the $[C2AcH\text{-}Re(CO)_3]^+$ conjugate in order to determine the location of binding of $[Re(CO)_3]^+$.(*3*) The trypsin digested fragments were subjected to LC-ESMS analysis. In the UV chromatogram post-trypsin digest of $[C2AcH\text{-}Re(CO)_3]^+$, several new peaks appeared with a rt between 32-35 min (Figure 2-7, A). A characteristic $^{185/187}$Re isotope pattern was associated with the ESI-

MS spectra obtained from these peaks. It was possible to identify the presence of three different fragments, all of which were conjugated to $[Re(CO)_3]^+$: $[LAAALEHHHHHH\text{-}Re(CO)_3]^+$ (*m/z* = 840.307 $[P_1 + Re(CO)_3 + H]^{2+}$), $[CK + LAAALEHHHHHH\text{-}Re(CO)_3]^+$ (*m/z* = 965.360 $[CK + P_1 + Re(CO)_3 + H]^{2+}$) and $[CKLAAALEHHHHHH\text{-}Re(CO)_3]^+$ (*m/z* = 956.724 $[P_2 + Re(CO)_3 + H]^{2+}$ where P_1 and P_2 represent CKLAAALEHHHHHH and LAAALEHHHHHH respectively (Figure 2-7, B and C). These data confirmed that the binding site of the $[Re(CO)_3]^+$ was located in the $(His)_6$-Tag region. In addition, the LC-ESMS revealed that for two of the fragments, as explained below, the CysLys residues remained coordinated to the Re metal centre.

Trypsin digest facilitates the digestion of a protein through cleavage at the carboxyl side of Lys and Arg amino acids. For the $[C2AcH\text{-}Re(CO)_3]^+$ protein cleavage would be expected at the Lys residues on either side of the Cys in the C-terminal sequence **K**C**K**LAAALEHHHHHH. The isomeric peaks at *m/z* = 965.360 corresponds to the $[CK + P_1\text{-}Re(CO)_3]^+$ fragment which is equivalent to the $[P_2\text{-}Re(CO)_3]^+$ C-terminal fragment with an additional 18 mass units.(Figure 2-7, C) These 18 mass units represent the addition of H_2O due to the trypsin-catalysed hydrolysis of the CK peptide bond. It appears that the hydrolysed CK dipeptide remains coordinated to the Re metal centre despite no longer being covalently linked to the $(His)_6$-Tag sequence. This supports the hypothesis that CysLys, in addition to the $(His)_6$-Tag, is directly involved in the coordination sphere to $[Re(CO)_3]^+$, most likely via a direct Re-S bond.

Another mass identified by LC-ESMS of the trypsin digested $[C2AcH\text{-}Re(CO)_3]^+$ appeared at *m/z* = 956.724 corresponding to the $[P_2\text{-}Re(CO)_3]^+$ fragment. The appearance of the $[P_2\text{-}Re(CO)_3]^+$ fragment indicates that despite expected cleavage at the Lys on the N-terminal side of the Cys being observed, the expected cleavage at the Lys on the C-terminal side of the Cys was not observed. This reduced rate of cleavage could be accounted for by the coordination of the Cys residue to $[Re(CO)_3]^+$ which could sterically hinder and change the conformation of the polypeptide sequence restricting access to trypsin. The P_2 fragment was absent from the ESI-MS data of the trypsin-digested unlabelled C2AcH protein confirming that without the $[Re(CO)_3]^+$ complex, efficient cleavage is obtained at the Lys residue on both sides of the Cys.

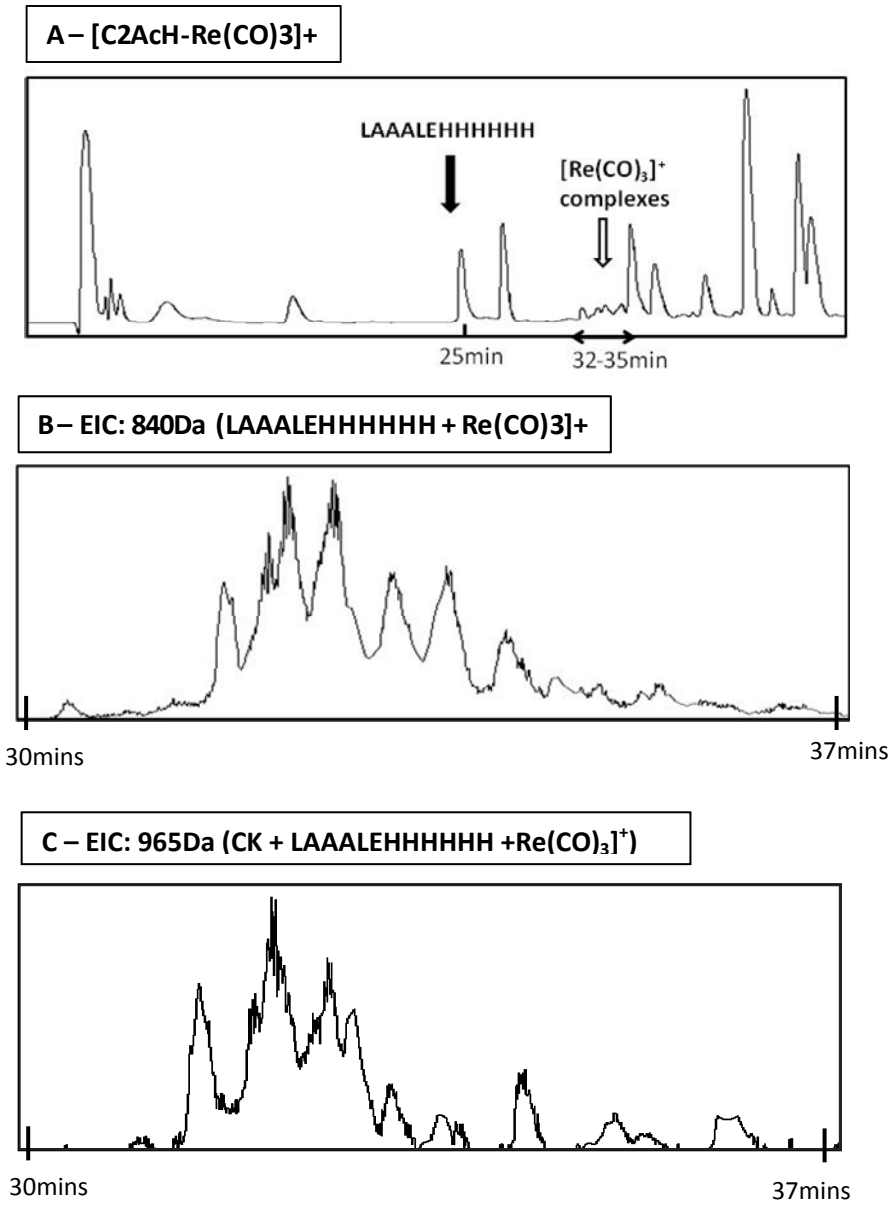

Figure 2-7. LC-MS data for $[C2AcH\text{-}Re(CO)_3]^+$ post trypsin digest. **A)** UV chromatogram of $C2AcH\text{-}Re(CO)_3]^+$ where the open arrow indicates the formation of multiple new peaks due to the P_1 and P_2 sequences, in the protein, bound to $[Re(CO)_3]^+$. **B)** EIC of *m/z* = 840.307 which corresponds to $[P_1\text{-}Re(CO)_3]^+$. **C)** EIC of *m/z* = 965.360 which corresponds to [CK + LAAALEHHHHHH-$Re(CO)_3]^+$.(*3*)

LC-ESMS analysis was also performed on a $[Re(CO)_3]^+$ conjugated C2AcH protein in which the Cys residue had been blocked with iodoacetamide, $[C2AcH\text{-}A\text{-}Re(CO)_3]^+$. In the ESI-MS of this construct it was not possible to detect any fragments in which the C_AK dipeptide, the alkylated CK peptide, remained bound to $[Re(CO)_3]^+$. This provides confirmation that alkylation of the Cys thiol prevents binding to the Re centre and it is highly probable that the Cys thiol is involved in direct coordination to the $[Re(CO)_3]^+$ complex. In Table 2-5 is a

summary of the LC-ESMS data post tryptic digest of the $[C2AcH\text{-}Re(CO)_3]^+$ complex, unlabelled C2AcH and the $[C2AcH\text{-}A - Re(CO)_3]^+$ construct in which the Cys has been blocked with an alkyl functionality. Schematic diagrams are also presented in Figure 2-8, representing the newly proposed structures of $[Re(CO)_3]^+$ binding to Cys containing sequences. The structures are based on the MS data obtained post tryptic digest of the $[C2AcH\text{-}Re(CO)_3]^+$ protein.

Protein (M)	Expected (Da)	Found (Da)
LAAALEHHHHHH	705.351 $[P + 2H]^{2+}$	705.348
LAAALEHHHHHH-$^{187/185}$**Re(CO)$_3$**	840.317 $[P_1 + Re(CO)_3 + H]^{2+}$	840.307
CKLAAALEHHHHHH	820.903 $[P_2 + 2H]^{2+}$	Not Observed
C_aKLAAALEHHHHHH	848.909 $[P_{2(a)} + 2H]^{2+}$	Not Observed
CKLAAALEHHHHHH-$^{187/185}$**Re(CO)**	956.373 $[P_2 + Re(CO)_3 + H]^{2+}$	956.421
C_aKLAAALEHHHHHH-$^{187/185}$**Re(CO)$_3$**	983.378 $[P_{2(a)} + Re(CO)_3 + H]^{2+}$	Not Observed
CK + LAAALEHHHHHH-$^{187/185}$**Re(CO)$_3$**	965.378 $[NH_2\text{-}CK\text{-}COOH + P_1 + Re(CO)_3 + H]^{2+}$	965.360
C_aK + LAAALEHHHHHH-$^{187/185}$**Re(CO)**	993.385 $[NH_2\text{-}C_aK\text{-}COOH + P_1 + Re(CO)_3 + H]^{2+}$	Not Observed

Figure 2-5. A table summarising the expected and observed ESI-MS data post tryptic digest of $[C2AcH\text{-}Re(CO)_3]^+$ and $[C2AcH\text{-}A - Re(CO)_3]^+$. **$P_1$** = LAAALEHHHHHH, **$P_2$** = CKLAAALEHHHHHH, **$C_a$** = abbreviation for **$C_{acetamide}$** for the protein with the alkylated Cys residue.(*3*)

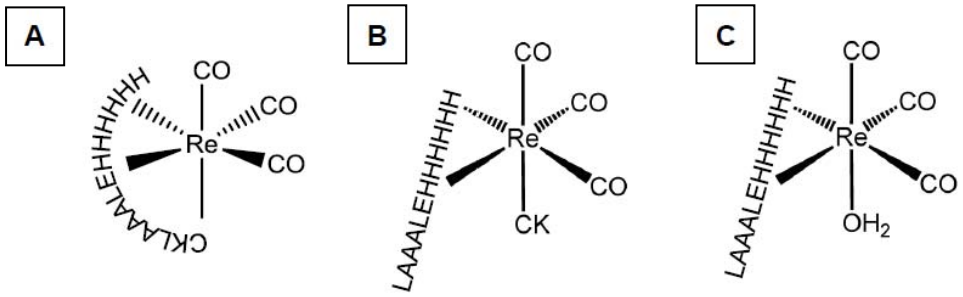

Figure 2-8. A schematic representation of the proposed structures of $[Re(CO)_3]^+$ binding to the $(His)_6$-Tag sequences post trypsin digest of $[C2AcH\text{-}Re(CO)_3]^+$ protein.(*3*) **A)** $[Re(CO)_3\text{-}CKLAAALEHHHHHH]^+$, **B)** $[Re(CO)_3\text{-}LAAALEHHHHHH + CK]^+$ and **C)** structure of $[Re(CO)_3]^+$ bound to a $(His)_6$-Tag as suggested (but unconfirmed experimentally) by Schibli et al.(*6*)

2.4.5B MS-MS analysis of the $[Re(CO)_3]^+$ Labelled LAAALEHHHHHH and CKLAAALEHHHHHH Sequences.

To further investigate the role of the Cys in coordination to $[M(CO)_3]^+$ complexes, MS-MS spectroscopy was obtained of the $[Re(CO)_3]^+$ labelled Cys/$(His)_6$-Tagged peptide and the equivalent non-Cys containing sequence; $[CKLAAALEHHHHHH\text{-}Re(CO)_3]^+$ ($[P_2\text{-}Re(CO)_3]^+$) and $[LAAALEHHHHHH\text{-}Re(CO)_3]^+$ ($[P_1\text{-}Re(CO)_3]^+$) respectively. The ESI-MS spectra for each of these peptide is displayed in Figure 2-13. For $[P_1\text{-}Re(CO)_3]^+$, peaks in the spectra are observed at *m/z* = 560.5487 for the $[P_1 + Re(CO)_3 + 2H]^{3+}$ ion and at *m/z* = 420.6638 for the $[P_1 + Re(CO)_3 + 3H]^{4+}$ ion (Figure 2-12, A). $[P_2\text{-}Re(CO)_3]^+$ appears in the spectra as its +3, +4 and +5 ions at *m/z* = 637.5834, *m/z* = 478.4402 and *m/z* = 382.9538 respectively (Figure 2-9, B). The characteristic splitting pattern associated with $^{185/187}$Re containing fragments is highlighted in the figure.

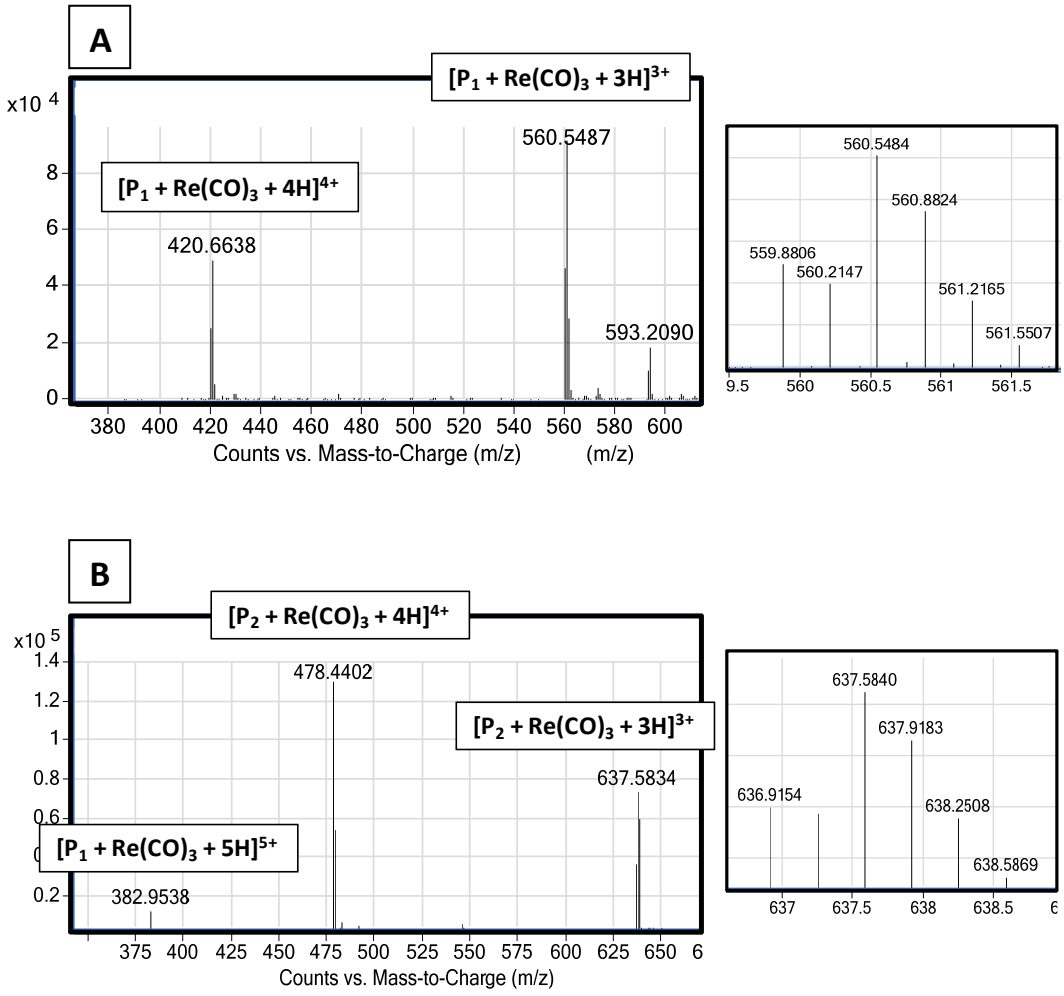

Figure 2-9. ESI-MS spectra for the $[Re(CO)_3]^+$ conjugated CKLAAALEHHHHHH and LAAALEHHHHHH peptides**. A)** $[LAAALEHHHHHH\text{-}Re(CO)_3]^+$ and P_1 = LAAALEHHHHHH. **B)** $[CKLAAALEHHHHHH\text{-}Re(CO)_3]^+$ where P_1 = CKLAAALEHHHHHH. The peak at *m/z* = 560.5487 and *m/z* = 637.5834 in graph A and B respectively have been blown up in the box on the right hand side. It is possible to see the characteristic $^{185/187}$Re pattern of the peaks (**right hand side**).

MS-MS is a common technique used for peptide sequencing and in this context it was used in an attempt to determine which amino acids were directly coordinated to the $[Re(CO)_3]^+$ complex.(*7-8*) When targeted with MS-MS, peptides primarily fragment along the peptide backbone in a reasonably well-documented manner. In this experiment, the parent ions of ions $[P_1\text{-}Re(CO)_3]^+$ and $[P_2\text{-}Re(CO)_3]^+$ complexes were targeted for MS-MS. Targeted MS-MS was performed at *m/z* = 560.5000 ($[P_1 + Re(CO)_3 + 2H]^{3+}$) and *m/z* = 637.6000 ($[P_1 + Re(CO)_3 + 2H]^{3+}$) for $[P_1\text{-}Re(CO)_3]^+$ and $[P_2\text{-}Re(CO)_3]^+$ respectively.

In the peptide backbone there are three different types of bond that can fragment including NH-CH, CH-CO and CO-NH. For every bond breakage two species are formed, a neutral and charged species. It is the charged species that can be monitored by mass spectrometry. When the charge is retained at the N-terminus the peptide fragments are referred to as a, b or c and when it is maintained on the C-terminus fragments are referred to as x, y or z according to the Roepstorff and Fohlman peptide fragmentation notation.(*8*) The most common fragmentation occurs at the amide bond, CO-NH and produces either the charged N-terminal fragment, an ammonium ion (b fragment), or the charged C-terminal fragment, a oxonium ion (y fragment). (Figure 2-10)

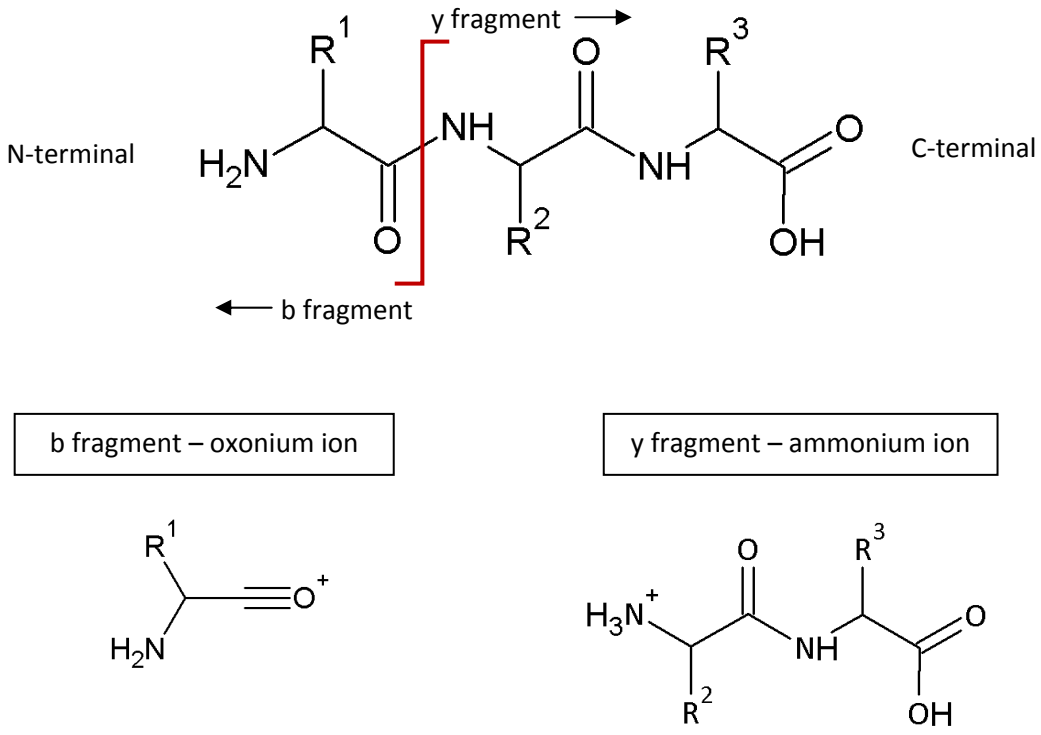

Figure 2-10 A diagram representing the most common backbone cleavage, CO-NH, during MS-MS targeting of peptide sequences. The charged ion recognised by the MS has also been included.

N-terminal fragmentation occurred for the $[P_1 + Re(CO)_3]^+$ complex and in the MS-MS spectra it was possible to clearly observe peaks corresponding to the b fragments: $[AAALEHHHHHH\text{-}Re(CO)_3]^+$, $[AALEHHHHHH\text{-}Re(CO)_3]^+$, $[ALEHHHHHH\text{-}Re(CO)_3]^+$ and $[LEHHHHHH\text{-}Re(CO)_3]^+$ fragments. For each newly formed fragment a single amino acid has

been cleaved from the N-terminal and produces the ammonium cations that are visible in the MS-MS spectra e.g. a Leu (L) is cleaved from the product ion, *m/z* = 560.5000 $[LAAALEHHHHHH + Re(CO)_3 + 2H]^{3+}$, by fragmentation at the CO-NH bond to produce the *m/z* = 782.7712 peak corresponding to $[AAALEHHHHH + Re(CO)_3 + H]^{2+}$. Figure 2-11

Fragmentation of the $[P_2 + Re(CO)_3]^+$ complex was somewhat different to that of the $[P_1 + Re(CO)_3]^+$ complex in that fragmentation primarily occurred from the C-terminal. In the MS-MS spectra peaks were observed at *m/z* = 878.8379, *m/z* = 809.8045 and *m/z* = 745.3064 that corresponded to the y fragmented ions: $[CKLAAALEHHHHH + Re(CO)_3 –OH + H]^{2+}$, $[CKLAAALEHHHH + Re(CO)_3 –OH + H]^{2+}$ and $[CKLAAALEHHH + Re(CO)_3 –OH + H]^{2+}$. (In the foregoing notation -OH means “minus OH”). C-terminal fragmented ions have been formed and this involves the loss of an OH group from the C-terminal to form the oxonium ion. In the MS-MS of $[P_2 + Re(CO)_3]^+$ three fragments have been produced as a result of the loss of His residues from the C-terminal. Despite the loss of 3 His residues from the C-terminal, the $[Re(CO)_3]^+$ still remains bound to the remaining sequences. If the $[Re(CO)_3]^+$ was only coordinated to the $(His)_6$-Tag sequence then fragmentation from N-terminal would be most likely as is demonstrated by the MS-MS of $[P_1\text{-}Re(CO)_3]^+$. Consequently this provides more evidence that the Cys is directly involved in coordination to $[Re(CO)_3]^+$.

Cleavage of the CK fragment from the N-terminal of $[P_2 + Re(CO)_3]^+$ was also observed however this resulted in the loss of the $[Re(CO)_3]^+$ complex. A peak at *m/z* = 705.3307 corresponded to the LAAALEHHHHHH sequence and did not contain the characteristic $^{185/187}$Re isotope. Again this supports the hypothesis that Cys is bound to $[Re(CO)_3]^+$ in addition to two of the $(His)_6$-Tag imidazole moieties. In the $[P_1 + Re(CO)_3]^+$ spectra peaks are observed at *m/z* = 430.1943 and *m/z* = 567.2535 that correspond to the presence of the respective HHH and HHHH fragments. Both peaks did not contain the characteristic $^{185/187}$Re splitting and represent 3 or 4 consecutive His residues that are uncoordinated to $[Re(CO)_3]^+$. In Figure 2-15 a schematic diagram representing the fragmentation pattern of $[P_2 + Re(CO)_3]^+$ can be seen.

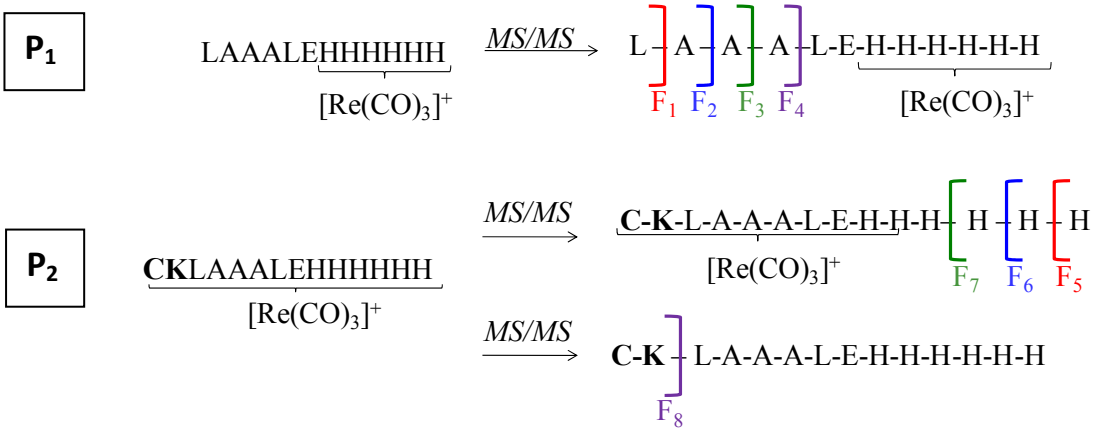

Fragment	Structure	z	m/z
	[LAAALEHHHHHH-Re(CO)$_3$]$^+$		
	Targeted Ion = 560.5000 (z=3)		
F$_1$	[AAALEHHHHHH-Re(CO)$_3$]$^+$	2	783.7751
F$_2$	[AALEHHHHHH-Re(CO)$_3$]$^+$	2	748.2575
F$_3$	[ALEHHHHHH-Re(CO)$_3$]$^+$	2	712.7760
F$_4$	[LEHHHHHH-Re(CO)$_3$]$^+$	2	677.219

Fragment	Structure	z	m/z
	[CKLAAALEHHHHHH-Re(CO)$_3$]$^+$		
	Targeted Ion = 637.6000 (z=3)		
F$_5$	[**CK**LAAALEHHHHH-Re(CO)$_3$]$^+$	2	878.3374
F$_6$	[**CK**LAAALEHHHH-Re(CO)$_3$]$^+$	2	809.8045
F$_7$	[**CK**LAAALEHHH-Re(CO)$_3$]$^+$	2	745.3064
F$_8$	LAAALEHHHHHH	2	705.3307

Figure 2-11. A schematic representation of the fragmentation patterns observed in the MS-MS analysis of [P$_1$-Re(CO)$_3$]$^+$ and [P$_2$-Re(CO)$_3$]$^+$.

2.4.6 Are multiple isomers formed during coordination of the [M(CO)$_3$]$^+$ to the His-Tag and can these isomers be reduced?

It has already been mentioned that the coordination of [M(CO)$_3$]$^+$ to the (His)$_6$-Tag involves the formation of multiple isomers. There is a possibility that this is due to the presence of 6 His residues, of which [M(CO)$_3$]$^+$ only requires two for coordination. To provide further insight into the coordination pattern of [M(CO)$_3$]$^+$ complexes to His-Tagged sequences, the LCMS of [LAAALEHHHHHH-Re(CO)$_3$]$^+$ (P$_1$-Re(CO)$_3$]$^+$) was carried out after labelling with a 3-fold molar excess of [Re(CO)$_3$]$^+$. In the UV chromatogram, Figure 2-12 A, a very broad peak with an RT between 13.5 and 32.5 mins was detected. According to the corresponding deconvoluted ESI-MS spectra, Figure 2-12B, this peak represents the formation of the

$[Re(CO)_3\text{-}P_1]^+$ complex. Evidently the broad peak in the UV chromatogram indicates that many different isomers and complexes have been formed during the coordination of $[Re(CO)_3]^+$ to P_1. ESI-MS spectrometry of $[Re(CO)_3\text{-}P_1]^+$ reveals that up to 3 $[Re(CO)_3]^+$ complexes can simultaneously coordinate to a $(His)_6$-Tag (Figure 2-16, C). Peaks at *m/z* = 1678.22, *m/z* = 1948.55 and *m/z* = 2216.44 correspond to the $[LAAALEHHHHHH\text{-}Re(CO)_3]^+$, $[LAAALEHHHHHH\text{-}([Re(CO)_3]^+)_2]$ and $[LAAALEHHHHHH\text{-}([Re(CO)_3]^+{}_3)]$ complexes respectively. This corroborates with the theory that $[Re(CO)_3]^+$ requires only 2 His residues for coordination and therefore with 6 His residues it is possible to have a total of 3 $[Re(CO)_3]^+$ complexes binding when excess $[Re(CO)_3]^+$ is available. There are approximately 13 peaks in the spectrum corresponding to isomers which probably represent the different possible combinations of labelling between $[Re(CO)_3]^+$ and 6 consecutive His residues.

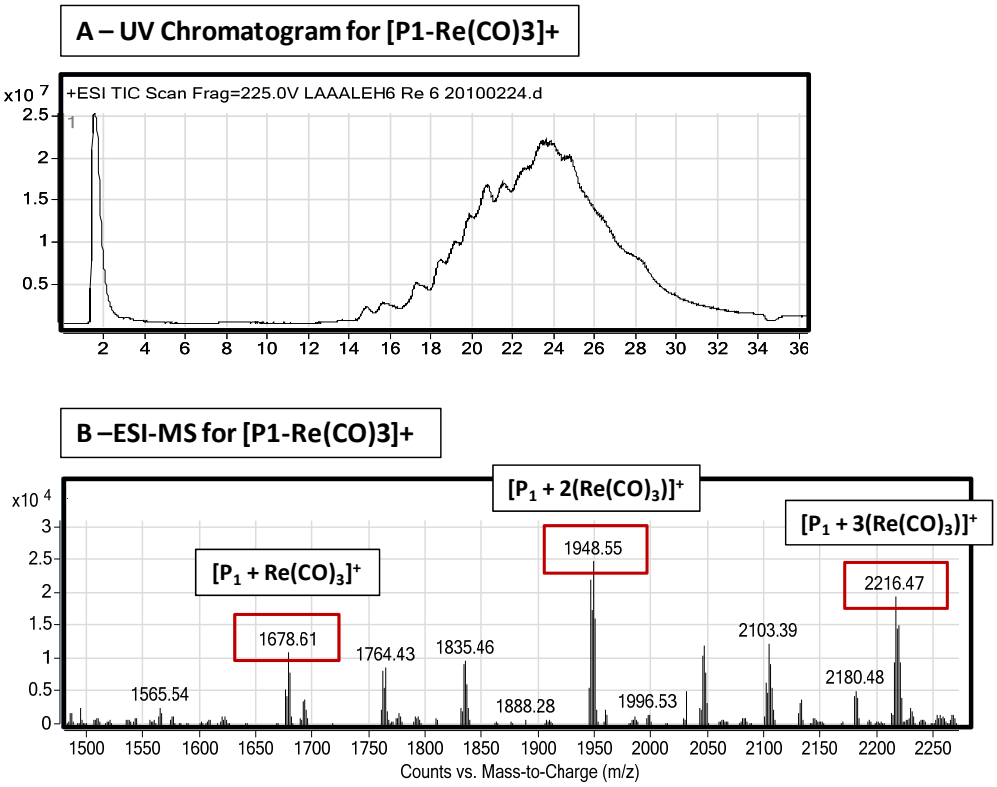

Figure 2-12. LCMS analysis of 3x molar excess of $[Re(CO)_3]^+$ binding to P_1 (LAAALEHHHHHH). A) UV chromatogram of the $[P_1\text{-}Re(CO)_3]^+$ complex, B Corresponding deconvoluted ESI-MS.

In an attempt to minimise the number of isomers present in the [peptide-$Re(CO)_3]^+$ complex, identical LCMS analysis was performed using a peptide with only 2 His residues, LAAALEHAHA (P_3). The UV chromatogram and corresponding deconvoluted ESI-MS can be seen in Figure 2-13 image B and D representing the [peptide-$Re(CO)_3]^+$ complex. Multiple peaks can still be detected in the UV chromatogram representing the $[P_3$-$Re(CO)_3]^+$ complex. All peaks have the same mass, *m/z* = 1272.46, which indicates that multiple isomers have been formed in the labelling of P_3 with $[Re(CO)_3]^+$ (Figure 2-13). There was no evidence in the MS that more than one $[Re(CO)_3]^+$ was simultaneously coordinated to P_3. Despite only having 2 His residues within the sequence, isomer formation was still apparent for the $[Re(CO)_3$-$P_3]^+$ complex. This suggests that there are more factors involved in the coordination between $[Re(CO)_3]^+$ and the peptide sequence.

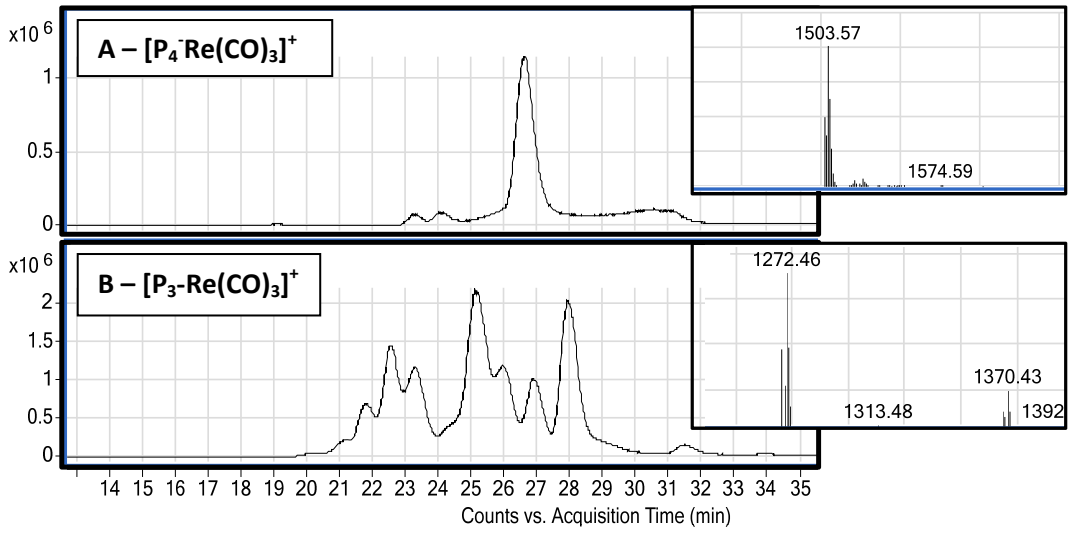

Figure 2-13. UV Chromatogram and corresponding ESI-MS for **A)** $[P_4$-$Re(CO)_3]^+$ and **B)** $[P_3$-$Re(CO)_3]^+$ where P_3 = LAAALEHAHA and P_4 = CKLAAALEHAHA

LCMS analysis was also carried out on the Cys containing peptide that had only 2 His residues, CKLAAALEHAHA (P_4). Interestingly in the UV chromatogram it was only possible to detect one major peak with an *m/z* = 1503.57, representing the $[P_4$-$Re(CO)_3]^+$ complex (Figure 2-13 image A). This implies that only one structural isomer had been formed between P_4 and $[Re(CO)_3]^+$. The difference between the P_4 and P_3 peptides is an additional CysLys motif at the C-terminal and consequently it can be deduced that the presence of the

CysLys residues are responsible for the reduction in isomer formation. In combination with the results previously observed during this Chapter, evidence suggests that for the CysLys containing sequences, it is the Cys residue that is involved in binding to the Re metal centre during labelling.

2.5 DISCUSSION & CONCLUSION

Data in this chapter provides several insights into the design and binding mode of His-Tagged sequences for binding the $[M(CO)_3]^+$ complex. It is now possible to answer some of the questions posed with particular emphasis on the influence of the Cys or CysLys on the coordination of $[M(CO)_3]^+$ complexes to His containing sequences. Firstly, radiolabelling the 10 Cys/His-Tagged peptide analogues confirmed that the CysLys/His combination does significantly improve labelling efficiencies in comparison to the His-Tag alone. This coincides with the observations reported by Tavare et al. in the labelling of the C2Ac protein that contained a $(His)_6$-Tag with a nearby CysLys. (Chapter 2.1). The reason behind the use of the CysLys motif was because it mimicked the sequences at the C-terminal of the C2Ac protein. The LCMS competition study between P_1 and P_2, LAAALEHHHHHH and CKLAAALEHHHHHH, for labelling with $[Re(CO)_3]^+$ also concurred that CysLys containing sequences substantially improved labelling efficiencies.

Prior to the studies performed within this Chapter, it was unclear why the labelling efficiencies increased in the presence of a CysLys residue. LCMS of the CysLys/His-Tag peptide analogues and the $[Re(CO)_3$-C2AcH$]^+$ protein provided some insight into the reasoning behind these observations. All data contributed towards the hypothesis that Cys is involved along with histidines in the coordination sphere of $[Re(CO)_3]^+$ to the peptide sequence.

It was initially proposed by Schibli et al. that the coordination sphere of $[Re(CO)_3]^+$ involved 2 His residues and the 6^{th} site was occupied by a H_2O molecule.(*6*) LCMS analysis of the tryspin digested $[Re(CO)_3$-C2AcH$]^+$ protein revealed that the $[Re(CO)_3]^+$ complex was site-specifically labelled to the C-terminal His-Tagged sequence. MS data demonstrated that in two of the three different Re fragments formed, Cys remained bound to the Re metal

centre even when the complex was unsupported by peptide bonds between Cys and the rest of the sequence. It was concluded that Cys is directly involved in the coordination to $[Re(CO)_3]^+$ and this was supported by further evidence acquired in the MSMS experiments of $[P_1\text{-}Re(CO)_3]^+$ and $[P_2\text{-}Re(CO)_3]^+$. Consequently, we now propose that binding of $[Re(CO)_3]^+$ to a Cys/His-Tagged peptide or protein involves three coordination sites comprising the imidazole group of 2 His residues and the thiol of a Cys.(Figure 2- 14)

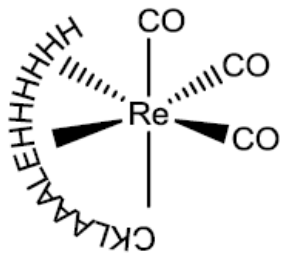

Figure 2-14. Schematic diagram representing the newly proposed coordination of $[Re(CO)_3]^+$ to a Cys/$(His)_6$-Tagged peptide sequence.

Multiple isomeric peaks in the UV chromatograms of $[Re(CO)_3\text{-peptide}]^+$ complexes are consistently observed. Initially this was believed to be associated with the regio- and stereoisomers formed, due to the presence of 6 His residues, of which $[M(CO)_3]^+$ required only two for coordination. However, the UV chromatogram of $[Re(CO)_3\text{-}P_3]^+$, where P_3 = LAAALEHAHA and only has 2 His residues, displayed multiple peaks with the same mass which represents different isomers formed during labelling. As there are only 2 His residues in the P_3 sequence, evidence indicates that other functional groups within the peptide sequence or buffer solution may be coordinating to the 6^{th} binding site of the Re metal and displacing the H_2O molecule. Another possibility is that the $[P_4\text{-}Re(CO)_3]^+$ complex forms a locked structural conformation. For $[P_3\text{-}Re(CO)_3]^+$, many different isomers were formed indicating that more than one factor was responsible for displacing the H_2O molecule. Examples of some of the functionalities of a peptide or in the labelling solution that have the potential to coordinate Re include: the amide backbone after deprotonation of the N-H group, the side chains of other amino acids such as Glu, the N-terminal amine, ACN in the labelling solution and phosphate ions or chloride from PBS buffer (although there is no evidence for any exogenous ions in the mass spectra).

The UV chromatogram, for the $[P_4\text{-}Re(CO)_3]^+$ complex, only 2 His residues, did not reveal multiple isomeric peaks. A single peak representing the $[P_4\text{-}Re(CO)_3]^+$ complex was detected indicating that only 1 type of coordination was formed between the peptide sequence and $[Re(CO)_3]^+$. Unlike P_3, P_4 contains a CysLys residue at the N-terminal of the sequence and results suggest that the thiol preferentially coordinates to the $[Re(CO)_3]^+$ above all other functionalities of the peptide producing a single complex. Again, this verifies the previous conclusions that Cys plays a role in the coordination sphere of $[Re(CO)_3]^+$ to a Cys containing His-Tag peptide sequence.

With respect to optimising and understanding the coordination of $[M(CO)_3]^+$ to the His residues, the 10 peptide sequences were designed to contain a variety of different His combinations e.g. HHHHHH, HHHH, HAHAHA, HAHA and HAAH. Radiolabelling studies revealed that a sequence of 6 consecutive His residues was the preferential number and arrangement of His within the sequence. Labelling efficiencies decreased in situations where the His residues were alternately spaced, for example as HAHAHA or HAAH. However, in terms of coordination, of the alternate arrangements HAHA was more favourable than the HAAH configuration according to the labelling efficiencies of these peptides.

Although some answers to the questions proposed have been provided by the above studies, structural NMR studies of the peptides coordinated to $[Re(CO)_3]^+$ would complement the data already obtained and potentially provide an "experimental model" of the binding.(*9*) The environment surrounding the amino acids post coordination of $[Re(CO)_3]^+$ is expected to change and comparison between the NMR of the $[Re(CO)_3]^+$ bound and unbound peptide sequence could identify the specific amino acids directly coordinated to $[Re(CO)_3]^+$. The protons in the side chains of the amino acids have typical ^1H chemical shift values and unique spectral properties, that are used to identify the specific amino acids within the sequence e.g. His has two C-H ring protons that are identifiable due to their sharp singlet peaks at a chemical shift between 6.5 and 8.5 ppm. A combination of TOCSY and COSY NMR should be able to decipher which peaks correspond to which amino acids and a difference in the chemical shift of a peak between the Re bound and unbound spectra can subsequently be associated with a specific amino acids. This may reveal to which amino acids the $[Re(CO)_3]^+$ is bound. NMR structural determination of the

coordination between $[Re(CO)_3]^+$ and the Cys/His-Tag peptides is definitely something that should be strongly considered for the future. One slight problem may be the production of a single pure isomer if a $(His)_6$-Tag is present. It may be worth considering the use of a peptide with a reduced number of His residues e.g CKLAAALEHAHA.

The experimental studies in this chapter have demonstrated how influential a single amino acid can be on the coordination between the His-Tag and the $[M(CO)_3]^+$ complex. In summary, a Cys in combination with a His-Tag significantly increases labelling efficiency with $[M(CO)_3]^+$ complexes. The influence of the Cys is at least partly due to its direct involvement in the coordination sphere of $[M(CO)_3]^+$ to the peptide sequence. As a result, reduced isomer formation is observed for the $[Re(CO)_3$-peptide$]^+$ complex when a Cys/His-Tag is present. It is likely that $[Re(CO)_3]^+$ binding involves three coordination sites to the peptide sequence: the imidazoles of two His residues and the thiol of a reduced Cys residue. Non-Cys containing peptide sequences demonstrated multiple isomeric peaks in which the 6^{th} coordination is more than likely occupied by one of a variety of different functional groups. Currently it can be concluded that other than the presence of His residues, the most important feature for efficient labelling is the incorporation of a Cys residue adjacent to the $(His)_6$-Tag.

REFERENCES

1. Tavare, R., Torres Martin De Rosales, R., Blower, P. J., and Mullen, G. E. (2009) Efficient site-specific radiolabeling of a modified C2A domain of synaptotagmin I with [99mTc(CO)3]+: a new radiopharmaceutical for imaging cell death, *Bioconjug Chem 20*, 2071-2081.
2. Lazarova, N., James, S., Babich, J., and Zubieta, J. (2004) A convenient synthesis, chemical characterization and reactivity of [Re(CO)(3)(H2O)(3)]Br: the crystal and molecular structure of [Re(CO)(3)(CH3CN)(2)Br], *Inorg Chem Commun 7*, 1023-1026.
3. Tavare, R., Williams, J., Howland, K., Blower, P. J., and Mullen, G. E. (2012) [Re(CO)(3)](+) labelling of a novel cysteine/hexahistidine tag: insights into binding mode by liquid chromatography-mass spectrometry, *J Inorg Biochem 114*, 24-27.
4. Binkley, S. L., Ziegler, C. J., Herrick, R. S., and Rowlett, R. S. (2010) Specific derivatization of lysozyme in aqueous solution with Re(CO)3(H2O)3(+), *Chem Commun (Camb) 46*, 1203-1205.
5. Zobi, F., and Spingler, B. (2012) Post-protein-binding reactivity and modifications of the fac-[Re(CO)3]+ core, *Inorg Chem 51*, 1210-1212.

6. Schibli, R., and Schubiger, P. A. (2002) Current use and future potential of organometallic radiopharmaceuticals, *Eur J Nucl Med Mol Imaging 29*, 1529-1542.
7. Johnson, R. S., and Biemann, K. (1989) Computer program (SEQPEP) to aid in the interpretation of high-energy collision tandem mass spectra of peptides, *Biomed Environ Mass Spectrom 18*, 945-957.
8. Roepstorff, P., and Fohlman, J. (1984) Proposal for a common nomenclature for sequence ions in mass spectra of peptides, *Biomed Mass Spectrom 11*, 601.
9. Williamson, M. P. (1993) Peptide structure determination by NMR, *Methods Mol Biol 17*, 69-85.

CHAPTER THREE

High-Through Put Screening of Peptide Libraries with $[^{99m}Tc(CO)_3]^+$

3.1 High Throughput Screening of the STKS-1 Celluspot™ Peptide Array

3.1.1 INTRODUCTION

3.1.1.1 Aims & Objective

Progress reported in the literature towards optimisation of the His-Tag design to improve labelling efficiency with $[M(CO)_3]^+$ synthons has been discussed in the previous chapters. The Cys/His-Tag sequences, incorporating a Cys close to the His-Tag, have demonstrated a moderate but significant improvement in the radiolabelling efficiency. It is common knowledge that the reactivity and behaviour of amino acid side chains can be significantly influenced by amino acids neighbouring in the sequence or those in close spatial proximity. In this chapter further investigations are discussed into the influence of individual amino acids on the coordination ability of the imidazole side chains, within the His-Tag, to the $[M(CO)_3]^+$ synthon. A high throughput screening technology, referred to as Celluspot™, is used and initial experimentation is performed using a trial STKS-1 Celluspot™ array. The aim of experiments with the STKS-1 Celluspot™ peptide array was to:

i) Develop a methodology suitable for screening the labelling efficiency of a library of peptides for coordination to $[M(CO)_3]^+$.

ii) Provide baseline data for random peptides to assist in designing a bespoke array

iii) Analyse the suitability of the method for further experimentation.

3.1.1.2 High Throughput Screening with Celluspot™ Peptide Arrays

SPOT synthesis technology is well known as a robust and efficient method of generating peptide libraries on membrane supports such as cellulose membrane sheets.(*1*) A bioanalytical German company, INTAVIS, developed the Celluspot™ peptide arrays based

on SPOT synthesis technology. Celluspot™ are arrays of peptide-cellulose conjugates that are spotted on to a planar surface. The peptides are synthesised on a modified cellulose support and the individual solutions of peptides, covalently bound to the cellulose, are then spotted on to glass slides. (Figure 3.1-1) They are often used as highthroughput screening methodologies for the detection of interactions between biological molecules and defined amino acid sequences that are presented on the chip surface, for example epitope mapping, enzyme-substrate and receptor-ligand interactions. The standard format of the Celluspot™ is a 26x67mm glass slide with up to 384 peptide-cellulose conjugates spotted in duplicate on the inert white membrane covering the glass surface. Peptide spots are approximately 1.2 mm apart. Generally 15-mer peptides are bound to the cellulose via their C-terminus and with an acetylated N-terminus. There is also a peptide-free control spot to test for non-specific binding. We propose that, in principle, Celluspot™ peptide arrays can be used as a combinatorial peptide library for the high throughput screening of genetically encodable tags suitable for the site-specific labelling of protein biomolecules with a radioisotope of choice. In particular, interest lies in the optimisation of the hexaHis sequence for labelling with [$M(CO)_3]^+$ complexes, but other labelling and bioconjugate modifications can be explored by the same approach.

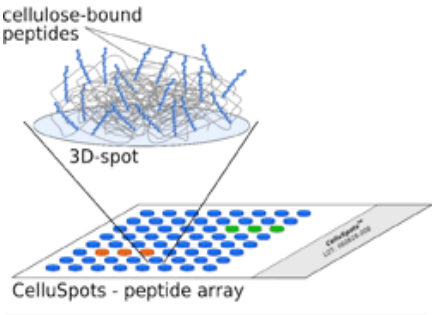

Figure 3.1-1. Diagram of the design of the Celluspot™ peptide array.

To test the principle, using an affordable trial array before investing in a bespoke array designed specifically for $[M(CO)_3]^+$ labelling, a Celluspot™ plate originally designed to screen for Serine/Threonine Kinase Substrate activity I (STKS-1) Array slides were obtained to test the suitability of the method for the labelling and detection of the peptides on the slide with $[M(CO)_3]^+$ complexes. The ability to use radioactive metals in conjunction with these

plates is invaluable as the binding of the radioactive $[^{99m}Tc(CO)_3]^+$ and $[^{186/188}Re(CO)_3]^+$ to the peptides can be observed using a phosphor imager. In order to evaluate the binding of $[^{99m}Tc(CO)_3]^+$ the presence of His residues within the peptide sequences was a requirement. It was expected that the presence of one or more His residues would be a requirement for Tc-binding. Although the STKS-1 array was not designed for specifically for the Tc-binding assay, it contained 68 peptide sequences with a single His amino acid and 16 peptide sequences with 2 or more His amino acids. The sequence of each peptide corresponding to the labelled spot is shown in Appendix 1 with the His-containing sequences highlighted in red. Figure 3.1-2 is an image of the STKS-1 Celluspot™ array. There are 386 spots in duplicate, 772 peptide spots in total. The duplicate spots are situated above and below each other as highlighted by the green boxes.

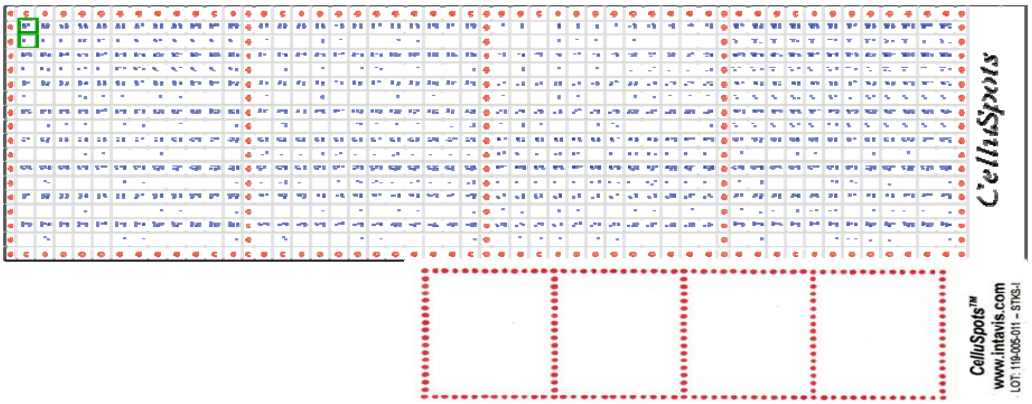

Figure 3.1-2. Template of the Celluspot™ STKS-1 peptide array. Each numbered letter represents a spot containing different peptide sequences i.e A1, A2, A3, A4 etc. There are duplicates of each numbered letter positioned in pairs above and below each other as highlighted by the green boxes (□). These duplicated spots have the same peptide sequence.

3.1.2 MATERIALS

^{99m}Tc was obtained as pertechnetate by elution in a Drytec generator (GE Healthcare, Amersham, UK) with 0.9% NaCl and converted to $[^{99m}Tc(CO)_3(OH_2)_3]^+$ using the Isolink kit (generously provided by Covidien, Petten , The Netherlands). Quality control of the $[^{99m}Tc(CO)_3(OH_2)_3]^+$ was carried out using glass backed silica gel 60 TLC plates (Merck Millipore, Darmstadt, Germany)analysed with a gamma-ray TLC scanner (Lablogic, UK). The STKS-1 Celluspot™ peptide arrays were generously donated by Intavis Bioanalytical

Instruments AG, Koeln, Germany. Analysis of the STKS-1 Celluspot™ array post radiolabelling was achieved using a Cyclone storage phosphor system and OptiQuant image analysis software (both from Perkin-Elmer). Solvents used during the experiments were purchased from Sigma Aldrich (ACN, conc. HCl, methanol, acetic acid) and PBS made using commercially available tablets (Sigma-Aldrich).

3.1.3 METHOD

3.1.3.1 $[^{99m}Tc(CO)_3]^+$ labelling of the STKS-1 Celluspot™ peptide array – Protocol 1

As previously discussed (Chapter 2.1) $[^{99m}Tc(CO)_3(H_2O)_3]^+$ was prepared using a standard Isolink kit and a quality control was carried out with glass backed silica TLC plates and a solvent phase of 1% HCl (concentrated) in methanol. The STKS-1 Celluspot™ array was incubated in a petri dish with 90MBq of $[^{99m}Tc(CO)_3]^+$ at 37°C for 1 hour. A solution of 70% ACN in H_2O was used to wash the array for 48 hours before an image was obtained using the phosphor imager. The Celluspot™ array was exposed to the phosphor film for 10 mins. Image processing was done using OptiQuant software associated with the phosphor imager. A square grid was placed around the Celluspot™ array image with an individual square surrounding each single spot. The intensity of each individual black spot was accounted for as in digital light units (DLU); an arbitrary relative value that once calibrated can be associated with radiochemical yield.

3.1.3.2 $[^{99m}Tc(CO)_3]^+$ labelling of the STKS-1 Celluspot™ peptide array – Protocol 2

$[^{99m}Tc(CO)_3]^+$ was prepared using the standard procedure and a quality control carried out. The Celluspot™ array was fully immersed in 50 ml of PBS buffer at pH 7.4 containing 8MBq of $[^{99m}Tc(CO)_3]^+$. This was heated at 37°C for 30 mins with gentle shaking. The array was then washed in 50 ml of 70% ACN in H_2O for 30 mins. Following this, an image of the array was generated using the phosphor imager with exposure to the phosphor film for 5 mins. All image processing was again achieved using the Opti-quant programme and the square grid method. A DLU value was recorded for the intensity of each black spot.

3.1.3.3 $^{99m}TcO_4^-$ Labelling of the STKS-1 Celluspot™ peptide array

The Celluspot™ peptide array was immersed in 50 ml of PBS buffer at pH 7.4 containing 8 MBq of $^{99m}TcO_4^-$ and heated at 37°C for 60 mins whilst gently shaking. An image was acquired by the phosphor imager following 10 mins of washing in a 70%ACN in H_2O solution.

3.1.4 RESULTS

3.1.4.1 Development of a method suitable for high-throughput screening using Celluspot™ Peptide Arrays

Radiolabelling the STKS-1 Celluspot™ peptide array confirmed that this is a suitable methodology for the high-throughput screening of multiple peptide sequences with $[^{99m}Tc(CO)_3]^+$ complexes. In terms of the analysis, the image obtained by the phosphor imager for the radiolabelled STKS-1 Celluspot™ peptide array has sufficient resolution for the detection of the individually bound peptide sequences as black dots on the plate surface. Using the OptiQuant software to isolate each black spot on a grid as an individual square it is possible to account for the intensity of the black spot as a digital light unit (DLU) value. This is an arbitrary value associated with radiochemical yield and can be used to compare the relative labelling efficiencies of the sequences. If the results from more than one array are compared then both arrays must be standardised according to each other. This is achieved by making sure that the labelling and imaging procedure for the arrays are identical with regards to the amount of radioactivity in the labelling solution, the exposure time of the array to the phosphor film and the intensity range in the phosphor image. The radioactive decay of the $[M(CO)_3]^+$ complex must also be taken into consideration. The relative intensity of the black spot correlates to the relative amount of $[^{99m}Tc(CO)_3]^+$ coordinated to the peptide. On the trial STKS-1 Celluspot™ arrays black spots can be identified in pairs above and below each other which represents the $[^{99m}Tc(CO)_3]^+$ bound peptides in duplicate. An overlay of the image onto the Celluspot™ template identifies the

location of the peptides that have been labelled and subsequently their corresponding sequences can be found. (Figure 3.1-3)

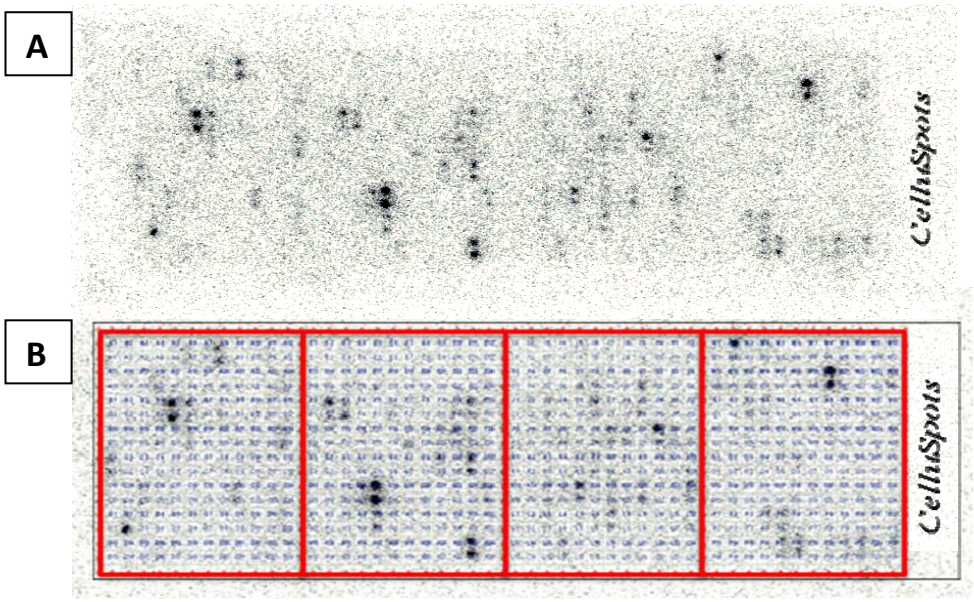

Figure 3.1-3. (A) Phosphor image of the $[^{99m}Tc(CO)_3]^+$ radiolabelled STKS-1 Celluspot™ peptide array post 48 hour wash in 70%ACN in H_2O. The black dots represent the peptides that have been radiolabelled. **(B)** An overlay of the phosphor image on the Celluspot™ template.

Two protocols were used for the radiolabelling of the trials STKS-1 Celluspot™ peptide arrays in order to optimise a suitable experimental method. Ultimately the peptide sequences are intended to be engineered into a protein and the radiolabelling would occur in solution, whereas the labelling in this experiment is on a solid phase. This should be taken into consideration when radiolabelling the Celluspot™ arrays and the experimental procedure should mimic the protein labelling conditions as much as possible. In protocol 1 the $[^{99m}Tc(CO)_3]^+$ in PBS buffer was placed on the array surface covering all the peptide spots and the petri dish containing the array placed in a 37°C environment. In protocol 2 however, the array was fully immersed into 50ml of PBS buffer containing the $[^{99m}Tc(CO)_3]^+$ complex and gently shaken at 37°C. In this instance, protocol 2 provides a better representation of the labelling conditions for a protein as the $[^{99m}Tc(CO)_3]^+$ is homogenously distributed across the array surface and each peptide sequence is in an identical environment.

In protocol 1 an excessive amount of radioactivity, 90 MBq, was added to the array and consequently a 48 hour washing period in 70%ACN/H_2O was required before a non-saturated image could be obtained on the phosphor imager. (Figure 3.1-4A) Modifications to this approach identified 7-8 MBq of $[^{99m}Tc(CO)_3]^+$ in 50 ml of buffer as a sufficient quantity of radioactivity suitable for the radiolabelling of the STKS-1 Celluspot™ peptides and their subsequent detection using the phosphor imager after shorter time periods. An image was obtained after 30 mins labelling and 30 mins washing in protocol 2. (Figure 3.1-4B)

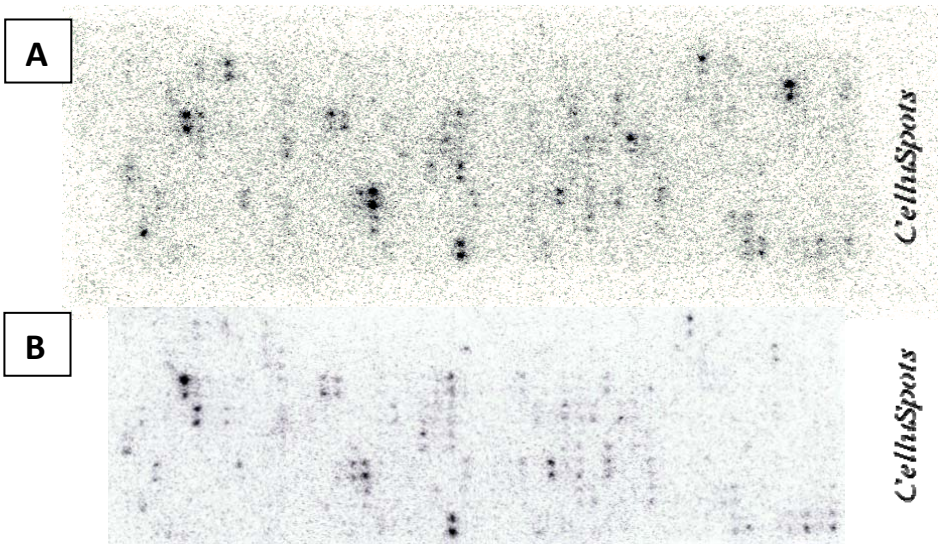

Figure 3.1-4. Phosphor image of the $[^{99m}Tc(CO)_3]^+$ radiolabelled STKS-1 Celluspot™ peptide arrays. **(A)** Image after protocol 1 methodology. **(B)** Image after protocol 2 methodology.

From the images obtained in Figure 3.1-4, it can be observed that the different experimental protocols adopted when labelling the STKS-1 Celluspot™ arrays have influenced the results obtained. In protocol 1 the Celluspot™ peptide array was washed for 48 hours and it is likely that any kinetically unstable $[^{99m}Tc(CO)_3$-peptide$]^+$ conjugates no longer appear as black spots on the array surface. Consequently the black spots present on the array surface (image A) correspond to the peptides that have formed thermodynamically favoured products with the $[^{99m}Tc(CO)_3]^+$ complex and once labelled are kinetically stable in the washing buffer 70%ACN in H_2O. The harsh washing conditions would have destroyed any unstable dative coordinate bonds formed between the His and $[^{99m}Tc(CO)_3]^+$ complexes. The image produced in protocol 2 (image B) was obtained after a significantly shorter 30 min wash and may reveals some information about the kinetically

unstable radiolabelled peptides. The increase in black spots present in image B demonstrates that a greater proportion of the peptide sequences are initially labelled with $[^{99m}Tc(CO)_3]^+$. For example (Figure 3.1-5), the blue circled black spots (image B) are no longer present in image A and represent peptide sequences that form kinetically favourable complexes with $[^{99m}Tc(CO)_3]^+$ but once radiolabelled are unstable in the washing solution. At these particular sites the reaction barriers for binding $[^{99m}Tc(CO)_3]^+$ are lower. Alternatively, the red circled spots in image A are not present in image B which implies that these are peptide sequences that have less favourable reaction kinetics towards the formation of the peptide-$[^{99m}Tc(CO)_3]^+$ complex. However, these peptides form thermodynamically favourable complexes with the $[^{99m}Tc(CO)_3]^+$ and once formed appear to be stable in the washing solution for 48 hours. There are some similarities between radiolabelled peptides on both arrays (green circles) and these peptides display characteristics that would be expected to be preferable when considering radiolabelling proteins. That is, they demonstrate fast reaction kinetics but also stability of the radiolabelled complex in a washing solution for a substantial period of time.

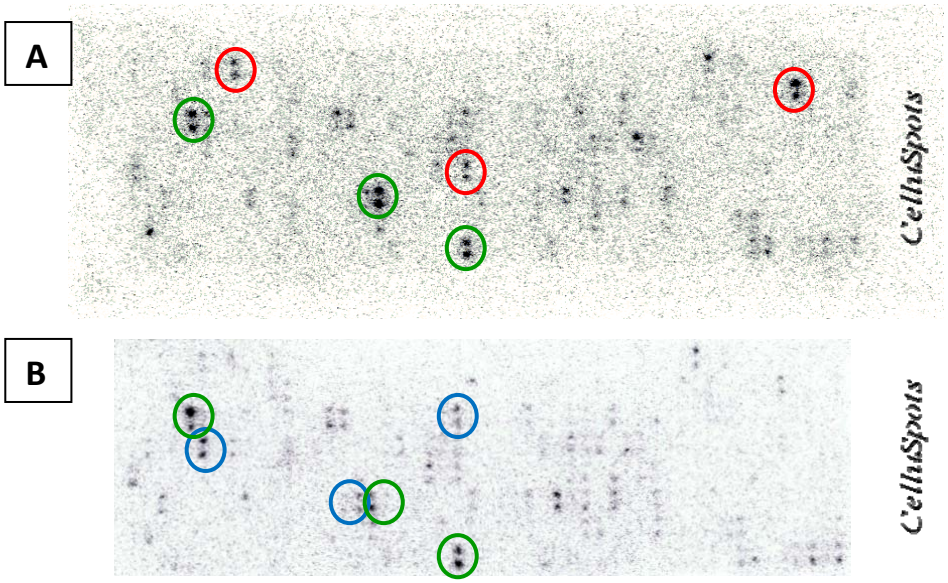

Figure 3.1-5. Phosphor image of the $[^{99m}Tc(CO)_3]^+$ radiolabelled STKS-1 Celluspot™ peptide arrays highlighting the differences and similarities in the results obtained by experimental protocol 1 **(Image A**) and protocol 2 **(image B). (Red circles) [**$^{99m}Tc(CO)_3]^+$ labelled peptides that appear only in image A**. (Blue circles)** $[^{99m}Tc(CO)_3]^+$ labelled peptides that appear only in image B. **(Green circles)** $[^{99m}Tc(CO)_3]^+$ labelled peptides that appear on both arrays, image A and image B.

3.1.4.2 Peptide Sequences that demonstrate preferential binding to $[^{99m}Tc(CO)_3]^+$ according to STKS-1 Celluspot™ Array

The binding efficiency of each peptide towards the $[^{99m}Tc(CO)_3]^+$ complexes was determined by obtaining the digital light unit data for each individual spot. The intensity of each spot correlates to the amount of radioactivity bound to that particular peptide; an intense black spot gives a high DLU value. The peptides were spotted in duplicate and an average of the digital light unit for both spots was taken and compared amongst other peptides on the plate. Figure 3.1-6 isolates the peptide sequences in the STKS-1 Celluspot™ peptide array that demonstrate the highest labelling efficiency towards the $[^{99m}Tc(CO)_3]^+$ complex in both protocol 1 (Table A) and protocol 2 (Table B). The peptides labelled A, B, C, D in Table A and A, B, C, D and E in Table B have the highest DLU values in comparison to all other peptides on the STKS-1 Celluspot™ array. Peptides labelled a-f and f-i, in table A and B respectively, demonstrate a reasonably high labelling efficiency in that they can be detected as black spots on the STKS-1 Celluspot™ array surface but do not have the same affinity for $[^{99m}Tc(CO)_3]^+$ as the more superior A-D (Table A) and A-E (Table B) sequences. (Figure 3.1-6)

As previously mentioned there are some variations between the peptides that show greatest affinity towards the $[^{99m}Tc(CO)_3]^+$ complex between both arrays due to the different protocols used in the experiment. In Table A (protocol 1) there are 4 sequences that have a DLU value significantly greater than any other sequence on the array. Of these, REEVPRRSGLSAGHR, GYLRKPKSMHKRFFV and EKKTKIRSLHNKLLN also have one of the highest DLU values in Table B and represent a peptide -$[^{99m}Tc(CO)_3]^+$ complex that has fast reaction kinetics but is also extremely stable after being washed for 48 hours. Of the 386 peptides present on the STKS-1 Celluspot™ array these 3 sequences would be most appropriate for the radiolabelling of a protein with $[^{99m}Tc(CO)_3]^+$.

A: Protocol 1

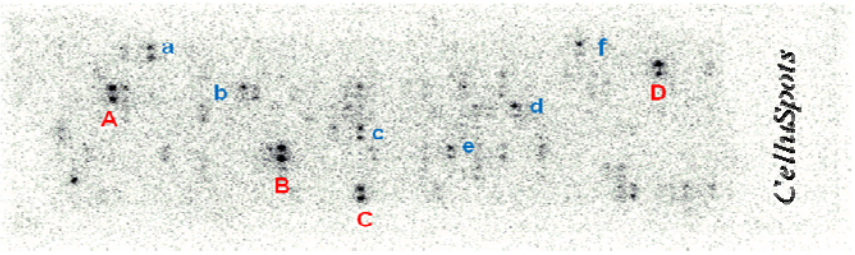

Spot	Peptide Sequence	pI	DLU
A	R-E-E-V-P-R-R-S-G-L-S-A-G-H-R	11.52	11, 418.60
B	G-Y-L-R-K-P-K-S-M-H-K-R-F-F-V	11.17	14,541.60
C	E-K-K-T-K-I-R-S-L-H-N-K-L-L-N	10.46	8,309.30
D	R-R-L-K-G-P-G-T-P-A-F-P-H-Y-L	11	14,371.40
a	Y-V-A-S-N-R-R-S-I-F-F-R-T-S-H	11.71	5,839.40
b	G-L-A-K-S-F-G-S-P-N-R-A-Y-T-H	9.99	6, 769.80
c	D-Y-F-L-L-S-H-S-L-L-P-A-L-C-D	4.51	6,445.90
d	H-V-Q-R-V-M-R-T-P-G-C-Q-S-P-G	10.35	6, 069.00
e	R-K-Q-H-A-R-V-ST-V-K-Y-D-R-R-E	10.93	5,791.90
f	K-K-K-S-E-P-S-S-P-D-H-G-S-S-T	8.51	5,987.40

B: Protocol 2

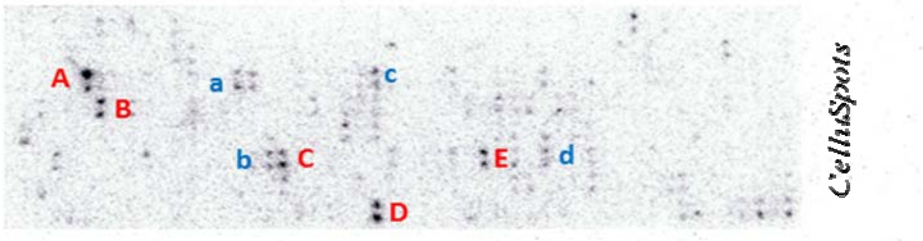

Spot	Peptide Sequence	pI	DLU
A	R-E-E-V-P-R-R-S-G-L-S-A-G-H-R	11.52	21,160.05
B	G-G-V-K-K-R-K-S-S-S-S-V-H-L-M	11.26	15,651.70
C	G-Y-L-R-K-P-K-S-M-H-K-R-F-F-V	11.17	13,792.50
D	E-K-K-T-K-I-R-S-L-H-N-K-L-L-N	10.46	17,746.45
E	R-K-Q-H-A-R-V-ST-V-K-Y-D-R-R-E	10.93	13,041.75
a	G-L-A-K-S-F-G-S-P-N-R-A-Y-T-H	9.99	10.449.25
b	G-P-R-V-W-Y-V-S-N-I-D-G-T-H-I	6.74	11,287.50
c	P-A-L-K-R-S-H-S-D-S-L-D-H-D-I	6.01	10,326.40
d	K-D-I-R-L-K-E-S-L-A-P-F-D-N-H	6.75	9,616.70

Figure 3.1-6. Highlights the peptides that have shown the greatest binding affinity towards the $[^{99m}Tc(CO)_3]^+$ complex in both experiments, protocol 1 and protocol 2. Their sequences, isoelectric point and DLU values are shown. **Table A**: Experimental results from protocol 1. **Table B**: Experimental results from protocol 2.

3.1.4.3 Peptide Sequences with a High Isoelectric Point (pI) have a High Labelling Efficiency to $[^{99m}Tc(CO)_3]^+$

In addition, a correlation between peptide sequences with exceptionally high labelling efficiencies to the $[^{99m}Tc(CO)_3]^+$ and peptide pI can be observed (Figure 3.1-6). The pI is defined as the pH at which the peptide sequences carry no net electrical charge and is strongly influenced by the presence of positively charged amino acids such as lysines (Lys) and arginines (Arg). The theoretical pI for all peptide sequences on the STKS-1 Celluspot™ array were calculated using the Compute pI/Mw tool provided by ExPASY Bioinformatics Resource Portal. In both Celluspot™ arrays all sequences identified as having the greatest DLU values, A-D in Table A and A-E in Table B, have a pI greater than 10.5. Furthermore in Table A, 8 out of the 10 best labelling peptides present have a pI greater than 9.5. There are two anomalies in Table A, DYFLLSHSLLPALCD and KKKSEPSSPDHGSST, with a pI of 4.51 and 8.51 respectively.

Similarly, table B also reveals that the majority of peptide sequences with high labelling efficiencies have a high pI, greater than 10. There is a slight discrepancy as three of the sequences have a pI of approximately 6.5: GPRVWYVSNIDGTHI, PALKRSHSDSLDHDI and KDIRLKESLAPFDNH. These are all sequences that initially form a kinetically favourable product but are no longer radiolabelled after a 24 hr wash in the 70%ACN/H_2O solution, according to the image of the Celluspot™ array after protocol 1 (Figure 3.1-6 Table A).

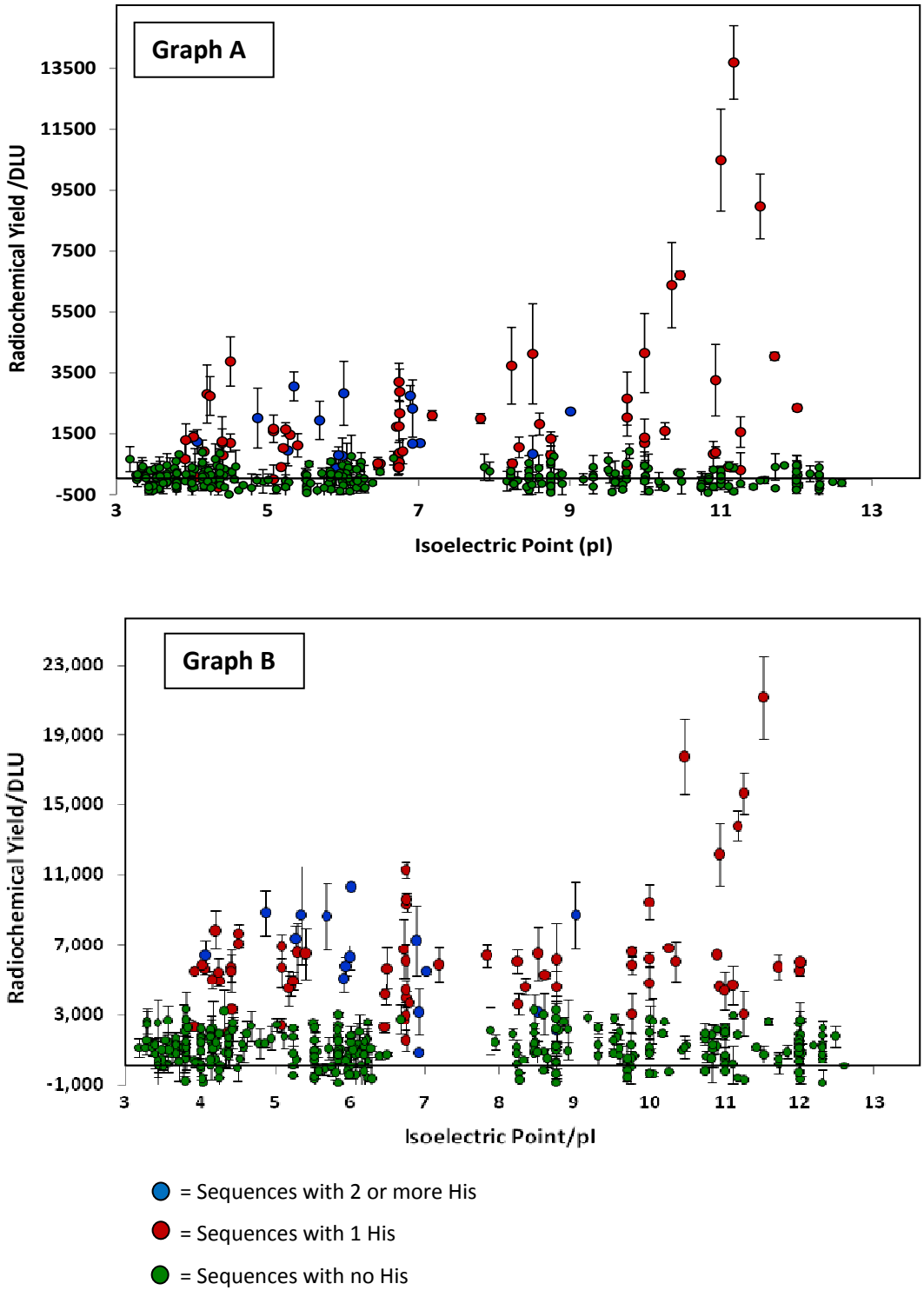

Figure 3.1-7. Positive correlation between isoelectric point of the STKS-1 Celluspot™ peptide sequences and their radiochemical yield for labelling with $[^{99m}Tc(CO)_3]^+$. **(Graph A)** Experimental results from protocol 1. **(Graph B)** Experimental results from protocol 2.

The positive correlation between the binding affinity and pI of the peptide sequences is further highlighted by the graphs in Figure 3.1-7. Peptide sequences with a pI > 9, to the

right of the marker, in both graph A and B (Figure 3.1-7) have demonstrated a substantially increased radiochemical yield in comparison to sequences with a lower pI. This is primarily evident in graph A, protocol 1 experiment, in which there is a clear distinction between the radiolabelling of sequences with a pI > 9 that contain a His and those His containing sequences with a pI = 3-7. In graph B, the difference in radiochemical yield between the His containing sequences that have a pI > 9.5 and a pI = 3-7 is less significant. This implies that the sequences with a pI = 3-7 form radiolabelled conjugates that are not kinetically stable in the washing buffer. Overall, a high pI contributes favourably to the labelling efficiency of the sequences to the $[^{99m}Tc(CO)_3]^+$ complex both in terms of fastest kinetics and greatest stability of the labelled product in the 70%ACN/H_2O wash solution.

3.1.4.4 His are Required for Coordination of the Peptide Sequences to $[^{99m}Tc(CO)_3]^+$

Further analysis of the tables in Figure 3.1-6 and graphs in Figure 3.1-7 reveal that each of the peptides demonstrating a high labelling efficiency to the $[^{99m}Tc(CO)_3]^+$ complex contain one or more His residues within the sequence. This is further emphasised by the graphs in Figure 3.1-8 which clearly shows that peptide sequences that did not contain His residues have extremely low labelling efficiency to the $[^{99m}Tc(CO)_3]^+$ complex. In both STKS-1 Celluspot™ array experiments, graph A for protocol 1 and graph B for protocol 2, all 300 non-His containing sequences present on the array surface have a radiochemical yield equivalent or similar to that of the controls, a peptide-free control spot (A2), in which there is no peptide bound to the cellulose membrane. This corresponds to the nonspecific binding of the $[^{99m}Tc(CO)_3]^+$ to the cellulose surface of the array. There are sequences on the STKS-1 Celluspot™ array that contain Cys but no His and these do not demonstrate a radiochemical yield greater than background level. Consequently, a high radiochemical yield for radiolabelling with $[^{99m}Tc(CO)_3]^+$ is dependent on the presence of His residues. This confirms that coordination to the $[^{99m}Tc(CO)_3]^+$ complex is achieved only through the His amino acids, presumably the imidazole side chains and confirms that only 1 His is required for binding.

Unexpectedly, peptide sequences containing two or more His residues did not demonstrate a particularly high labelling efficiency to $[^{99m}Tc(CO)_3]^+$ compared to peptides with a single His In protocol 1 (Figure 3.1-8 graph A) coordination to $[^{99m}Tc(CO)_3]^+$ primarily occurred in

sequences that contained a single His residue and in protocol 2 (Figure 3.1-8 graph B) only a slight increase in radiochemical yield can be observed for the sequences containing more than 1 His residue. The majority of the 16 sequences containing multiple His had a maximum of 2 His and these were not adjacent to each other. In addition, the highest pI of the sequences with multiple His is 9.0 and therefore it does not feature in the pI region in which high labelling efficiencies were mainly observed. In protocol 2 (Figure 3.1-8 graph B), the slight increase in radiochemical yield for the multiple containing His sequences is probably due to the kinetic favourability of a sequence containing more than 1 His residue which increases the entropy of activation (and hence decreases the free energy of activation). In this instance, the $[^{99m}Tc(CO)_3]^+$ radiolabelled peptides were unstable due to the decrease in radiochemical yield post washing (Figure 3.1-8 graph B) and it is likely that the His were not in a favourable environment.

Considering that the requirements for a high radiolabelling yield include the presence of a His and a high pI value, it is surprising that there are some sequences that possess such characteristics but demonstrate a very low binding affinity to $[^{99m}Tc(CO)_3]^+$. The length of the peptide sequences, 15 amino acids, could be responsible for this discrepancy. In some situations the positively charged amino acids contributing to the high pI are not situated within an influential proximity to the His. Further investigations with a specifically designed His-tagged Celluspot™ peptide array would be able to clarify if a correlation between efficient labelling sequences and high pI exists.

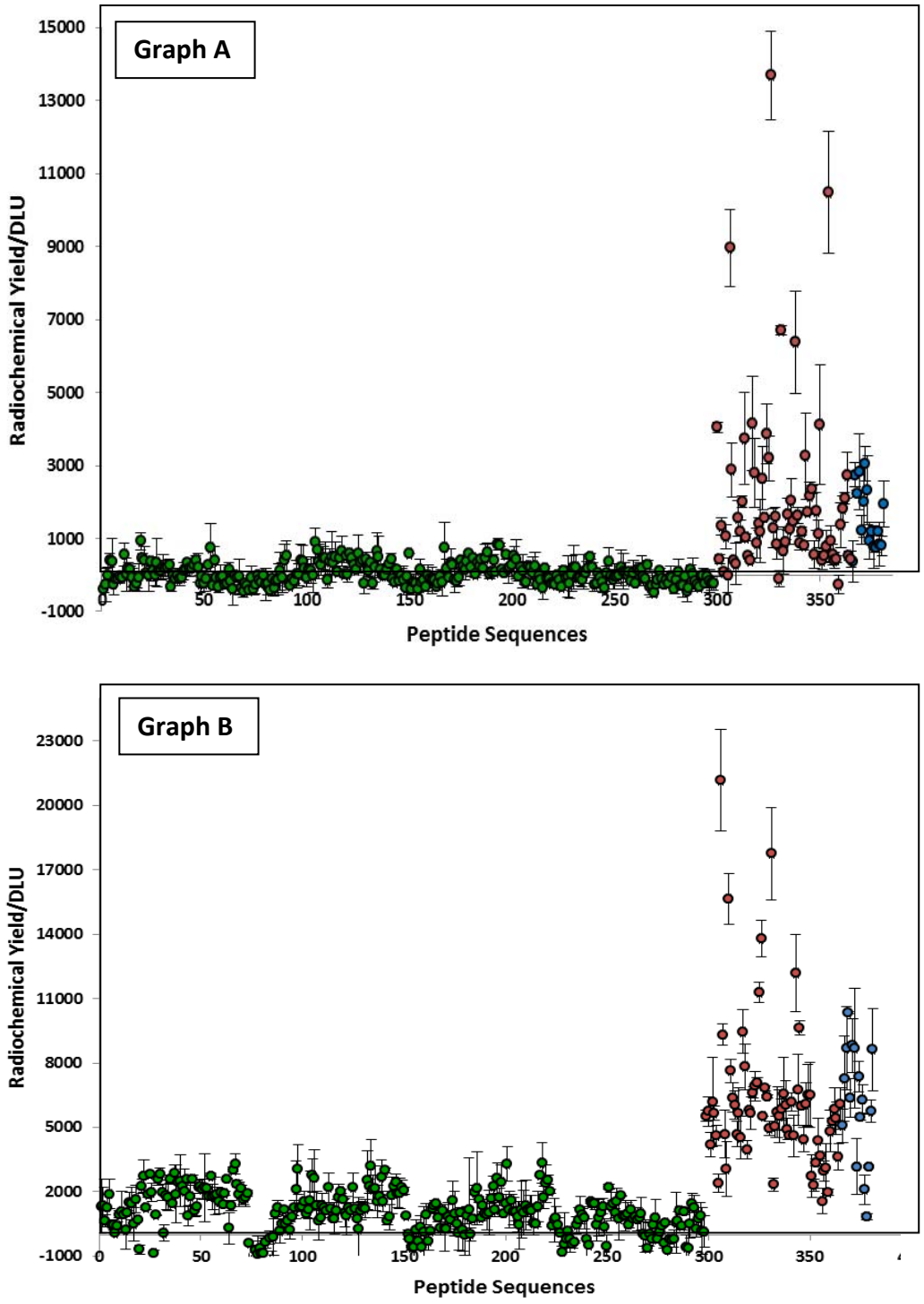

Figure 3.1-8 STKS-1 Celluspot^{TM} peptide array: Binding affinity of the peptide sequences to the $[^{99m}Tc(CO)_3]^+$ complex. The peptides have been categorised according to how many His are within the sequence: **(GREEN)** No his residues, **(RED)** 1 his residue and **(BLUE)** multiple His residues. **(Graph A)** Results after experimental protocol 1. **(Graph B)** Results after experimental protocol 2.

3.1.4.5 Unreduced $^{99m}TcO_4^-$ does not bind to Celluspot™ Peptide Array

Often the $[^{99m}Tc(CO)_3]^+$ solution used in the radiolabelling experiments will have a 98-99% radiochemical purity due to incomplete reduction of the $^{99m}TcO_4^-$. To eliminate the possibility that $^{99m}TcO_4^-$ binds non-specifically to the cellulose membrane coating, the analysis of the STKS-1 Celluspot™ peptide array was performed post incubation with $^{99m}TcO_4^-$ solution as a control. It is not possible to identify any peptides coordinated to the $^{99m}TcO_4^-$ or radioactivity bound to the cellulose membrane in the image produced. (Figure 3.1-9) This provides confirmation that the $^{99m}TcO_4^-$ does not bind independently to amino acids and its presence in the radiolabelling solution will not interfere with the data acquired from the $[^{99m}Tc(CO)_3]^+$ labelling of the Celluspot™ peptide array.

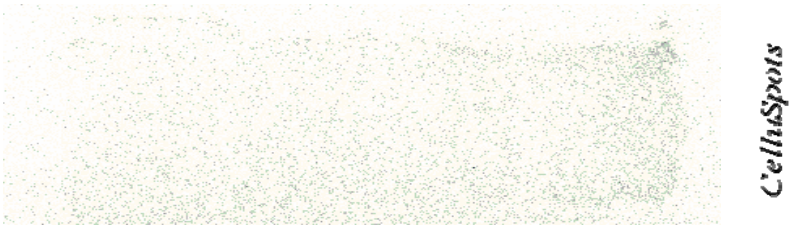

Figure 3.1-9. Phosphor image of the STKS-1 Celluspot™ peptide array after labelling with $^{99m}TcO_4^-$. Image after 10min wash with 70%ACN in H_2O.

3.1.5 DISCUSSION & CONCLUSION

Our overall goal in this project is to analyse and subsequently optimise the binding of $[M(CO)_3]^+$ complexes to peptide sequences. The development of a high throughput screening methodology is a prerequisite before the large scale analysis of a peptide library can be accomplished. The STKS-1 Celluspot™ peptide array has provided the opportunity to develop such a method and analyse its suitability for future use in identifying peptide sequences with preferential binding to $[^{99m}Tc(CO)_3]^+$. Due to the different protocols used in the experiments, the results acquired from the STKS-1 Celluspot™ peptide arrays do not provide information with regards to the reproducibility of the arrays. However, they do confirm the phosphor imager has sufficient resolution to discriminate between individual peptide spots on the array surface. In the library, the peptides have been spotted in

duplicate and in most instances the radiolabelled peptide can be identified as two black spots above and below each other demonstrating the reliability of the array. Furthermore, incubation of the Celluspot™ array with $^{99m}TcO_4^-$ confirmed that there was no non-specific binding to the cellulose membrane and therefore any unreduced $^{99m}TcO_4^-$ present in the radioactive solution will not interfere with the results. Despite the simplicity of the high-throughput screening method, it is of note that the peptide sequences may behave differently bound to the cellulose membrane than in solution. A comparison between the labelling efficiencies of the sequences on the Celluspot™ array and of the same sequences in solution was accomplished and the results are discussed in Chapter 3.3..

In terms of the experimental methods used with the STKS-1 Celluspot™ array, protocol 2 best mimics the labelling requirements of a protein. Firstly, the array is fully immersed in the radiolabelling solution providing a homogenous surrounding for the peptides and secondly, it would be straightforward to modify protocol 2 to include experimentations that involve different conditions such as a change in temperature, pH, salt concentration and buffer. From this, information would be obtained about the optimum radiolabelling conditions which would contribute to the overall aim to improve protein labelling with $[M(CO)_3]^+$ complexes.

Due to the nature of the $[^{99m}Tc(CO)_3]^+$ labelling protocols used, the data obtained after protocol 1 primarily assessed the kinetic stability of the $[^{99m}Tc(CO)_3]^+$ labelled peptides. Once bound to the $[^{99m}Tc(CO)_3]^+$ the peptides were subjected to a 48 hour wash in relatively harsh conditions that should destroy any unstable dative coordinate bonds formed between the His and $[^{99m}Tc(CO)_3]^+$ complexes. In protocol 2 more information was obtained with regards to the kinetically unfavourable $[^{99m}Tc(CO)_3]^+$ conjugates as the wash time was only 30mins and some of the sequences demonstrating fast labelling kinetics but poor stability could still be identified. Combining the data provides an overall understanding of the peptides that radiolabel with $[^{99m}Tc(CO)_3]^+$ in terms of their kinetic favourability and also stability of the labelled complexes. This identifies REEVPRRSGLSAGHR, GYLRKPKSMHKRFFV and EKKTKIRSLHNKLLN as the sequences most suitable for the $[^{99m}Tc(CO)_3]^+$ labelling of proteins, in comparison to other sequences on the STKS-1 Celluspot™ arrays. These sequences have the fastest reaction rate whilst maintaining the stability of the $[^{99m}Tc(CO)_3]^+$-product after a 48 hour wash under harsh conditions. In future Celluspot™ peptide array experiments it would be preferable, and feasible, to obtain information with

regards to reaction kinetics, thermodynamics and stability of the radiolabelled products in the same procedure. Consequently, experimental protocols will incorporate different steps in which the radiolabelling can be monitored at time intervals and the stability of the $[^{99m}Tc(CO)_3]^+$-peptide complexes analysed under different conditions, including buffer solutions, serum and in competition with His/Cys rich solutions.

An initial contribution to the optimisation of the His-Tag as a labelling sequence for $[M(CO)_3]^+$ complexes has been achieved with the preliminary results provided by the trial STKS-1 Celluspot™ peptide array. Key characteristics have been identified for the efficient labelling of peptide sequences with $[^{99m}Tc(CO)_3]^+$: His are required for coordination of the peptide sequence to the ^{99m}Tc core, and sequences with a high pI are preferable. Of the 386 peptide sequences, 300 did not contain a His residue and did not demonstrate any coordination to $[^{99m}Tc(CO)_3]^+$. Due to the quantity of non-His containing sequences there is sufficient evidence to conclude that the presence of a His residue is required for $[^{99m}Tc(CO)_3]^+$ coordination. This should be taken into consideration in the design of future peptide libraries investigating $[^{99m}Tc(CO)_3]^+$ coordination. The peptide sequences should contain His residues and modifications made to the amino acids surrounding the His in order to analyse their influence on the reactivity of the His.

An indication has been made from the STKS-1 Celluspot™ array results that peptide sequences with a high pI demonstrate preferential binding to $[^{99m}Tc(CO)_3]^+$. Peptide sequences are typically amphoteric as they contain both positive and negative charges depending on the functional groups present in the molecule. Therefore, the net charge on a peptide is affected by the surrounding pH. The pI dictates at which pH the negative and positive charges on the peptide sequence are balanced culminating in an overall neutral charge. Peptide sequences will have a higher pI the more basic amino acid residues are present as the basic side chain introduces “extra” positive charges into the sequence. More basic conditions are required for such a peptide to exist in its neutral form. Amino acid residues such as Lys and Arg are the most basic with side chain pKa values of 10.53, 12.48 and 6.10 respectively. Taking into account coordination to $[^{99m}Tc(CO)_3]^+$ occurs via His residues, the STKS-1 Celluspot™ results imply that a His in combination with basic residues, Arg and Lys, has a higher labelling efficiencyto the $[^{99m}Tc(CO)_3]^+$ complex.

This trend is inconclusive as there were some irregularities in which peptide sequences containing His residues and a high pI, pI > 9, did not coordinate to $[^{99m}Tc(CO)_3]^+$. Other His sequences, such as DYFLLSHSLLPALCD, demonstrated high labelling efficiencies but had a low pI of 4.51. In this instance, further analysis of the DYFLLSHSLLPALCD sequence revealed that a Cys residue was present 6 amino acids away from the His which could be responsible for the unexpectedly high labelling efficiency. As previously discussed (Chapter 2), the presence of a Cys residue adjacent to the his-tag has a positive influence on the coordination of the peptide sequence to $[^{99m}Tc(CO)_3]^+$. This was demonstrated for sequences in which the Cys residue was 7 amino acids away from the His. Information regarding the best position of the Cys in relation to the His was investigated using a specifically designed His-tagged Celluspot™ peptide array at a later stage and the results are discussed in Chapter 3.3.

Further discrepancies in the trend observed between an increase in pI and an increase in labelling efficiency was present in the results obtained from protocol 2. Three of the sequences with high labelling efficiencies had an unexpectedly low pI of approximately 6.5: GPRVWYVSNIDGTHI, PALKRSHSDSLDHDI and KDIRLKESLAPFDNH. However, these were all sequences that initially formed a kinetically favourable product but were no longer radiolabelled after a 24hour wash in the 70%ACN/H_2O solution. Consequently the radiolabelled peptides were unstable and would not be suitable as a method for the labelling of proteins with $[^{99m}Tc(CO)_3]^+$.

Clearly there are other factors to consider before reaching a definitive conclusion that a sequence containing His residues and positively charged amino acids to give a high pI are the optimal sequence for labelling $[M(CO)_3]^+$ complexes. Further investigations can be accomplished using the specifically designed His-tagged Celluspot™ peptide array with particular focus on the influence of charge on coordination of the His to $[^{99m}Tc(CO)_3]^+$.

To conclude, the Celluspot™ peptide array provides an efficient methodology for the analysis of multiple peptide sequences as suitable tags for the coordination of $[M(CO)_3]^+$ complexes. It provides a straightforward method in which labelling conditions including pH, temperature and buffers can be easily controlled. Protocol 2 is a suitable experimental procedure that best mimics protein labelling requirements (fast labelling, high kinetic stability) and should be applied to future Celluspot™ arrays. Through the STKS-1

Celluspot™ peptide array it has been established that preferential binding to $[^{99m}Tc(CO)_3]^+$ can be observed for peptide sequences that, in order of importance (a) contain His residues and (b) have a high pI value. Using the information obtained, a Celluspot™ peptide array can be designed to include His containing peptide sequences in which the environments surrounding the His residues are modified according to other amino acids used.

REFERENCES

1. Frank, R. (2002) The SPOT-synthesis technique. Synthetic peptide arrays on membrane supports--principles and applications, *J Immunol Methods 267*, 13-26.

3.2 Section 3.2: Design of the His-tagged Celluspot™ Peptide Array

3.2.1 Introduction

Results obtained from the trial STKS-1 Celluspot™ array confirmed the suitability of the peptide array as a method for simultaneously screening a library of peptide sequences for coordination towards metal $[M(CO)_3]^+$ sequences. In the next step, a Celluspot™ peptide array was specifically designed for screening with $[^{99m}Tc(CO)_3]^+$ complexes and its analogue $[^{186/188}Re(CO)_3]^+$. Identification of sequences with high binding affinities can be achieved through phosphor imaging of the array post radiolabelling. Optimisation of the reaction conditions for the radiolabelling of the Celluspot™ peptides is also possible and investigations will include suitable buffers and temperature.

In the manufacture of the designed His-Tagged Celluspot™ peptide array, the peptide sequences are attached chemically to the cellulose through the C-terminal. The peptide-cellulose conjugates are spotted on the slides and attached to the surface via cohesive attraction. The arrays are stable in aqueous buffers (PBS, imidazole and saline are suitable). A 3,6-dioxa-octanoic acid linker is used between the C-terminal amino acid of the peptide and the cellulose. In addition N-terminal acetylation blocks the amine group on the N-terminal from contributing to the ability of the peptide tag to coordinate to $[M(CO)_3]^+$. As the C-terminal of the peptide sequences is attached to the cellulose the His-Tag has been primarily positioned at the N-terminal in order to represent the freedom of movement available for the His-Tag in a protein environment. Unlike the trial STKS-1 Celluspot™ array, the 384 peptide-cellulose-conjugate spots are printed on both the right and left hand side of the slide and in Figure 3.2-1 the duplicated spots have been highlighted by the green boxes.

Figure 3.3- 1 A) Template of the His-Tagged CelluspotTM peptide array. **B)** An example of a CelluspotTM peptide array containing 386 peptides sequence representing *Borrelia* antigen fragments on both the left and right hand side of the plate. The green boxes (☐) represent duplicated spots, that is spots that has the same peptide sequence.

3.2.2 Aims & Objectives

Here we aim to describe the design of the His-Tagged Celluspot™ array based on a series of questions proposed in relation to which amino acids influence the labelling efficiency of a sequence for $[M(CO)_3]^+$ complexes. The analysis of the trial Celluspot ™ array (Chapter 3.1) and also the His/Cys Tagged peptides in solution (Chapter 2) contributed significantly towards the questions from which the design of the 384 peptide library was made. It is not possible to evaluate the effect of all 19 proteogenic amino acids on the coordination of the His-Tag to $[M(CO)_3]^+$ due to limitations in the number of different peptide sequence spots available on the His-Tagged Celluspot™ array. Therefore when designing the remaining sequences for the His-tagged Celluspot™ array, focus has been on using amino acids with unique characteristics as neighbouring residues to the His-Tag in the peptides. The peptide sequences will ultimately be placed into categories based on the characteristic features of the amino acids that surround the His residues.

3.2.3 What is the Optimum Number and Arrangement of His Residues?

An important consideration was the presence of His residues in the sequences. According to the literature (Chapter 1), his-tagged proteins have typically contained a His-Tag sequence, 6 consecutive His, for purification and/or radiolabelling with $[^{99m}Tc(CO)_3]^+$. Based on the experimental data currently reported in this thesis, His are an absolute requirement for effective $[^{99m}Tc(CO)_3]^+$ coordination and the "standard" six-His His-Tag demonstrated a higher binding affinity than 4 consecutive His (HHHH), 3 His in a HAHAHA format or 2 His in HAHA and HAAH format (Chapter 2). Other than the necessary control spots, all sequences in the newly designed Celluspot™ peptide array will therefore include at least 2 His with the majority containing a standard His-Tag. Consequently the designed array is henceforth referred to as the His-tagged Celluspot™ peptide array.

3.2.4 What is the Influence of the Cys and the Optimum Distance of the Cys from the His Residues?

Preliminary results aiming to identify a genetically encodable tag for efficient labelling to $[M(CO)_3]^+$ complexes highlighted peptide conjugated sequences combining a free Cys and a His-tag as a potential improvement on the His-tag alone. Radiolabelling studies of His/Cys Tag sequences in solution with $[M(CO)_3]^+$ confirmed the importance of the Cys in increasing the labelling efficiency of the His-Tag. This was discussed in Chapter 2 and previously published by our group in the $[^{99m}Tc(CO)_3]^+$ labelling of the C2A domain of synaptotagmin.(*1-2*) The ten His/Cys Tag peptide analogues discussed in Chapter 2 contained His-Tag sequences in order to analyse the preferred coordination of the $[M(CO)_3]^+$ to the His: HHHHHH (generic His-Tag), HHHH (reduced His-Tag sequence), HAHAHA, HAHA and HAAH.(Table 3.2-1) These sequences were included in the 384 peptides in the His-tagged Celluspot™ array and form a basic template around which the majority of other sequences were designed. Due to the presence of the Cys/His-Tag sequences on the His-tagged Celluspot™ array and their extensive analysis in solution an platform with excellent $[M(CO)_3]^+$ binding properties has been provided as a baseline to which other potential labelling sequences can be directly compared. In addition, it is a possibility that the radiolabelling of peptide sequences attached to the cellulose membrane

is not analogous to the radiolabelling of peptides in solution. For protein labelling, the sequences will usually be in solution. Embedding the ten His/Cys Tag analogues that have been labelled in solution in the array provides a comparator for the correlation between the labelling efficiency of the peptide sequences in solution and in solid phase. Consequently, the reliability of the results obtained from the Celluspot™ peptide array in predicting which sequence has the highest binding efficiency towards $[^{99m}Tc(CO)_3]^+$ in solution will be known.

His-Tag Sequence Analogues	His/Cys Tag	His/Cys Tag without Cys
HHHHHH (generic His-Tag)	CKLAAALEHHHHHH	LAAALEHHHHHH
HHHH (reduced His-Tag)	CKLAAALEHHHH	LAAALEHHHH
HAHAHA	CKLAAALEHAHAHA	LAAALEHAHAHA
HAHA (1-3 coordination)	CKLAAALEHAHA	LAAALEHAHA
HAAH (1-4 coordination)	CKLAAALEHAAH	LAAALEHAAH

Table 3.1- 1. Table showing the difference combination of His-Tags included on the Celluspot™ array. The 10 peptide sequences in the table, in pairs with and without Cys, form the basis of the Celluspot™ array design.

In the His-tagged Celluspot™ peptide array the sequences are conjugated to the cellulose via the C-terminal and therefore in order to mimic the His/Cys tag environment of the C2A protein(*1*) and the 10 peptides previously synthesised the His-tag has been positioned at the N-terminal e.g. HHHHHHELAAALKC. This enables the His-tag to have the greatest freedom of movement for coordination. The His/Cys Tag sequences have also been included in the array with the His positioned at the C-terminal conjugated to the 3,6-dioxa-octanoic acid linker which is attached to the cellulose. This enables an albeit comparison of the labelling efficiency between sequences with C-terminal or N-terminal His.
In the original His/Cys Tag sequences, CKLAAALEHHHHHH, the Cys is positioned eight amino acids away from the His-Tag in the direction of the N-terminus i.e. there are 7 amino acids in between the Cys and the nearest His residue. With the His-tagged Celluspot™ peptide

array, sequences have been included in which the distance of the Cys with respect to the His-Tag has been varied. Using the same sequences as the His/Cys Tag the Cys has been placed at amino acid positions 7, 6, 5, 4, 3, 2 and 1 away from the His-tag to determine the optimum position of the Cys for the improved labelling ability of the His-Tag to $[M(CO)_3]^+$.

Another sequence containing His residues with a nearby Cys included in the His-Tagged Celluspot™ was HHHCHHH. Here, the His residues have been separated into two sets of three by the Cys. According to preliminary data from the analysis of the His/Cys Tags in solution (Chapter 2) and reported by Schibli et al.(*3*), $[M(CO)_3]^+$ coordination occurs via alternate His. Consequently with a HHHCHHH sequence two $[M(CO)_3]^+$ complexes can potentially bind to the His on either side of the Cys. The Cys itself could potentially influence the binding affinity of both sets of His towards $[M(CO)_3]^+$ and thus increase the labelling efficiency.

3.2.5 What is the Influence of the Lys Residue?

In Chapter 2, it wasn't definitive as to whether the Cys or Lys was influencing the labelling efficiency of the His-Tagged sequences. The C2A-His-Tagged protein contained a Cys/His-Tag sequence that once subjected to a trypsin digest was cleaved at the Lys residues on both sides of the Cys in the C-terminal sequence KCKLAAALEHHHHHH. When the His-Tag was labelled with $[Re(CO)_3]^+$ the CK fragment remained bound to the metal centre despite the trypsin cleavage.(*2*) The assumption was that coordination of the CK fragment to the metal was due to the free Cys however, Lys contains an amino group on its side chain which also has the potential to form a dative coordinate bond to the metal centre. This has been demonstrated with the synthesis of new *fac*-$[M(CO)_3]^+$ complexes (M=Re, ^{99m}Tc) in which N-donor tridentate and bidentate ligands have efficiently replaced the weakly bound H_2O ligands of the reduced $[M(CO)_3(H_2O)_3]^+$ complex.(*4-7*) Consequently, in the Celluspot™ array sequences have been included in which the Cys or Lys have been omitted e.g. CLAAALEHHHHHH and KLAAALEHHHHHH sequences. Comparisons in the rate of labelling between these sequences should provide information in relation to the presence of which amino acid demonstrates a higher labelling efficiency and is more likely coordinate to $[^{99m}Tc(CO)_3]^+$.

3.2.6 What is the Influence of a His-Tag Embedded in a Labelling Sequence?

Another approach not yet considered is the insertion of the His-tag within a sequence surrounded on both sides by amino acids. In the His-Tagged Celluspot™ array, sequences have been designed in which the His-Tag is embedded within a chain of up to 15 amino acids rather than at the x-terminus. It is possible that individual amino acids may have a stronger influence on the coordination between the His and $[M(CO)_3]^+$ complex when situated on one specific side of the His-Tag. Different combinations of His-Tags have been embedded into a labelling sequence. These include the $(His)_6$-Tag, HHH, HAHAHA, HAHA and HAAH.

3.2.7 What is the Influence of two Cys Residues on the Labelling?

Some sequences with a His-Tag embedded in the middle of a labelling sequence include two Cys residues; a Cys on either side of the His-Tag. The distance of the Cys from the His-Tag on both the C and N terminal varies from position 4, 2, 1 amino acids away from the nearest His. The presence of two Cys residues in a labelling sequence is unfavourable due to problems with the formation of disulphide bonds between free Cys. A protein with two free Cys at the C or N-terminal is very likely to cyclise in solution. Information provided through analysis of the labelling efficiencies obtained by the double Cys sequences may contribute towards understanding the favoured coordination between $[M(CO)_3]^+$ and a His/Cys-Tagged sequence and help identify the optimum position of the Cys in relation to the His.

3.2.8 What is the Influence of Positively, Negatively or Neutrally Charged Sequences on Labelling with $[^{99m}Tc(CO)_3]^+$?

The sequences discussed above have been focused primarily on the influence of the Cys with regards to labelling His with $[M(CO)_3]^+$ complexes. However, there are a number of other amino acids that have unique properties which should be taken into consideration. Initial results reported from the trial STKS-1 Celluspot™ array, suggested that the pI of the

peptide sequence is an influential factor in the efficiency of labelling His-Tags. The pI of a labelling peptide sequence is influenced by the presence of amino acids with electrically charged side chains. At physiological pH (7.4), Arg and Lys are amino acids are positively charged, having an exceptionally high pKa of around 12.1 and 10.6 respectively. Aspartic acid and glutamic acid have negatively charged side chains at physiological pH, having a low pKa of 3.7 and 4.1 respectively. Within the His-Tagged Celluspot^{TM} array, sequences have been included that investigate directly the influence of the positively or negatively charged amino acids with respect to the $[M(CO)_3]^+$ labelling of His. A peptide sequence with a high pI is directly associated with the presence of multiple arginine and/or Lys residues in the sequence whereas a low pI is directly associated with the presence of glutamic acid and/or aspartic acid amino acids within the sequence.

Peptide sequences have been designed with a pI ranging from 12.6 (RHRHRHGRGGR) to 4.26 (DHDHDHGDGGDC). Other intermediate pI values have been accounted for with at least one peptide sequence on the His-tagged Celluspot^{TM} array. The number of Arg, Lys, Glu or Asp residues present in the sequence ranges from 1 to 5. There are no sequences that contain a mixture of Arg and Lys or Glu and Asp. Positions of the negatively or positively charged amino acids with respect to the His are varied in order to investigate optimum distance for improving binding affinities of the His-Tag towards $[M(CO)_3]^+$. Some sequences have been included in which the His residues have been separated with Arg, Lys, Asp or Glu amino acids for example HRHRHR,HKHKHK, HDHDHD and HEHEHE. Furthermore, sequences have been included in which the negatively or positively charged amino acids are substituted for neutral hydrophobic residues such as Ala, Gly and Leu. This can be used to evaluate the difference in labelling efficiency between charged and neutral sequences.

There are sequences present that contain no amino acids with charged side chains other than the requisite His residues. These are referred to as the neutral His sequences. In addition, Ala, Gly and Leu have been used in many sequences as spacers due to their characteristics as small and uncharged with side chains that are chemically inert.

3.2.9 Can Met Replace Cys to Avoid Dimerisation?

Met like Cys is a sulphur-containing amino acid with a thioether group rather than a thiol. Thioethers, like thiols, are recognised as donor groups for $[M(CO)_3]^+$ complexes and consequently, it is possible that Met behaves similarly to Cys with reference to the significance Cys has on the binding of $[M(CO)_3]^+$ to His.(*8*) This would be advantageous for recombinant proteins as, unlike Cys, Met cannot be oxidised to form a disulphide bond. Peptide sequences have been included that contain Met rather than the Cys using the His/Cys Tag as a template structure. The distance of the Met from the His, the presence of two Mets on either side of the His-Tag and the combination of Mets with positively and negatively charged amino acids has been taken into consideration in the design. Due to its inability to form disulfide bonds, multiple Met residues within a peptide sequence is not unfavourable and could be an advantage if the labelling affinity of $[M(CO)_3]^+$ improves.

3.2.10 What is the Influence of Pro on the Labelling Efficiency?

Proline is unique amongst the 20 proteogenic amino acids as it is the only one that has a distinctive cyclic structured side chain, forming a 5-membered ring that includes the backbone nitrogen. This geometry gives proline an exceptional conformational rigidity in comparison to other amino acids and generally introduces breaks or kinks into the polypeptide chain. Proline is unable to donate its amide hydrogen to complete the H-bonding chain of the helix and its side chain interferes sterically with the backbone of the preceding turn preventing Pro from adapting to the helical geometry. A bend of about 30^o is forced into the helical axis of the peptide sequence. The addition of Pro amino acids to the His/Cys labelling sequence could have an impact on coordination to $[M(CO)_3]^+$ as a turn in the straight chain peptide sequence could help the His-Tag to encompass the metal centre more easily or it may limit the availability of the His-Tag for access to $[^{99m}Tc(CO)_3]^+$. Currently, it has been implied that when Cys is present in the labelling sequence it forms the 6^{th} coordination site to the metal centre. If this is correct then a Pro positioned between the His and Cys could provide the flexibility required in the chain to help the Cys fold around the $[M(CO)_3]^+$ complex. This could produce a structurally favourable coordination site for $[M(CO)_3]^+$ and lead to a faster rate of labelling and a more stable product. In the His-Tagged Celluspot™ peptide array, labelling sequences with Pro amino acids have been

designed based on the following positions of the proline with respect to the His: HHHPHHH, HHHHHHPXXXXXXC and, HHHHHHXXXPXXC.

3.2.11 What is the Influence of Glu on the Labelling Efficiency?

In contrast to Pro, Gly does not have a side chain and allows high flexibility in the polypeptide chain. It has 3 different unique capabilities: smallest side group which is advantageous when peptide sequences must approach each other very closely; assumes a conformation normally forbidden due to close contact with the R groups, and, it is more flexible than any other amino acid which is valuable for sections of the backbone that need to hinge/move. Using this information, Gly has been frequently included in the sequences as spacers in between important amino acids. It is intended that the flexibility of Gly will increase the freedom of movement within the peptide sequence to optimise the geometry required for efficient $[M(CO)_3]^+$ coordination.

3.2.12 Can Catalytic Reactions be used to Improve Labelling Efficiency?

In a biological context specific amino acids are often found inside the active sites of enzymes and work together to generate a chemical reaction. An example of this is the catalytic triad in chymotrypsin which refers to a set of three specific residues that function together and are directly involved in catalysis. A well known example of a catalytic triad is present in chymotrypsin where a Ser, Asp and His trigger a reaction sequence that ultimately enables the cleavage of a peptide bond. The COOH on Asp forms a low-barrier hydrogen bond with His which simultaneously increases the pKa of its imidazole nitrogen from 7 to 12. This allows the His to act as a base and deprotonate the Ser. The deprotonated Ser serves as a nucleophile and triggers hydrolysis of the amide bond. With this in mind, peptide sequences were designed to include Ser and Asp amino acids on either side of the His. The combination of Ser, Asp and His could contribute to improving the radiolabelling efficiencies of the His residues.

3.2.13 Controls

The remaining peptide sequences primarily include controls. There are two spots present in which no peptides are conjugated to the cellulose in order to assess any unspecific binding to the cellulose membrane. One of these spots includes the 3,6-dioxa-octanoic acid linker to eliminate the possibility that this linker could interfere with $[M(CO)_3]^+$ labelling of His residues. Two non-His containing peptides with random combinations of amino acids have also been included on the His-Tagged Celluspot™ array. They do not contain any His residues in order to confirm that His residues are required for the radiolabelling. In addition, the 4 sequences with the highest radiochemical yield from the trial STKS-1Celluspot™ array are represented and two sequences that have recently been published by Tolmachev et al. for the radiolabelling of a HER-2 binding affibody with $[^{99m}Tc(CO)_3]^+$.

3.2.14 Peptide Categories for Data Analysis

For data analysis, the peptide sequences have been placed into categories according to the characteristic features of the amino acids that surround the His residues and the arrangement of these amino acids with regards to the His residues. The categories have been summarised below and a small explanation given with each group:

- **His/Cys Peptides:** 10 peptide sequences analysed in Chapter 2 based on the CKLAAALEHHHHHH labelling sequence engineered at the C-terminal of the C2A protein for $[^{99m}Tc(CO)_3]^+$ labelling. These 10 sequences contained different His-Tags and are present in duplicate with and without an adjacent CK dipeptide. Sequences are CKLAAALEHHHHHH, LAAALEHHHHHH, CKLAAALEHHHH, LAAALEHHHH, CKLAAALEHAHAHA, LAAALEHAHAHA, CKLAAALEHAHA, LAAALEHAHA, CKLAAALEHAAH, LAAALEHAAH.
- **Distance from C (Nt His-Tag):** His/Cys sequences in which the position of the Cys has been varied with respect to the His residues. Cys is positioned between 7-1 amino acids away from the nearest His. The His-Tag is at the N-terminal (Nt) of the sequence
- **C-terminal His-Tag:** His/Cys peptide sequences with a C-terminal His-Tag
- **His/Cys Tag with no Lys:** His/Cys sequences without the Lys residues.

- **His-Tag in the middle:** His-Tag is embedded within the sequence and surrounded by amino acids on either side. The surrounding amino acids are based on the composition of the His/Cys peptide and include Leu, Ala, Glu, Cys or Lys.
- **Double Cysteine:** Two Cys residues within a His containing peptide sequence. One is on the N-terminal and one is on the C-terminal side of the His.
- **HHHCHHH:** Sequences with a Cys separating two sets of 3x His residues
- **Proline:** Proline has been included in the His containing sequences at different positions e.g. HHHPHHH, HHHHHHP, HHHPHHHXXXP and HHHHHHXXXP, where X is equivalent to any other amino acid.
- **Methionine:** Methionines have been included in the His containing sequences to replace the Cys. Very similar to Cys but cannot be oxidised to form disulphide bonds.
- **Neutral:** His containing sequences with no charged amino acids. Sequences include hydrophobic spacers such as Leu, Ala or Gly.
- **Negatively Charged Amino Acids:** Sequences with 2 or more Glu and/or Asp residues surrounding the His.
- **Positively Charged Amino Acids:** Sequences with 2 or more Arg and/or Lys residues surrounding the His.
- **Serine:** Sequences with multiple Ser residues surrounding the His.
- **Catalytic Sequences:** Sequences with $(His)_6$-Tags and amino acid combinationsthat form catalytic triads e.g. Ser, Asp and His.
- **Controls:** 4 spots on the CelluspotTM peptide array surface: 2 blank spots on the cellulose membrance and two randomly generated peptide sequences that contain no His. All other amino acids are included at least once in one of the sequences.
- **HEHEHE Tag**: 2 His containinglabelling sequences previously published by Tolmachevet al. for the radiolabelling of proteins with $[^{99m}Tc(CO)_3]^+$.

REFERENCES

1. Tavare, R., Torres Martin De Rosales, R., Blower, P. J., and Mullen, G. E. (2009) Efficient site-specific radiolabeling of a modified C2A domain of synaptotagmin I

with [^{99m}Tc(CO)$_3$]$^+$: a new radiopharmaceutical for imaging cell death, *Bioconjug Chem 20*, 2071-2081.
2. Tavare, R., Williams, J., Howland, K., Blower, P. J., and Mullen, G. E. (2012) [Re(CO)(3)](+) labelling of a novel cysteine/hexahistidine tag: insights into binding mode by liquid chromatography-mass spectrometry, *J Inorg Biochem 114*, 24-27.
3. Schibli, R., and Schubiger, P. A. (2002) Current use and future potential of organometallic radiopharmaceuticals, *Eur J Nucl Med Mol Imaging 29*, 1529-1542.
4. Perera, T., Marzilli, P. A., Fronczek, F. R., and Marzilli, L. G. (2010) Several novel N-donor tridentate ligands formed in chemical studies of new fac-Re(CO)3 complexes relevant to fac-^{99m}Tc(CO)3 radiopharmaceuticals: attack of a terminal amine on coordinated acetonitrile, *Inorg Chem 49*, 2123-2131.
5. Alberto, R. (2003) [Tc(CO)(3)](+) chemistry: a promising new concept for SPET?, *Eur J Nucl Med Mol I 30*, 1299-1302.
6. Christoforou, A. M., Marzilli, P. A., Fronczek, F. R., and Marzilli, L. G. (2007) fac-[Re(CO)(3)L](+) complexes with N-CH(2)-CH(2)-X-CH(2)-CH(2)-N tridentate ligands. synthetic, X-ray crystallographic, and NMR spectroscopic investigations, *Inorg Chem 46*, 11173-11182.
7. Chiotellis, A., Tsoukalas, C., Pelecanou, M., Raptopoulou, C., Terzis, A., Papadopoulos, M., Papadopoulou-Daifoti, Z., and Pirmettis, I. (2008) Convenient route leading to neutral fac-M(CO)3(NNO) complexes (M = Re, ^{99m}Tc) coupled to amine pharmacophores, *Inorg Chem 47*, 2601-2607.
8. Lazarova, N., Babich, J., Valliant, J., Schaffer, P., James, S., and Zubieta, J. (2005) Thiol- and thioether-based bifunctional chelates for the {M(CO)3}+ core (M = Tc, Re), *Inorg Chem 44*, 6763-6770.

3.3 High Throughput Screening of His-Tagged Celluspot™ Peptide Array with $[^{99m}Tc(CO)_3]^+$

3.3.1 INTRODUCTION

3.3.1.1 Aim and Objective

The aim is to distinguish which characteristics of a peptide sequence are beneficial or detrimental towards the coordination of $[M(CO)_3]^+$ complexes. In Chapter 3.2, a His-Tagged Celluspot™ array was specifically designed based on a series of questions in relation to what amino acids could influence the labelling of His residues. Here, results are described of the radiolabelling of the His-Tagged array with $[^{99m}Tc(CO)_3]^+$, performed to screen a large number of the designed sequences for $[^{99m}Tc(CO)_3]^+$ binding and answer the questions. Another aim is to determine the most appropriate buffer and pH suitable for the efficient radiolabelling of His-Tagged peptides with $[^{99m}Tc(CO)_3]^+$. Ultimately the objective is to arrive at an optimal sequence for incorporation into a protein and for highly efficient site-specific labelling with $[^{99m}Tc(CO)_3]^+$.

The design of the His-Tagged Celluspot™ peptide array in Chapter 3.2 was focused on a series of questions and these questions will be addressed when analysing the $[^{99m}Tc(CO)_3]^+$ conjugated array in this chapter. Specific questions tackled within this chapter include:

i) What is the correlation between the radiolabelling peptides in solution and on solid phase?
ii) What is the influence of the Cys including its preferred position within the sequence?
iii) What is the influence of positively charged amino acids?
iv) What is the influence of negatively charged amino acids?
v) What is the optimum number and arrangement of His residues?
vi) Can Met replace Cys in a labelling sequence and give equal labelling efficiency?
vii) What is the best labelling sequence and how does it compare to sequences within the literature?

viii) Do any trends in radiolabelling efficiency change over time?

Radiolabelling efficiencies of the His-Tagged Celluspot™ peptide were monitored after 15, 30, 60 and 90 mins total incubation time.

ix) What is the kinetic stability of the $[^{99m}Tc(CO)_3]^+$ labelled peptides on the plate?

His-tagged Celluspot™ experiments were designed to analyse the stability of the labelled product in buffer, human serum and in competition with a 1000 molar excess His/Cys containing solution.

x) What is the influence of buffer and pH on the labelling efficiency of the peptides?

In the His-tagged Celluspot™ array experiments a citrate buffer at pH 5.5 and a tris-HCl buffer at pH 8.8 were used in addition to the standard PBS buffer at pH 7.4.

3.3.1.2 His-Tagged Celluspot™ Array Layout

For these experiments, the His-tagged Celluspot™ array used has a layout of the peptides as demonstrated in figure 3.3-2. 384 peptide-cellulose-conjugate spots are printed on both the right and left hand side of the array and the duplicated spots have been highlighted by the green boxes. Spot-to-spot distance is approximately 1.2 mm and the concentration of peptide in each spot is approximately 4.2 μg. The peptide sequences have been conjugated via their C-terminal to a 3,6-dioxa-octanoic acid linker and the N-terminus is acetylated.

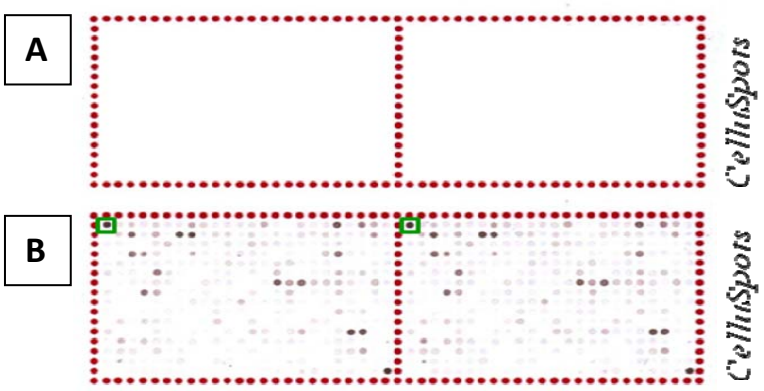

Figure 3.3- 1 A) Template of the His-Tagged Celluspot™ peptide array. **B)** An example of a Celluspot™ peptide array containing 386 peptides sequence representing *Borrelia* antigen fragments on both the left and right hand side of the plate. The green boxes ( ) represent duplicated spots, that is spots that has the same peptide sequence.

3.3.2 MATERIALS

Unless otherwise specified, materials were obtained and equipment used as previously described for the radiolabelling experiments of the STKS-1 Celluspot™ peptide array in Chapter 3.1.2. For the stability experiments, serum was isolated from fresh human blood.

3.3.3 METHODS

3.3.3.1 Calculation of pI Values for Peptide Sequences on the His-Tagged Celluspot™ Array

The theoretical pI of all peptide sequences on the His-Tagged Celluspot™ peptidearray has been calculated using compute pI/Mw by ExPASy Bioinformatics Resource Portal. pI/Mw is a tool which allows the computation of the theoretic pI and Mw (molecular weight) for a list of UniProt Knowledgebase (Swiss Prot or TrEMBL) entries or for user entered sequences.

3.3.3.2 $[^{99m}Tc(CO)_3]^+$ Labelling in PBS Buffer pH 7.4

$[^{99m}Tc(CO)_3]^+$ was synthesised using the standard Isolink procedure and a TLC quality control carried out to confirm that the radiochemical yield was >95% (Chapter 2). The His-tagged Celluspot™ peptide array was fully immersed in a Falcon tube containing 50 ml of a pH 7.4 PBS solution and 7-8 MBq of $[^{99m}Tc(CO)_3]^+$. Incubation of the array in the solution was carried out for 15mins at 37^oC with gentle shaking. After 15 minutes the array was placed in 50 ml of non-radioactive PBS for 3 seconds to wash off any unbound $[^{99m}Tc(CO)_3]^+$ and padded dry with filter paper. The surface of the plate cannot be rubbed only gently pressed. There should be minimal activity on the filter paper. The plate was then exposed to the phosphor film for 5 minutes and the film placed in the phosphor imager to generate an image. Re-immersion of the Celluspot™ peptide array in the original PBS buffer solution containing the $[^{99m}Tc(CO)_3]^+$ complex was carried out and left for another 15 minutes to give an total incubation time of 30 minutes. The process of washing and imaging was repeated again to obtain results at a 30 minute time point. In addition to 15 and 30 minutes, images were also obtained similarly at 60, 90 and 120 minute time points. The $[^{99m}Tc(CO)_3]^+$

radiolabelling of the His-Tagged Celluspot™ peptide array was repeated for 3 slides in order to report the results as n=6 (two arrays per slide).

3.3.3.3 Stability of the $[^{99m}Tc(CO)_3]^+$ Labelled Peptides

Following exposure to the phosphor film after a total incubation time of 120 minutes, the His-Tagged Celluspot™ peptide arrays were incubated in 50 ml of either human serum, non-radioactive PBS buffer or a 1000 molar excess of a Cys containing solution followed by a 1000 molar excess of a His containing solution. PBS was prepared in the same way as the PBS buffer used in the radiolabelling procedure and its pH adjusted to 7.4. Human serum was isolated from fresh human blood and diluted with saline in a 1:4 ratio (serum:saline). The 1000 molar excess solution of Cys or His was prepared according to the estimate that the concentration of a peptide spot on the array is approximately 4.19μmol. The Cys and His were dissolved in PBS buffer and adjusted to pH 7.4. Immersion of the $[^{99m}Tc(CO)_3]^+$ labelled His-Tagged Celluspot™ peptide array in 50ml of either the PBS buffer, serum or Cys/His rich solutions was carried out for 60 minutes at 37°C with gentle shaking. The array was removed from the solutions, washed for 3 seconds in 50 ml of PBS buffer and padded dry with filter paper. Exposure to the phosphor film occurred for 5 minutes before an image was generated and analysed with OptiQuant software as described above. The arrays were re-immersed into their specific solutions and the process of obtaining an image was repeated after a total incubation time of 2 hrs and 24 hrs for the PBS buffer and human serum and 3 hrs for the Cys and His containing solution. At 3 hrs and 24 hrs the arrays were exposed to the film for 10 mins and 30 mins respectively in order to sufficiently detect the $[^{99m}Tc(CO)_3]^+$ bound to the peptides after radioactive decay. For each of the stability tests, PBS buffer, human serum and His or Cys rich solutions, the results are reported as n=2 (1 array with 2 peptides).

For the stability analysis of the $[^{99m}Tc(CO)_3$-peptide$]^+$ conjugates the DLU for each peptide on the Celluspot™ peptide array post incubation with the washing buffers are compared with the DLU of each peptide at the end of the 120 minute radiolabelling period. This effectively converts the yields at the start of the stability analysis to 100% regardless of the degree of radiolabelling of each peptide and makes interpretation of the stability data simpler. In order to account for the radioactivity decay, the background activity on the

Celluspot™ at each time point of the stability analysis was compared with the background activity at the start of the stability analysis (i.e. the phosphor image after 120min incubation with $[^{99m}Tc(CO)_3]^+$) and this was factored into the calculation of DLU for each peptide spot.

3.3.3.2 $[^{99m}Tc(CO)_3]^+$ Labelling in Citrate Buffer at pH 5.5 and Tris-HCl Buffer at pH 7.4 and 8.8.

The same procedure was used as is reported above for the $[^{99m}Tc(CO)_3]^+$ labelling of the His-Tagged Celluspot™ peptide array in PBS buffer. Instead of PBS buffer, the arrays were fully immersed in either a solution of citrate buffer at pH 5.5 or Tris-HCl buffer at pH 8.8 or pH 7.4. Images were generated at the 15, 30, 60, 90 and 120 minute total incubation time points. After 120 minutes incubation, the stability of the $[^{99m}Tc(CO)_3]^+$ labelled peptides was assessed in the respective buffers for 3 hours. All results are reported for n=2 (1 slide with 2 arrays).

3.3.3.3 Data Analysis of the $[^{99m}Tc(CO)_3]^+$ Radiolabelled His-Tagged Celluspot™ peptide Arrays

Image processing was done using the Opti-quant programme associated with the phosphor imager. A grid was placed around the image with each square surrounding a single spot. The intensity of each black spot was then recorded as a DLU (digital light unit), an arbitrary unit that can be associated with radiochemical yield. The radiochemical yield values were reproducible for a given exposure time and activity. When more than one slide was used for the same data, it was necessary to compare the background activity of both slides and factor the difference into the calculation of DLU for each peptide spot.Once the radiochemical yields had been collected, two tailed tests (T TEST) were performed on the data collected to evaluate the significant difference in radiochemical yield between specific peptides and generate p values.

3.3.4 RESULTS A: $[^{99m}Tc(CO)_3]^+$ Labelling in PBS Buffer pH7.4

Through radiolabelling the trial STKS-1 Celluspot^{TM} peptide arrays, it has already been established (Chapter3.1) that His residues are required for $[^{99m}Tc(CO)_3]^+$ coordination. From these earlier data $^{99m}TcO_4^-$ it is clear that does not bind to the peptide sequences or to the array substrate surface and there appears to be a correlation between sequences with a high pI and a high labelling efficiency. Images generated from the phosphor imager had sufficient resolution to be able to detect the individually bound peptide sequences and generate a DLU value from the intensity of the black spots on the plate surface. Figure 3.3-3 displays the images generated from the $[^{99m}Tc(CO)_3]^+$ radiolabelled His-Tagged Celluspot^{TM} array post 15, 30, 60 and 120 minute total incubation time. Visually it is possible to see that over time the radiochemical yield of the peptide sequences increases so that by 120 minutes the majority of peptides appear as a black spot on the array and have therefore coordinated to the $[^{99m}Tc(CO)_3]^+$ complex. Isolating each black spot on a grid as an individual square enabled a DLU value to be assigned to the individual peptide sequences. The DLU value is associated with the labelling efficiency of the peptide and was used as a comparative marker. Radiolabelling experiments of the His-Tagged Celluspot^{TM} array in PBS buffer were performed on 3 separate arrays to give n=6, increasing the consistency and reliability of the results.

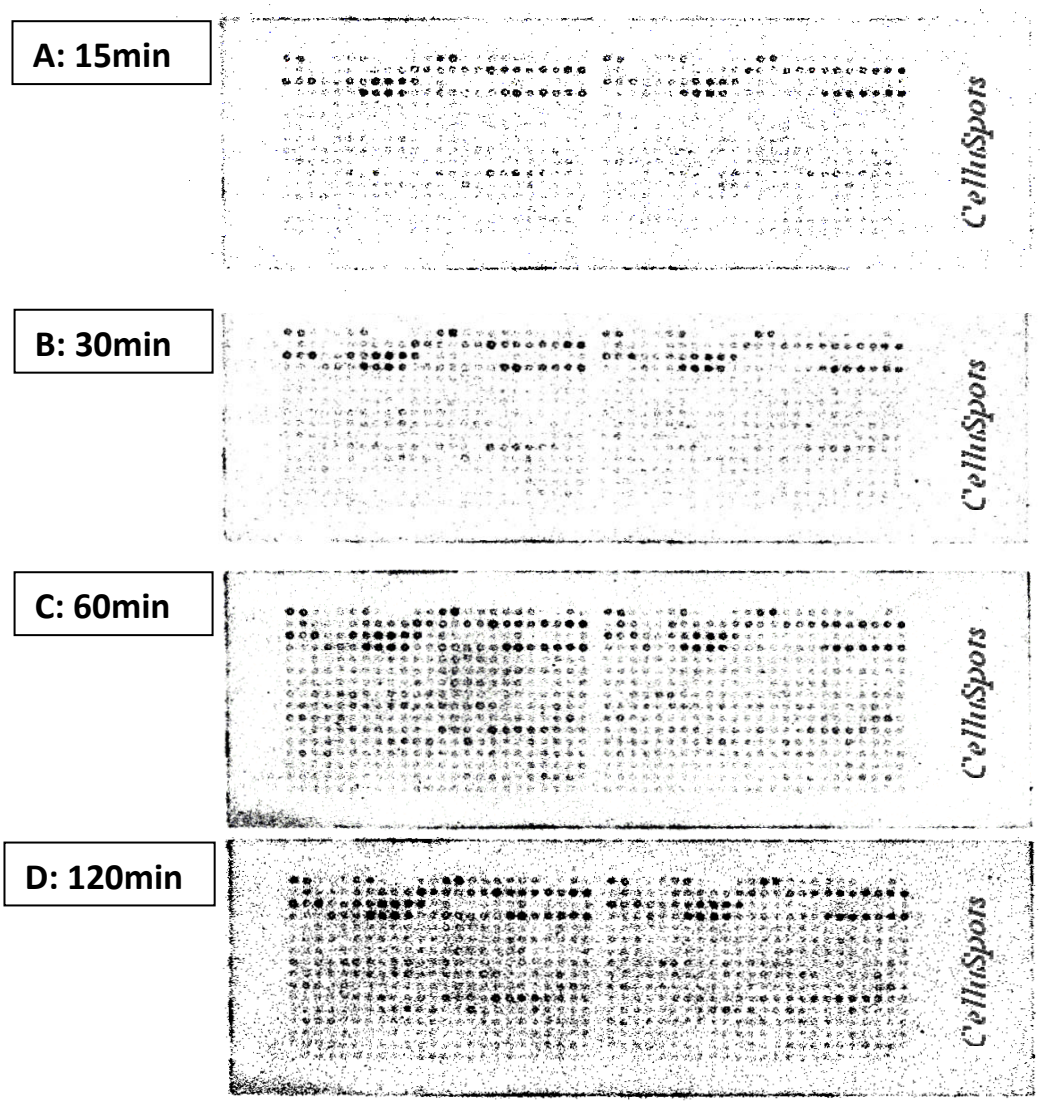

Figure 3.3- 2. Phosphor image of the $[^{99m}Tc(CO)_3]^+$ radiolabelled His-Tagged Celluspot™ peptide array. Each black spot represents a peptide sequence. **A)** Image after 15 minutes total incubation time, **B)** Image after 30 minute total incubation time, **C)** Image after 60 minute total incubation time and **D)** Image after 120 minute incubation time.

The aim of experiments with the His-Tagged Celluspot™ peptide array was to identify features that improve the labelling kinetics of peptide sequences with $[^{99m}Tc(CO)_3]^+$ and to ultimately minimise the time required for the $[^{99m}Tc(CO)_3]^+$ labelling of proteins, maximise specific activity, site specificity and labelling efficiency and minimise the rate of loss of radiolabel under simulated biological conditions. The phosphor images generated after 15 minutes incubation (the shortest) reveal the peptide sequences most suitable for

applications in protein labelling. Although several later time points were evaluated, the most importance is attached to the data obtained from the 15 minute time point.

3.3.4.1 Is there a Good Correlation between Radiolabelling in Solution and on Solid Phase?

For protein labelling the peptide sequences will be in solution whereas the sequences on the His-Tagged Celluspot™ array are attached to a solid phase; they are conjugated to the array surface. In Chapter 2, 10 peptide sequences were analysed in solution that contain His-Tag analogues and for each analogue the sequence was synthesised with and without an adjacent Cys residue. These 10 peptide sequences were also included on the His-Tagged Celluspot™ peptide array. Consequently, a direct comparison between the radiochemical yield of these sequences in solution (Chapter 2) and on solid phase will clarify whether there is a good correlation between the labelling in the different situations. Results confirm that there is an excellent correlation between the radiochemical yield of the peptides in solution and on solid phase at the 15, 30, 60 and 120 mins time points. The R2 values are 0.9129, 0.9287, 0.9303 and 0.902 for the 15, 30, 60 and 120 mins incubation times respectively (Figure 3.1-4). Therefore, the labelling efficiencies generated through analysis of the $[^{99m}Tc(CO)_3]^+$ labelled His-Tagged Celluspot™ array can be considered as providing an accurate prediction of the labelling in solution.

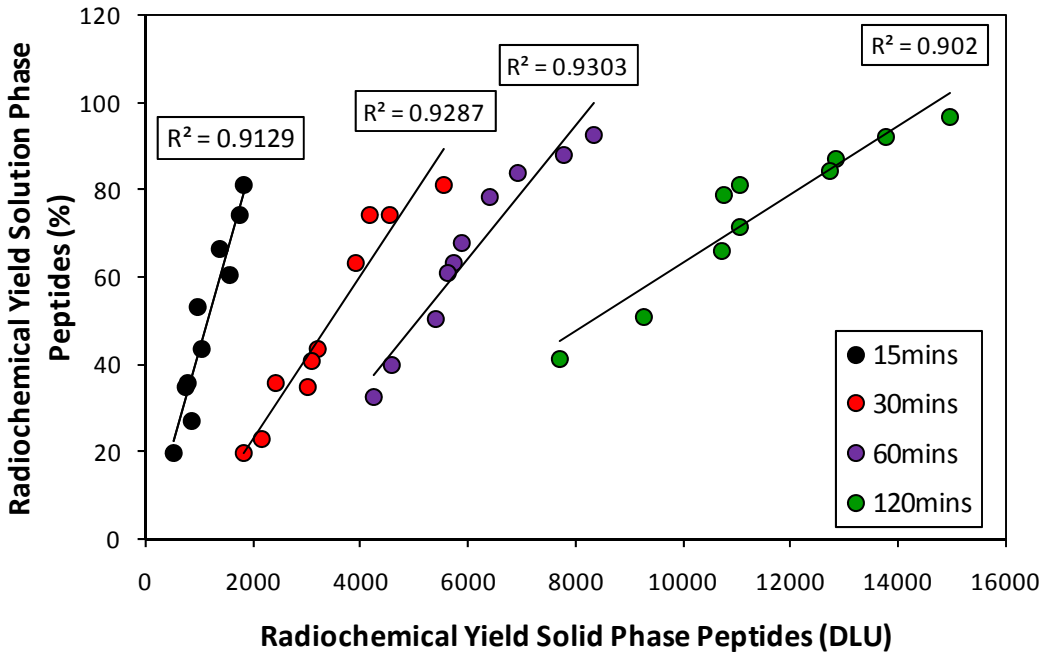

Figure 3.3- 3 Correlation between the radiochemical yield of the Cys/His Tag peptide sequence (Chapter 2) in solution and on solid phase after 15, 30, 60 and 120mins incubation with $[^{99m}Tc(CO)_3]^+$.

3.3.4.2 What is the Influence of the Positively Charged Amino Acids?

The analysis of the His-Tagged Celluspot™ array will coincide with the questions asked during the design of the array in Chapter 3.2. Looking at the phosphor image obtained after 15 minutes incubation time, it is evident that some peptide sequences demonstrate superior reaction kinetics for radiolabelling with $[^{99m}Tc(CO)_3]^+$. Figure 3.3-5 highlights these peptide spots on the array image with green circles. Plotting the radiochemical yield (DLU) of all peptide sequences from the His-Tagged Celluspot™ array confirms this observation and clearly identifies the sequences that contain positively charged amino acids to be the ones that have the highest rate of labelling. (Figure 3.3-6). The peptide sequences have been placed into categories (Section 3.2) according to the characteristic features of the amino acids that surround the His residues and the arrangement of these amino acids with regards to the His residues. The categories have been explained in Chapter 3.2.

In the graph (Figure 3.3-6), the importance of positively charged amino acids is demonstrated by the substantial difference in radiochemical yield of the peptides in the "Positively Charged Amino Acids → Arg, Lys" (purple) category in comparison to the majority of other peptides present on the array surface. In the "Positively Charged Amino

Acids → Arg, Lys" category all amino acids have at least 2 Lys or Arg residues with a maximum of 4 Arg or 4 Lys residues.

The extent to which the positively charged amino acids improve the labelling efficiency is highlighted when comparing to the labelling of the 10 peptide sequences from Chapter 2 (Cys/His-Tag peptides). Chapter 2, CKLAAALEHHHHHH (Cys/$(His)_6$-Tag) was identified as the peptide demonstrating superior labelling efficiency for $[M(CO)_3]^+$ complexes. According to the results in figure 3.3-6, all sequences within the "Positively Charged Amino Acid → Arg, Lys" category have a higher radiochemical yield than the Cys/$(His)_6$ Tagged sequence (black category). A black horizontal line on the graph (figure 3.3-6) draws attention to the difference in radiochemical yield between the Cys/$(His)_6$-Tagged peptides and the positively charged peptides.

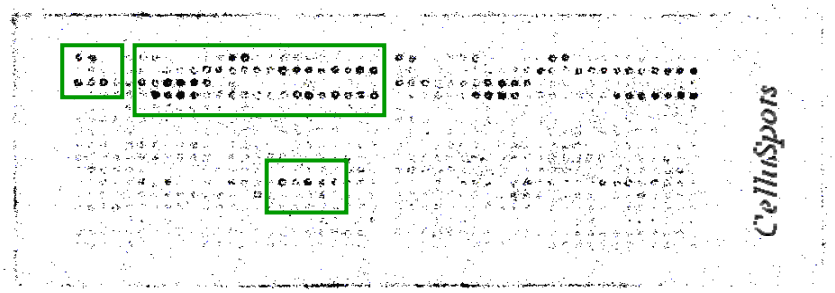

Figure 3.3- 4 Phosphor image of the $[^{99m}Tc(CO)_3]^+$ radiolabelled His-Tagged Celluspot™ array after 15 minute incubation time. **Green Boxes:** Highlights the peptide spots with the superior labelling efficiency on the left hand side of the plate. The right hand side is an identical copy of the sequences on the left hand side.

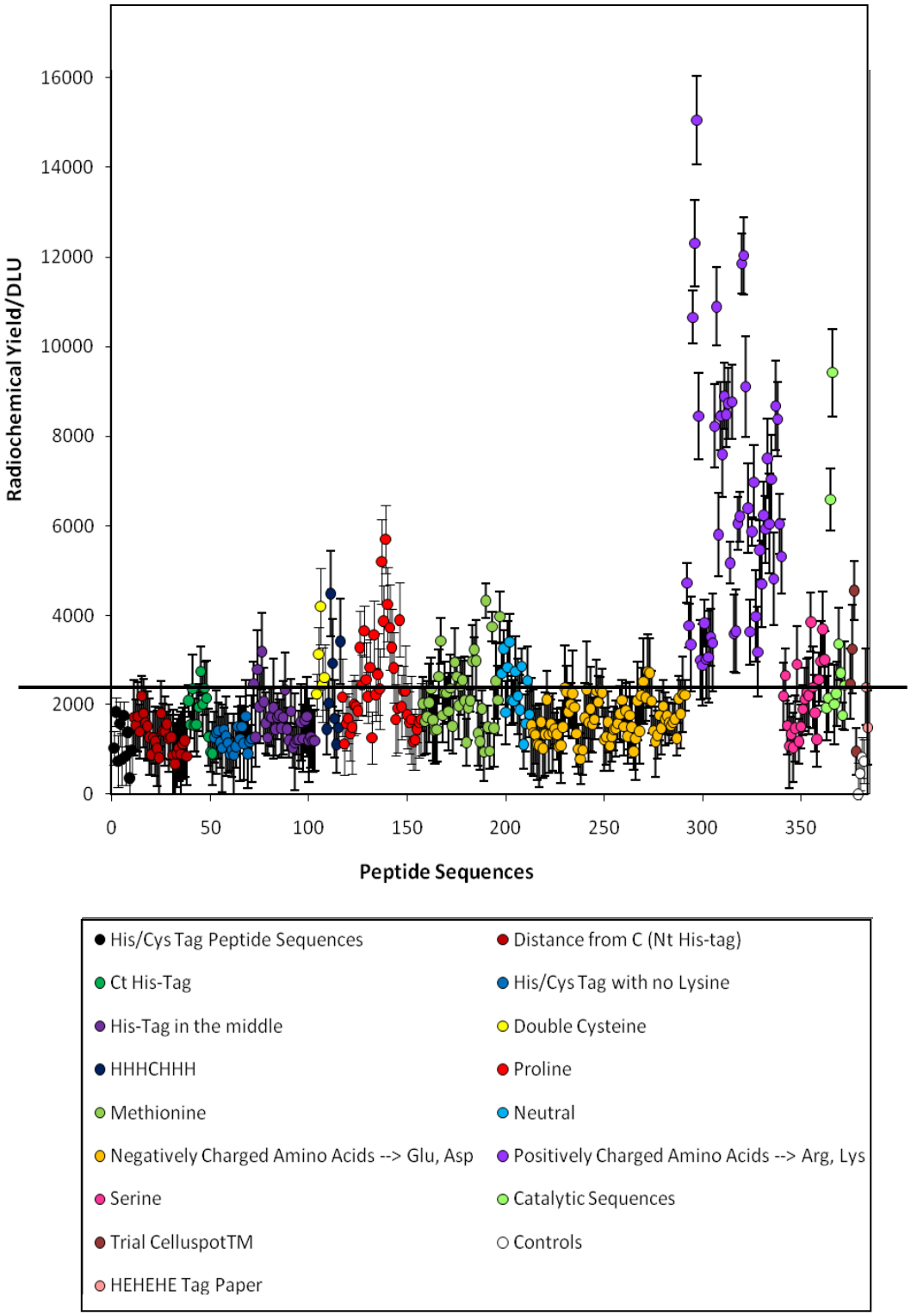

Figure 3.3- 5. Radiochemical yield of all 384 peptides on the Celluspot^{TM} peptide array post radiolabelling with $[^{99m}Tc(CO)_3]^+$ after 15 minutes incubation time in PBS at pH 7.4. Results and standard deviations are calculated based on 6 sets of data. The peptide are categorised according to their characteristic features of the amino acids that surround the His residues and the arrangement of these amino acids with regards to the His residues. The black horizontal line on the graph emphasises the clear boundary between the His/Cys Tag Peptides analysed in Chapter 2 (**black category)** and the peptides containing 2 or more Arg/Lys residues (**purple category).**

Images generated from the phosphor imager of the His-Tagged Celluspot™ peptide array after incubation with $[^{99m}Tc(CO)_3]^+$ for a total of 30, 60 and 120 minutes can be seen in Figure 3.3-3. At a first glance it is apparent that over time the radiochemical yield of the peptide sequences increases so that by 120 minutes all peptides appear as a black spot on the array and therefore have all to some extent coordinated to the $[^{99m}Tc(CO)_3]^+$ complex. As previously carried out for the images at 15 minute time points, the black spots were isolated on a grid as individual squares and a DLU value obtained for each spot which represents the labelling efficiency of the corresponding peptide sequence. Data for the 30, 60 and 120 minute time points was also acquired on 3 separate arrays to give n=6 and standardised against each other according to the background DLU values.

3.3.4.3 What is the influence of the positively charged amino acids at 30, 60 and 120 mins?

Comparisons between the radiochemical yields of all sequences at 15, 30, 60 and 120 minute total incubation times demonstrates that nothing particularly changes in the labelling efficiency trend. (figure 3.3-21) The sequences in the "positively charged amino acid → Arg, Lys" (purple) category remain as those that have the highest labelling efficiencies throughout the 2 hours of incubation with $[^{99m}Tc(CO)_3]^+$. In addition there are 2 sequences in the "Catalytic Sequences" (mint green) category that continue to show an equally as high radiochemical yield as that of the purple category throughout the incubation period. These two sequences have a HHHHHHGRCRG and RCRGHHHHHHGRCR composition and pI values of 10.35 and 11.35 respectively. These graphs (figure 3.3-21) highlight the importance of positively charged amino acids in improving the labelling efficiency of the $(His)_6$-Tag. There is an increase in the radiochemical yield of the majority of other sequences over time and by 120 mins all sequences containing His residues have demonstrated some coordination to $[^{99m}Tc(CO)_3]^+$. Radiochemical yields at all time points have been presented on the same scale. The differences in radiochemical yields for the sequences containing positively charged amino acids are not as significant after 120 minutes. The four sequences having the lowest radiochemical yields correspond to the peptides in the "Controls" (white) category. Here the spots on the array either contain no peptides or peptides with no His residues.

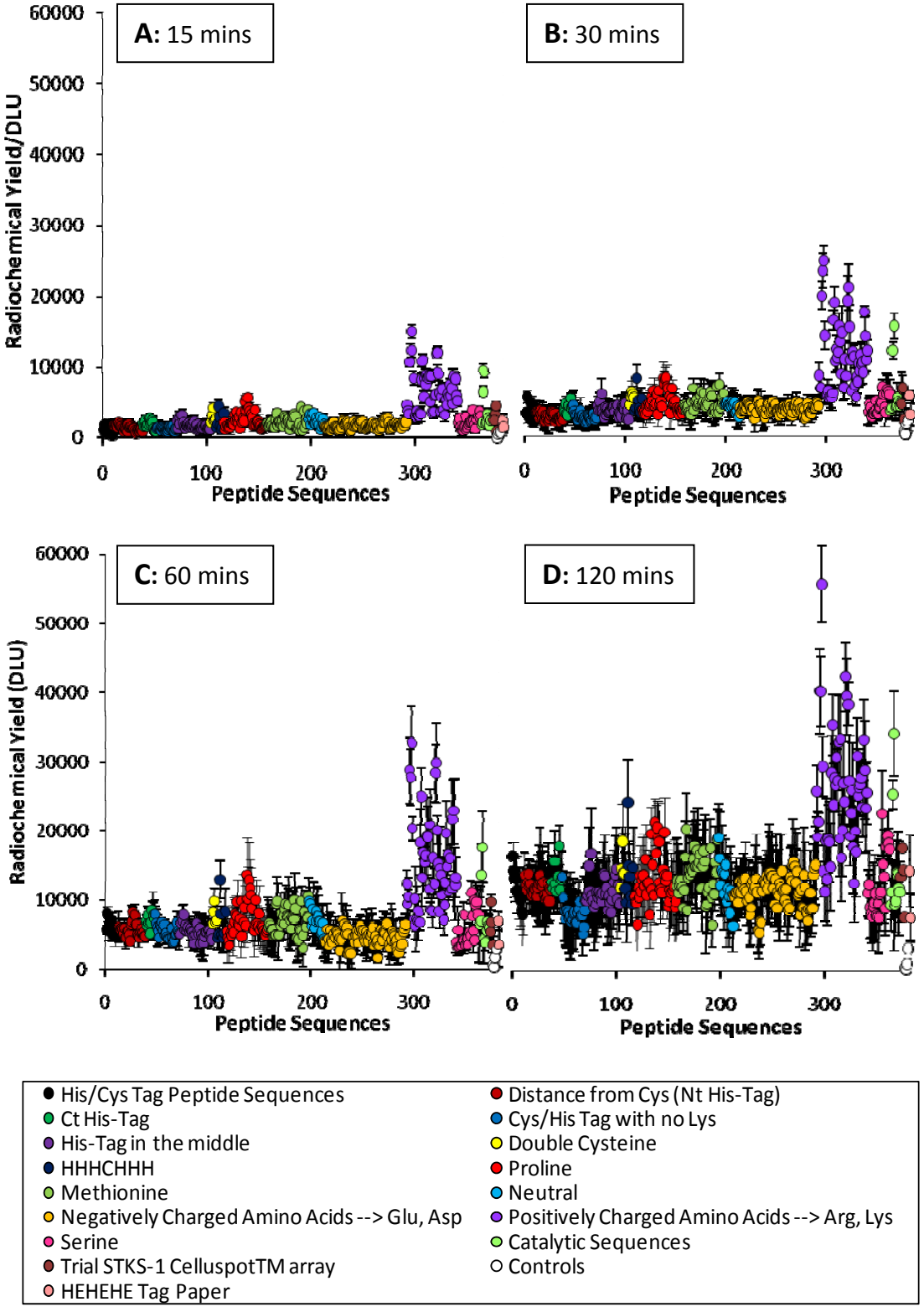

Figure 3.1-21. Radiochemical yield of all 384 peptides on the His-Tagged Celluspot™ peptide array post radiolabelling with $[^{99m}Tc(CO)_3]^+$ in PBS at pH 7.4. Results and standard deviations are calculated based on 6 sets of data. Peptides are categorised according to their characteristics and these categories are listed in the legend (a summary can be seen in Chapter 3.2). **A)** After 15mins incubation time, **B)** after 30mins incubation time, **C)** after 60mins incubation time, **D)** after 120mins incubation time.

3.3.4.4 Positively Charged Amino Acids VS Negatively Charged Amino Acids?

To further evaluate the influence of the positively charged amino acids on the radiolabelling of the His containing peptides with $[^{99m}Tc(CO)_3]^+$ complexes, a comparison between the labelling of peptide sequences with multiple negatively charged amino acids and positively charged amino acids has been made (Figure 3.3-7). In figure 3.3-7 there are 78 sequences in the negatively charged amino acid group in which a mixture of Glu and Asp amino acids, pka 4.15 and 3.71 respectively, are included and surround the His residues. Each sequence contains at least 2 negatively charged amino acids and a maximum of 4 in combination with a nearby generic His-Tag (HHHHHH) or His residues arranged as XHXHXHX, XHHHXHHHX, XHXHX and XHXXH where X is either Glu or Asp. In the positively charged amino acid category there are 49 sequences that contain a mixture of Lys and Arg amino acids, pKa of 10.67 and 12.10 respectively, surrounding the His residues. Similarly, each sequence contains between 2-4 positively charged amino acids in combination with a nearby generic His-Tag (HHHHHH) or His residues arranged as XHXHXHX, XHHHXHHHX, XHXHX and XHXXH where X is either Arg or Lys. The average pI for the negatively charged and positively charged sequences compared in Figure 3.3-7 are 5.4 and 11.1 respectively, which demonstrates the influence of the Arg or Lys and Glu or Asp on the overall charge of the peptide sequence. From the graph, a significant difference, $p<0.005$, can be observed between the average labelling efficiency of the sequences containing negatively charged amino acids and those with positively charged amino acids. In addition, there is no overlap between the radiochemical yields of the sequences containing multiple positively charged amino acids or negatively charged amino acids. The highest radiochemical yield of the Glu/Asp sequences is lower than the lowest radiochemical yield of the Arg/Lys sequences.

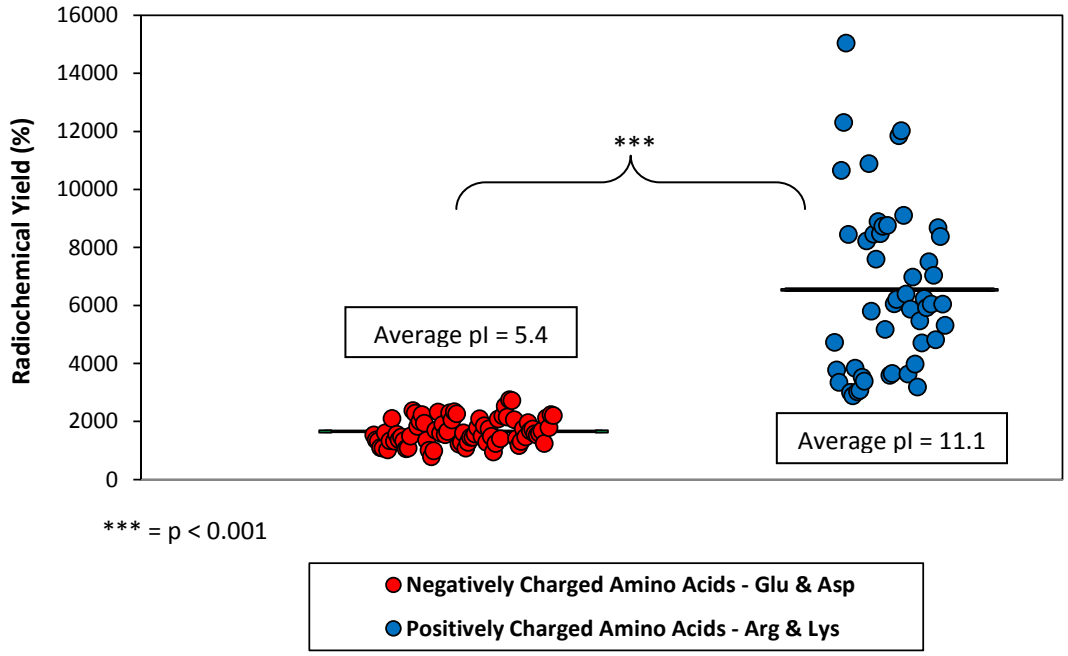

Figure 3.3- 6 Comparison between the $[^{99m}Tc(CO)_3]^+$ radiolabelling of peptide sequences with multiple negatively charged amino acids and positively charged amino acids. Sequences include at least 2 negatively charged amino acids (Glu and/or Asp) or 2 positively charged amino acids (Arg and/or Lys). The black lines represent the average radiochemical yield for both the negatively charged amino acid sequences and positively charged amino acid sequences.

The superiority of sequences containing basic amino acids for improved labelling efficiency is emphasised in Figure 3.3-8 in which a direct comparison has been made between 7 different peptide sequences with a single amino acid substituted for either Glu or Arg. For all sequences when an Arg is present there is a significantly higher radiochemical yield with $p<0.001$ (***) for 5 sequences and $p<0.01$ (**) for the other 2 sequences.

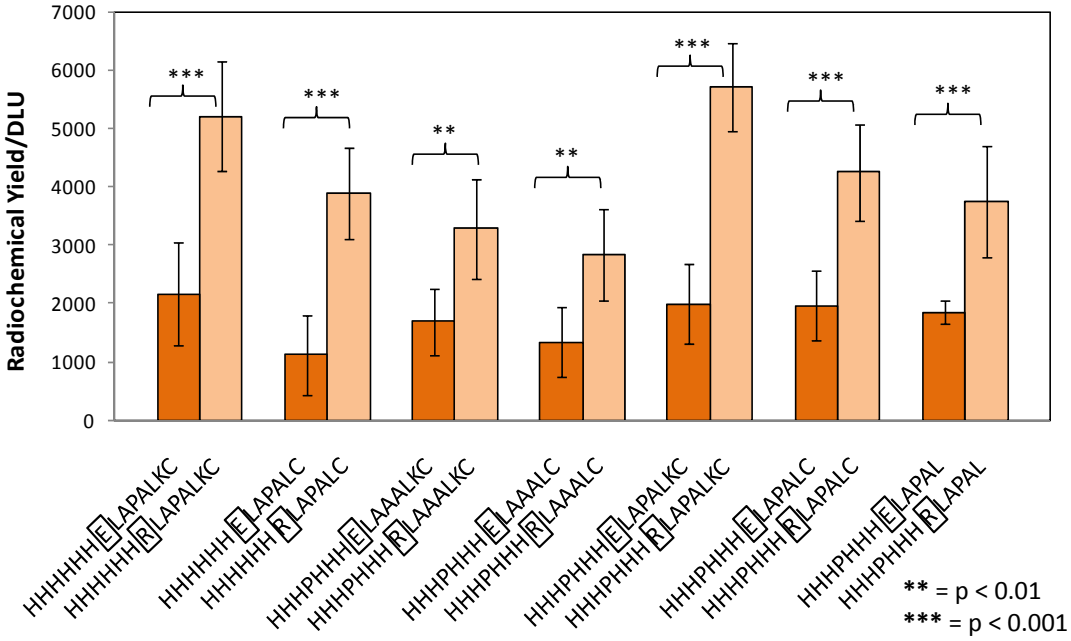

Figure 3.3- 7. Comparison between the radiochemical yield of Glu and Arg containing sequences. A single amino acid has been changed at an identical position within the sequences.

In addition to positively charged amino acids having a positive impact on the labelling of His residues, it is also possible to say that negatively charged amino acids are detrimental to the labelling of His containing sequence with $[M(CO)_3]^+$ complexes in comparison to the sequences containing neutrally charged amino acids and have a pI nearer to 7. This has been demonstrated in a set of graphs that focus on the influence of a single amino acid within a sequence to compare direct effects on the labelling of the His residues (Figure 3.6-9). The amino acids that are varied include Glu, Asp, Lys, Arg, Ser and Gly. Of these, Asp and Lys are basic and positively charged, Glu and Asp are acidic and negatively charged, Gly is a flexible neutrally charged amino acid and Ser is a small nucleophilic amino acid also neutrally charged at physiological pH 7.4. In all the 6 different sequences analysed in figure 3.6-8, Glu and Asp have the lowest labelling even in comparison to the neutrally charged Gly and Ser residues. The Arg and Lys containing sequences have a radiochemical yield significantly higher than the neutrally charged Gly and Ser sequences in addition to the acidic Glu and Asp sequences, $p<0.001$. These graphs evidently demonstrate the considerable influence a single amino acid can have on the labelling efficiency of His residues with $[^{99m}Tc(CO)_3]^+$.

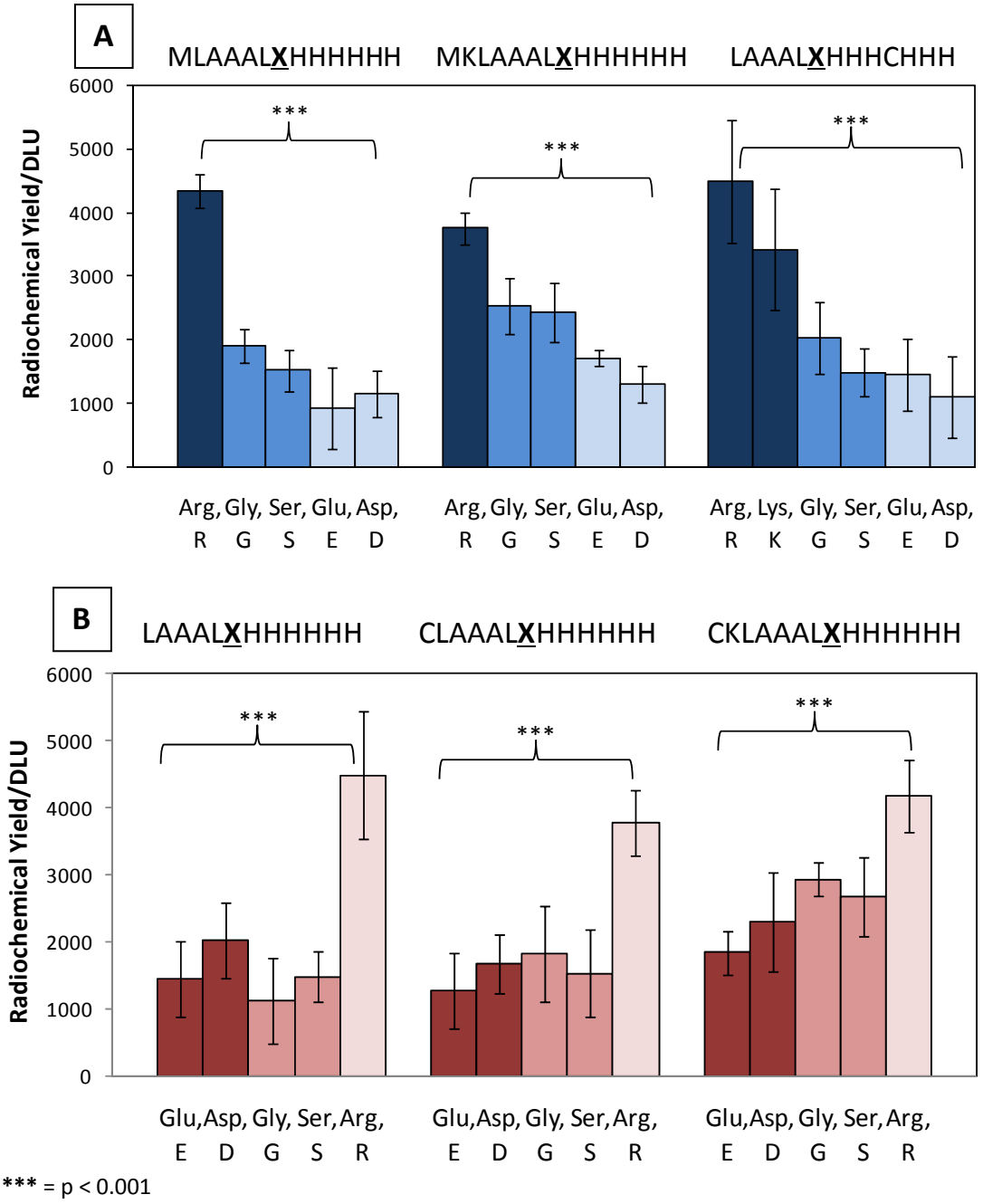

*** = $p < 0.001$

Figure 3.3- 8 Comparison between the radiochemical yield of labelling sequences containing an Arg, Lys, Gly, Ser, Glu and Asp amino acids. A single amino acid has been replaced in the 'X' position within each sequence **A:** MLAAALXHHHHHH, MKLAAALXHHHHHH and LAAALXHHHCHHH sequences, **B:** LAAALXHHHHHH, CLAAALXHHHHHH, CKLAAALXHHHHHH sequences.

3.3.4.5 What is the Correlation between pI and Labelling Efficiencies?

Coinciding with the results already observed, peptide sequences with a high pI also show remarkably enhanced labelling efficiencies for the $[^{99m}Tc(CO)_3]^+$ complex. pI is the pH at

which a protein carries no net charge and is largely influenced by the presence of amino acids with electrically charged side chains such as Glu, Asp, Arg and Lys. A peptide sequence at a pH below its pI will carry a net positive charge and above its pI a net negative charge. The presence of positively charged amino acids in a sequence will increase the pI and therefore a high pI is also associated with a high radiochemical yield. In figure 3.3-10 there are 5 graphs in which pI has been plotted against radiochemical yields of peptide sequences that have a His-Tag (HHHHHH), an abbreviated His-Tag (HHHH), 3 His residues with an alternate spacer (HXHXHX), 2 His residues with an alternate spacer (HXHX) and 2 His with 2 spacers (HXXH). His residues coordinate the $[^{99m}Tc(CO)_3]^+$ and therefore when analysing the effect of pI on the labelling efficiency, comparisons were made between sequences that contained the same number and positioning of His residues.

In every graph there is a positive correlation between sequences with a high pI and a high radiochemical yield. A more dramatic increase in radiochemical yield is observed for sequences with a pI > 9.5 which results in a slight exponential relationship between pI and radiochemical yield. On the graphs a black dotted line represents a pI of 9.5. There are a limited number of sequences in the array with an abbreviated His-Tag (HHHH) and of these peptides the highest pI is only 8.5 (Graph B – Figure 3.3-10). As a consequence, it is difficult to observe the exponential relationship between pI and radiochemical yield in graph B (Figure 3.3-10) as the data do not exist for peptides with a HHHH Tag and a pI value in the region demonstrating greatest radiochemical yield i.e > 9. Not all peptide sequences coincide with the trend that a pI > 9.5 corresponds to an increase in radiochemical yield. In graph A and C, figure 3.3-10, it is possible to see peptides with a pI of 11 and 12 respectively that demonstrate a lower radiochemical yield than expected when comparing to other sequences of a similar pI.

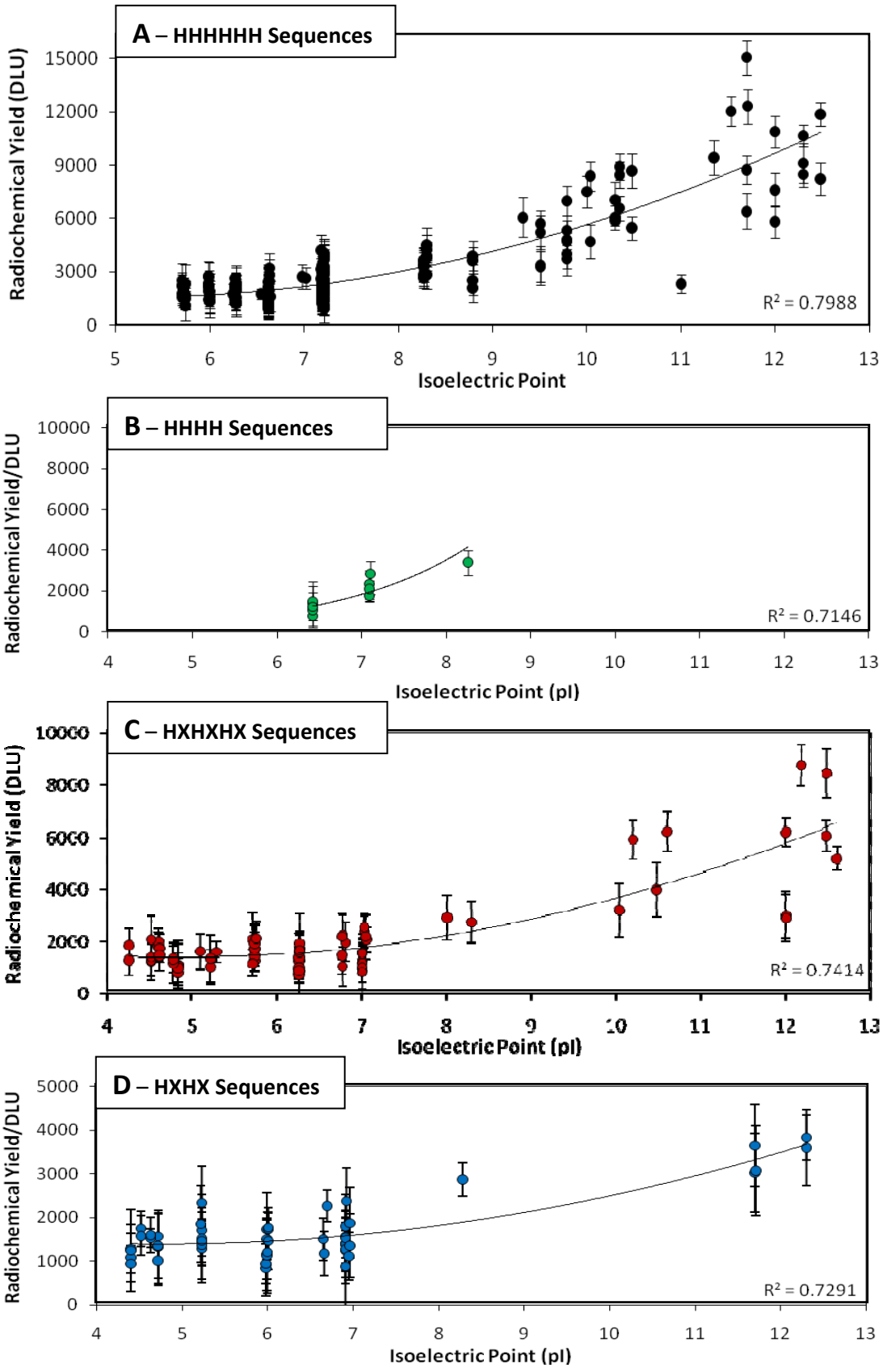
A – HHHHHH Sequences
Radiochemical Yield (DLU)
15000
12000
9000
6000
3000
0
5
6
7
8
9
10
11
12
13
Isoelectric Point
R² = 0.7988
B – HHHH Sequences
Radiochemical Yield/DLU
10000
8000
6000
4000
2000
0
4
5
6
7
8
9
10
11
12
13
Isoelectric Point (pI)
R² = 0.7146
C – HXHXHX Sequences
Radiochemical Yield (DLU)
10000
8000
6000
4000
2000
0
4
5
6
7
8
9
10
11
12
13
Isoelectric Point (pI)
R² = 0.7414
D – HXHX Sequences
Radiochemical Yield/DLU
5000
4000
3000
2000
1000
0
4
5
6
7
8
9
10
11
12
13
Isoelectric Point (pI)
R² = 0.7291

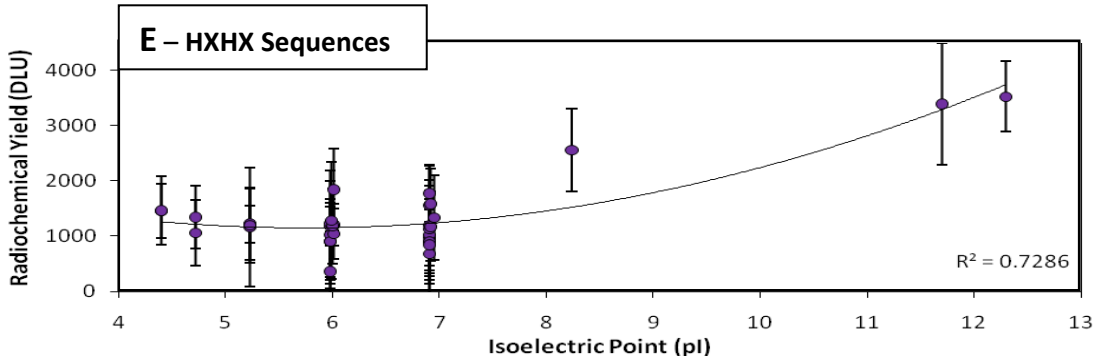

Figure 3.3- 9. A comparison between the radiochemical yield and pI of the peptide sequences. Graphs have been plotted according to the number and position of His residues included in the peptide sequences. Radiochemical yield has been plotted against pI for peptide sequences with: **A)** 6 His residues, HHHHHH; **B)** 4 His residues, HHHH; **C)** 3 His residues in a HXHXHX motif; **D)** 2 His residues in a HXHX motif; and, **E)** 2 His residues in a HXXH motif.

3.3.4.6 How many Positively Charged Residues are Required?

The above sections establish that for the most efficient and fastest radiolabelling with $[^{99m}Tc(CO)_3]^+$, peptide sequences require a high pI which corresponds with the presence of positively charged amino acids near the His residues. Present on the His-tagged Celluspot™ peptide array are sequences that contain between 1 and 4 Arg or Lys residues in combination with a standard His-Tag, 6 consecutive His residues (HHHHHH). Analysis of the data reveals that to obtain a pI greater than 9.5 and hence a fast labelling efficiency, between 2-4 Arg residues or 3-4 Lys residues are required within the sequence. For Arg-containing sequences, figure 3.3-11 demonstrates that there is an increase in pI and radiochemical yield with the number of Arg residues present in the sequence. However, the most significant increase in radiochemical yield is between peptides containing 1 or 2 Arg residues where $p<0.001$ (Graph A – Figure 3.3-11). Also, peptide sequences with 2 Arg residues have an average pI of 11.01 which is greater than the requisite pI of 9.5 (Graph B – Figure 3.3-11). Increasing the number of Arg residues to 3 or 4 within the sequence does not substantially increase the radiochemical yield or the pI. Consequently it appears that the minimum number of Arg residues required for an efficient labelling sequence is 2.

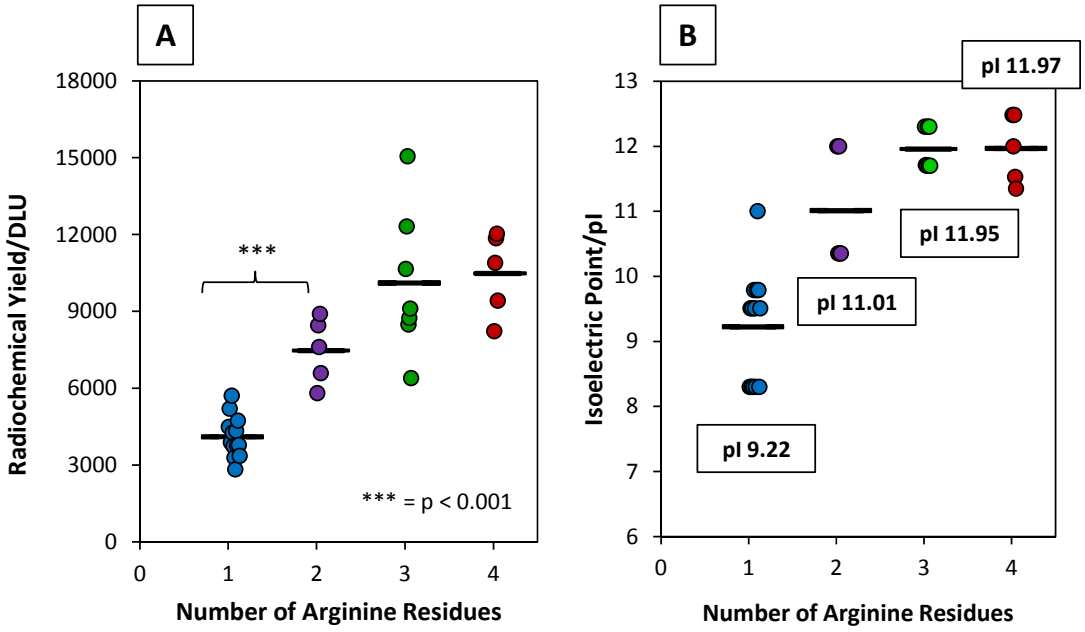

Figure 3.3- 11. Number of Arg residues within a peptide sequence plotted against the radiochemical yield of the sequence (**A**) and pI (**B**). All sequences include a His-Tag, HHHHHH and the Arg are positioned on either side of the $(His)_6$-Tag, both sides of the $(His)_6$-Tag or in between the His residues.

Similarly, for Lys containing sequences, the pI and radiochemical yield of the peptides increases with the number of Lys residues present in the sequence. Lys has a side chain with a lower pKa value than Arg and therefore more Lys residues are needed in the sequence to give an equivalent pI to that of the Arg containing sequences. This is evident in Figure 3.3-12 where a significant difference in radiochemical yield is now observed between sequences containing 2 and 3 Lys residues. In addition, in order to have a pI greater than 9.5 a minimum of 3 Lys residues must be included in the sequence. Increasing the number of Lys residues to 4 does not greatly increase the radiochemical yield or pI. As a result, the minimum number of Lys residues required for an efficient labelling sequence is 3.

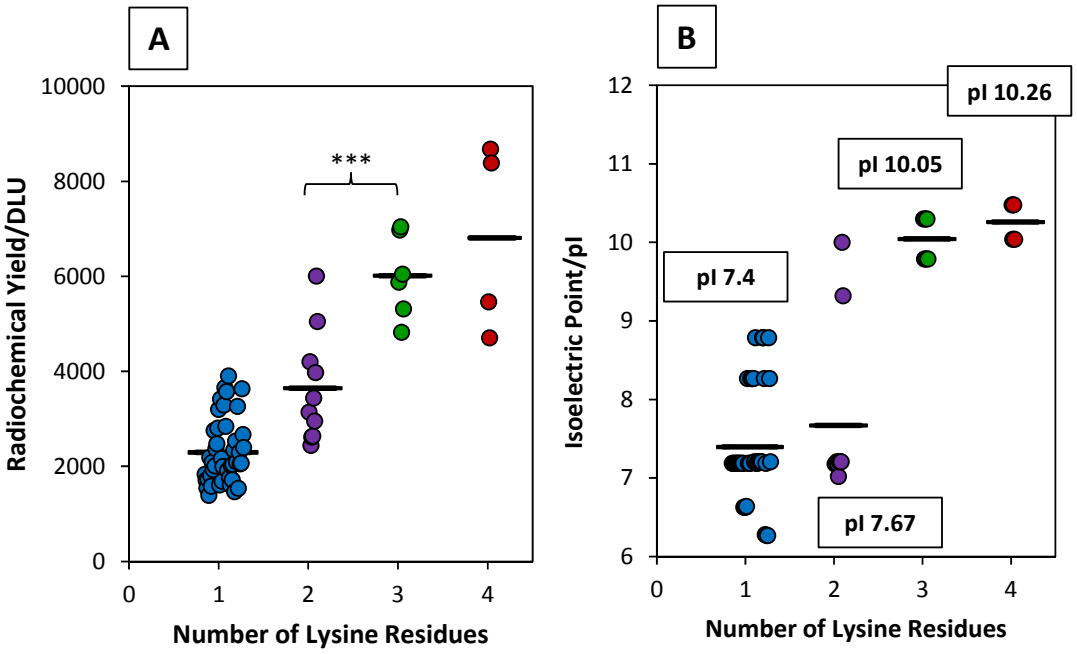

Figure 3.3- 12. Number of Lys residues within a peptide sequence plotted against the radiochemical yield of the sequence (**A**) and pI (**B**). All sequences include a His-Tag, HHHHHH and the Lys are positioned: on either side of the $(His)_6$-Tag, both sides of the $(His)_6$-Tag or in between the His residues.

The combined data, Figure 3.3-13, for the Arg and Lys containing peptide sequences plotted against pI and radiochemical yield clearly highlights that Arg is on average more positively charged and has a greater influence on the increase of pI and subsequently the radiochemical yield of a peptide. More Lys residues are required in the labelling sequence to compensate for the lower pka and to equal the same labelling ability as the Arg containing sequences.

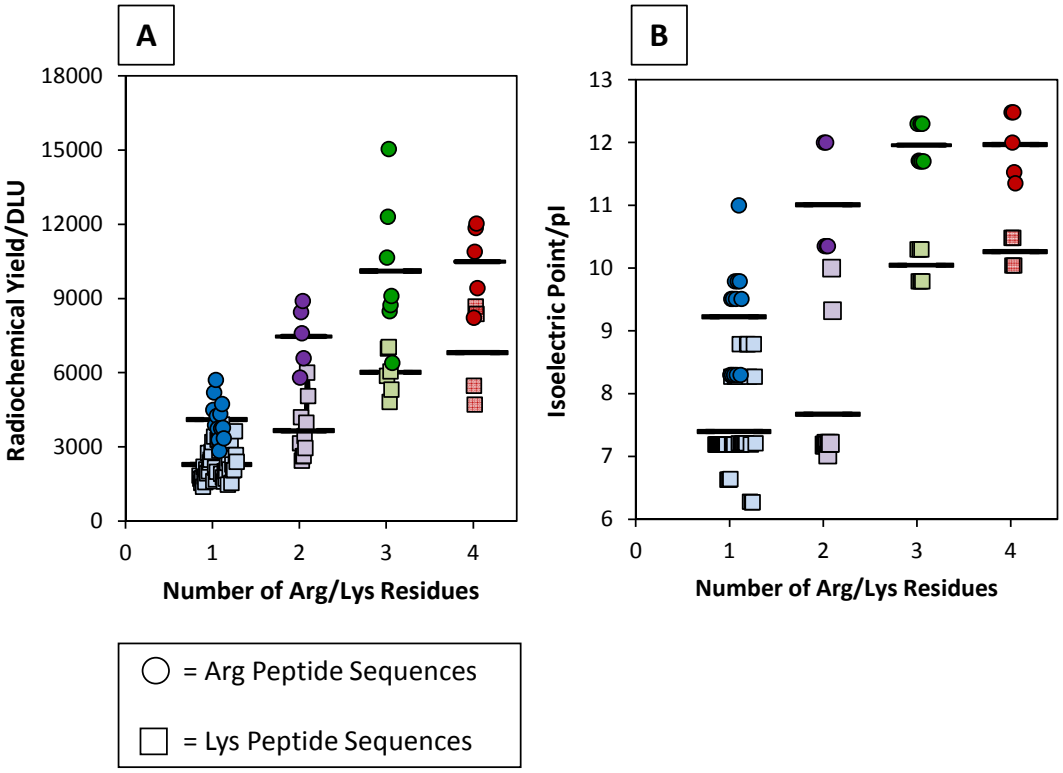

Figure 3.3- 13. Combined data for the number of Lys and Arg residues within a peptide sequence plotted against the radiochemical yield of the sequence (**A**) and pI (**B**). Arg containing sequences are better than Lys containing sequences at improving radiochemical yield. All sequences include a $(His)_6$-Tag, HHHHHH.

3.3.4.7 What is the Optimum Position of the Arg Residues in Relation to His?

Further evaluation on the influence of Arg focused on the preferred position of the Arg residues in relation to the His. Within the His-Tagged Celluspot™ array, there are many different varieties of sequences containing Arg residues. The sequences have been separated into three broad categories that have included: i) His-Tags with Arg residues in combination with other amino acids (X) positioned on one side e.g. HHHHHH-$(Arg/X)_{seq}$; ii) His-Tags with Arg residues in combination with other amino acids (X) positioned on both sides e.g. $(Arg/X)_{seq}$-HHHHHH-$(Arg/X)_{seq}$; iii) His residues with Arg inserted into the sequence of histidines e.g. HRHRHR-$(X)_{seq}$, HRHR-$(X)_{seq}$ and RHRRHR-$(X)_{seq}$. (Figure 3.3-14). Analysing the labelling efficiency of Arg containing sequences based on these principles identified sequences with Arg residues separating the His amino acids and a reduced number of His amino acids as being unfavourable for $[^{99m}Tc(CO)_3]^+$ coordination. The HRHRHR-$(X)_{seq}$, HRHR-$(X)_{seq}$ and RHRRHR-$(X)_{seq}$ sequences demonstrated the lowest

radiochemical yields. Sequences with 2 His amino acids separated by Arg are least favourable. The preferred labelling sequence according to figure 3.3-14 features the HHHHHHXXRRR motif. However, it is difficult to obtain any further information with regards to the positional arrangement of Arg when surrounding a $(His)_6$-Tag e.g. for the HHHHHH-$(Arg/X)_{seq}$ and $(Arg/X)_{seq}$-HHHHHH-$(Arg/X)_{seq}$ sequences. These sequences all have relatively similar labelling efficiencies.

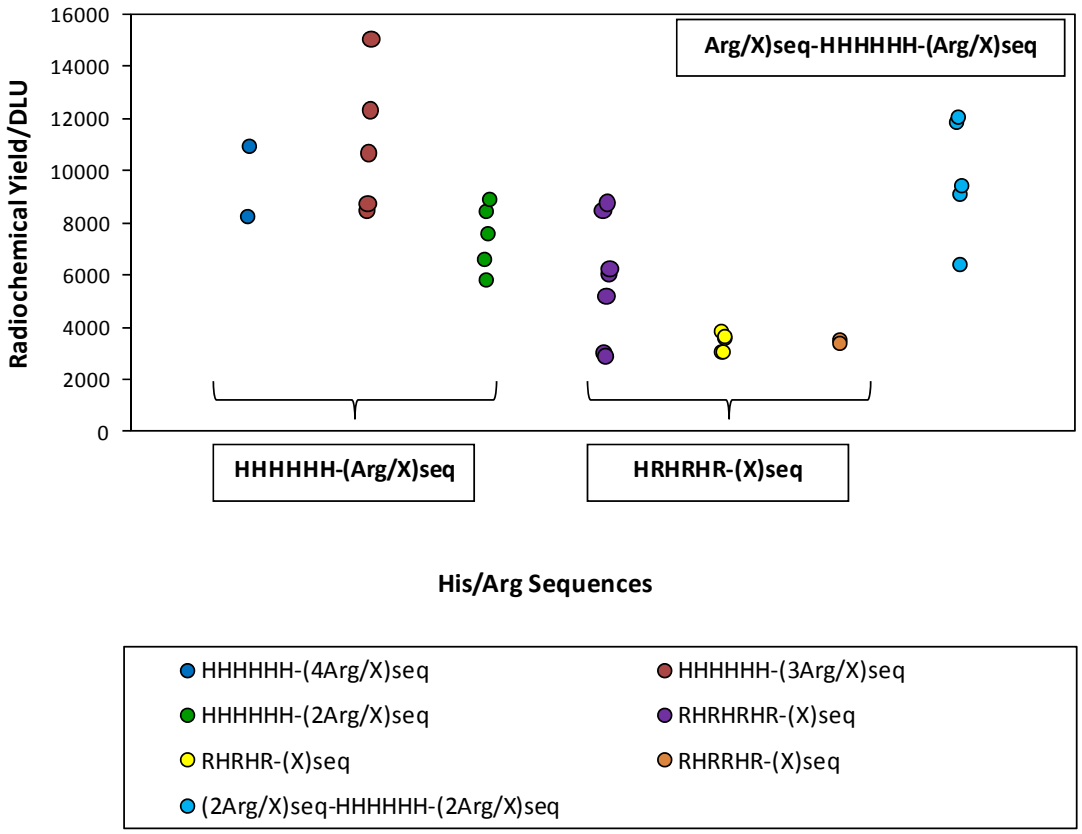

Figure 3.3- 14. Comparisons between positions of the Arg residues in the labelling sequence with respect to the His amino acids. The sequences have been categorised according to the positioning of the His residues: **HHHHHH-(Arg/X)seq**, **HRHRHR-(X)seq** and **(Arg/X)seq-HHHHHH-(Arg/X)seq**. X = any other amino acid other than Arg or His.

3.3.4.8 What is the Optimum Number and Arrangement of His Residues?

Other factors emphasised in the design of the His-Tagged Celluspot™ array that were previously considered to be particularly influential in the labelling efficiency of His sequences with $[^{99m}Tc(CO)_3]^+$ include the quantity of His residues required in the sequence. Sequences were included in the array with different combinations of amino acids. These

include the generic $(His)_6$-Tag (HHHHHH), an abbreviated His-Tag with 4 consecutive His residues (HHHH), HXHXHX, HXHX and HXXH arrangements in which X is equivalent to any other amino acid except His. From figure 3.3-15, sequences with 6 consecutive His residues (His-Tag) demonstrated a superior labelling efficiency compared to the other His combinations. In addition, sequences without His residues show no labelling; which coincides with the results from the trial STLS-1 Celluspot™ array (Chapter 3.1). In chapter 2, the labelling of the Cys/His-Tag analogues highlighted a reduction in radiochemical yield with a reduction in the number of His residues in the sequence. This is evident from the results in figure 3.3-15 where the labelling efficiency of the $(His)_6$-Tag > HXHXHX > HXHX > HXXH.

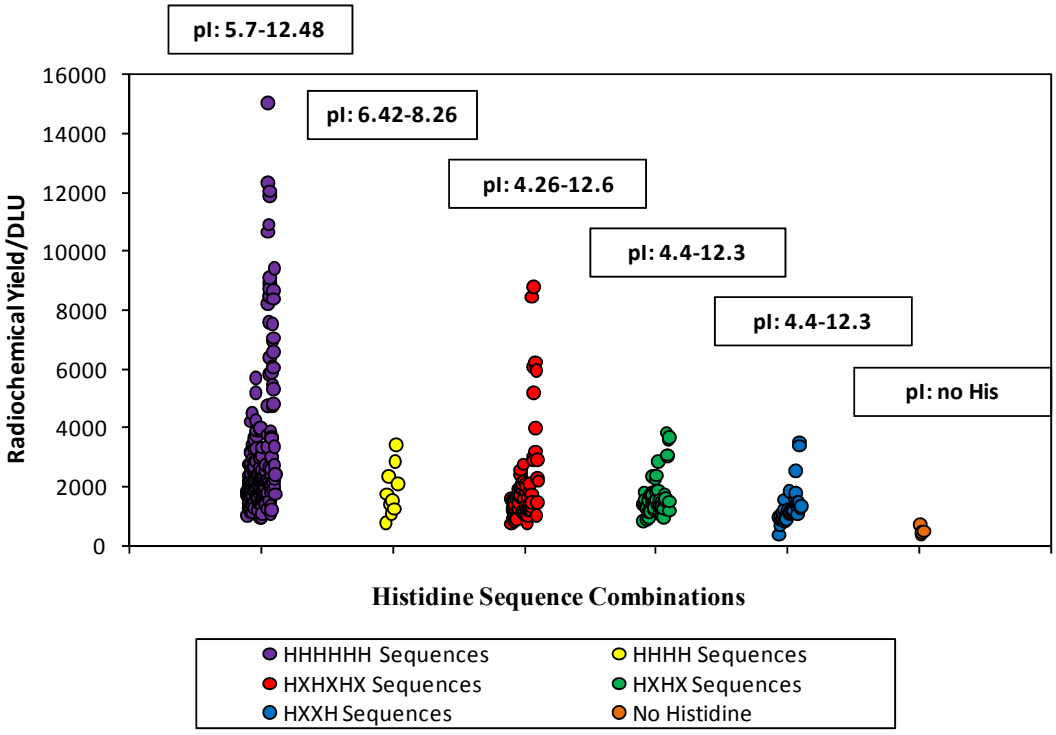

Figure 3.3- 15. Comparison between the radiochemical yield of peptide sequences with HHHHHH, HHHH, HXHXHX, HXHX and HXXH combinations of His amino acids. X= Any amino acid other than His.

The proportional relationship between the number of His residues and the labelling efficiency of the sequences does not apply to the abbreviated His-Tag, HHHH according to the results displayed in figure3.3-16. The abbreviated His-Tag sequences show a lower radiochemical yield than that of the HXHXHX containing sequences which only have 3 His residues. This result must be interpreted cautiously: among sequences in the array containing an abbreviated His-Tag the highest pI is 8.5. This is considerably lower than that

of sequences with other His combinations in which there are at least a few peptides with a pI greater than 12.The pI is an important factor that must be taken into consideration as it has a strong influence on the labelling efficiency. It is unfair to compare labelling efficiencies of sequences based on their His combinations unless for each combination sequences are included with high and low pIs, above and below 9.5. For this reason, the exponential relationship between the pI and radiochemical yield for the different His combinations was plotted in figure 3.3-16. For HHHHHH, HXHXHX, HXHX and HXXH, there are sequences present with pIs ranging from 5 to at least 12. The abbreviated His-Tag sequences have not been included in the pI vs radiochemical yield graph (figure 3.3-16) as it is an unfair comparison considering the maximum pI is 8.5.

Figure 3.3-16 confirms the superiority of the His-Tag in comparison to the HXHXHX, HXHX and HXXH arrangements of His residues. In addition the graph shows that the trend in radiochemical yield, according to the exponential lines of best fit, increases proportionally to the number of His residues within a sequence e.g. HXXH <HXHX < HXHXHX < HHHHHH. For example, among sequences with a high pI (pI>9.5) the presence of 6 His residues, HHHHHH, is more beneficial to the labelling efficiency than the other combinations. There are 2 sequence combinations that have 2 His residues, HXHX or HXXH, and a slight preference for labelling of $[^{99m}Tc(CO)_3]^+$ is observed for His residues in a 1-3 rather than 1-4 arrangement, HXHX > HXXH.

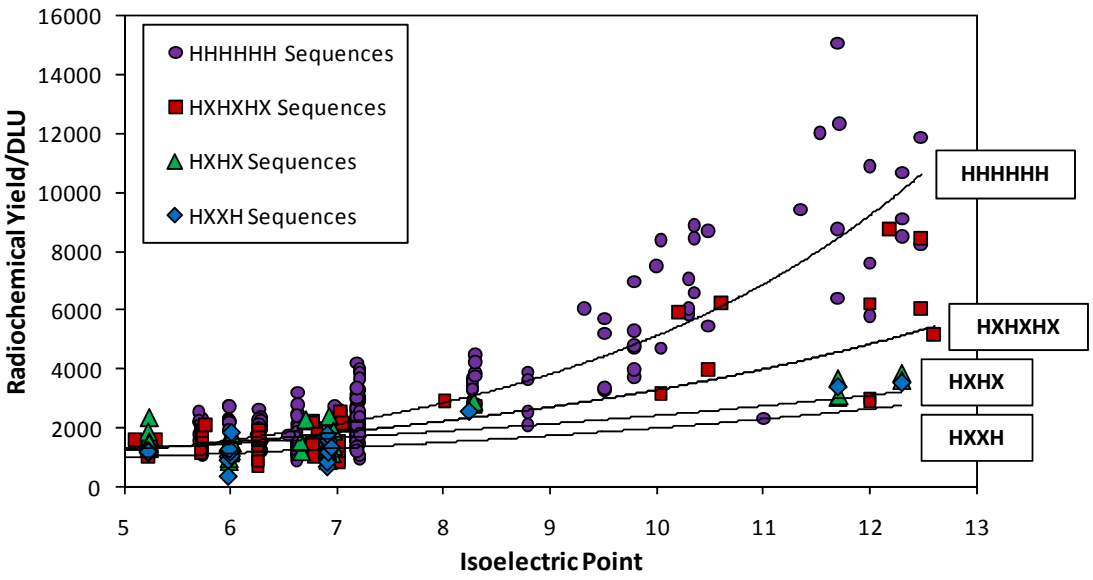

Figure 3.3- 16. The exponential relationship between pI and radiochemical yield plotted for separately for sequences with HHHHHH, HXHXHX, HXHX and HXXH combinations of His residues. X = any amino acid other than His.

3.3.4.9 What is the Influence of the Cys?

A substantial emphasis was placed on the importance of the Cys whilst designing the His-Tagged Celluspot^{TM} array (Chapter 3.2). In Chapter 1.2 and 2 the application of CKLAAALEHHHHHH was discussed and it was concluded that the addition of a Cys significantly improved labelling efficiencies of His with $[M(CO)_3]^+$ complexes. Consequently, many sequences were included on the His-tagged Celluspot^{TM} peptide array to fully analyse the importance of the Cys such as: the optimum distance of the Cys from the His, the possibility of replacing Cys with Met to avoid disulfide bond formation in proteins and, the role it plays in the coordination of $[M(CO)_3]^+$ to His residues. All of the 10 sequences that demonstrate the best labelling efficiency are featured in the "Positively Charged Amino Acid" category and contain multiple Arg residues. Seven of the top 10 sequences also include a Cys amino acid.

A direct comparison has been made between the $[^{99m}Tc(CO)_3]^+$ labelling of the best sequences with and without a Cys residue (Figure 3.3-17). With the exception of the GGRHHHRHHHRGGC sequence, all other peptides have a higher radiochemical yield when a Cys is included within the chain. For three of the sequences, CLRRRLAHHHHHH, CRRAARRHHHHHH and CRGGRGHRHRHR, a significantly higher radiochemical yield is achieved in the presence of a Cys residue than in the (otherwise) identical sequence where the Cys has been excluded ($p<0.01$ for CRRAARRHHHHHH and $p<0.001$ for CLRRRLAHHHHHH and CRGGRGHRHRHR). Results from the CelluspotTM array show that in comparison to other factors, Cys does not make a significant difference to the labelling efficiency of a peptide sequence. It may be contributing somewhat towards improving the coordination of $[^{99m}Tc(CO)_3]^+$ to the His sequences as the majority of the 10 best labelling sequences do contain a Cys. However, it is definitely not the most influential factor.

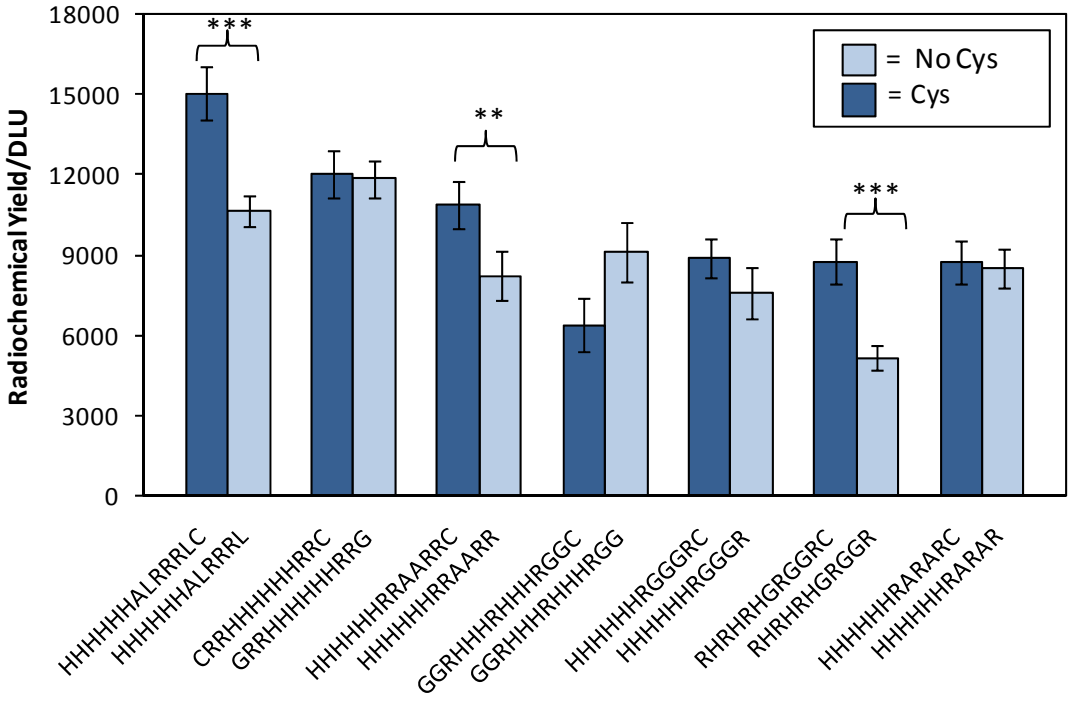

10 Best Labelling Sequences	
HHHHHHALRRRLC	1
HHHHHHALRRRLKC	2
CRRHHHHHHRRC	3
GRRHHHHHHRRG	4
HHHHHHRRAARRC	5
HHHHHHALRRRL	6
RCRGHHHHHHGRCR	7
GGRHHHRHHHRGG	8
HHHHHHRGGGRC	9
RHRHRHGRGGRC	10

Figure 3.3-17. Top: Radiochemical yield for the 10 sequences with the highest labelling efficiency. Data is shown for the 10 sequences with and without the presence of a Cys. **Left:** Table showing the 10 best labelling sequences. **Blue** = Cys containing sequences.

*** = $p < 0.001$
** = $p < 0.05$

With regards to the optimum position of the Cys in relation to the His residues, the results are somewhat inconclusive. Variations in the position of the Cys were altered from 1-8 amino acids away from the His residues. Figure 3.3-18 reveals that there is a slight increase in radiochemical yield for sequences where the Cys is 3-4 or 7-8 amino acids away from the His residues. This trend can be seen for sequences with a HHHHHH, HAHAHA and HAHA combination of His amino acids. Results for the HAAH sequences cannot be taking into consideration as the radiochemical yields are very low and the results appear to be inconsistent (large error bars). The least favoured positions of the Cys with regards to the His residues is 1 or 5 amino acids away.

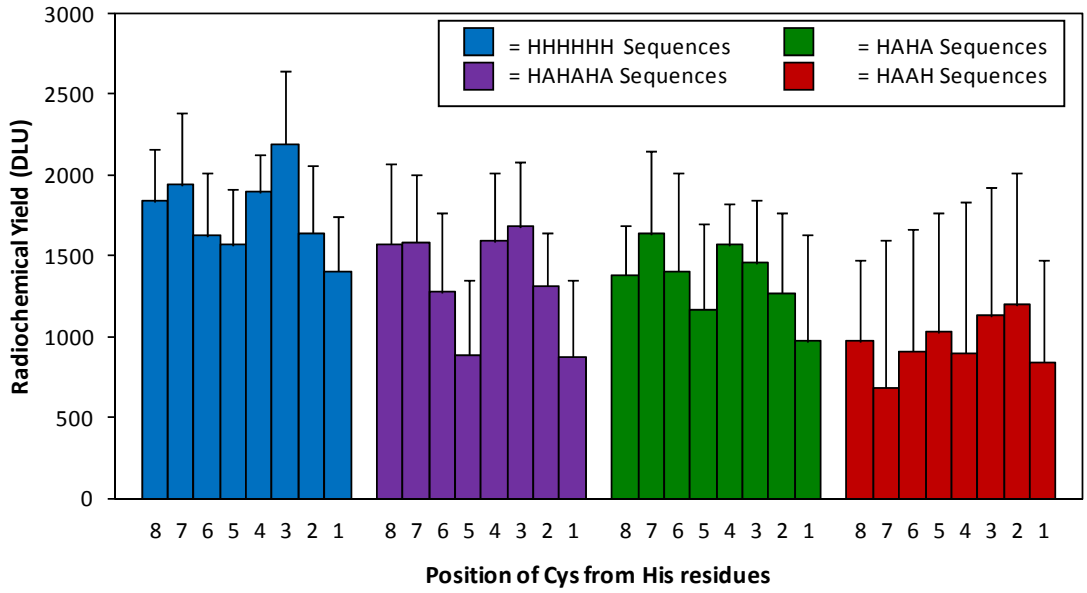

Figure 3.3-18. Radiochemical yield of sequences in which the position of the Cys with regards to the His residues has been altered from 1-8 amino acids away. Data has been included for sequences with a HHHHHH, HAHAHA, HAHA and HAAH combination of His residues.

3.3.4.10 Can Cys be Replaced with Met?

Data provided by the His-Tagged Celluspot™ peptide array has agreed with previous research and shown that Cys appears to be a contributing factor towards increasing the $[^{99m}Tc(CO)_3]^+$ labelling efficiency however, it is definitely not the most influential factor and makes a minor contribution compared to arginines and lysines. The inclusion of a Cys residue sometimes causes problems with the dimerisation of proteins due to formation of disulfide bonds. A comparison between the labelling efficiency of identical sequences in which a Cys is replaced by Met can be seen in figure 3.3-19. The difference in radiochemical yield for the Met or Cys containing sequences in figure 3.3-19 is insignificant and therefore Met could be used instead of a Cys to give an almost identical rate of labelling. Due to the alkyl side chain of the Met amino acid, the formation of disulfide bonds is avoided. In figure 3.3-19 there are 4 sequences in which a comparison is made between the Cys or Met containing sequences and those without either.

There is a definite decrease in radiochemical yield when the Met and Cys are removed entirely. The decrease in radiochemical yield observed when the Met or Cys are removed is far more significant that what was observed earlier when analysing the top labelling sequence with and without a Cys residue. (Chapter 3.3.4.8) This is possibly due to the lack

of positively charged residues within these sequences. Therefore it may be a possibility that Cys does considerably contribute towards the labelling efficiency but it is definitely not the most influential factor. In the presence of multiple Arg residues the effect of a Cys in increasing the labelling efficiency is not significant.

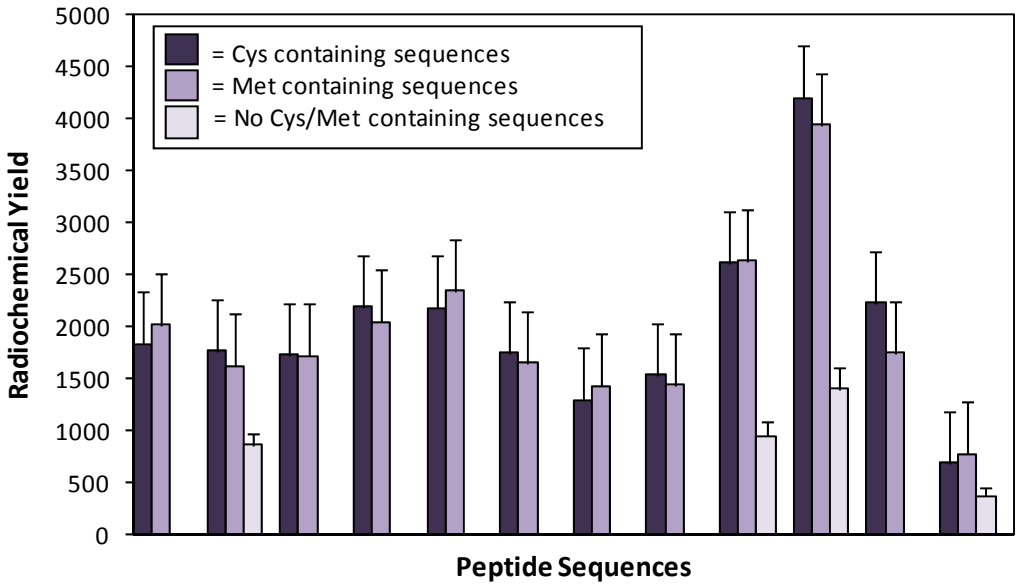

Figure 3.3- 19. A comparison between the radiochemical yield of identical peptide sequences in which a Cys residue has been replaced by a Met amino acid. For four of the sequences, the radiochemical yield has been included for the sequence excluding any Cys or Met amino acids.

3.3.4.11 What is the Peptide Sequence Demonstrating the Highest Labelling Efficiency for $[^{99m}Tc(CO)_3]^+$ and How it Compares with Typical His-Tags in the Literature ?

Overall, CLRRRLAHHHHHH is the sequence that demonstrates the fastest rate of labelling and is consequently the most favourable in coordinating to $[^{99m}Tc(CO)_3]^+$ after 15 minutes. Peptide sequences previously published for the labelling of proteins with $[^{99m}Tc(CO)_3]^+$ have been included in the His-tagged Celluspot^{TM} array and their radiolabelling efficiencies are directly compared to that of CLRRRLAHHHHHH in Figure 3.3-20. The superiority of the CLRRRLAHHHHHH sequence for labelling with $[^{99m}Tc(CO)_3]^+$ complexes is clearly evident from the graph. A significant increase in radiochemical yield was observed for the CLRRRLAHHHHHH sequence in comparison to: LAAALEHHHHHH and CKLAAALEHHHHHHH previously published by Tavare et al. for $[^{99m}Tc(CO)_3]^+$ labelling of the C2A protein;

KNDVQLHHHHHHSSG and EKNFKNEAEHEHEHM published by Tolmachev et al. for $[^{99m}Tc(CO)_3]^+$ labelling of HER2 antibody; and the equivalent sequences with negatively charged Glu and Asp amino acids replacing the positive Arg residues. There is a significant 8 fold higher rate of labelling at 15 minutes between CLRRRLAHHHHHH and the previously used His-containing sequences.

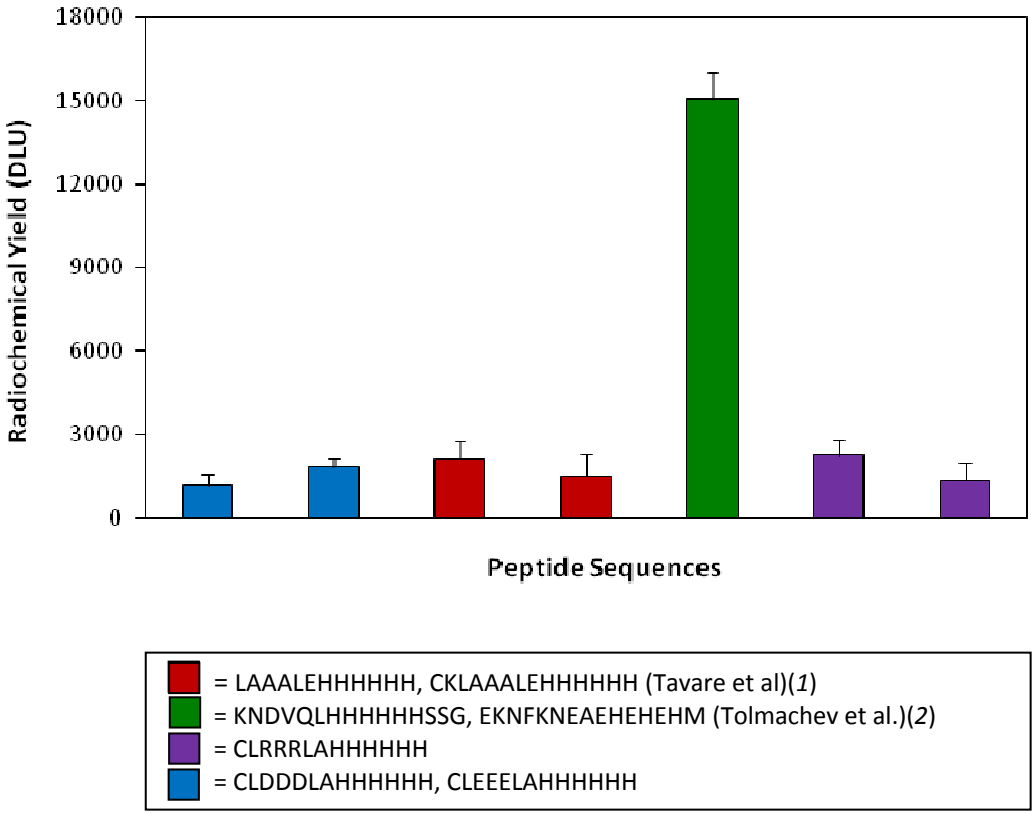

Figure 3.3- 19. A comparison between the radiochemical yield of sequences previously used in the literature for protein labelling with $[^{99m}Tc(CO)_3]^+$, LAAALEHHHHHH, CKLAAALEHHHHHH, KNDVQLHHHHHHSSG and EKNFKNAEHEHEHM, and the sequence demonstrating the highest labelling efficiency according to the His-Tagged Celluspot™ array, CLRRRLAHHHHHH. The labelling efficiencies of sequences from the array equivalent to that of CLRRRLAHHHHHH with negatively charged amino acids (Glu and Asp) replacing the positively charged Arg residues have been included in the bar chart.

The sequences containing multiple positively charged amino acids continued to display a significant increase in radiochemical yield in comparison to the majority of other sequences on the array surface over the 2hr incubation period. This is emphasised in figure 3.3-22 in which a comparison is made between the previously published $(His)_6$-Tag sequences and CLRRRLAHHHHHH sequence after 30, 60 and 120mins total incubation times. CLRRRLAHHHHHH consistently demonstrated the highest labelling efficiency at all time points. Significant differences in radiochemical yields are observed at all time points

between CLRRRLAHHHHHH and the LAAALEHHHHHH and CKLAAALEHHHHHHH sequences previously published by Tavare et al, and KNDVQLHHHHHHSSG and EKNFKNEAEHEHEHM sequences published by Tolmachev et al. (*1, 3*)The equivalent sequence to CLRRRLAHHHHHH, in which the positively charged Arg residues have been substituted for negatively charged Glu and Asp, demonstrates the lowest radiochemical yield throughout the labelling experiment. This confirms that negatively charged amino acids are detrimental to the labelling efficiencies.

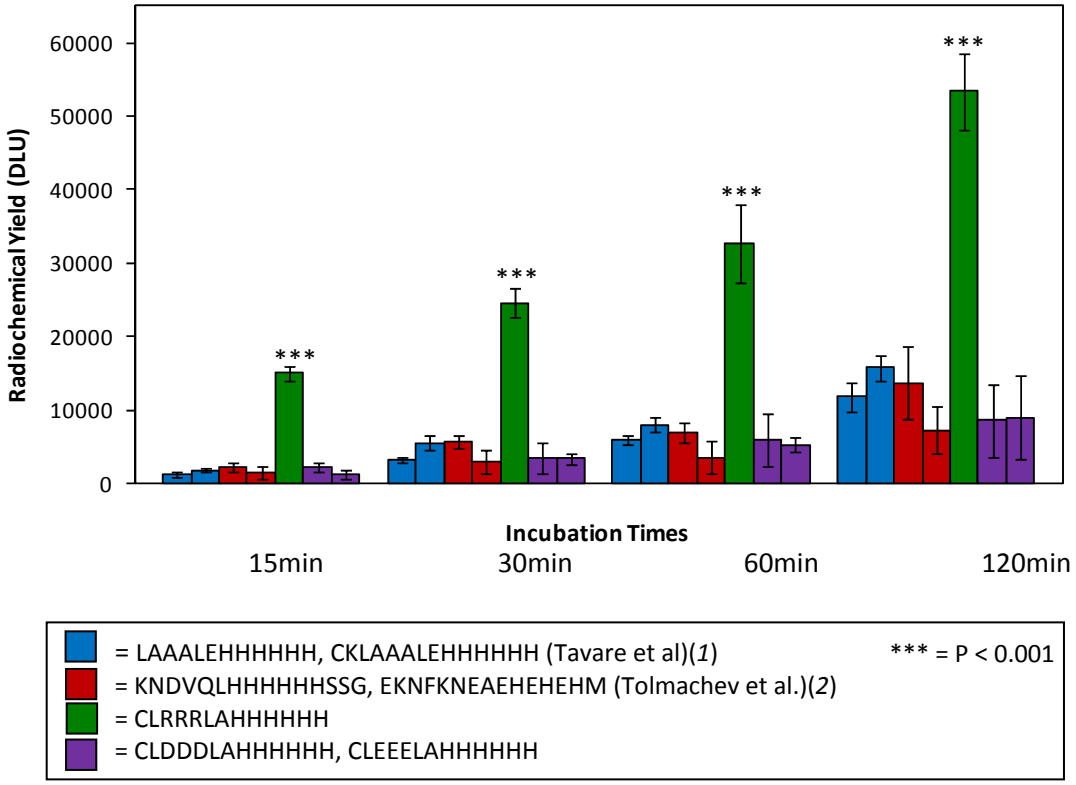

Figure 3.3- 22. A comparison between the radiochemical yield of sequences in the array that have previously used in the literature for protein labelling with $[^{99m}Tc(CO)_3]^+$, LAAALEHHHHHH, CKLAAALEHHHHHH, KNDVQLHHHHHHSSG and EKNFKNAEHEHEHM, and the sequence demonstrating the highest labelling efficiency according to the His-Tagged Celluspot™ array, CLRRRLAHHHHHH. The labelling efficiencies of sequences corresponding to CLRRRLAHHHHHH but with negatively charged amino acids (Glu and Asp) replacing the positively charged Arg residues have been included in the bar chart. The data have been reported for total incubation times of 15, 30, 60 and 120 minutes.

3.3.5 RESULTS B: $[^{99m}Tc(CO)_3]^+$ Labelling in Citrate Buffer (pH 5.1) and Tris Buffer (pH 7.4 and 8.8)

In the His-tagged Celluspot™ array experiments a citrate buffer at pH 5.5 and a tris-HCl buffer at pH 8.8 were used in addition to the standard PBS buffer at pH 7.4. This enabled analysis of the radiolabelling in both a slightly acidic and basic environment. It is important that the buffer used in $[^{99m}Tc(CO)_3]^+$ labelling of proteins is suitable for biological use and can effectively maintain the required pH of the protein post addition of the $[^{99m}Tc(CO)_3]^+$. Citrate and Tris-HCl buffer have a buffering capacity from pH 3.0 to 6.2 and pH 7.2-9.0 respectively. As a control, $[^{99m}Tc(CO)_3]^+$ labelling of the His-tagged Celluspot™ array was also performed in tris-HCl buffer at pH 7.4, a pH within its buffering capacity. A comparison between results of the Tris-HCl experiments and PBS experiments at pH 7.4 will be able to distinguish whether it is the buffer or pH that is influential on the labelling abilities of the His-tagged peptides. Consequently when performing the radiolabelling in Tris-HCl buffer at pH 8.8 it will be possible to distinguish whether it is the buffer or pH that effects the labelling efficiencies. This control is not possible for citrate buffer as pH 7.4 is not in its buffering capacity. Investigations into the labelling of the His-Tagged Celluspot™ peptide arrays under different conditions has provided a greater understanding of the optimal labelling conditions required with regards to the buffering solutions and pH.

3.3.5.1 $[^{99m}Tc(CO)_3]^+$ Labelling in Citrate Buffer at pH 5.1

Phosphor images generated post $[^{99m}Tc(CO)_3]^+$ labelling of the His-Tagged Celluspot™ array in citrate buffer at pH 5.1 can be seen in figure 3.3-29. Image A and B represent the radiochemical yields of the peptides after a total incubation time of 15 and 120mins, while image C represents the radiochemical yields after subsequent exposure of the array to a 1000 molar excess solution of His for 3hrs. Visibly, it is apparent that the coordination of $[^{99m}Tc(CO)_3]^+$ to the sequences is not favourable in the presence of citrate buffer at pH 5.1. After 120mins of incubation (figure 3.3-29, image B), black spots are detectable on the array surface in the image however, they are significantly less well defined than those obtained with similar activities when labelling occurred in PBS buffer. This suggests that the radiochemical yields of the sequences in citrate buffer are very low. The phosphor images

generated after 30mins and 60mins total incubation time have not been included as the image at 120mins signifies the maximum labelling efficiency of the sequences.

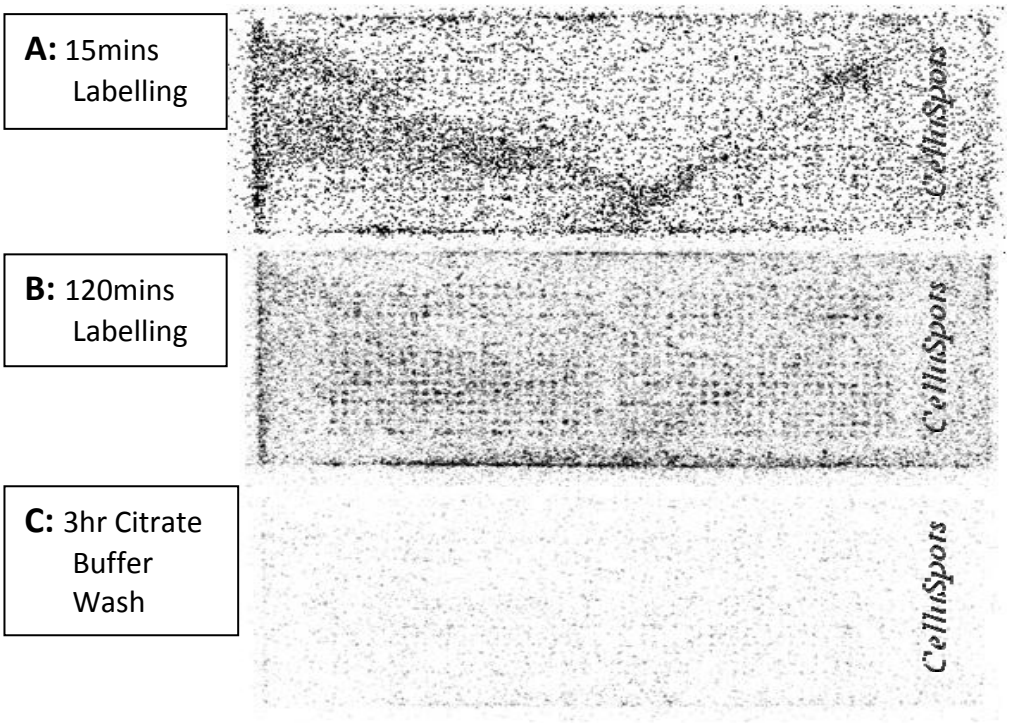

Figure 3.3-29. Phosphor images of the $[^{99m}Tc(CO)_3]^+$ radiolabelled His-Tagged Celluspot™ peptide array after radiolabelling had been performed in citrate buffer at pH 5.1 and a subsequent wash in a 1000 molar excess solution of His amino acids. **A)** Image after radiolabelling for 15mins with $[^{99m}Tc(CO)_3]^+$, **B)** Image after radiolabelling for 120mins with $[^{99m}Tc(CO)_3]^+$. **C)** Image after exposure to a His containing solution for 3hrs.

Exposure to a PBS buffered solution containing excess His amino acids was performed in an attempt to reduce the background radioactivity on the plate surface and potentially reveal sequences that may have been radiolabelled with $[^{99m}Tc(CO)_3]^+$. Image C in figure 3.3-29 summarises the results and it was found that any $[^{99m}Tc(CO)_3]^+$ bound to the peptides or the array surface had completely dissociated in the presence of the His amino acids. Little radioactivity could be detected on the His-Tagged Celluspot™ peptide array in image C. Interestingly, in citrate buffer not only is binding a lot slower but also more reversible. The $[^{99m}Tc(CO)_3$-peptide$]^+$ conjugates present after 120mins incubation are kinetically unstable post washing in citrate buffer. Consequently, citrate buffer at pH 5.1 is not suitable for labelling His-Tagged sequences or proteins with $[^{99m}Tc(CO)_3]^+$ and should not be pursued for further experiments.

3.3.5.2 $[^{99m}Tc(CO)_3]^+$ Labelling in Tris-HCl Buffer at pH 8.8

Radiolabelling of the His-Tagged Celluspot™ array in Tris-HCl buffer at pH 8.8 was very similar to that of labelling in citrate buffer. Figure 3.3-30 displays the phosphor images generated after a total incubation period of 15, 30, 60 and 120mins (images A, B, C and D respectively). After 15 mins, it was found that the peptides had not been efficiently radiolabelled with $[^{99m}Tc(CO)_3]^+$ and only faint black spots were identified on the array in the image (figure 3.3-30, image A). A similar outcome was observed after 30mins and 60mins incubation. However, at 120mins somewhat stronger black spots were detected in the image suggesting that a low radiochemical yield had been achieved by the peptide sequences. (Figure 3.3-20, image B).

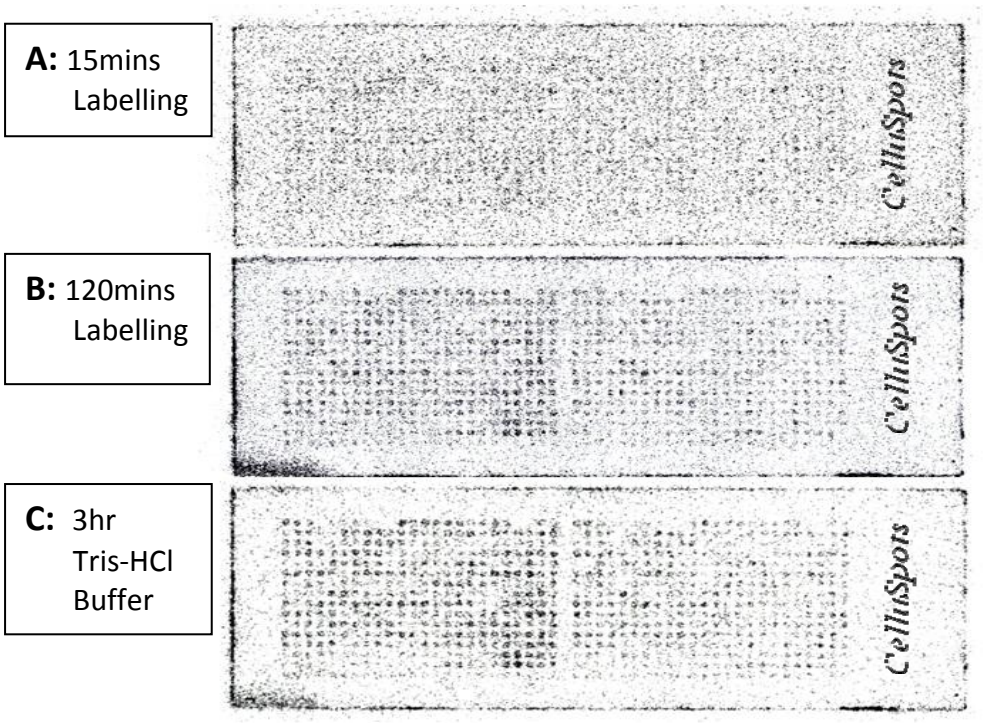

Figure 3.3-29. Phosphor images of the $[^{99m}Tc(CO)_3]^+$ radiolabelled His-Tagged Celluspot™ peptide array after radiolabelling had been performed in citrate buffer at pH 5.1 and a subsequent wash in a 1000 molar excess solution of His amino acids. **A)** Image after radiolabelling for 15mins with $[^{99m}Tc(CO)_3]^+$, **B)** Image after radiolabelling for 120mins with $[^{99m}Tc(CO)_3]^+$. **C)** Image after exposure to Tris-HCl buffer for 3hrs.

Plotting the radiochemical yields of the peptide sequences revealed that complexation with $[^{99m}Tc(CO)_3]^+$ had occurred (Figure 3.3-30 graph A). However, unlike the labelling in PBS, no preferential coordination was demonstrated for the peptides containing multiple positively

charged amino acids. All His-containing sequences appeared to demonstrate roughly equal labelling efficiencies that were greater than those of the sequences in the "Controls" category that either contained no His residues or no amino acids. No obvious specific trends in labelling efficiencies were detected with regards to the different characteristics of the sequences.

The radiochemical yields for the labelling in Tris-HCl buffer after 120mins has been compared with radiochemical yields obtained for the sequences after labelling in PBS buffer for 15mins. In Figure 3.3-30, graph A and B correspond with the radiolabelling efficiency of the His-Tagged Celluspot^{TM} array after 120mins in citrate buffer and 15mins in PBS buffer respectively. In order to achieve this comparison, the amount of $[^{99m}Tc(CO)_3]^+$ used in the labelling solution and the exposure time of the Celluspot^{TM} array to the film was equivalent in both procedures and consequently the graphs have been plotted on the same scale. In PBS buffer the radiochemical yields displayed by the sequences in the "Positively Charged Amino Acids → Arg and Lys" category (purple) after 15mins labelling were significantly higher by approximately 6 fold than the labelling efficiencies shown by any of the sequences after 120mins labelling in tris-HCl buffer at pH 8.8.

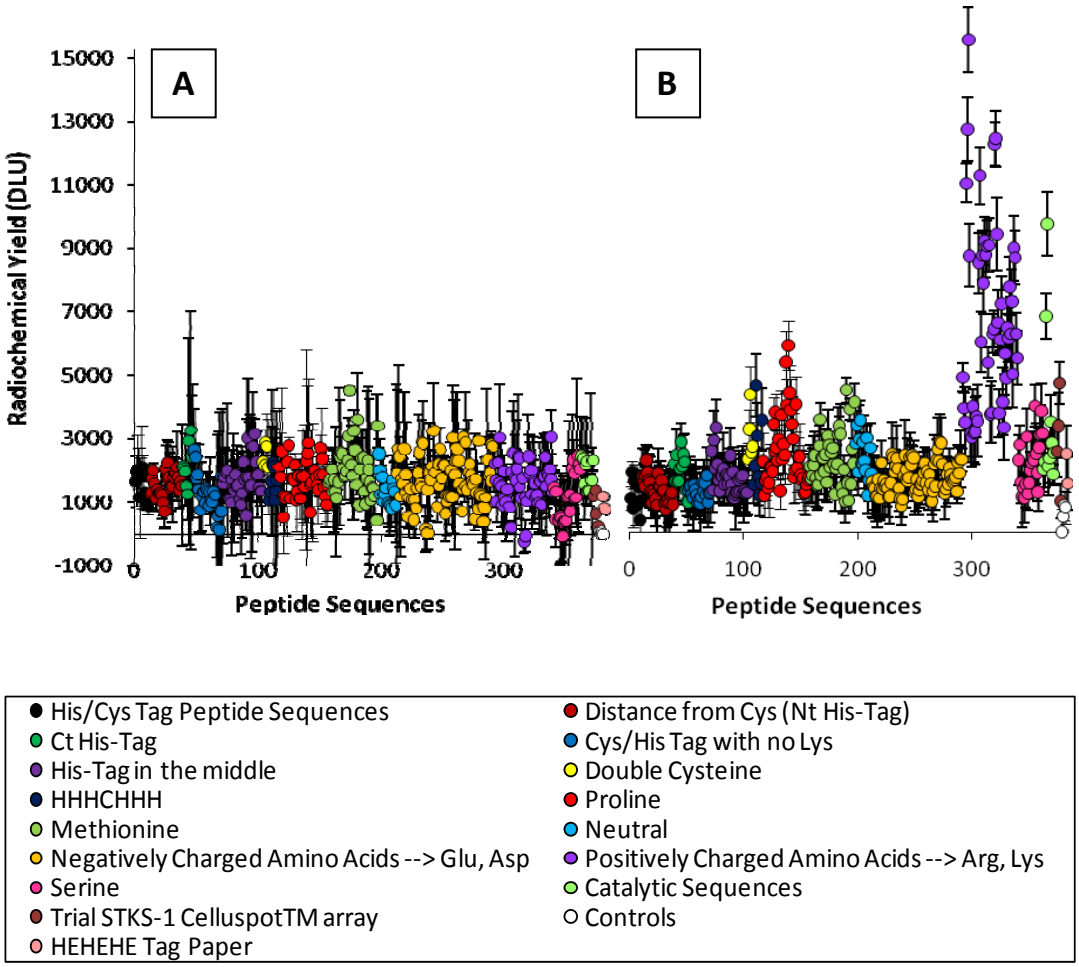

Figure 3.3-30. Comparisons between the radiochemical yields obtained after: **A)** 120mins reaction time in $[^{99m}Tc(CO)_3]^+$ tris-HCl buffered solution at pH 8.8 and, **B)** 15mins reaction time in $[^{99m}Tc(CO)_3]^+$ PBS buffered solution. The graphs have been plotted to the same scale.

After 120mins the radiolabelled Celluspot^{TM} array was washed in Tris-HCl buffer at pH 8.8 for 3 hours in an attempt to both remove some of the unspecifically bound $[^{99m}Tc(CO)_3]^+$ from the array surface and potentially better visualise the labelling of the sequences and to evaluate radiochemical stability. Some background activity was removed but no changes were observed in the radiochemical yields of the peptide sequences according to the phosphor image in figure 3.3-30, image C. This confirms that once labelled in Tris-HCl buffer (pH 8.8), the conjugates were stable for the duration of the washing procedure. The reduction in the $[^{99m}Tc(CO)_3]^+$ background of the array surface suggests that Tris may act to some extent as a chelator for the $[^{99m}Tc(CO)_3]^+$ complex or it could just be a dilution effect.

3.3.5.3 $[^{99m}Tc(CO)_3]^+$ Labelling in Tris-HCl Buffer at pH 7.4

The radiolabelling in Tris-HCl buffer at pH 7.4 (matching the pH of the PBS labelling conditions) was carried out as a control to differentiate between the effect of changing the buffer identity and the pH on labelling efficiencies of the peptides. Phosphor images representing the His-Tagged Celluspot™ array post labelling in Tris-HCl buffer after 15, 60 and 120mins are shown in figure 3.3-32 image A-C respectively.

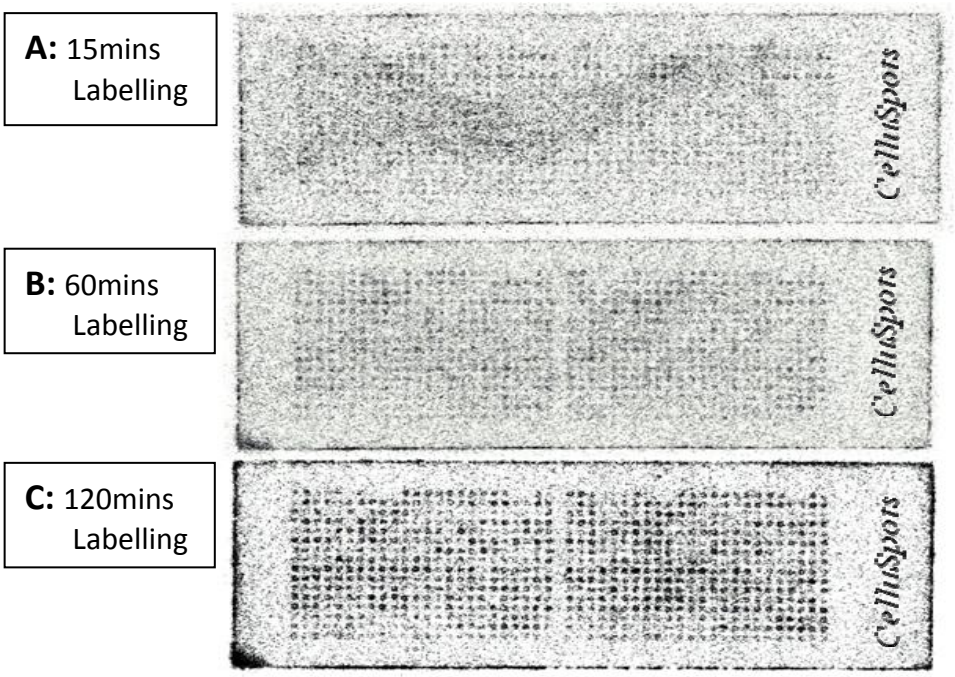

Figure 3.3-31. Phosphor images of the $[^{99m}Tc(CO)_3]^+$ radiolabelled His-Tagged Celluspot™ peptide array after radiolabelling had been performed in Tris-HCl buffer at pH 7.4. **A)** Image after radiolabelling for 15mins with $[^{99m}Tc(CO)_3]^+$, **B)** Image after radiolabelling for 60mins with $[^{99m}Tc(CO)_3]^+$. **C)** Image after radiolabelling for 120mins with $[^{99m}Tc(CO)_3]^+$.

Similarly to the Tris-HCl labelling at pH 8.8, $[^{99m}Tc(CO)_3]^+$ radiolabelling yield was low after 15mins (figure 3.3-32, image A). However, increased coordination of $[^{99m}Tc(CO)_3]^+$ was observed at 60mins reaction time with the appearance of black spots on the array surface representing the radiolabelled peptides. (Figure 3.3-32, image B) The intensity of the spots was insufficient to calculate a comparative radiochemical yield for the individual sequences. Over the subsequent hour, the radiolabelling increased substantially and prominent black spots were detected in the image at 120mins (figure 3.3-32, image C). These were plotted

as radiochemical yields for the sequences and comparisons were made with the radiochemical yields obtained after 120mins labelling in Tris-HCl buffer (pH 8.8) and 15mins labelling in PBS buffer (pH 7.4) (figure 3.3-33, graph A, B and C respectively). In order to compare the data on the same scale, the $[^{99m}Tc(CO)_3]^+$ labelling of all Celluspot™ arrays in the different buffers was performed under the same conditions; the equivalent amout of $[^{99m}Tc(CO)_3]^+$ was added to the labelling solution and the array was exposed to the phosphor film for the same amount of time.

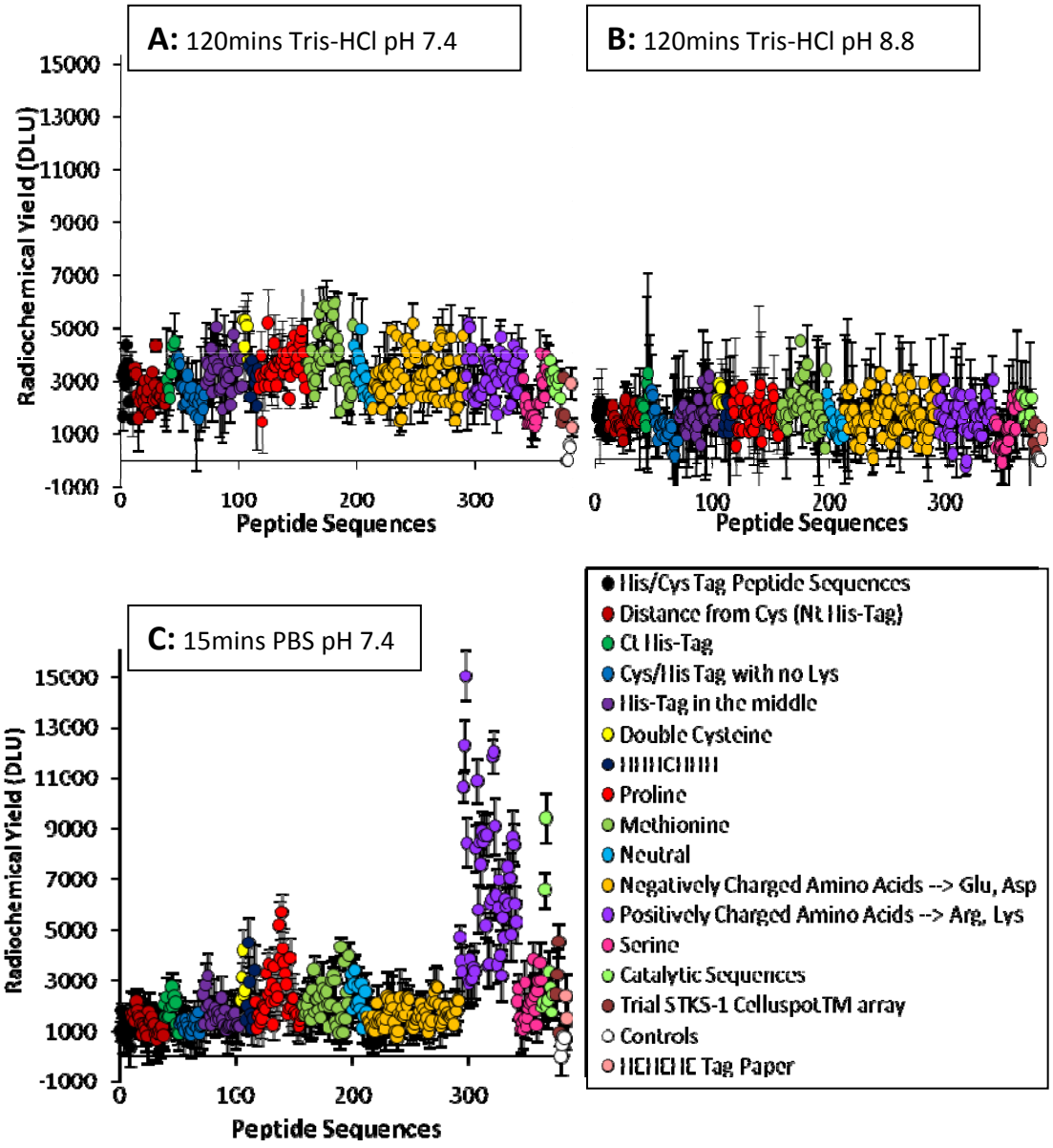

Figure 3.3-32. Comparisons between the radiochemical yields obtained after: **A)** 120mins reaction time in $[^{99m}Tc(CO)_3]^+$ Tris-HCl buffered solution at pH 7.4, **B)** 120mins reaction time in $[^{99m}Tc(CO)_3]^+$ Tris-HCl buffered solution at pH 8.8 and, **B)** 15mins reaction time in $[^{99m}Tc(CO)_3]^+$ PBS buffered solution. The graphs have been plotted to the same scale and the data standardised according to the background $[^{99m}Tc(CO)_3]^+$ values from the arrays.

A two fold increase in radiochemical yield was demonstrated by the peptides labelled in Tris-HCl buffer at pH 7.4 rather than pH 8.8 after 120mins. (figure 3.3-32, image A and B). Average radiochemical yield values (DLU) for the sequences labelled in tris buffer (pH 7.4) were 3,000-4,000 whereas labelling in Tris-HCl buffer (pH 8.8) gave average radiochemical yields of approximately 1500 to 2,000. No preferential coordination was shown for any of the specific peptide categories and it was not possible to identify specific amino acid characteristics that led to an increased labelling efficiency in Tris-HCl buffer at pH 7.4. In conjunction with the labelling at pH 8.8, all His containing peptides demonstrated an equal labelling efficiency for $[^{99m}Tc(CO)_3]^+$ which was greater than the labelling efficiency of the non-His containing peptide controls .

The difference between the labelling efficiencies in Tris-HCl at pH 7.4 and 8.8 is minor in comparison to the labelling efficiencies demonstrated by the multiple positively charged sequences after 15mins labelling in PBS buffer. Figure 3.3-32 compares the radiochemical yields of the sequences at pH 7.4 in either Tris-HCl (graph A) or PBS buffer (graph C). $[^{99m}Tc(CO)_3]^+$ labelling of the peptides in Tris-HCl buffer at pH 7.4 is more successful than the use of Tris-HCl buffer at pH 8.8. However, all labelling with Tris-HCl buffers is inferior in contrast to the use of PBS buffer at pH 7.4 as the labelling condition.

3.3.6 RESULTS C: Stability of $[^{99m}Tc(CO)_3]^+$-Peptide Conjugates

The data for the radiochemical stability of the $[^{99m}Tc(CO)_3$-Peptide$]^+$ conjugates was obtained using the same procedure as previously applied to the analysis of the Celluspot™ arrays after 15, 30, 60 and 120 minute incubation times. After incubating the plates with $[^{99m}Tc(CO)_3]^+$ the solution was replaced with Tc-free PBS, serum, histidine solution or cysteine solution and incubated at 37°C. Stability of the $[^{99m}Tc(CO)_3$-peptide$]^+$ conjugates was assessed in PBS buffer and human serum after 1hr, 2hr and 24hrs incubation and a 1000 molar excess solution of His or Cys after 3hrs incubation.

Ideally for the efficient radiolabelling of a protein it is important that the coordination of the $[^{99m}Tc(CO)_3]^+$to the His residues is kinetically favourable to give a rapid reaction and that

once the $[^{99m}Tc(CO)_3]^+$ labelled product is formed it is completely stable under biological conditions. Therefore a peptide that demonstrates a high labelling efficiency after 15 minutes (high DLU value) and remains coordinated to $[^{99m}Tc(CO)_3]^+$ after immersion in the buffer, serum or His/Cys rich solution is theoretically the most promising sequence for applications in site-specific protein radiolabelling.

3.3.6.1 $[^{99m}Tc(CO)_3$-Peptide$]^+$ Conjugate: Stability in PBS Buffer at pH 7.4

The phosphor images in figure 3.3-23 represent the comparison between the His-Tagged Celluspot™ peptide array after incubation with $[^{99m}Tc(CO)_3]^+$ for 120 minutes followed by incubation in PBS buffer at 37°C for 1hr, 2hrs and 24hrs. Image A represents the point at which the sequences have achieved their individual maximum radiochemical yield during the experiment. According to the subsequent phosphor images, figure 3.3-23 B, C and D, the majority of the peptides appear to retain their conjugation to the $[^{99m}Tc(CO)_3]^+$ throughout the incubation in PBS buffer. In image D, most peptides can be seen as a black spot on the array surface which represents the $[^{99m}Tc(CO)_3]^+$ bound to the sequence.

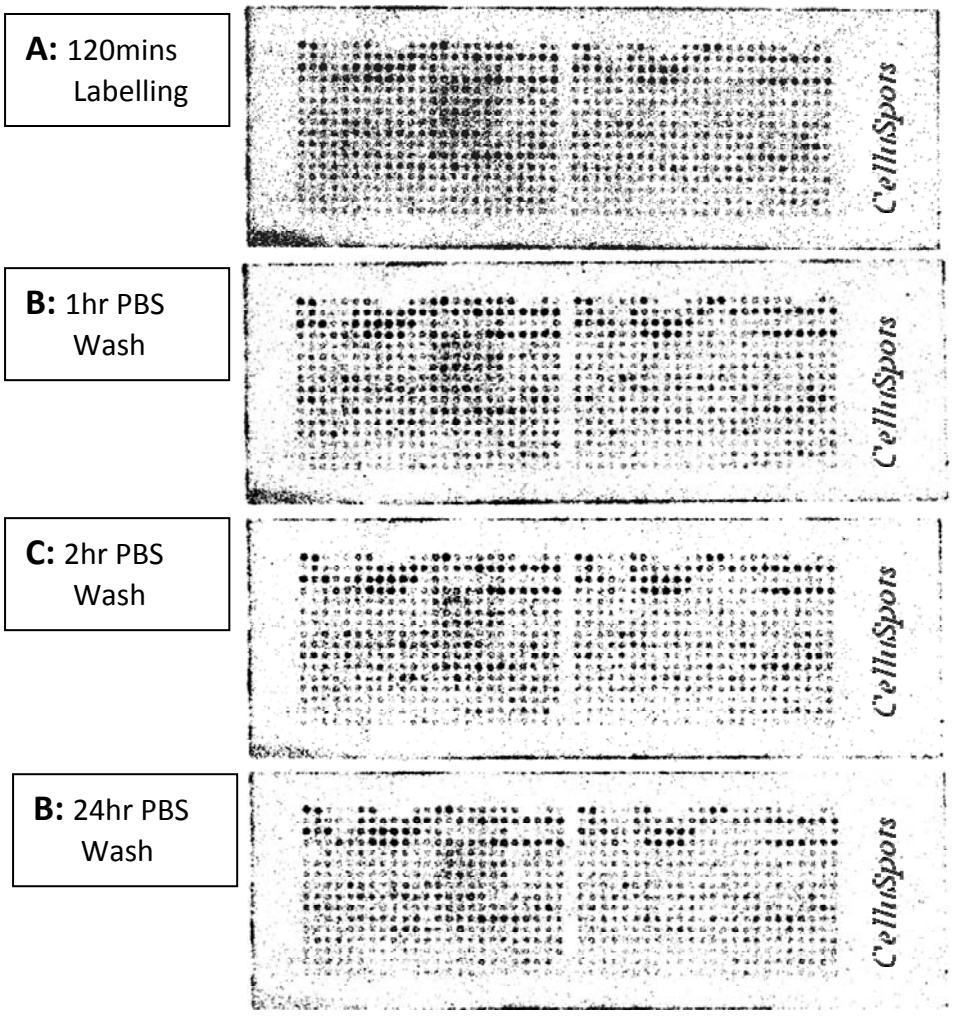

Figure 3.3-23. Phosphor image of the $[^{99m}Tc(CO)_3]^+$ radiolabelled His-Tagged Celluspot™ peptide array at 120 minutes and after incubation in PBS buffer for up to 24hrs. Each black spot represents a peptide sequence. **A)** Image after radiolabelling for 120mins with $[^{99m}Tc(CO)_3]^+$, **B)** Image after incubation in PBS buffer for 1hr, **C)** Image after incubation in PBS buffer for 2hrs and **D)** Image after incubation in PBS buffer for 24hrs.

Further analysis, figure 3.3-24 presents a more quantitative representation of the peptide stabilities and displays the data as the remaining $[^{99m}Tc(CO)_3]^+$ activity bound to the peptide after 1 hr, 2 hrs and 24 hrs incubation in non-radioactive PBS buffer as a percentage of the corresponding activity after 120 min incubation with ^{99m}Tc. Generally the data demonstrates that all peptides, with the exception of the "controls" category (white) peptides, have approximately equal stability in PBS buffer. The calculated %Bound $[^{99m}Tc(CO)_3]^+$ for all His containing sequences was consistently between 84-125% for the duration of the 24hr exposure to PBS buffer. No his-containing peptides were found to demonstrate a significant difference in their stability (i.e. loss of radiolabel) over time (Controls (white) category). Values above 100% were observed at all time points and are

accounted for by experimental error/statistical variation. It is concluded that that sequences with a %Bound [^{99m}Tc()CO)$_3$]$^+$ greater than 100% are completely stable in the PBS buffer. A decrease of up to 16% was detected in the %bound [^{99m}Tc(CO)$_3$]$^+$ after 1hr incubation and remained constant for the duration of the stability assay. This suggests that there may be some instability in the [^{99m}Tc(CO)$_3$]$^+$ conjugated peptide complexes. However, the consistency of the decrease in %bound[^{99m}Tc(CO)$_3$]$^+$ suggests that that the [^{99m}Tc(CO)$_3$-peptide]$^+$ conjugates are stable in PBS buffer and the range in %Bound [^{99m}Tc(CO)$_3$]$^+$ is due to experimental errors or statistical variations

A gradual decrease in %bound [^{99m}Tc(CO)$_3$]$^+$ overtime would be expected for labelled peptides that are kinetically unstable and dissociation of the [^{99m}Tc(CO)$_3$]$^+$ complex has occurred. This was demonstrated by the peptide sequences in the “Controls” category (white) that contained no His residues. After 1hr incubation a decrease in %bound [^{99m}Tc(CO)$_3$]$^+$ to 81% and 66% was observed which further decreased after 24hrs to 6% and 12% for the GQLVNEREGASPPWY and RKNDDSTYAGMIMFE sequences respectively. [^{99m}Tc(CO)$_3$]$^+$ labelled sequences with no His residues are clearly weakly coordinated to [^{99m}Tc(CO)$_3$]$^+$ and are thermodynamically and kinetically unstable when immersed in PBS buffer, free of [^{99m}Tc(CO)$_3^+$. Overtime, a gradual dissociation of the [^{99m}Tc(CO)$_3$]$^+$ complex occurred to give a greater than 85% reduction in the amount of [^{99m}Tc(CO)$_3$]$^+$ bound to the peptides after 24hrs. In summary, there was no detectable loss of radiolabel from any histidine-containing peptides during incubation in PBS for 24 h, whereas histidine-free peptides showed substantial loss of radiolabel.

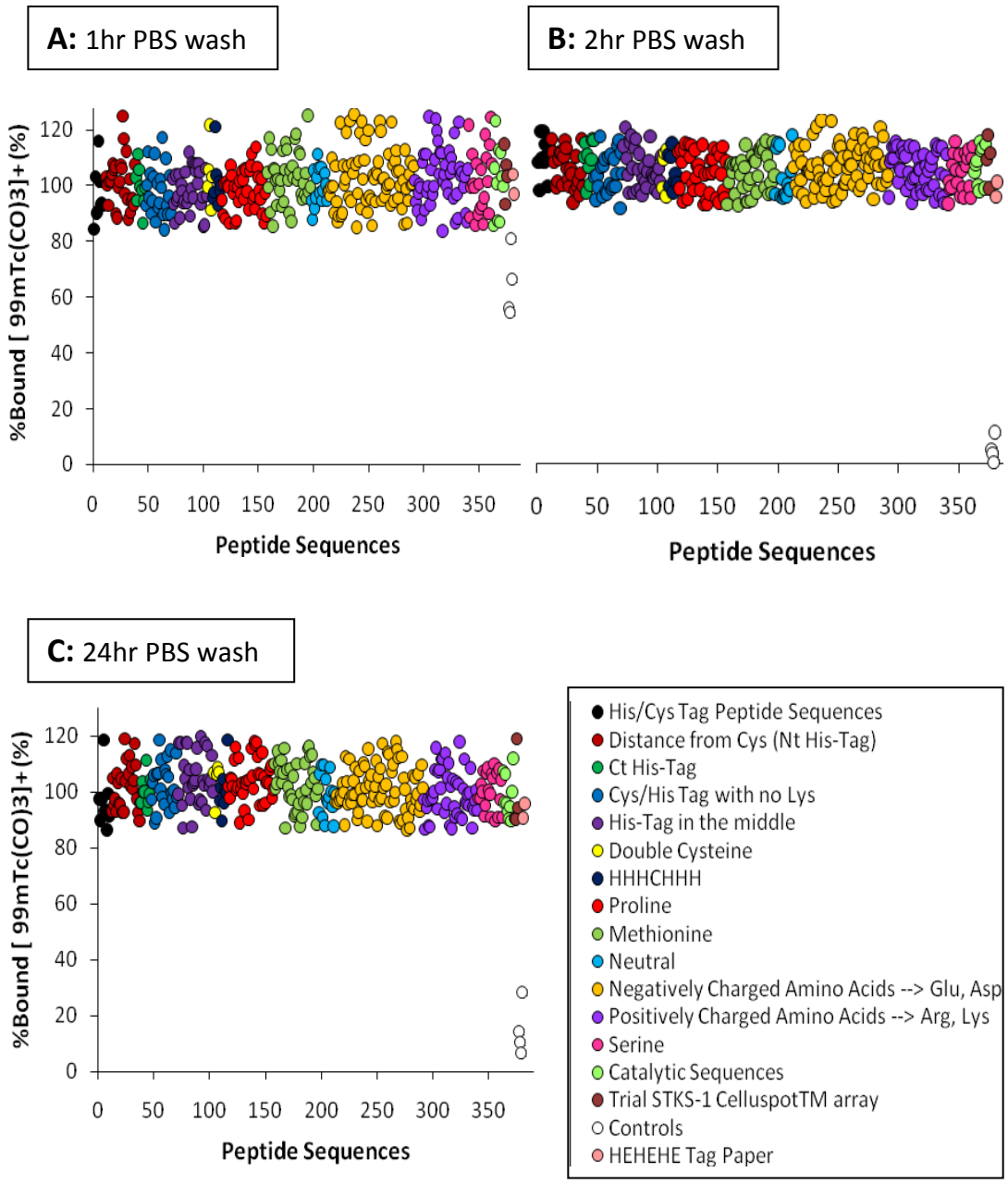

Figure 3.3-24. The calculated %Bound $[^{99m}Tc(CO)_3]^+$ for all peptide sequences after exposure to PBS buffer for 1hr, 2hrs and 24hrs. The data has been presented according to the categories previously established based on the characteristics of the peptide sequences. **A)** Exposure to PBS buffer for 1hr. **B)** Exposure to PBS buffer for 2hrs. **C)** Exposure to PBS buffer for 24hrs. The peptides in the "Controls" category (white circles) correspond to 2 spots on the array with no peptide sequences and 2 spots on the array with peptide sequences that do not contain His amino acids.

3.3.6.2 $[^{99m}Tc(CO)_3$-Peptide$]^+$ Conjugate: Stability in Human Serum

The %Bound $[^{99m}Tc(CO)_3]^+$ for the radiolabelled Celluspot^{TM} array after exposure to human serum for 1, 2 and 24hrs was comparable to that of the stability assay in PBS buffer. In

figure 3.3-25 the phosphor images again reveal that the majority of the peptides remain coordinated to $[^{99m}Tc(CO)_3]^+$ and appear as black spots on the array surface after 1hr, 2hrs and 24hrs incubation in human serum. Image A represents the point at which the sequences have achieved their individual maximum radiochemical yield during the experiment (after 2 hr of incubation with $[^{99m}Tc(CO)_3]^+$). There is not much visible difference between image A and the image obtained following a 24hr exposure to human serum (image D). This suggests that the peptides retain their coordination to $[^{99m}Tc(CO)_3]^+$ whilst subjected to the presence serum proteins. The serum proteins do however bind to the $[^{99m}Tc(CO)_3]^+$ that has unspecifically bound to the Celluspot^{TM} array surface and the background contamination can be seen to decrease overtime.

A complete analysis of the data obtained from the phosphor images can be seen in Figure 3.3-26 which reports the stability as the remaining %bound of $[^{99m}Tc(CO)_3]^+$. All His containing peptides demonstrated a remaining %bound $[^{99m}Tc(CO)_3]^+$ between 84-114% at all time points throughout the 24hr incubation period. The graphs in figure 3.3-26 look identical with the exception of the sequences in the "Controls" category. Of the four peptides in the "Controls" category (white), 2 are peptide free spots on the array and 2 are His-free peptides. Due to the consistent %bound $[^{99m}Tc(CO)_3]^+$ values overtime it can be concluded that the histidine-containing $[^{99m}Tc(CO)_3$-peptide$]^+$ conjugates are stable in human serum and dissociation of the $[^{99m}Tc(CO)_3]^+$complex did not occur. Discrepancies in the %Bound$[^{99m}Tc(CO)_3]^+$ data from demonstrating a 100% stability for the sequences are a consequence of experimental error and statistical variation.

A dramatic decrease in %bound $[^{99m}Tc(CO)_3]^+$ was observed for the non-His containing peptides in the "Controls" category after only 1hr exposure to human serum. Reductions of greater than 85% in bound $[^{99m}Tc(CO)_3]^+$ were detected for these peptides after 1hr incubation (figure 3.3-26, graph A) which increased to 95% after 24hrs incubation (figure 3.3-26, graph B). Dissociation of ^{99m}Tc from His free peptides was faster in serum than in PBS. This suggests that for sequences with no His residues, preferential coordination of $[^{99m}Tc(CO)_3]^+$ for the serum proteins occurs and almost complete dissociation of $[^{99m}Tc(CO)_3]^+$ from the peptide occurred. Consequently, $[^{99m}Tc(CO)_3$-peptide$]^+$ conjugates with no His residues are very unstable in human serum and are not suitable for further applications in clinical studies.

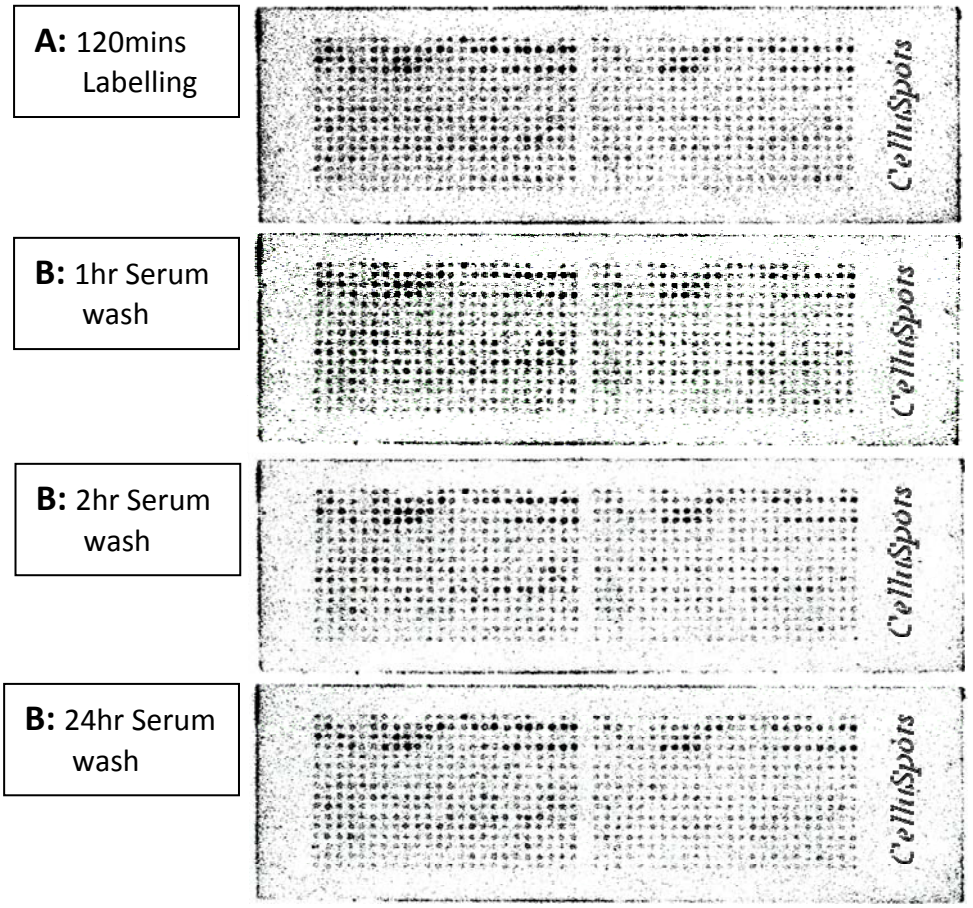

Figure 3.3-25. Phosphor image of the $[^{99m}Tc(CO)_3]^+$ radiolabelled His-Tagged Celluspot™ peptide array at 120 minutes and after incubation in Human Serum for up to 24hrs. Each black spot represents a peptide sequence. **A)** Image after radiolabelling for 120mins with $[^{99m}Tc(CO)_3]^+$, **B)** Image after incubation in PBS buffer for 1hr, **C)** Image after incubation in PBS buffer for 2hrs and **D)** Image after incubation in PBS buffer for 24hrs.

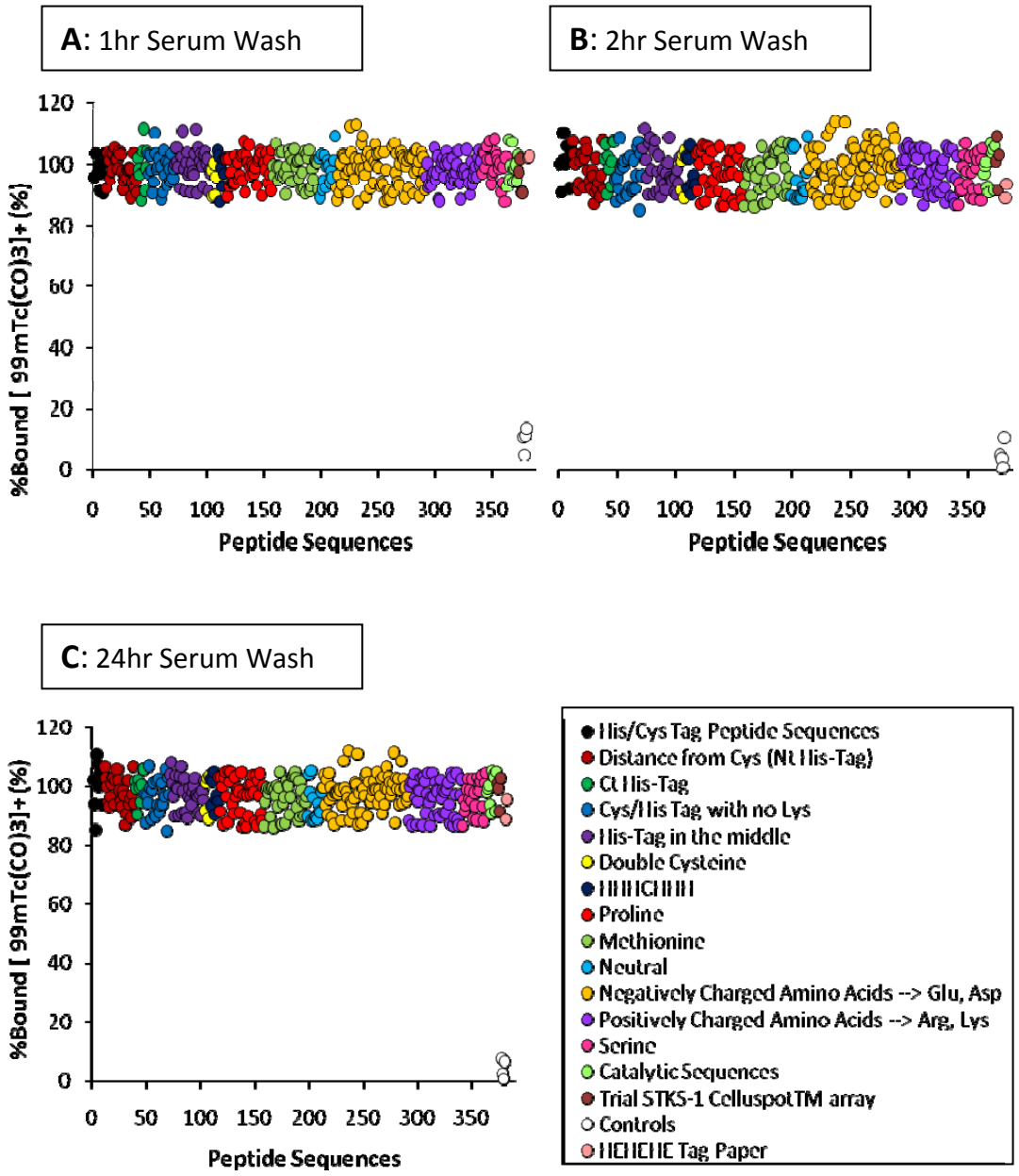

Figure 3.3-26. The calculated %Bound $[^{99m}Tc(CO)_3]^+$ for all peptide sequences after exposure to human serum for 1hr, 2hrs and 24hrs. The data has been presented according to the categories previously established based on the characteristics of the peptide sequences. **A)** Exposure to human serum for 1hr. **B)** Exposure to human serum for 2hrs. **C)** Exposure to human serum for 24hrs.

3.3.6.3 [^{99m} Tc(CO)$_3$-Peptide]$^+$ Conjugate: Stability in 1000 Molar Excess Cys and His Rich Solution

The [^{99m}Tc(CO)$_3$]$^+$ labelled Celluspot^{TM} array was initially incubated in a nominal 1000-fold molar excess solution of the Cys amino acid for 3 hours. After an image had been obtained, the array was subsequently incubated in a nominal 1000 molar excess solution of the His amino acid for 3 hours. The exact molar excess is unknown as the calculation was based on the estimation that the peptide concentration for each spot was approximately 4.19 μmol. A 1000 molar excess was used to guarantee that an excess amount of Cys or His was present in the solution. Visibly, when comparing the phosphor images, it appears qualitatively as though all [^{99m}Tc(CO)$_3$-peptide]$^+$ conjugates maintained their stability throughout both incubations. (Figure 3.3-28) Image A again represents the maximum radiochemical yield achieved by a peptide during the experiment (i.e. after 2 hr incubation with ^{99m}Tc(CO)$_3$]$^+$) and the black spots present in image A are replicated in image B and C. A reduction in the radioactive background from the array surface has occurred post exposure to His and Cys which is predictable as Cys and His are well known chelators for [^{99m}Tc(CO)$_3$]$^+$.

The intensity of the black spots were analysed and a remaining %bound[^{99m}Tc(CO)$_3$]$^+$ calculated for each peptide sequence. (Figure 3.3-29) As previously observed with the serum and PBS buffer stability assays, all His containing peptides maintained a constant %bound [^{99m}Tc(CO)$_3$]$^+$ in the range of 78-118% for the duration of the incubation in excess Cys and His solutions (Figure 3.3-29, graph A and B). None of the His containing sequences demonstrated any unique behaviour, they all had very similar values for the remaining %bound [^{99m}Tc(CO)$_3$]$^+$. In addition it was found that there were no significant differences in %bound [^{99m}Tc(CO)$_3$]$^+$ from the maximum radiochemical yield achieved pre exposure to His and Cys. The consistency of the results implies that all His containing peptides are strongly coordinated to [^{99m}Tc(CO)$_3$]$^+$ and despite the presence of excess His and Cys residues, that could compete thermodynamically for binding sites on the [^{99m}Tc(CO)$_3$]$^+$, the stability of the labelled peptides have been maintained. The Tc-his-tag interaction therefore appears to be highly stable kinetically. Values for %Bound [^{99m}Tc(CO)$_3$]$^+$ above and below 100% are likely to be due to experimental error.

Peptides in the "Controls" category (white) with no His residues again demonstrated a gradual decrease in the remaining [^{99m}Tc(CO)$_3$]$^+$ bound to the sequences during exposure to

Cys and His solutions.(Figure 3.3-27) Like serum proteins, His and Cys demonstrated a more favourable coordination to $[^{99m}Tc(CO)_3]^+$ in comparison to the non His containing peptides. A reduction of 50% in %bound $[^{99m}Tc(CO)_3]^+$ was observed after the first 3hrs incubation in the Cys rich solution (figure 3.3-27, graph A) and after exposure to His, less than 10% $[^{99m}Tc(CO)_3]^+$ remained bound to the sequences (figure 3.3-27, graph B). Coinciding with the previous results for the stability of the $[^{99m}Tc(CO)_3$-peptide$]^+$ conjugates, His residues are necessary to retain coordination to the $[^{99m}Tc(CO)_3]^+$ complex in the presence of cysteine or histidine in the medium.

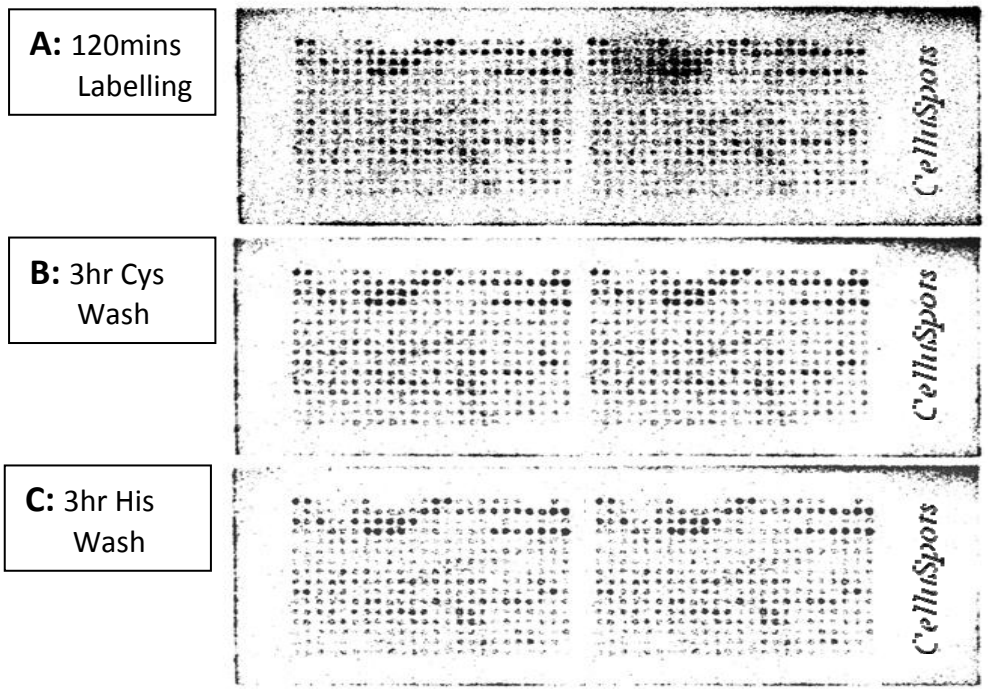

Figure 3.3-27. Phosphor image of the $[^{99m}Tc(CO)_3]^+$ radiolabelled His-Tagged Celluspot™ peptide array at 120 minutes and after incubation in a 1000 molar excess of a Cys and His containing solution for 3hrs consecutively. Each black spot represents a peptide sequence. **A)** Image after radiolabelling for 120mins with $[^{99m}Tc(CO)_3]^+$, **B)** Image after incubation in an excess Cys solution, and **C)** Image after incubation in an excess His solution.

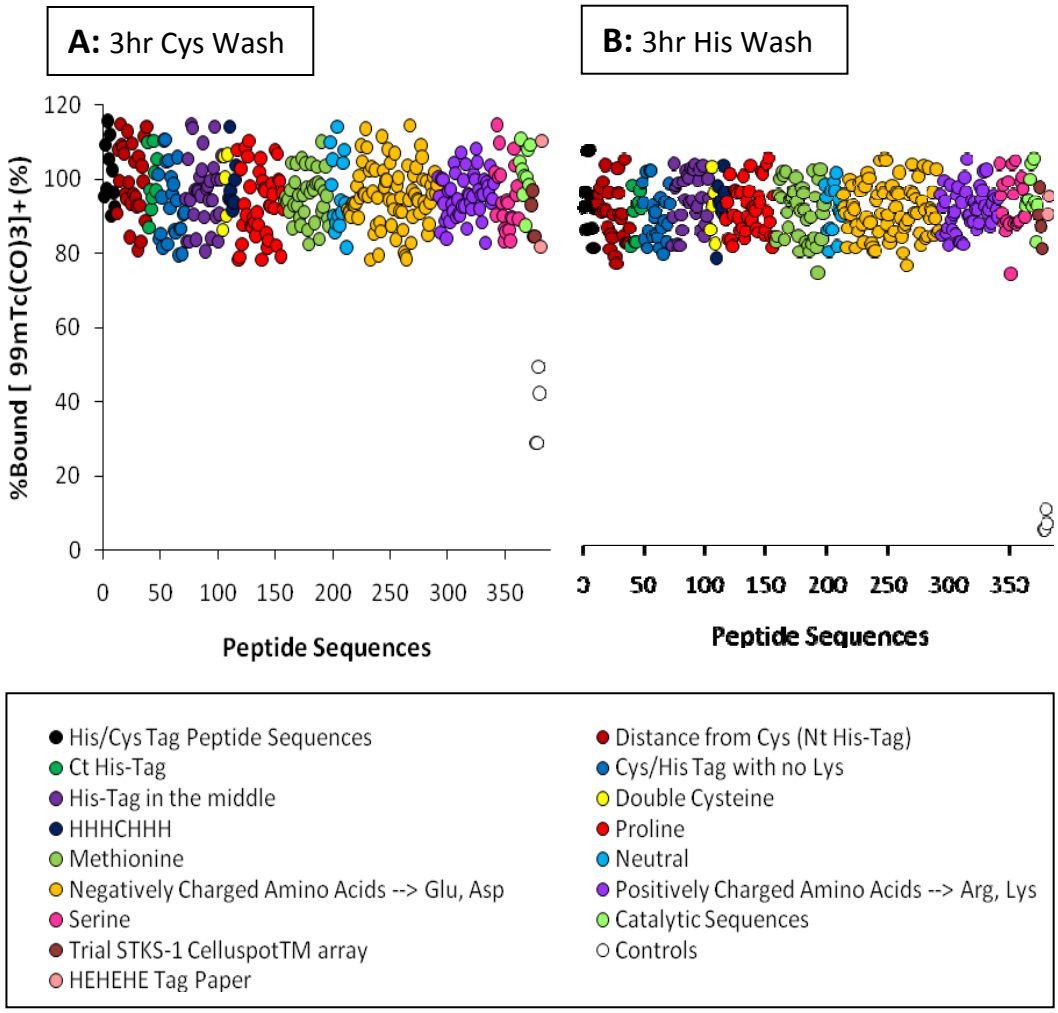

Figure 3.3-26. The calculated %Bound $[^{99m}Tc(CO)_3]^+$ for all peptide sequences after exposure to molar excess Cys and His solutions for 3hrs each consecutively. The data has been presented according to the categories previously established based on the characteristics of the peptide sequences. **A)** Exposure to a Cys rich solution for 3hrs. **B)** Exposure to His rich solution for 3hrs.

3.3.7 DISCUSSION & CONCLUSION

3.3.7.1 $[^{99m}Tc(CO)_3]^+$ Labelling in PBS Buffer at pH 7.4

In chapter 2, it was observed that the addition of a Cys to a His-Tagged peptide significantly improved the labelling efficiency of the sequence with $[^{99m}Tc(CO)_3]^+$. It was concluded that the Cys was responsible for the substantial improvement in labelling efficiency as it coordinated to the $[^{99m}Tc(CO)_3]^+$ complex in addition to 2 His residues (as detected by

tryptic digest and mass spectrometry). Consequently the presence of a Cys adjacent to the His residues became a focal point in the design process of the His-Tagged Celluspot™ array (Chapter 3.2). In addition, the 10 Cys/His peptide sequences previously synthesised and analysed, provided a useful method of assessing the reliability of the data produced by the Celluspot™ array in predicting solution-phase labelling efficiency. The correlation between the labelling efficiency of the Cys/His Tag peptides in solution and on solid phase after 15 minutes incubation time was good and demonstrated that the peptide behaviour on the array was a predictive representation of their behaviour in solution. A similar correlation was observed at the 30, 60 and 120 minute time points. This analysis was carried out to ensure that at the later time points the labelling efficiencies of the peptides would continue to provide an accurate interpretation of what would happen in solution.

Results from the His-Tagged Celluspot™ array revealed that overall, the importance of the Cys for labelling with $[^{99m}Tc(CO)_3]^+$ was not as dominant. Analysis of the array revealed that for sequences, that were identical except for the presence/absence of a Cys residue, the presence of the Cys did improve the labelling efficiency. However the difference in labelling efficiency was not as significant as had been anticipated based on the results of chapter 2. Of the 10 best labelling sequences in the His-tagged array, only 7 contained a Cys and indeed the addition of a c-terminal Cys to the sequence GGRHHHRHHHRGG actually decreased the labelling efficiency. Another consideration was the positioning of the Cys with respect to the His amino acids. Results highlighted that there was very little difference in labelling when the Cys was positioned between 1 to 8 amino acids away from the His residues. A marginal trend suggested that a Cys positioned 1 or 5 amino acids away from the His was least favoured. This could be a result of the Cys attempting to coordinate to the $[^{99m}Tc(CO)_3]^+$ complex. With a Cys next to the His, there will be no flexibility in the peptide chain between the Cys and His which may restrict the ability of the Cys to coordinate to the $[^{99m}Tc(CO)_3]^+$ complex. In addition, peptide chains form alpha helices with approximately 3.6 residues per turn and a Cys, 5 amino acids from the His may be in a structural orientation facing away from the $[^{99m}Tc(CO)_3]^+$ which may prohibit coordination of the $[^{99m}Tc(CO)_3]^+$ to 2 His residues and the Cys simultaneously.

From the array, evidence suggested that Cys can be replaced by Met whilst maintaining the labelling efficiency of the sequence. Dimerisation of proteins is a problem associated with the presence of Cys residues due to their tendencies to form disulphide bonds at a neutral

pH. Met with an alkyl substituent cannot be oxidised to form disulfide bonds. However, the comparable labelling efficiencies observed between the Met and Cys containing sequences suggests that the thiol in Met behaves similarly to that of thiol in Cys in relation to coordination with the $[^{99m}Tc(CO)_3]^+$ complex. In chapter 2 it was revealed that Cys coordinates to the $[^{99m}Tc(CO)_3]^+$ complex and it is a possibility that Met does the same

Met was not present in the 10 sequences with the greatest affinity for $[^{99m}Tc(CO)_3]^+$ due to the lack of sequences that contained a Met residue in combination with multiple Arg or Lys residues on the array surface. When designing the His-Tagged Celluspot™ array, the extent to which the positively charged residues and a high pI influenced the labelling was not yet known. Consequently, the highest pI of a Met containing sequences was 7.21 which does not meet the pI threshold of 9.5 to guarantee a high labelling efficiency. Sequences with both arginines and methionines should be tested to see if further gains in labelling efficiency can be made.

Cys has maintained some influence over the labelling efficiencies of His-Tagged peptides with $[^{99m}Tc(CO)_3]^+$ however it is no longer the most important contributing factor. Instead, sequences with a high pI, preferably greater than 9.5, containing multiple positively charged amino acids in combination with 6 His residues, have demonstrated a superiority for labelling with $[^{99m}Tc(CO)_3]^+$. After 15 minutes incubation time, the phosphor image generated clearly identifies a small subset of peptides as black spots with exceptional affinity for the $[^{99m}Tc(CO)_3]^+$. When comparing the radiochemical yield of all sequences, the dominance of the peptides from the "Positive Charged Amino Acid → Arg and Lys" category for coordinating $[^{99m}Tc(CO)_3]^+$ was clearly evident. This was highlighted in situations where the replacement of a single neutrally charged amino acid to an Arg or Lys significantly increased the labelling efficiency.

Positively charged amino acids increase the pI of a peptide sequence and a slight exponential trend was observed between pI and labelling efficiency. It was not possible to compare the radiochemical yield against pI for all sequences present on the array due to variations in the number and position of His residues within the sequences. The presence of His is the vital and primary requirement for coordination to $[^{99m}Tc(CO)_3]^+$ and an increase in His residues from 2 to 6 has a dramatic effect on the labelling efficiency, independent of the sequence pI. Sequences were classified according to the number and arrangement of His

residues and individual exponential curves reflecting the correlation between pI and labelling efficiency were produced HHHHHH, HHHH, HXHXHX, HXHX and HXXH peptides. The R2 values for these curves ranged from 0.72 to 0.75. This does not indicate an excellent fit between the curves and data points and suggests that the exponential relationship between pI and labelling efficiency is very vague. The range of different sequences compared within each exponential graph is very broad and the only similarities between the sequences is the position and number of His residues. This could be another reason as to why the relationship between pI and labelling efficiency is quite tenuous. Visually, it is clear that once a pI of 9.5 has been reached the radiochemical yield increases quite rapidly in proportion to the increase in pI. For sequences below a pI of 9.5 there are very small differences in radiochemical yield in the pI range of 4.5-9.5.

Arg and Lys are both basic positively charged amino acids with high pKa values and have the greatest contribution towards increasing the pI of a sequence to 9.5, the pI above which a high radiochemical yield is obtained. Data identified that 2-4 Arg residues or 3-4 Lys residues was optimal for a high labelling efficiency. This is primarily because 2 Arg or 3 Lys were the minimum amount of basic residues required in a sequence to give a pI equal or greater than 9.5. Once the 9.5 pI threshold had been reached a significant difference in labelling efficiencies was observed, for example between sequences containing 1 and 2 Arg residues or 2 and 3 Lys residues. An increase in the number of basic residues above the minimum requirement, 2 Arg and 3 Lys, did not considerably improve the labelling efficiencies much further.

Overall, the Arg containing sequences demonstrated a greater affinity for the $[^{99m}Tc(CO)_3]^+$ than the Lys containing sequences which is most probably related to the higher pI achieved by the Arg sequences corresponding to an increase in labelling efficiencies. The Arg side chain has a greater basicity and higher pKa than that of the Lys side chain which coincides with a stronger influence on the pI of a sequence. More Lys residues are therefore required in a labelling sequence to compensate for the lower pKa of its side chain. On the His-tagged Celluspot™ array there were no sequences with more than 4 Lys or 4 Arg residues. Comparisons were made between the number of Arg and Lys residues required in sequences with a $(His)_6$-Tag. For sequences with abbreviated His-Tags, e.g. HHHH, HXHXHX , HXHX and HXXH, there were not enough data to determine how many Arg and Lys residues were required to generate a high labelling efficiency.

Arg has been established as having the greatest influence on the labelling efficiencies of a sequence. The exact preferred position of the Arg with respect to the His is not completely known. It was identified that sequences in which the Arg separates the His, HRHRHR, HRHR and HRRHR, demonstrated the lowest radiochemical yields which could be either due to the positioning of the Arg or the number of His residues. Arg could sterically hinder the imidazole side chains of the His residues and interfere with their coordination to $[^{99m}Tc(CO)_3]^+$. Another possibility is that for HRHRHR, HRHR and HRRHR sequences there are less His residues than the His-Tag and consequently complexation is entropically less favourable. Sequences with 2 His residues definitely showed the lowest radiochemical yield. For $(His)_6$-Tag sequences there are no apparent rules for the positioning of the Arg in relation to the His other than the HHHHHHXXRRRX sequence which showed preferential coordination to $[^{99m}Tc(CO)_3]^+$ in comparison to other Arg and $(His)_6$-Tag combinations. However, the amount of data available to properly analyse the optimal position of the Arg with respect to His was not sufficient.

Not only does the addition of positively charged amino acids to the sequence improve labelling but replacing the residues with negatively charged Glu and Asp is detrimental to the labelling efficiency when labelling occurs in PBS buffer. Comparisons made between sequences in which single amino acids were substituted for a negative, positive or neutrally charged residue revealed that negatively charged amino acids further decreased the labelling efficiency. Amino acids with uncharged side chains, Gly and Ser, had a slightly higher labelling efficiency than the same sequences with a Glu or Asp substitution. This was confirmed in the observation that an increase in pI of the sequence correlates with an increase in labelling efficiency. Negatively charged amino acids, Glu and Asp, have side chains with a pKa of 4.15 and 3.71 respectively which due to the negative charges gives a low pI. The exponential relationship between pI and labelling efficiency implies that the sequences containing the most negatively charged amino acids have the lowest labelling efficiencies. Substituting a Glu or Asp for a neutrally charged amino acid such as Gly or Ser is beneficial.

The superiority of the positively charged amino acids for increasing labelling efficiency remained after a total incubation time of 30, 60 and 120 minutes. Over time other peptide sequences began to demonstrate an increase in radiochemical yield however, no other characteristics could be identified that accelerated the labelling of a peptide sequence with

$[^{99m}Tc(CO)_3]^+$. By 120 minute all peptides had been radiolabelled to a certain extent with $[^{99m}Tc(CO)_3]^+$. For applications in protein radiolabelling, the information obtained after 15 minutes incubation time is most valid as it reveals the most kinetically favourable products. Labelling sequences from the His-Tagged Celluspot™ peptide array with a high radiochemical yield after 15 minutes should enable fast and efficient protein radiolabelling despite the low protein concentrations present. The superiority of the CLRRRLAHHHHHH for chelating $[^{99m}Tc(CO)_3]^+$, in comparison to all other sequences on the Celluspot™ array, has been established throughout the incubation period demonstrating the highest radiochemical yield at 15, 30, 60 and 120 minutes. Comparisons between the radiochemical yields of the previously published $(His)_6$ sequences and the newly identified Arg/$(His)_6$ sequence revealed that a significant 8 fold improvement in labelling efficiencies had been achieved. Theoretically, CLRRRLAHHHHH should significantly improve the labelling affinity of a protein for $[^{99m}Tc(CO)_3]^+$ by 8 fold providing the opportunity to facilitate a fast and efficient labelling procedure at low protein concentrations whilst maintaining a specific activity suitable for clinical and pre-clinical applications.

Emphasis has currently been focused on the influence of the neighbouring amino acids for improving labelling efficiency. However, the importance of the His residues must not be ignored. Ultimately, according to the STKS-1 Celluspot™ peptide array (Chapter 3.1), His residues are essential for coordination to the $[^{99m}TYc(CO)_3]^+$ complex and all sequences included on the His-Tagged Celluspot™ peptide array included at least 2 His residues except the four sequences in the “Controls” category. As expected, there was a proportional increase between radiochemical yield and the number of His residues within a sequence. Sequences with 6 His residues are entropically more favourable and the coordination to $[^{99m}Tc(CO)_3]^+$ is more probable.

$(His)_6$-Tagged sequences or even HXHXHX sequences demonstrate a significantly higher labelling efficiency than sequences with 2 His-residues which helps reduce the doubt associated with whether radiolabelling a $(His)_6$-Tagged protein occurs site-specifically. A sequence containing a $(His)_6$-Tag in a medium sized protein with several other individual His residues dotted around should provide a method of site-specific labelling for $[^{99m}Tc(CO)_3]^+$ according to the Celluspot™ array results. In addition, the presence of the Arg increased labelling of the $(His)_6$-Tag by 8-fold and the favourability of the $[^{99m}Tc(CO)_3]^+$ complex to an Arg/$(His)_6$-Tagged protein should guarantee site-specific labelling.

Surprisingly, in this study, HXHXHX (3 His) sequences have an overall higher radiochemical yield than HHHH (4 His) which contradicts the theory that the more His residues in a sequence the more beneficial it is for the labelling efficiencies . However, the data available for the HHHH sequences are limited and only cover a narrow range of different neighbouring amino acids. HXHXHX sequences have been included with pIs in the range of 4.26 to 12.48 whereas HHHH sequences have pIs in the range of 6.42 to 8.26. For 4 consecutive His residues there are no sequences with a pI > 9.5, the threshold at which a high radiochemical yield has been observed. Consequently, this indicates that for a peptide sequence to achieve high labelling efficiencies a balance between the number of His residues and the pI of the sequence is required. It is not solely dependent on either characteristic but a combination of both factors. Sequences with a pI greater than 9.5 are influenced by the number of His residues. A $(His)_6$-Tag demonstrates a significantly higher radiochemical yield in comparison to HXHXHX, HXHX and HXXH motifs. HXHX and HXXH containing sequences have the lowest radiochemical yields which are primarily associated to the presence of only 2 His residues within the sequence. There is a slight preference for HXHX implicating that $[^{99m}Tc(CO)_3]^+$ favours coordination to the structural arrangement of alternate His residues rather than in a 1-4 separation. Addtional sequences combining HHHH with arg and/or lys should be evaluated, along with met-containing sequences suggested earlier.

Given the results from the His-Tagged Celluspot™ peptide array focus has now been redirected towards the influence of neighbouring positively charged amino acids and the overall pI of the sequence. An optimised labelling sequence for $[^{99m}Tc(CO)_3]^+$ is primarily dependant on the combination between the number of His residues and the overall pI of the sequence, which is influenced by the addition of positively charged amino acids. It is uncertain as to why the positively charged amino acids have such a powerful influence on the labelling efficiencies of the peptide sequences. At a labelling pH of 7.4, sequences containing multiple Arg residues will be positively charged. Considering that $[^{99m}Tc(CO)_3]^+$ is also presumed to be positively charged the favourable coordination between Arg sequences and $[^{99m}Tc(CO)_3]^+$ is surprising. A further discussion with regards to the role of the positively charged amino acids in $[^{99m}Tc(CO)_3]^+$ coordination to His-Tagged sequences will be pursued in Chapter 5.

3.3.7.2 Stability of the [^{99m}Tc(CO)$_3$-peptide]$^+$ Conjugates in PBS Buffer, Human Serum and His or Cys Rich Solutions

Stability of the [^{99m}Tc(CO)$_3$-peptide]$^+$ conjugates was assessed in PBS buffer, human serum and in competition with a solution of a large excess of free histidine and cysteine. These challenges model the potential scenarios in which a [^{99m}Tc(CO)$_3$]$^+$ labelled His-Tagged protein may be subjected to during pre-clinical or clinical experimentation. Prior to injection, the radiolabelled protein may be required to remain in solution at room temperature or 37^{o}C. Subsequent to injection, the [^{99m}Tc(CO)$_3$]$^+$ labelled protein will be considerably diluted by human serum and surrounded in excess by serum proteins which can also coordinate to [^{99m}Tc(CO)$_3$]$^+$. In both situations it would be detrimental if the [^{99m}Tc(CO)$_3$]$^+$ dissociated from the labelled protein. It is required that a labelling sequence is designed to strongly coordinate [^{99m}Tc(CO)$_3$]$^+$ and remain stable forn solution and once injected into the blood stream. The kinetic stability of the coordination was tested through incubation of the labelled Celluspot^{TM} array in a solution containing approximately 1000 molar excess of His or Cys amino acid. Both, in particular His, are well established for binding to [^{99m}Tc(CO)$_3$]$^+$.

Overall all His-Tagged [^{99m}Tc(CO)$_3$]$^+$ peptides on the array labelled in PBS buffer demonstrated an excellent kinetic stability in PBS, human serum and His or Cys rich solutions. The %bound [^{99m}Tc(CO)$_3$]$^+$ values generally varied between 80-125% for all peptide sequences containing a His-Tag at the 1hr, 2hr and 24hr time points. The maximum decrease of 20% in %bound [^{99m}Tc(CO)$_3$]$^+$ could potentially be accounted for by the thermodynamic and kinetic instability of the [^{99m}Tc(CO)$_3$-peptide]$^+$ conjugates. However, if kinetically unstable the %bound [^{99m}Tc(CO)$_3$]$^+$ of the peptide conjugates would be expected to gradually decrease overtime due to the dissociation of the [^{99m}Tc(CO)$_3$]$^+$ complex from the peptides. The decrease in %bound [^{99m}Tc(CO)$_3$]$^+$ remains at a constant level throughout the assay and is not associated with a specific sequence or sequences in a specific category. This suggests that it is a result of experimental error. Coinciding with this is the unrealistic increase in %bound [^{99m}Tc(CO)$_3$]$^+$, up to 25%, which was consistently observed at all time points and is again likely to be associated with experimental error and or/statistical variation. The washing buffers in which the His-Tagged Celluspot^{TM} arrays were immersed did not contain any radioactive [^{99m}Tc(CO)$_3$]$^+$ and therefore it is impossible that an increase in radiochemical yield of the peptides occurred. Experimental error could be associated

with a number of different factors; inaccuracies in assigning a DLU value to each peptide sequence; the exposure of the array to the phosphor film; and, the inconsistencies in the radioactive background of the array which has only been represented by a single DLU value for standardising the data. For the stability assays, only a single Celluspot^{TM} peptide array was used with each washing buffer which could account for the large range in %bound $[^{99m}Tc(CO)_3]^+$. The experiment could be repeated to increase the accuracy of the data.

All $(His)_6$-tagged peptides maintained a constant %bound $[^{99m}Tc(CO)_3]^+$ throughout incubation in all washing buffers. From the similarity in %bound $[^{99m}Tc)(CO)_3]^+$ throughout the stability assay, it is possible to conclude that the $[^{99m}Tc(CO)_3$-peptide$]^+$ conjugates are stable in PBS buffer and human serum for up to 24hrs. Once conjugated to a $(His)_6$-Tagged containing peptide the $[^{99m}Tc(CO)_3]^+$ remains coordinated despite competition from the serum proteins and 1000 molar excess of His or Cys amino acids. As a consequence the His-Tagged sequences are suitable for applications in pre-clinical or clinical experiments as they can demonstrate a high stability for adequate periods of time.

Peptides not containing a His residue were unstable in human serum, PBS buffer and competition with a 1000 molar excess Cys and His solutions. This coincides with the principle that His residues are required for $[^{99m}Tc(CO)_3]^+$ coordination. The non-His containing peptides are unspecifically bound to $[^{99m}Tc(CO)_3]^+$ after 120 minute incubation. In competition with serum proteins and excess free His and Cys residues, the $[^{99m}Tc(CO)_3]^+$ rapidly dissociates over 1hr leading to greater than 90% reduction in $[^{99m}Tc(CO)_3]^+$ bound to the peptide. In PBS buffer the dissociation is more gradual as PBS does not compete for coordination to $[^{99m}Tc(CO)_3]^+$, but a reduction of 85% in $[^{99m}Tc(CO)_3]^+$ bound to the peptide was still observed after 24hrs. To conclude $[^{99m}Tc(CO)_3]^+$ conjugated non-His containing peptides are thermodynamically and kinetically unstable. It is essential that His residues are included in the sequence both for high labelling efficiencies and for stability of the $[^{99m}Tc(CO)_3$-peptide$]^+$ conjugate in buffered solutions and human serum. However, it is also clear that once labelled, His-containing sequences all have adequate stability to justify in vivo evaluation and so the primary criterion for selection of the best sequence would be labelling efficiency and not stability.

3.3.7.3 $[^{99m}Tc(CO)_3]^+$ Labelling in Citrate Buffer (pH 5.1) and Tris-HCl Buffer (pH 7.4 and pH 8.8)

A substantial decrease in radiochemical yield was observed for the $[^{99m},Tc(CO)_3]^+$ labelling of peptides in PBS buffer in comparison to citrate buffer and tris-HCl buffer at pH 5.1, 7.4 and 8.8 respectively. It is difficult to differentiate whether it is the influence of the pH or the buffer that has a negative impact on labelling. With PBS demonstrating narrow buffering capacity it was not possible to use the buffer at an acidic or basic pH within a large enough range suitable for the comparison studies. Therefore citrate buffer was chosen for the acidic pH of 5.1 and Tris-HCl for the basic pH of 8.8 and control at pH 7.4.

Citrate buffer was suitable for the labelling experiments at an acidic pH as it is a biological buffer and appropriate for clinical use. However, in terms of the labelling conditions required for $[^{99m}Tc(CO)_3]^+$ conjugation, a citrate buffer environment at pH 5.1 is definitely not the optimal buffer to be used. No coordination to $[^{99m}Tc(CO)_3]^+$ was demonstrated by the peptide sequences. Tris is also a biological buffer and suitable for clinical use. In hindsight, tris may have not been the most appropriate buffer to provide a basic environment for $[^{99m}Tc(CO)_3]^+$ labelling due to its ability to coordinate $[^{99m}Tc(CO)_3]^+$ through the primary amine in its structure. Tris could have competed against the His-Tagged sequences for the coordination sites of $[^{99m}Tc(CO)_3]^+$ and as a result a low radiochemical yield was observed for the peptides on the array. When washing was performed in Tris-HCl buffer the $[^{99m}Tc(CO)_3]^+$ background was reduced on the Celluspot^{TM} array. One possibility is that that Tris-HCl has a preferential coordination to $[^{99m}Tc(CO)_3]^+$ than the cellulose membrane and unspecifically bound $[^{99m}Tc(CO)_3]^+$ to the array dissociates in the presence of Tris. Peptide sequences demonstrated conjugation to $[^{99m}Tc(CO)_3]^+$ in Tris-HCl buffer at pH 8.8 and at pH 7.4 after 120mins and once a $[^{99m}Tc(CO)_3$-peptide$]^+$ conjugate had formed it was stable despite washing in non-radioactive Tris-HCl for 3 hrs. A two fold increase in labelling efficiency was achieved in Tris-HCl at pH 7.4 rather than pH 8.8, however this was not comparable with the significantly higher labelling efficiencies of the peptide sequences in PBS buffer. Initial conclusions suggest that optimal labelling conditions for $[^{99m}Tc(CO)_3]^+$ are PBS buffer and a pH of 7.4 is preferable to an acidic or basic pH.

Consideration must be taken that Tris-HCl is able to coordinate $[^{99m}Tc(CO)_3]^+$ and even though it is appropriate to conclude that Tris-HCl buffer is detrimental for labelling, it cannot be completely deduced that a basic pH is also not suitable. There was a slight

preference for radiolabelling at pH 7.4 with Tris-HCl buffer rather than 8.8 but the difference was not significant enough to accurately reach a definitive answer. The nature of the buffer, probably because of its effect on the sequence or the $Tc(CO)_3$ complex, appears to be critical therefore further investigations into the use of a wide range of buffers at neutral or basic pH should be carried out. In particular, some publications involving the $[^{99m}Tc(CO)_3]^+$ labelling of $(His)_6$-Tagged proteins have implemented a carbonate buffer at pH 9 as the labelling condition.(*4*) In that work, to optimise the labelling conditions investigations were reported in which the pH was monitored from pH 4 to 10 using an acetate buffer, 2-[N-morpholino] enthanesulfonic acid buffer (MES) and carbonate buffer. The carbonate buffer proved to be most suitable in the labelling studies. No comparisons were made to PBS buffer. The His-Tagged Celluspot™ array provides the opportunity to further easily analyse multiple conditions simultaneously and also to observe whether different characteristics of a labelling sequence will perform better under different buffering conditions.

In PBS buffer, Arg containing sequences demonstrated a significant 8 fold increase in radiochemical yields in comparison to all other His-Tag sequences after 15mins. Significantly lower radiochemical yields for the positively charged sequences were observed when radiolabelling took place in citrate and Tris-HCl buffer. In these buffers, all peptides demonstrated equivalent radiochemical yields throughout the reaction time period. This indicates that a specific role for PBS buffer may be a factor that needs to be taken into consideration when attempting to explain the influence of the positively charged Arg on the coordination between the His and $[^{99m}Tc(CO)_3]^+$ complex.

It is presumed that in Tris-HCl buffer low radiolabelling is observed perhaps due to the interference of the Tris in binding $[^{99m}Tc(CO)_3]^+$. It is not thought that Tris has preferential $[^{99m}Tc(CO)_3]^+$ binding over the His-Tag sequences as labelling does occur after 60-120mins incubation. However in a labelling situation, Tris is in a large excess in comparison to the small concentration of the peptides on the array. Currently, no explanation can be given for the complete lack of radiolabelling in citrate buffer. In chapter 5, further discussions have been made in relation to the reasoning behind the poor radiochemical yields observed for the peptides when labelling occurs in Tris-HCl and citrate buffer.

3.3.7.4 Conclusion and Future

In summary,preferential chelation to $[^{99m}Tc(CO)_3]^+$ was observed for sequences with at least 2 Arg residues , an adjacent $(His)_6$-Tag and a pI > 9.5 In terms of the labelling conditions, PBS at pH 7.4 was identified as the most appropriate buffer to use. CLRRRLAHHHHHH, the sequence demonstrating the highest labelling efficiencies at all time points, coincides with the requirements identified as being most important when designing labelling sequences for $[^{99m}Tc(CO)_3]^+$ coordination. The significantly higher radiochemical yields achieved with CLRRRLAHHHHHH will be most beneficial when radiolabelling a protein with $[^{99m}Tc(CO)_3]^+$. This will improve the labelling efficiency allowing for the labelling to occur at lower protein concentrations whilst maintaining high levels of specific activity and site-specificity suitable for pre-clinical applications and avoiding purification steps in the production procedure. In addition, the site specificity of the labelling reaction should be achieved under mild conditions regardless of the nature of other domains of the protein. Considering the non-His and Cys containing sequences labelled at orders of magnitude less efficiently than CLRRRLAHHHHHH a $[^{99m}Tc(CO)_3$-protein$]^+$ conjugate with high structural homogeneity and site-specificity with intact biological recognition activity should be achieved. As a labelling sequence, CLRRRLAHHHHHH has the potential to be incorporated into libraries of trial recombinant proteins for the large scale evaluation of their suitability as radiopharmaceuticals.

The Arg containing $[^{99m}Tc(CO)_3$-peptide$]^+$ conjugates also demonstrated an excellent resistance to loss of the $[^{99m}Tc(CO)_3]^+$ complex in PBS buffer, human serum and when exposed to the competitive 1000 molar excess His or Cys containing solution. This provides the evidence required to proceed with the engineering of the CLRRRLAHHHHHH and other sequences of similar labelling efficiency into a recombinant for subsequent radiolabelling and in vivo studes.

Analysis of the labelling conditions identified PBS at pH 7.4 as the most appropriate buffering system. However comparisons were only made between citrate buffer at a acidic pH of 5.1 and Tris-HCl at a basic pH 8.8 and neutral pH 7.4. Other buffering systems should be investigated in parallel with PBS in particular carbonate buffer at pH 9-10 as this has been already used in the $[^{99m}Tc(CO)_3]^+$ labelling of proteins. Celluspot™ array provides a method in which the analysis of multiple buffering systems can be quickly assessed and can

potentially provide a greater understanding with regards to the optimal labelling conditions.

This chapter has described how Celluspot™ peptide array has identified CLRRRLAHHHHHH as a sequence demonstrating superior labelling efficiencies for $[^{99m}Tc(CO)_3]^+$. The engineering of this sequence into a recombinant protein can now be accomplished and subsequent analysis performed to examine whether the superior affinity for $[^{99m}Tc(CO)_3]^+$ in translational into a protein context.

REFERENCES

1. Tavare, R., Torres Martin De Rosales, R., Blower, P. J., and Mullen, G. E. (2009) Efficient site-specific radiolabeling of a modified C2A domain of synaptotagmin I with [99mTc(CO)3]+: a new radiopharmaceutical for imaging cell death, *Bioconjug Chem 20*, 2071-2081.
2. Tolmachev, V., Hofstrom, C., Malmberg, J., Ahlgren, S., Hosseinimehr, S. J., Sandstrom, M., Abrahmsen, L., Orlova, A., and Graslund, T. (2010) HEHEHE-tagged affibody molecule may be purified by IMAC, is conveniently labeled with [(m)Tc(CO)](+), and shows improved biodistribution with reduced hepatic radioactivity accumulation, *Bioconjug Chem 21*, 2013-2022.
3. Tolmachev, V., Hofstrom, C., Malmberg, J., Ahlgren, S., Hosseinimehr, S. J., Sandstrom, M., Abrahmsen, L., Orlova, A., and Graslund, T. (2010) HEHEHE-tagged affibody molecule may be purified by IMAC, is conveniently labeled with [(9)(9)(m)Tc(CO)(3)](+), and shows improved biodistribution with reduced hepatic radioactivity accumulation, *Bioconjug Chem 21*, 2013-2022.
4. Waibel, R., Alberto, R., Willuda, J., Finnern, R., Schibli, R., Stichelberger, A., Egli, A., Abram, U., Mach, J. P., Pluckthun, A., and Schubiger, P. A. (1999) Stable one-step technetium-99m labeling of His-tagged recombinant proteins with a novel Tc(I)-carbonyl complex, *Nat Biotechnol 17*, 897-901.

CHAPTER FOUR

$[^{99m}Tc(CO)_3]^+$ Radiolabelling of a Protein with an Arg/$(His)_6$-Tag

4 Effect of Novel Optimised His-Tags on $[^{99m}Tc(CO)_3]^+$ Radiolabelling and Biological Properties of Targeting Proteins.

4.1. INTRODUCTION

4.1.1 Aim & Objective

Radiolabelling the CelluspotTM peptide array identified Arg containing $(His)_6$-Tag (Arg/His) sequences as having the highest affinity for the $[^{99m}Tc(CO)_3]^+$. These sequences are expected to provide an efficient method for the fast labelling of proteins at low concentrations, if their properties are preserved when they are part of a full protein. To evaluate this concept an Arg/His sequence was engineered into the J591 single chain antibody (scFv) at the C-terminal.

Comparative radiolabelling studies were performed with other non-Arg containing $(His)_6$-Tag proteins to determine whether the favourable radiolabelling characteristics of the optimised sequences persist when incorporated into proteins and whether the sequences affect the biological properties of the proteins. The aim was to investigate whether the Arg containing sequences can provide faster labelling, at lower protein concentration, at lower temperature, with more site specificity and without the additional purification step, compared with conventional $(His)_6$-Tagged proteins.

Another objective was to evaluate the affinity of the J591scFvJWT protein for the PSMA target to investigate the effect of the Arg containing sequence on the biological properties of the protein. To achieve this, cell binding assays were performed on the J591scFvJWT and two other His-Tagged control proteins; J591scFv and huJ591scFv.

In the following sections (4.1.2), preceding Methods and Results, background information is provided on the example proteins used in this work.

4.1.2 J591 targeting Prostate Specific Membrane Antigen (PSMA)

J591(scFv) is an antibody derived from the monoclonal antibody J591 which recognises an extracellular epitope of prostate specific membrane antigen (PSMA). Also known as Glutamate Carboxypeptidase II (GPCII), PSMA is a well-established marker for prostate carcinoma which is one of the most commonly diagnosed cancers.(*1*) In 1990s in the US approximately 38% of deaths of men 50 years or older were accounted for by prostate cancer.(*2*) PSMA is a marker that demonstrates elevated levels of expression for virtually all prostate cancers with a further increase observed for metastatic disease and aggressive carcinomas.(*3-5*) It has been used in diagnostic applications in which ProstaScint, the ^{111}In labelled monoclonal antibody 7E11-C5, has been one of the most recognisable tools for targeting PSMA on prostatic cell surfaces.(*6-8*) Due to its restricted expression in non-malignant tissues and its increased expression with cancer progression, PSMA has been identified as having excellent target properties for the detection and possible therapy of prostate tumours.(*9-10*) The Prostascint scan revealed an increased sensitivity and specificity in comparison to the conventional CT and MRI methods in prostatic cancer patients.(*11*) Despite its success, any further enhancements to the diagnostic value of ProstaScint were limited due to the intracellular localisation of its antigen, and as a result, the production of a variety of antibodies targeting extracellular domains of PSMA was carried out.(*12-13*)

A deimmunised version of the mAb J591 was one of the first antibodies described and characterised for targeting extracellular domains of PSMA in a number of different clinical studies.(*14-17*) Two combined phase I trials with ^{111}In-J591/^{90}Y-JF591 for imaging followed by immunotherapy and ^{177}Lu-J591 for imaging, demonstrated that J591 accurately targets bone and soft tissue lesions; the lesion detectability was 94% for bone lesions and 72% for soft tissue lesions as compared to CT and bone scans.(*17*) Similarly, a sensitivity of 67% for soft tissue and 93% for bone lesions with 100% selectivity was reported in an ^{111}In labelled J591 study, and a phase I study identified ^{111}In-J591 as a suitable imaging agent for selective and safe targeting of the vasculature of prostate tumours.(*14-15*) Excellent targeting properties were observed for the mAb J591 but, due to the use of a full length antibody conjugate, a long circulation time was observed and to obtain a sufficient contrast in the images, scans had to be performed days after the injection of the tracer. For pre-clinical

studies with ^{89}Zr-J591 and ^{64}Cu-J591, PET scans had to be performed 24hr and 16hr respectively post tracer injection to obtain clear images.(*18-19*) The use of isotopes with a shorter half life, such as ^{99m}Tc, in combination with intact antibodies with correspondingly long biological half lives can be detrimental to obtaining images with good target to background contrast. To compensate, a higher dose of ^{99m}Tc is required which gives a higher radiation dose to the patient. A higher radiation dose to patients also occurs when using the intact antibodies radiolabelled with longer lived radioisotopes as they circulate for much longer periods of time. Increasing the radiation exposure to patients should be avoided at all costs.

4.1.3 Antibodies, Diabodies and Single Chain Antibodies

The engineering of an antibody into smaller fragments is possible whilst largely retaining the antigen binding properties.(*20-22*) Smaller antibody fragments are providing solutions to some of the challenges of imaging with intact antibodies. Protein engineering strategies have been designed to engineer fragmented antibodies specifically for imaging and therapeutic applications as a strategy for improving and optimising the targeting and clearance properties of full length antibodies.(*23*) Advantages have included improvements in the diffusion and transport of smaller fragments into tumours or other target tissues. The smaller size allows for more rapid and even tissue penetration which leads to a larger accumulation in the target. In addition, smaller antibody fragments often accelerate blood clearance which when conjugated to radioactive or therapeutic probes lowers their exposure times to healthy tissues. Due to the rapid pharmacokinetics of the smaller antibody fragments, imaging can potentially occur at a 1hr to 8hr time point post tracer injection. This reduces patient exposure to the toxicity of the radioisotope and biological activity of the antibody whilst minimising the total procedure time. One limitation that must be considered is the high uptake and retention of radiolabelled antibody fragments in the kidney which increases radiotoxicity and can lead to kidney failure.(*24*) However, many strategies have been investigated in an attempt to overcome this problem such as the use of lysine infusion or polyglutamic acid and succinylated gelatine combination to reduce the renal uptake of ^{111}In-labelled-DTPA or ^{111}In-labelled-DOTA conjugated antibody fragments.(*24-25*)

The smallest fragments engineered are single chain antibody Fv fragments (scFv approx 25 kDa) which consist of variable light VL and heavy VH domains connected by a short peptide linker of 10 to 25 amino acids (Figure 4-1). ScFvs demonstrate rapid blood clearance, $t_{1/2}$ Blood = 0.5-2hrs, but as a result reach lower activity levels in the tumours compared to whole antibodies.(*26*) Diabodies are scFv dimers (approximately 55 kDa) and are the smallest antibody fragments that retain the bivalency of the parental antibody (Figure 4.1-1). As a result, in combination with a slightly longer blood half life ($t_{1/2}$ Blood = 3-7hrs), a significant improvement can be seen in tumour retention times.(*27*) Other larger fragments such as minibodies and scFv-Fcs, 80kDa or 105kDa respectively, have been produced by fusing the scFv to the CH3 domain or the Fc fragment of the antibody.

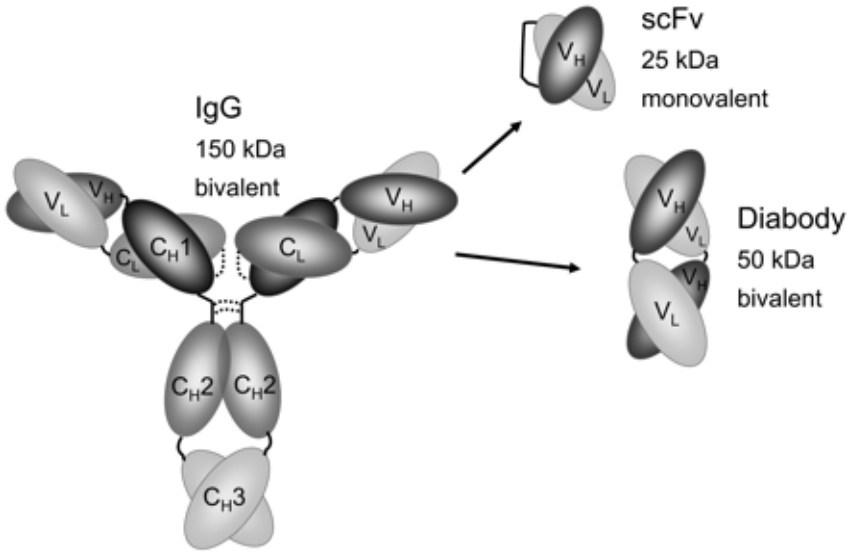

Figure 4-1. Schematic representation of an intact antibody (IgG) and its scFv and diabody fragments. The scFv fragment consists of the variable light and heavy chain domains and the diabody is a dimer of the scFv which maintains the bivalency of the antibody. scFv and diabodies have a molecular weight of approximately 25kDa and 50kDa respectively.(*28*)

Diabodies and scFvs have been engineered against a variety of antigens and radiolabelled for preclinical imaging mainly with PET radioisotopes.(*29-33*) For example, the C6.5 scFv diabody demonstrated efficient targeting and excellent uptake in HER2 positive tumours with a longer tumour retention time which is advantageous for applications as delivery vehicles for therapeutic agents.(*34*) Studies have suggested that these smaller antibody fragments are suitable for clinical translation as diagnostic tracers. Diabodies and scFv fragments are potential formats for radiolabelling with relatively short-lived isotopes such

as ^{99m}Tc and therefore were selected as a model system for the purpose of this study. The antiPSMA antibody, J591, was expressed as scFv and diabody fragments with Arg/$(His)_6$ containing sequences at the C-terminal for site specific labelling with ^{99m}Tc and subsequent SPECT imaging of PSMA expression in prostate cancer models.

4.1.4 J591diaJWT-Cys, J591 scFv JWT, J591diaJWT Proteins and Control Proteins

From the results of the His-Tagged CelluspotTM peptide array (Chapter 3.3), CLRRRLAHHHHHH was identified as the sequence that demonstrated the best labelling efficiency for the $[^{99m}Tc(CO)_3]^+$ complex. Consequently, a diabody was synthesised based on the anti PSMA J591 antibody and engineered to contain the CLRRRLAHHHHHH (JWT-CYS) sequence at the C-terminal. This protein was referred to as the J591diaJWT-Cys. The JWT-Cys tag provides a Cys and Arg containing $(His)_6$ labelling sequence. Previously, the influence of the CysLys for improving $(His)_6$ labelling with $[^{99m}Tc(CO)_3]^+$ was demonstrated with the C2A protein (Chapter 2) whereas the Arg influence has only been analysed in peptide sequences on a solid phase.(*35*) An Arg/$(His)_6$ labelling sequence without the Cys residue, LRRRLAHHHHHH (JWT) was also engineered at the C-terminal of a J591 diabody and scFv producing the respective J591diaJWT and J591scFvJWT.

Several other available protein fragments with standard $(His)_6$ Tags, but with no Arg residues, were used as controls. Comparisons of the radiolabelling efficiency and in vitro and in vivo analysis should reveal whether the Arg/$(His)_6$-Tag is suitable as a standardised method for efficient site-specific labelling of proteins with $[^{99m}Tc(CO)_3]^+$ without compromising the binding of the protein for the target. ScFv fragments derived from the mAb J591 were produced and engineered to contain C-terminal $(His)_6$-Tags without the Arg residues. These include J591(scFv) and a humanised version of J591 scFv. In addition, scFv fragments of an antibody directed against mouse vascular cell adhesion molecular 1 (VCAM-1) were obtained for further comparative experiments.(*36*) These antibodies, referred to as 6C7.1scFv and 6C7.1-CscFvys, contain a $(His)_6$-Tag at the C-terminal and will determine whether the Arg/$(His)_6$ system can demonstrate a superior labelling efficiency over other types of $(His)_6$-Tagged protein independently of the protein. For the 6C7.1-CscFv antibody, a Cys residue is present at the C-terminal side of the $(His)_6$-Tag. This provides a

direct comparison between the previously successful Cys/$(His)_6$-Tag system and the newly developed Arg/$(His)_6$-Tag combination for labelling proteins with $[^{99m}Tc(CO)_3]^+$. The range of control proteins used in the comparative studies against the J591scFvJWT will provide sufficient evidence to determine whether the presence of Arg residues in combination with a $(His)_6$-Tag in a protein mimics the superior behaviour of the Arg/$(His)_6$ peptides from the His-Tagged CelluspotTM array. A summary of all the different $(His)_6$-Tagged proteins used in this study, including their properties and purpose, can be seen in figure 4-2.

4.1.5 $[^{99m}Tc(CO)_3]^+$ Radiolabelling Efficiencies

In chapter 2.1 figure 1.2-5, a summary of the conditions used and yields obtained post labelling of $(His)_6$-Tagged proteins with $[^{99m}Tc(CO)_3]^+$ is displayed. This highlights many of the issues currently associated with the site-specific radiolabelling of His-Tagged proteins with $[M(CO)_3]^+$ complexes. In order to use the [protein-$^{99m}Tc(CO)_3$] conjugate in pre-clinical studies, the radiochemical purity must typically be at greater than 95%. Often this is not the case and to achieve a > 95% radiochemical purity a purification step, namely a PD-10 column, must be included in the radiolabelling protocol. Not only is a purification step time consuming, but also involves the loss of protein and reduces the concentration of the protein.(*37-43*) Loss of protein can be costly depending on the type of protein used and the ease at which it can be produced. Procedures involving a loss of protein are preferably avoided when preparing radiolabelled protein conjugates for clinical use. For pre-clinical and clinical applications an ideal situation would involve a labelling sequence that can be engineered into a protein and demonstrates a high labelling efficiency (greater than 95%) to avoid the need for post-labelling purification, at a low protein concentration (less than 1mg/ml) in the fastest possible time (quicker than 60 minutes).

Once radiolabelled, the stability of the $[^{99m}Tc(CO)_3$-protein$]^+$ conjugate was assessed in human serum. Preliminary studies to evaluate the biological affinity of $[^{99m}Tc(CO)_3$-J591scFvJWT$]^+$ and $[^{99m}Tc(CO)_3$-huJ591scFv] to the target were performed in a cell binding competition assay.

4.2 MATERIALS

Protein purification was carried out using the AKTA-FPLC-900 System with a Fraction collector-950 (GE Healthcare Life Sciences) using a Ni-NTA column (Superflow Cartridge, Qiagen, Manchester, UK) and a Superdex 75 HR 10/30 column (GE Healthcare, Little Chalfont, UK) for gel filtration. All buffers were prepared in house with chemicals and solvents obtained from Sigma-Aldrich (Dorset, UK) unless otherwise specified. Sterile water was used to prepare the buffers. Vivaspin2 ultracentrifugation tubes with a 5,000 molecular weight cut-off were purchased from Sartorius (Epsom, UK) for protein concentration and protein concentration measured by UV spectrometry using a Nanodrop 2000c Spectrophotometer (ThermoScientific, UK). Proteins were analysed using SDS-PAGE analysis with NuPAGE 12% gels (Invitrogen, Paisley, UK), MOPS buffer (Life Technologies, Paisley UK) and an Invitrogen Novex Mini Cell chamber (Life Technologies). For western blot development, antiPentaHis, goat anti mouse – horse radish peroxidise (Gam:HRP) and SigmaFastDAB were obtained from Qiagen, Millipore and Sigma-Aldrich respectively. The Novex Sharp prestained protein standard for SDS-PAGE and Western Blot was obtained from Life Technologies. High performance liquid chromatography (HPLC) analysis was carried out on an Agilent 1200 series system with an in-line UV (280nm) detector and a BioSepSEC-s 2000 (Phenomenex, Cheshire, UK) size exclusion column (SEC). DNA sequencing was performed by Beckman Coulter Genomics, Takeley, UK. For radiolabelling experiments and quality controls, materials were obtained and equipment used as previously described for the radiolabelling experiments of the Cys/His-Tag Peptides in Chapter 2. Dr Florian Kampmeier kindly provided the DU145 cells and the DU145 cells expressing PSMA (DU145-PSMA).(*44*)

4.3 METHOD & EXPERIMENTAL

4.3.1 Antibody construction and expression

A single chain fragment variable (scFv) of J591 in VH-VL orientation was PCR amplified from the SFG P28z vector and subcloned into a hybrid expression vector based on Psectag2 (Life Technologies) and Pires-Egfp (Clonetech) sequences.(*45*) J591JWT-CYS and J591JWT were

generated by insertion of annealed overlapping oligonucleotides (Integrated DNA Technologies) with NotI/EcoRI overhangs replacing the original $(His)_6$ sequence in the expression vector.

Oligo sequences:

JWT-CYS_forward: 5' ggccgcATGCCTGAGAAGAAGGCTGGCCCACCACCACCACCACTGAG 3'
JWT- reverse: 5' AATTCTCAGTGGTGGTGGTGGTGGTGGGCCAGCCTTCTTCTCAGGCATgc 3'

JWT-forward: 5' ggccgcACTGAGAAGAAGGCTGGCCCACCACCACCACCACTGAG 3'
JWT- reverse: 5' gcACTGAGAAGAAGGCTGGCCCACCACCACCACCACCACTGAGAATT 3'

For the diabodies, the scFv of J591 was converted by shortening the linker to GGGGS using overlapping primers. As opposed to the mainly monomeric scFv, diabodies form a stable dimer as a result of the short linker. Cloning of the diabody was performed into mammalian expression vectors, pMs, with a C-terminal JWT-CYS or JWT tag and a N-terminal Ig-kappa-leader.

A published, humanised sequence of the J591 scFv was synthesised by Geneart and subcloned into the target expression vector. The sequence coding for the 6C7.1scFv scFv was kindly provided by Prof S. Duebel, University of Braunscheig, Germany. The 6C7.1scFv scFv sequence was PCR amplified from a source vector and subcloned into the target expression vector. 6C7.1scFv scFv with a C-terminal cysteine (6C7.1-CscFvy(scFv)) was used as an additional control. All sequences were verified by DNA sequencing. Dr Florian Kampmeier kindly provided the expression vectors for all contructs and produced the purified 6C7.1scFvscFv and 6C7.1-CscFvysscFv with a > 95% purity.

For protein production, HEK393T cells were transfected with the respective expression vector and transfected cells were selected with 100μg/ml of Zeocin. Cells were then expanded to triple layer flasks and culture supernatants containing the recombinant protein were collected.

4.3.2 Antibody purification

Purification was achieved by a combination of immobilised metal ion chromatography and size exclusion chromatography. The scFv and diabodies were extracted from HEK293T culture supernatant on the AKTA-FPLC using Ni-NTA chromatography with a 5ml Ni-NTA column which had previously been equilibrated with 5 column volumes (CV) of 1x Ni-NTA binding buffer (50mM NaH_2PO_4, 300mM NaCl, 10mM imidazole, pH 8). Before loading the Ni-NTA column at approximately 1.5ml/min, the supernatant was filtered to remove residual dead cells and diluted with 4x Ni-NTA binding buffer in a 3:1 ratio (supernatant to Ni-NTA binding buffer). Once loaded, the $(His)_6$-Tagged proteins bind to the Ni-NTA column and an initial washing step was performed to remove impurities from the culture media using 5 CV of Ni-NTA washing buffer with 35mM imidazole (35mM imidazole, 50mM NaH_2PO_4, 300mM NaCl, pH 8). The proteins were then eluted from the NiNTA column with 250mM imidazole Ni-NTA elution buffer (250mM imidazole, 300mM NaCl, 50mM NaH2PO4, pH 8).

A size exclusion gel filtration step (SEC, Superdex 75 HR 10/30) using the AKTA-FPLC further purified the antibody fragments separating from each other the impurities from the culture media, dimerised scFv fragments, diabodies and monomeric scFv. 500µl fractions of the unpurified proteins were loaded onto the SEC column for purification and the separated products collected as 1ml fractions. The purified monomeric scFv and diabody proteins in PBS at pH 7.4 were concentrated using VivaSpin membrane spin filter columns with a 5,000 molecular weight cut off to > 0.9 mg/ml. Protein concentration was measured by UV spectrometry with a UV absorption of 280nm using a Nanodrop device. A molar extinction coefficient and molecular weight of the respective protein was determined from the primary amino acid sequence using the ProtParam online tool, assuming all cysteines are present as cystines. These data are displayed in Table 4-1. All aliquots were stored in PBS buffer at pH 7.4 at -80^{o}C.

Protein	Extinction Coefficient (E_{280nm}) (M^{-1} cm^{-1})	$MW_{monome}R$ (kDa)	Labelling Sequence	pI of Labelling Sequence	Comments
J591diaJWT-Cys	51130	27.70	CLRRRLAHHHHHH	11.70	Diabody against J591mAb with JWT-CYS-Tag
J591scFvJWT	51130	28.23	ALRRRLAHHHHHH	12.40	scFv against J591mAb with JWT-Tag
J591diaJWT	51130	27.60	ALRRRLAHHHHHH	12.40	Diabody against J591mAb with JWT-Tag
J591scFv	51130	27.07	KRAAALEHHHHHH	6.62	scFv against J591mAb with $(His)_6$-Tag
huJ591scFv	51130	27.28	IKAAALEHHHHHH	6.62	Humanised scFv against J591mAb with $(His)_6$-Tag
C67.1 scFv	48610	28.78	PTAAALEHHHHHH	6.62	scFv against VCAM-1 with $(His)_6$ Tag
C67.1-C scFv	48610	28.89	TAAALEHHHHHHC	6.62	scFv against VCAM-1 with Cys/$(His)_6$-Tag

Table 4-1. Extinction coefficient and molecular weight data for the primary amino acid sequence for all 7 antibody fragments expressed. The labelling sequence and its pI has also been included for the protein fragments. Data obtained using ExPASy ProtParam online tool assuming all cysteines are present as (reduced) cysteines.

4.3.3 Biochemical Characterisation: SDS Page, HPLC and Western Blot

Purity of the scFv protein fragments was assessed by SDS-PAGE/ Coomassie brilliant blue staining, by analytical size exclusion HPLC and a Western Blot. 12% precast polyacrylamide gels (Nu-PAGE) were used to separate and visualise the proteins. Protein samples were

mixed with a 1/4 volume of 4x SDS-PAGE loading buffer and 1/10 volume of 10x SDS-PAGE reducing buffer where reduction of covalent disulfide bonds was necessary for the protein samples. For 5 minutes at 98^{o}C the proteins were denatured before loading onto the NuPAGE 12% gels. Gels were run under constant voltage, 200V, for 55 minutes in an Invitrogen protein gel electrophoresis chamber with MOPS buffer. A Novex Sharp prestained protein standard was used to provide a molecular weight ladder as a reference. Gels were either visualised with Coomassie Brilliant blue G250 staining or proteins were transferred to nitrocellulose membranes for subsequent Western blot detection. For Western blotting, nitrocellulose membranes with the transferred proteins were blocked for 1hr at room temperature with 0.05% polyabsorbate 20 (Tween20) in PBS. After 2x 1hr washes in PBS-Tween20 (PBST), membranes were incubated for 1hr with the primary antibody, anti Penta His, diluted 1:4000 in a 0.05% BSA in PBS solution. The membranes were washed 3x for 5min with PBST before a 1hr incubation at room temperature with the secondary antibody, GaM:HRP, diluted 1:5000 in PBS. Another 3x 5min washing procedures with PBST were carried out before the blots were developed with SigmaFastDAB as the HRP substrate. A sharp Pre-Stained Protein Standard was used as a size reference. Size exclusion HPLC was peR$_f$ormed with PBS, pH 7.4, as the mobile phase and a flow rate of 1ml/min.

4.3.4 Conversion of $^{99m}TcO_4^-$ to $[^{99m}Tc(CO)_3]^+$

The J591scFvJWT, J591scFv, huJ591scFvscFv, 6C7.1scFv and 6C7.1-CscFvys, proteins were labelled with $[^{99m}Tc(CO)_3]^+$ via the C-terminal $(His)_6$-tag for the comparative radiolabelling studies. Preparation of the $[^{99m}Tc(CO)_3]^+$ was performed as previously described for the radiolabelling of the Cys/His-Tag peptides in Chapter 2.

4.3.5 Preparation of ScFv Proteins for $[^{99m}Tc(CO)_3]^+$ Radiolabelling

ScFv proteins in PBS at pH 7.4 were prepared to a concentration of: 42μM (1.2mg/ml) for J591scFvJWT, J591scFv and huJ591scFvscFv; 21μM (0.6mg/ml) for 6C7.1scFv; and 10.5μM (0.3mg/ml) for 6C7.1-CscFvs. Protein concentrations were determined by UV absorption at 280nm using a Nanodrop spectrophotometer. For J591scFvJWT, J591scFv and huJ591scFvscFv, 20 μl samples were aliquotted and a 2:1 dilution series performed to give 6

different protein concentrations: 42 μM, 21 μM, 10.5 μM, 5.25 μM, 2.625 μM and 1.312 μM. The same procedure was carried out for 6C7.1scFv and 6C7.1-CscFvys proteins starting from a concentration of 21 μM and 10.5 μM respectively. There were therefore five 6C7.1scFv samples and four 6C7.1-CscFvs samples. Once diluted with $[^{99m}Tc(CO)_3]^+$ the desired protein concentration, as reported in the results, was reached.

4.3.6 $[^{99m}Tc(CO)_3]^+$ Radiolabelling of scFv Proteins

To the scFv proteins, 10 ul of approximately 50 MBq of $[^{99m}Tc(CO)_3]^+$ was added to give 2 MBq/μg for the protein samples with the highest concentration. The $[^{99m}Tc(CO)_3]^+$-protein solutions were incubated at 37°C for up to 2 hrs. Aliquots were taken at 15, 30, 60, 90 and 120 minutes for analysis by TLC using the equivalent method to that of the Cys/His-Tagged peptides in Chapter 2. 1.5μl of the $[^{99m}Tc(CO)_3]^+$-protein solutions were spotted at the origin of the iTLC-SA paper, and the strip allowed to air-dry before development in a mobile phase of 0.1 M citrate buffer at pH 5. The iTLC-SA strips were cut in half and the radioactivity in each half recorded, using a gamma counter, as counts per minute (cpm). The percentage radiochemical yield was calculated by dividing the cpm recorded from the lower half of the strip with the total cpm for the whole strip, that is the cpm for the top and bottom halves of the strip.

$$\text{Radiochemical yield (\%)} = \left(\frac{\text{Cpm from lower half of TLC strip}}{\text{Total cpm from TLC strip}} \right) \text{X } 100$$

The comparative radiolabelling study for the scFv proteins was repeated in order to report the data in duplicate with error bars recorded as standard deviations.

4.3.7 $[^{99m}Tc(CO)_3]^+$ Radiolabelling of J591scFvJWT: Comparison between 25°C and 37°C

J591scFvJWT was incubated at 37°C and 25°C with $[^{99m}Tc(CO)_3]^+$ in a 5 MBq/ug ratio for up to 2 hours. Aliquots were taken at 15, 30, 60, 90 and 120 minutes for radiochemical yield

monitoring by iTLC-SA in 0.1 M citrate buffer at pH 5.5. (iTLC-SA: $R_f = 0$ for protein and $R_f = 1$ for $[^{99m}Tc(CO)_3]^+$ and unreduced $^{99m}TcO_4$-). The iTLC-SA strips were cut in half and the radioactivity in each half recorded using the gamma counter as cpm. Percentage radiochemical yield was calculated from the gamma counter data and a comparison made between radiolabelling at 25°C and 37°C. Protein concentration post addition of $[^{99m}Tc(CO)_3]^+$ was 14.1 μM (0.4mg/ml) for the labelling at 37°C and 25°C.

4.3.8 Serum Stability of $[^{99m}Tc(CO)3$-J591scFvJWT$]^+$ Conjugate

J591scFvJWT was radiolabelled with $[^{99m}Tc(CO)_3]^+$ as previously described (Chapter 4.2). Once the radiochemical yield had reached 95%, the $[^{99m}Tc(CO)_3]^+$-J591scFvJWT conjugate was incubated in a 1:1 v/v ratio with fresh human serum at 37°C. Human serum was isolated from fresh human blood. Aliquots were taken at 0, 15, 30, 60, 120 and 240 minutes for TLC analysis using ITLC-SA chromatography paper and a mobile phase of 0.1M citrate buffer at pH 5. Additional samples were also obtained at the same time points and instantly frozen in liquid nitrogen. Once all samples were collected, they were separated by SDS-PAGE (12% NuPAGE, Invitrogen) which was analysed by Coomassie blue staining and autoradiography using a phosphor imager.

4.3.9 Cell Binding Studies

A homologous cell binding competition was performed for the $[^{99m}Tc(CO)_3]^+$ conjugated J591scFvJWT, J591scFv and huJ591scFvscFv to analyse the binding properties of the proteins. DU145 cells expressing PSMA were used as the target and DU145 cells were used as a negative control (prepared by Dr Florian Kampmeier). In a 86 well plate, cells (4 x 104 DU145/DU145-PSMA cells/well) were seeded and grown overnight. The following day they were incubated with a serial dilution of J591scFvJWT, J591scFv and huJ591scFvscFv with concentrations ranging from 3559 nM to 0.06 nM. A constant concentration of ^{99m}Tc conjugated scFvs (1 nM) was added to each well for 45 mins at 4°C. Post incubation cells were washed 3x with 100 ul cold PBS and lysed 2x with 50 μl of 0.5 M NaOH. The cell-associated radioactivity was counted using the gamma counter and data collected analysed

by graph Pad Prism using a “one site total binding algorithm” to plot the data. The experimental Kd was calculated based on the value for IC_{50}-[$^{99m}Tc(CO)_3$-scFv protein].

4.4 RESULTS

4.4.1 ScFv and Diabody Protein Sequences

All scFv and diabody fragments were successfully constructed, expressed and purified. The sequences of all scFv and diabodies expressed were confirmed by DNA sequencing. In this project, the labelling sequences were defined as the 13 amino acids at the C-terminal of the protein which includes the $(His)_6$-Tag and 7 of its surrounding amino acid residues. 6C7.1-CscFv (Figure 4-2 above) contains information about the amino acid composition of the labelling sequence and its local pI value. A $(His)_6$-Tag in combination with multiple Arg residues was successfully incorporated as the labelling sequence at the C-terminal of the J591diaJWT-Cys, J591diaJWT and J591scFvJWT proteins. J591diaJWT-Cys has a ACLRRRLAHHHHHH labelling sequence with a pI of 11.70. The same sequence without the Cys residue, pI 12.40, has been engineered into the J591diaJWT and J591scFvJWT proteins.

The control proteins were chosen due to the minimal number of Arg residues at the C-terminal in close proximity to the $(His)_6$-Tag (Figure 4-2). Apart from the labelling sequence J591scFv protein has an identical amino acid composition to that of the J591scFvJWT fragment. Its labelling sequence, KRAAALEHHHHHH, with a pI of 8.79, contains 1 Arg and 1 Lys residue 6 and 7 amino acids away from the $(His)_6$-Tag. To analyse the effect of this Arg on labelling, an additional version of the J591scFv was used for comparison, humanised (hu) J591scFv, with a labelling sequence not containing the Arg. The huJ591scFvscFv labelling sequence, IKLAAALEHHHHHH, has a pI of 7.21. The Lys 7 amino acids away from the $(His)_6$-Tag is still present.

6C7.1scFv and 6C7.1-CscFvys scFvs have identical amino acid composition other than an additional Cys residue at the C-terminal side of the His-Tag in the 6C7.1-CscFvys scFv. The labelling sequences for 6C7.1scFv and 6C7.1-CscFvys are PTAAALEHHHHHH and TAAALEHHHHHHC respectively and the pI is 6.53 for both.

4.4.2 J591diaJWT-Cys – Expression and Purification

The J591diaJWT-Cys was produced in HEK239T cells with yields of purified protein (purity > 95%) of 1.5 mg/L culture supernatant. Expression of purified J591diaJWT-Cys was lower in comparison to other $(His)_6$-Tagged J591dia proteins, which on average demonstrated a yield of 4-6 mg/L of culture supernatant. A SDS-PAGE was performed on the purified J591diaJWT-Cys in parallel with a J591-Cysdia protein provided by Dr Florian Kampmeier. J591-Cysdia has an identical amino acid composition to that of the J591diaJWT-Cys other than in the $(His)_6$-Tag labelling sequence. J591-Cys Cdia has a labelling sequence that also contains a single Cys residue but it is at the C-terminal of the $(His)_6$-Tag, RLAAALEHHHHHHC. Due to the similarities in sequences, J591diaJWT-Cys and J591dia-Cys should demonstrate a similar behaviour on the SDS-PAGE with molecular weights of 55.4 kDa and 54.36 kDa for the diabody and 27.70 kDa and 27.18 kDa for the monomer. It is expected that both J591diaJWT-Cys and J591dia-Cys appear primarily as dimers in the SDS-PAGE due to the Cys residue at the C-terminal which leads to the formation of a covalent bond that will not be reduced during the SDS-PAGE procedure. J591diaC can therefore act as a reference to evaluate whether the Cys/Arg/$(His)_6$-Tag effects the expression of the J591 diabody.

Figure 4-2 reveals the results from the SDS-PAGE of the J591diaJWT-Cys and J591Cdia samples. When performing the SDS-PAGE both diabody fragments were loaded onto the gel in both their non-reduced and reduced forms. J591Cdia was present as a dimer of 54 kDa, lane C, with the C-terminal cysteines forming a stabilising disulfide bond in about 85-90% of the protein. In the non-reduced J591Cdia sample (lane C) a single band was observed at 28 kDa corresponding to 10% of the protein. This was confirmed in the reduced sample (lane D) in which all covalent disulfide bonds have been reduced to yield the monomer product in 100% yield.

The formation of the covalent dimer for J591dia-Cys is an indication that proper folding has occurred. In the non-reduced sample (lane A) of the J591diaJWT-Cys, it was not possible to see a comparable amount of dimer formation which suggests that the correct folding has not taken place. J591diaJWT-Cys appears primarily as a monomer of 28 KDa with only 20% of the protein present as a covalent dimer at 55 kDa. In addition the band representing the monomer in both the non-reduced and reduced sample (lane A and B) are in fact double bands that are very close together. These results suggest that the JWT-Cys tag has

interfered with the folding of the diabody and that two proteins with slightly different structures have been produced. It is possible that the Cys in the JWT-Cys labelling sequence could be impacting on the folding of the diabody and therefore the J591diaJWT and J591scFvJWT were expressed excluding the Cys from the labelling sequence. J591diaJWT-Cys was not pursued any further in this study.

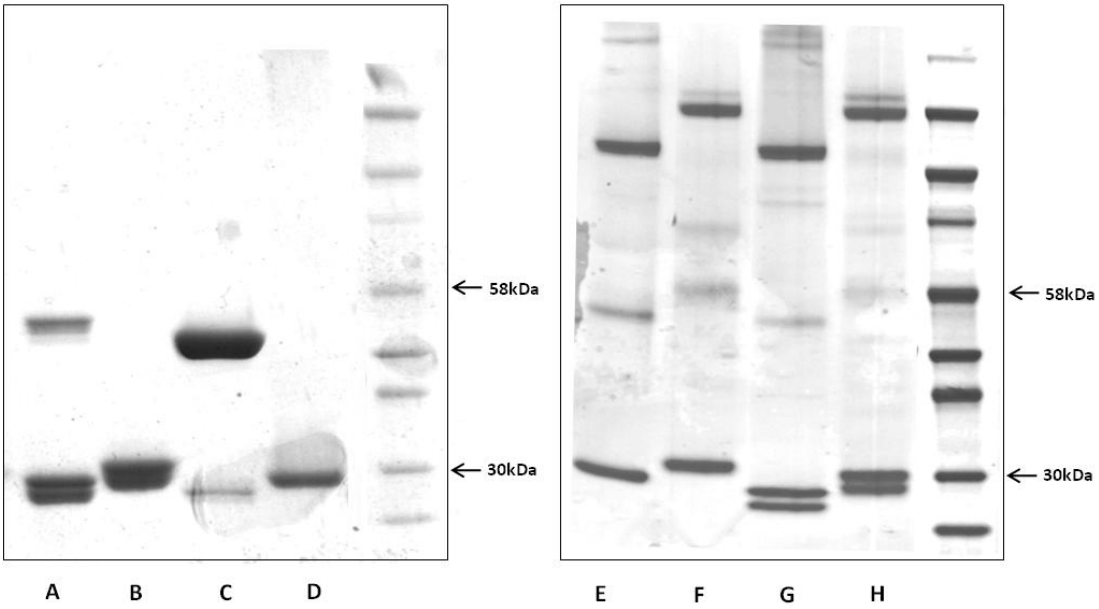

Lane	Sample	Lane	Sample
A	Purified J591diaJWT-Cys non-reduced sample	**E**	Unpurified J591scFvJWT non-reduced sample
B	Purified J591diaJWT-Cys reduced sample	**F**	Unpurified J591diaJWT reduced sample
C	Purified J591Cdia non-reduced sample	**G**	Unpurified J591diaJWT non-reduced sample
D	Purified J591Cdia reduced sample	**H**	Unpurified J591diaJWT reduced sample

Figure 4-2. Image on the Left (Lane A-D): SDS-PAGE analysis of the purified J591diaJWT-Cys and J591Cdia proteins. Both proteins have been loaded onto the NuPAGE gel in their reduced and non-reduced form. **Image on the Right (Lane E-H):** SDS-PAGE analysis of the unpurified J591scFvJWT and unpurified J591diaJWT. All proteins have been loaded onto the NuPAGE gel in their reduced and non-reduced form.

4.4.3 J591scFvJWT and J591diaJWT – Expression

The scFv and diabody proteins with JWT tags were also produced in HEK239T cells with yields for the purified protein of approximately 2 mg/L culture supernatant. The SDS-PAGE for the unpurified J591scFvJWT and J591diaJWT can be seen in Figure 4-2 (image on the right). Both samples have been loaded onto the NuPAGE gel in their reduced and non-reduced forms. The JWT tagged protein fragments do not carry a Cys residue at the C-terminal in the labelling sequence and therefore the formation of a covalent diabody is not possible. On the SDS-PAGE the diabody and scFv proteins are both expected to appear as a monomer at 28 kDa due to the disruption of all secondary and tertiary structure during the SDS-PAGE protocol.

The SDS-PAGE in Figure 4-2 reveals that as predicted both the J591diaJWT and J591scFvJWT are primarily present as a monomer at 28 kDa in 95% abundance. Confirmation of this was provided by the reduced samples in lanes F and H respectively for J591scFvJWT and J591diaJWT. However, for the diabody the monomer appears as two distinct bands at 28 kDa in both the reduced and non-reduced samples. This implies that two different protein structures have been formed and again the assumption has been made that the JWT Tag has somewhat interfered with protein folding. As a result, the J591diaJWT was no longer pursued in this study.

The J591scFvJWT demonstrated a far more promising outcome. The non-reduced and reduced samples revealed a single band representing the J591scFvJWT monomer at 28 kDa. This implies that the protein folding has not been compromised and a homogenous J591scFvJWT protein has been formed. As a result of the successful expression, J591scFvJWT was reproduced and purified in parallel with the J591scFv control protein for further comparative studies including radiolabelling efficiencies and binding to PSMA.

4.4.4 J591scFvJWT and J591scFv (Control Protein) – Large Scale Expression and Purification

The large scale production of J591scFvJWT and J591scFv produced the 2 mg/L and 7 mg/L respectively of the purified proteins. Evidence suggests that the JWT Tag influences the

expression of the J591scFv protein and resulting in smaller amounts of the protein. Production and purification steps were monitored by SDS PAGE and Western blotting and are displayed in Figure 4-3) and 4-5 for the J591scFvJWT and J591scFv respectively. The J591scFvJWT (Figure 4-3) appears as a monomer of 28 kDa. Lanes A-C in the SDS-PAGE monitor the progress of extracting J591scFvJWT from the culture supernatatant. $(His)_6$ recombinant proteins such as J591scFvJWT have a high affinity and selectivity for the Ni-NTA and as a result, the majority of protein impurities present in the supernatant, lane A, are discarded in the flowthrough of the Ni-NTA purification system. Other impurities from the culture media unspecifically bound to the NiNTA are removed with addition of the Ni-NTA washing buffer containing 35 mM imidazole, row B. J591scFvJWT was eluted from the column by competition with a 250 mM imidazole solution in the Ni-NTA elution buffer, row C.

Three peaks appeared in the SEC purification step of the J591scFvJWT and samples from each were loaded onto the SDS PAGE and can be seen in rows D-F. The first peak corresponded to serum proteins from culture media, row D, whilst the second peak corresponded to dimeric aggregates of J591scFvJWT protein, row E. The dimeric aggregates formed were non-covalent dimers and on the SDS-PAGE appear as single monomers at 28 kDa due to the SDS procedure disrupting the secondary and tertiary structures of the protein. J591scFvJWT was eluted as a purified protein in the third peak, row F, and concentrated to 1.3 mg/ml, row G. The corresponding western blot confirms the appearance of the J591scFvJWT as a single band at 28 KDa on the SDS-PAGE. The primary antibody used in the western blot, antiPentaHis, specifically detects the $(His)_6$ tag.

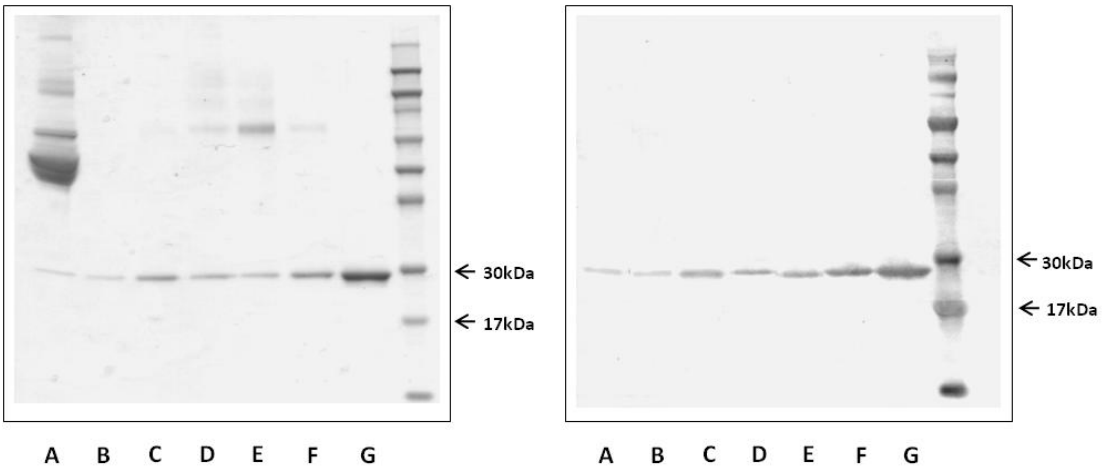

Row	Sample
A	Culture Supernatant
B	35mM imidazole wash of the NiNTA column
C	J591scFvJWT elution from NiNTA column (250 mM imidazole)
D	SEC Purification: Fraction 1 – BSA Protein
E	SEC Purification: Fraction 2 – Non-covalent dimers of J591scFvJWT
F	SEC Purification: Fraction 3 – Purified monomeric J591scFvJWT
G	Concentrated J591scFvJWT – 1.3 mg/ml

Figure 4-3. SDS-PAGE and Western Blot of the extraction and purification process of the J591scFvJWT protein from the culture supernatant**. Left**: SDS-PAGE with rows from A-G. **Right:** Western Blot of the SDS-PAGE with rows from A-G. J591scFvJWT sample runs as a single band corresponding to the size of the monomer, 28 kDa.

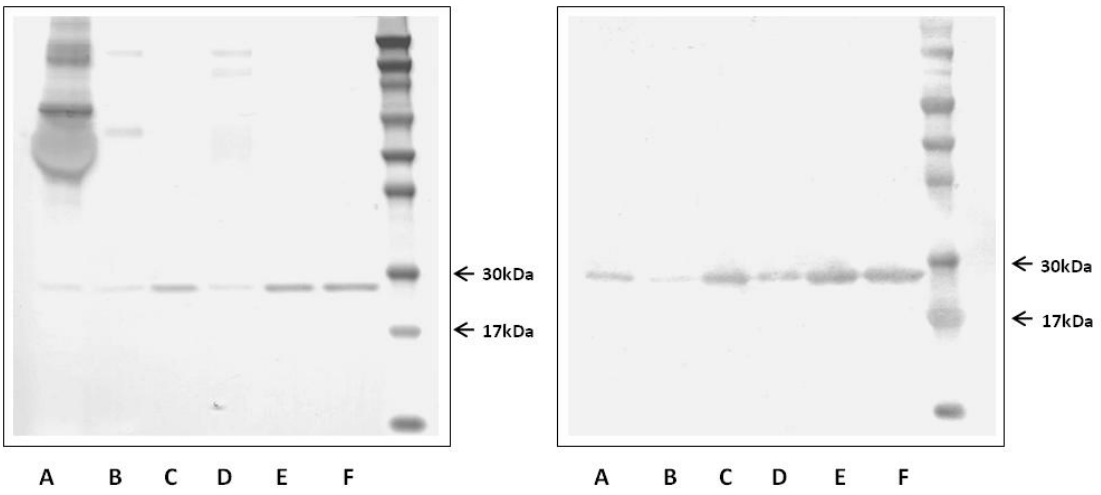

Row	Sample
A	Culture Supernatant
B	35 mM imidazole wash of the NiNTA column
C	J591scFv elution from NiNTA column (250 mM imidazole)
D	SEC Purification: Fraction 1 – BSA Protein
E	SEC Purification: Fraction 2 – Non-covalent dimers of J591scFv
F	SEC Purification: Fraction 3 – Purified monomeric J591scFv

Figure 4-4. SDS-PAGE and Western Blot of the extraction and purification process of the J591scFv protein from the culture supernatant**. Left**: SDS-PAGE with rows from A-F. **Right:** Western Blot of the SDS-PAGE with rows from A-F. J591scFv sample runs as a single band corresponding to the size of the monomer, 27 kDa.

SDS-PAGE and Western Blot monitoring for the process of extracting and purifying the J591scFv protein is shown in Figure 4-4. Again, rows A-C represent the extraction of the protein from the culture supernatant and rows D-F represent the purification fractions from the SEC. The J591scFv appears as a monomeric protein at 27 kDa and the purified (purity > 95%) sample can be seen in row F concentrated to 1.35 mg/ml. Confirmation of the presence of J591scFv is given by the Western blot which highlights the position of the $(His)_6$ containing proteins on the SDS-PAGE (Figure 4-4). The same procedures for production and purification were used for the huJ591scFv, 6C7.1scFv and 6C7.1-CscFv proteins and assessed by SDS-PAGE and Western Blot.

SEC HPLC analysis confirms that for J591scFvJWT, J591scFv and huJ591scFv, the protein exists as a monomer, rt = 9:10-9:30 min, with between 90-100% purity (Figure 4-5). The peak observed at rt = 8:15-8:30 min, represents the formation of non-covalent dimers and accounts for less than 10% of the protein samples.

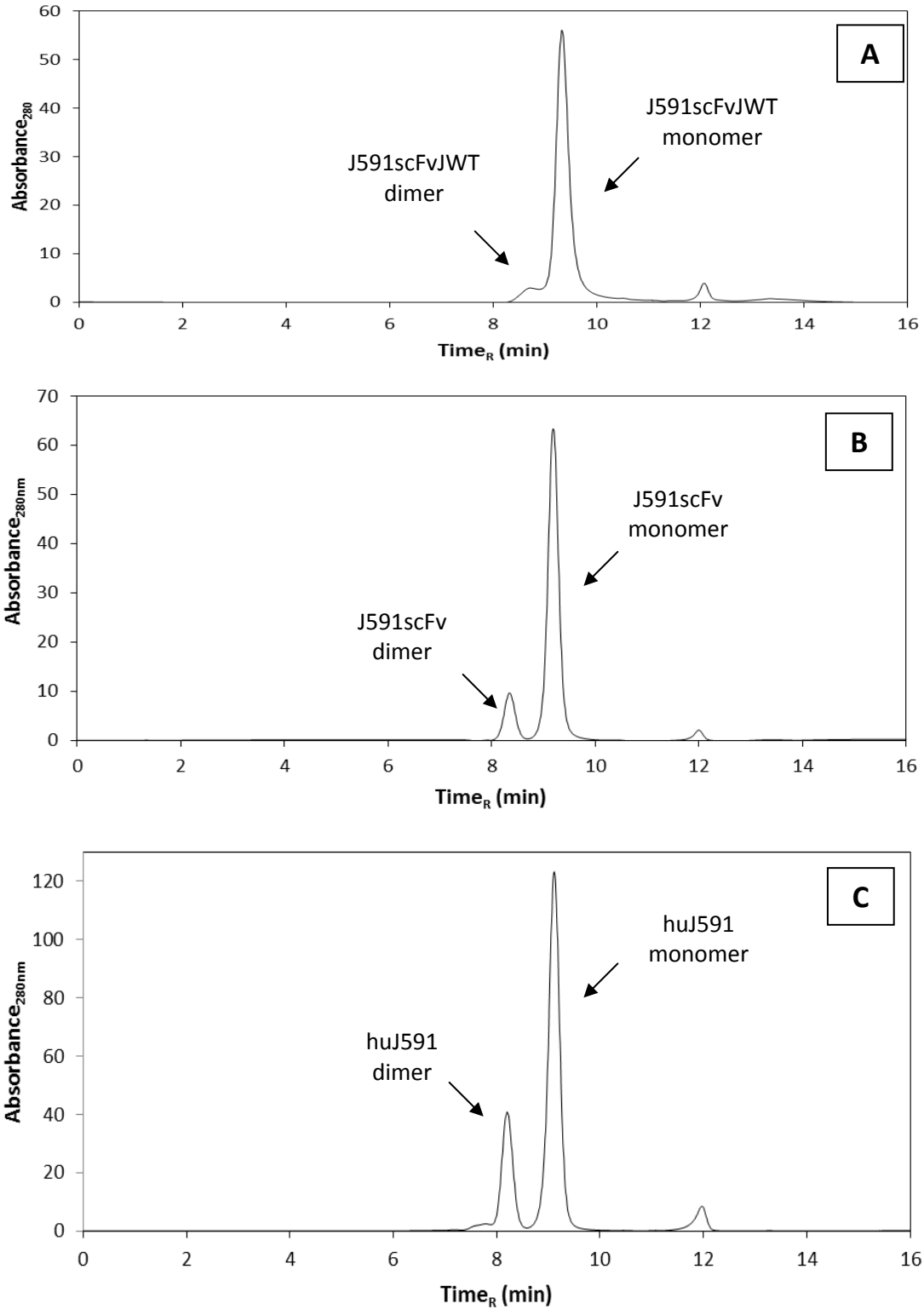

Figure 4-5. HPLC SEC analysis of the scFv proteins shows elution primarily as a single monomeric species at a TimeR in the region of 9:10 - 9:30min. The peak in the region with a TimeR between 8:15-8:30min represents the non-covalent dimers of the scFv protein. **A)** J591scFvJWT protein. **B)** J591scFv protein. **C)** huJ591scFv protein.

4.4.5 TLC Techniques for Identifying Percentage Radiochemical Yields

All purified scFv proteins were radiolabelled with $[^{99m}Tc(CO)_3]^+$. ^{99m}Tc was obtained from the generator in its $^{99m}TcO_4^-$ form and reduced to $[^{99m}Tc(CO)_3]^+$. A TLC method was used as a quality control to assess the conversion of $^{99m}TcO_4^-$ to $[^{99m}Tc(CO)_3]^+$. For these experiments, a radiochemical yield of 99% was achieved for $[^{99m}Tc(CO)_3]^+$ post reduction of $^{99m}TcO_4^-$ according to the TLC quality control (Figure 4-6). As mentioned in Chapter 2, in the TLC (3 cm x 7.5 cm, origin = 10 mm, solvent front = 65 mm), unreduced $^{99m}TcO_4^-$ has an $R_f = 0.9$, $[^{99m}Tc(CO)_3]^+$ has an $R_f = 0.2$-0.8 and any ^{99m}Tc-colloids present remain at the baseline with an $R_f = 0$. The area under the peak provides the abundance of each complex present within the sample. No further purification was required before use of the $[^{99m}Tc(CO)_3]^+$ complex in the radiolabelling of the scFv fragments.

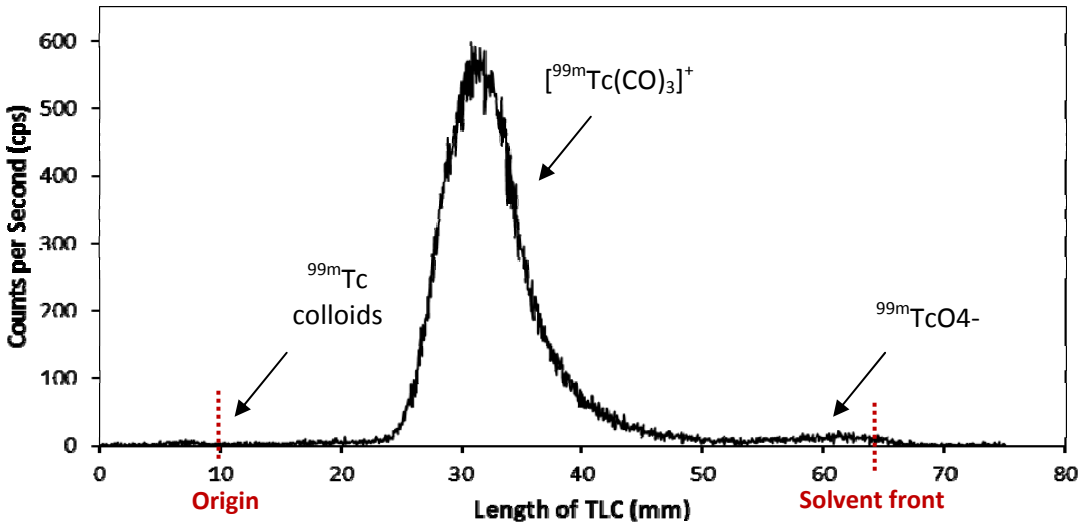

Figure 4-6. TLC quality control of $^{99m}TcO_4^-$ reduction to $[^{99m}Tc(CO)_3]^+$ for use in the radiolabelling of the scFv fragments: **R_f = 0.9** for $^{99m}TcO_4^-$, **R_f = 0** for ^{99m}Tc colloids and **R_f = 0.2-0.8** for $[^{99m}Tc(CO)_3]^+$.

The iTLC-SA method previously used to determine the labelling efficiencies of the Cys/His-Tag peptides in Chapter 2 was also suitable for use in the scFv protein radiolabelling experiments. It was able to separate the $[^{99m}Tc(CO)_3]^+$ labelled scFvs from the unbound $[^{99m}Tc(CO)_3]^+$ and unreduced $^{99m}TcO_4^-$. In Figure 4-7 an iTLC-SA image representing the purified radiolabelled J591scFvJWT protein can be seen and this is compared to the iTLC-SAs of other likely impurities present in the labelling solution. The radiolabelled scFv fragments behave similarly to the labelled Cys/His-Tag peptides and have an $R_f = 0$. Therefore a definitive separation can be detected between the free $[^{99m}Tc(CO)_3]^+$ and

$^{99m}TcO_4^-$, (R_f =1), and the radiolabelled protein. This is beneficial as it enables the accurate calculation of the percentage radiochemical yield. Also it allows for the iTLC-SA strips to be analysed using the gamma counter as previously demonstrated for the Cys/His-Tag peptides. An iTLC-SA image in Figure 4-8 of theJ591scFvJWT labelling reaction demonstrates that a clear separation is obtained between [^{99m}Tc(CO)3-J591scFvJWT]$^+$ conjugate at the baseline, 80% abundance, and the unbound [$^{99m}Tc(CO)_3]^+$ and unreduced $^{99m}TcO_4^-$ at the solvent front, 20% abundance.

The inability to separate the ^{99m}Tc colloids from the radiolabelled Cys/His-Tag peptides was a disadvantage with the iTLC-SA methodology. This remains a difficulty in the radiolabelling experiments of the scFvs as both [$^{99m}Tc(CO)_3$-scFv]$^+$ and ^{99m}Tc colloids remain at the baseline (R_f = 0) after development of the strip. As established with the Cys/His-Tag peptides, information related to the abundance of ^{99m}Tc-colloids in the labelling solution can be obtained from the quality control TLC of [$^{99m}Tc(CO)_3]^+$ (Figure 4-6) and an iTLC-SA analysis of the labelling solution without any proteins present. In all experiments carried out for the radiolabelling of the scFvs, the percentage of ^{99m}Tc colloids was negligible. Furthermore in the iTLC-SA it was not possible to separate the peaks corresponding to [$^{99m}Tc(CO)_3]^+$ and $^{99m}TcO_4^-$. The percentage of $^{99m}TcO_4^-$ in the labelling solution was acquired from the initial TLC quality control of [$^{99m}Tc(CO)_3]^+$ (Figure 4-6). If there was more than 10%, the [$^{99m}Tc(CO)_3]^+$ labelling solution would have been purified prior to its use. However in this instance, this was not necessary as radiochemical purity of [$^{99m}Tc(CO)_3]^+$ was always > 95%.

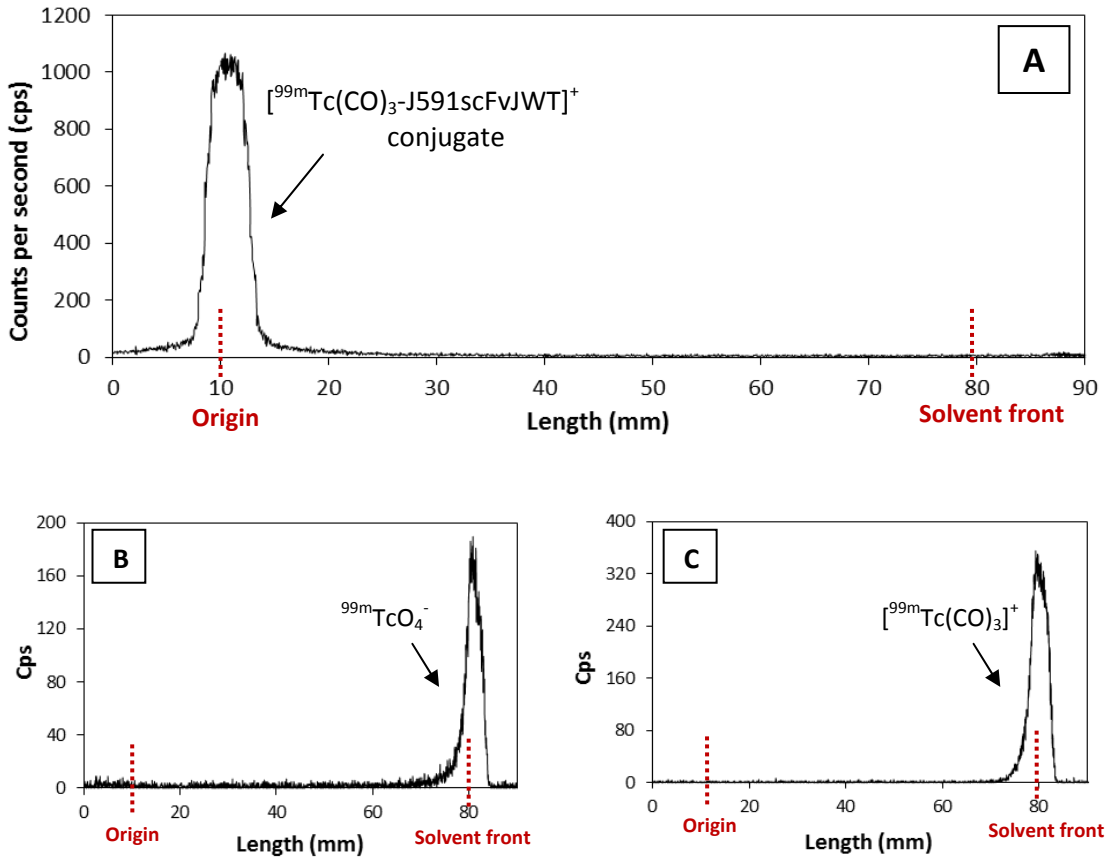

Figure 4-7. iTLC-SA chromatograms of the individual components present in the labelling reaction. The strips (7.5 x 90 mm) had an origin at 10 mm and a solvent front at 80 mm. **A)** Purified by PD-10 J591scFvJWT protein with an $R_f = 0$. **B)** Unreduced $^{99m}TcO_4^-$ with an $R_f = 1$. **C)** Unbound $[^{99m}Tc(CO)_3]^+$ complex with an $R_f = 1$.

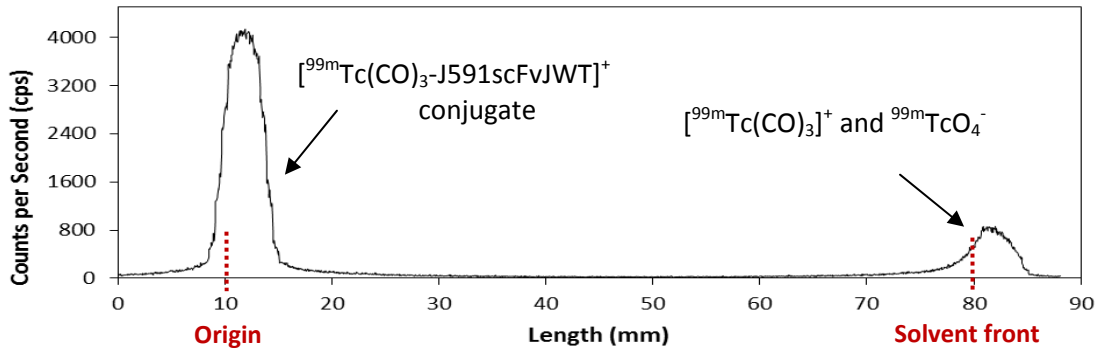

Figure 4-8. iTLC-SA of the J591scFvJWT labelling reaction. The strips (7.5 x 90mm) had an origin at 10 mm and a solvent front at 80 mm. The components of the reaction can be identified as follows: $R_f = 0$ for $[^{99m}Tc(CO)_3\text{-J591scFvJWT}]^+$ and $R_f = 1$ for $[^{99m}Tc(CO)_3]^+$ and $^{99m}TcO_4^-$.

4.4.6 $[^{99m}Tc(CO)_3]^+$ Radiolabelling Efficiencies of the scFv proteins at Different Concentrations

All scFv protein fragments were radiolabelled by site-specific chelation of $[^{99m}Tc(CO)_3]^+$ via the $(His)_6$ Tag at the C-terminal. The proteins were radiolabelled at a range of 6 different concentrations in a 2:1 dilution series. Protein concentrations were calculated post addition of the $[^{99m}Tc(CO)_3]^+$ radiolabelling solution. The highest concentration achieved for the protein in the $[^{99m}Tc(CO)_3]^+$ radiolabelling solution was 28.2 μM which for the J591scFvJWT, J591scFvJWT and huJ591scFvscFv proteins is equivalent to 0.8 mg/ml. The subsequent 5 protein concentrations in the dilution series were 14.1 μM, 7 μM, 3.5 μM, 1.76 μM and 0.88 μM. Concentrations of the purified 6C7.1scFv and 6C7.1-CscFvys were not high enough to enable the protein concentration to reach 28.2μM in the $[^{99m}Tc(CO)_3]^+$ labelling solution because of restricted availability. Consequently, for 6C7.1scFv and 6C7.1-CscFvys the highest protein concentrations achieved in the labelling reaction were 14.1 μM and 7 μM respectively.

To determine the relative efficiency of radiolabelling, the radiochemical yield was plotted against protein concentration (log[protein]) for each time point (Figure 4-9). J591scFvJWT with the Arg/His labelling sequence clearly shows a superior labelling efficiency in comparison to all other comparators with labelling sequences that do not contain multiple Arg residues. This can be seen at 15, 30, 60, 90 and 120 minutes. Other scFv proteins (J591scFv, huJ591scFv, 6C7.1 and 6C7.1-Cys) have lower labelling efficiencies and behave similarly to each other according to the graphs in Figure 4-9. Among these, a slight increase in the radiochemical yield was observed for the J591scFv. This is probably due to the labelling sequence of J591scFv that contains an Arg residue 6 amino acids away from the $(His)_6$. For huJ591scFv, 6C7.1 and 6C7.1-Cys, the Arg amino acid has been replaced by a Lys or Leu residue and these proteins displayed the lowest radiochemical yield at all time points.

Protein Concentration (μM)	Protein Concentration (mg/ml)	Log[Concentration] (μM)
28.2	0.8	1.45
14.1	0.4	1.15
7	0.2	0.85
3.5	0.1	0.54
1.76	0.05	0.25
0.88	0.025	-0.06

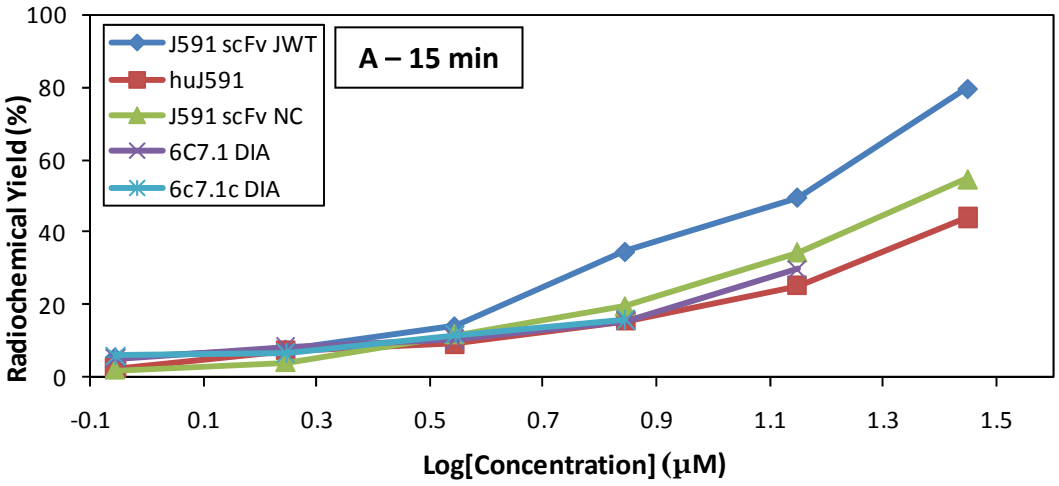

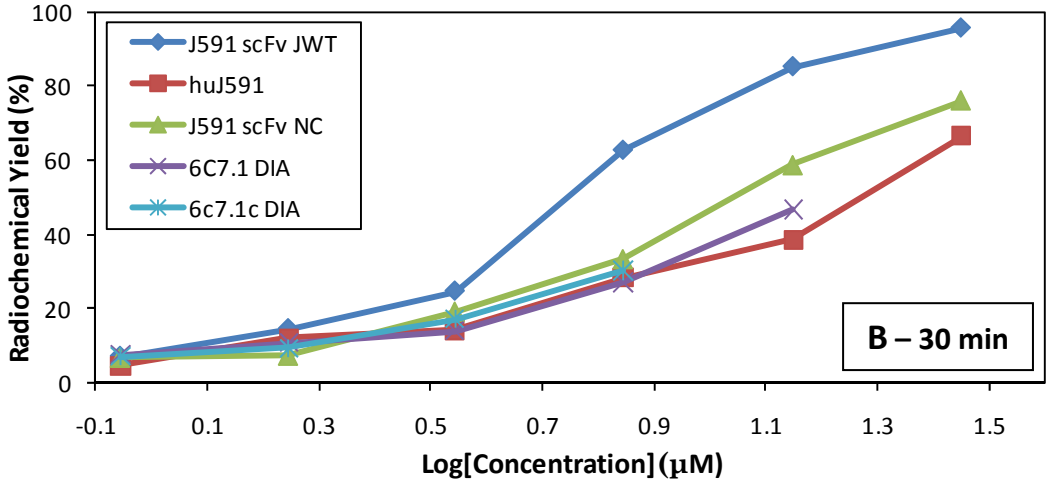

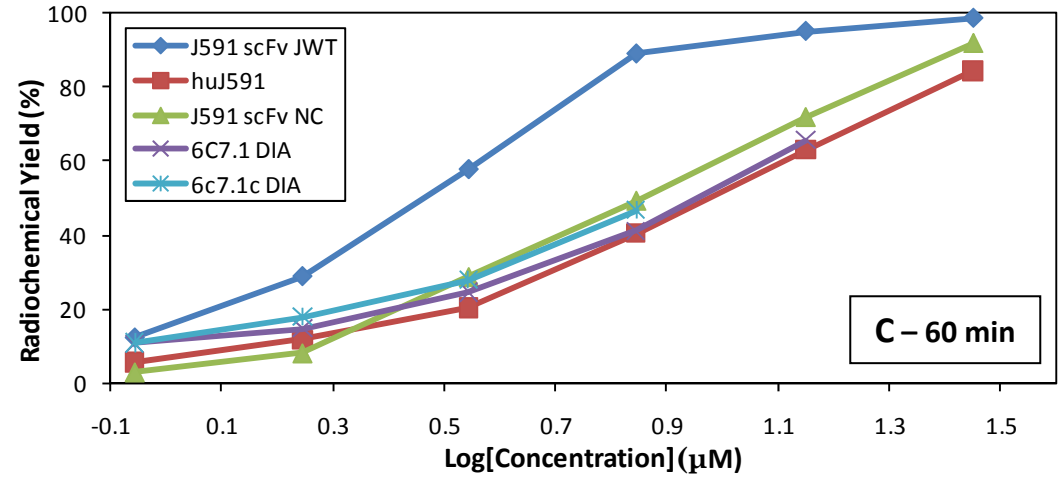

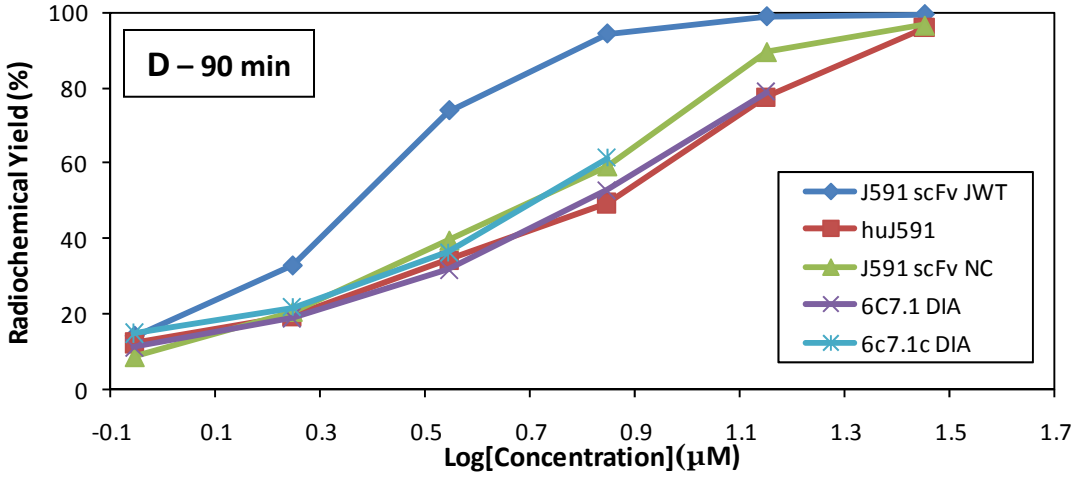

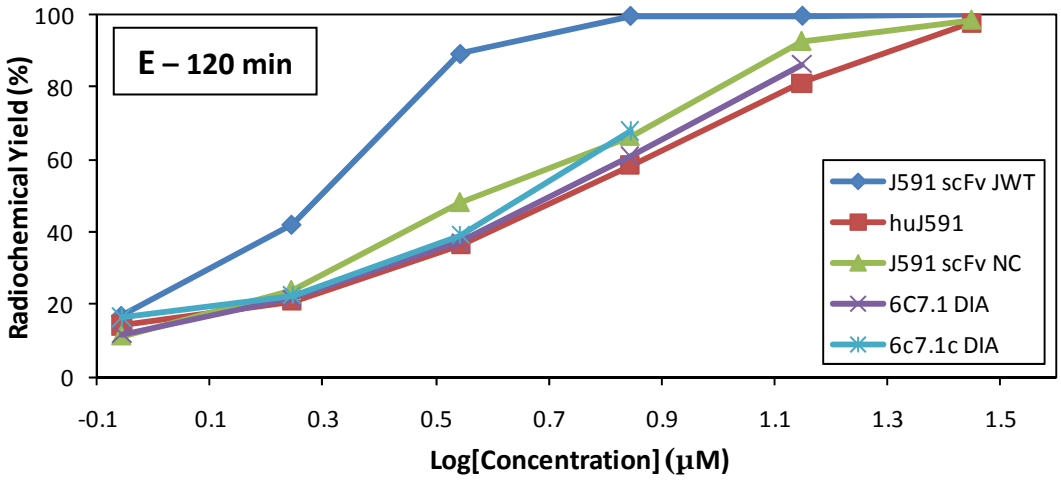

Figure 4-9 Radiolabelling efficiencies of the J591scFvJWT, J591scFv, huJ591scFv, 6C7.1 and 6C7.1-Cys proteins under increasingly dilute conditions expressed as % radiochemical yield against log[concentration] of scFv protein. The table reveals the concentration in µM and mg/ml corresponding to the log[concentration] data points on the graphs. The labelling efficiency was recorded at 5 different time points: **A)** 15 minutes, **B)** 30 minutes, **C)** 60 minutes, **D)** 90 minutes and E) 120 minutes.

To further highlight the superiority in labelling efficiency of the J591scFvJWT protein, the radiochemical yield of J591scFvJWT, J591scFv and huJ591scFv proteins at a concentration of 14.1 μM (0.4mg/ml) were plotted against time. (Figure 4-11)

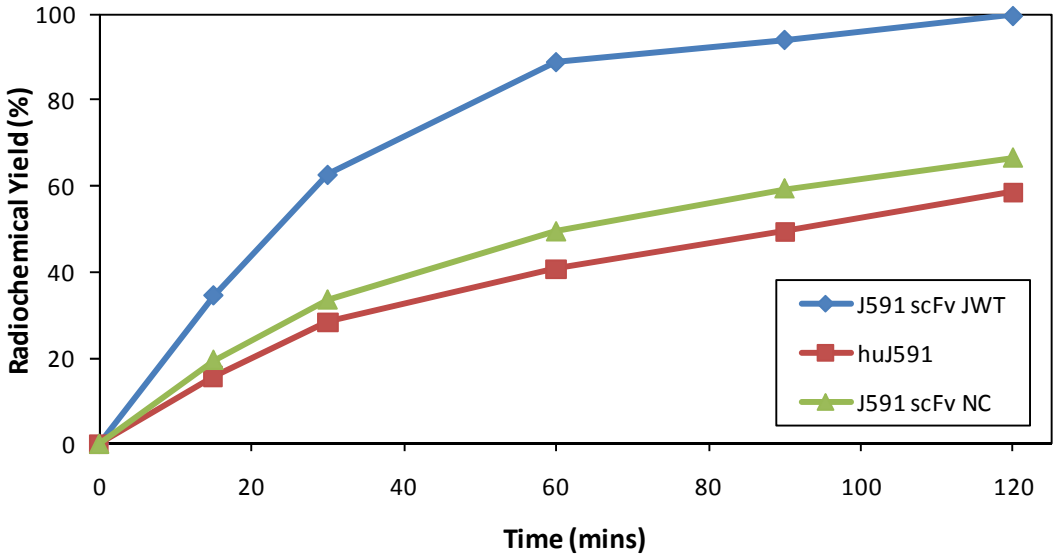

Figure 4-10. Radiolabelling efficiencies of J591scFvJWT, J591scFv and huJ591. Radiochemical yield plotted against total incubation times; 15, 30, 60, 90 and 120 mins. The concentration of the protein in the labelling solution was 7 μM (0.2mg/ml).

When analysing the data obtained from the comparative radiolabelling studies, an important consideration is the concentration and time at which a threshold radiochemical yield of 95% has been reached. This is typically the minimum radiochemical purity required for pre-clinical and clinical applications. Table 4-2 is a table that reveals the incubation time and protein concentration at which the scFv proteins were able to reach a 95% radiochemical yield.

	15min	30min	60min	90min	120min
28.2uM		J591scFvJWT = 96%	J591scFvJWT = 99%	J591scFvJWT = 99% J591scFv = 97% huJ591scFv = 96%	J591scFvJWT = 100% J591scFv = 99% huJ591scFv = 98%
14.1uM			J591scFvJWT = 95%	J591scFvJWT = 98%	J591scFvJWT = 99%
7uM				J591scFvJWT = 95%	J591scFvJWT = 99%
3.5uM					
1.76uM					
0.88uM					

Figure 4-2. Protein concentrations and incubation times at which scFv proteins demonstrate a radiochemical yield greater than or equal to 95%. Only the proteins and radiochemical yield achieved that were greater than 95% have been included in the table.

From the data in Table 4-2 it is also evident that at a given concentration, the protein containing the JWT tag labelled faster than the others, and reached the 95% threshold more quickly. Again, it is obvious that by this criterion J591scFvJWT exceeds the efficiency shown by the other proteins with standard $(His)_6$ sequences. From Table 4-2 it is clear that J591scFvJWT achieved a radiolabelling efficiency greater than 95% at the lowest protein concentration, 7 μM, after incubation for 90 minutes. For the non Arg/His containing proteins, the lowest protein concentration at which a radiochemical yield greater than 95% was achieved was 28.2 μM after 90 minutes, for J591scFv and huJ591scFv. This reveals that an Arg/His Tag has demonstrated an identical radiolabelling efficiency to that of a generic $(His)_6$ tag when there is a significant 4 fold decrease in protein concentration at 90 minutes.

Often for $(His)_6$ tagged proteins incubation with $[^{99m}Tc(CO)_3]^+$ is standardised to 60 minutes at 37°C followed by a PD-10 purification in order to yield a $[^{99m}Tc(CO)_3]^+$ conjugated protein for in vivo use. In the comparative radiolabelling experiments, the non-Arg containing

proteins did not reach a radiochemical yield of greater than 95% after 60 minutes. This was only achieved after a minimum of 90 minutes and only at the highest protein concentration. However, J591scFvJWT after 60 minutes demonstrated a greater than 95% radiochemical yield for both the highest and second highest protein concentrations. In addition, after 90 minutes, the third highest protein concentration also reached the minimum requirement of 95% radiochemical yield.

In all cases the concentrations at which the scFv proteins were radiolabelled were not high enough to give a radiolabelling efficiency greater than 95% after 15 minute incubation times. However, at 30 minutes J591scFvJWT at the highest protein concentration, 28.2 μM, has a radiochemical yield of 96% which enables it to be directly used for in vivo experimentations without a purification procedure. Consequently for J591scFvJWT protein, with a concentration of 28.2 μM or higher in the $[^{99m}Tc(CO)_3]^+$ labelling solution, the total synthesis time would be 30 minutes or less. To achieve the same outcome with non Arg/$(His)_6$ containing proteins, total incubation time required would be 90 minutes. This is an extra 60 minute incubation time which for ^{99m}Tc corresponds approximately to an 10% decrease in radioactivity.

For high concentrations and long incubation times, it was observed that J591scFvJWT precipitates in solution when heated to 37^oC whereas the other proteins do not. To overcome this issue, the radiolabelling of J591scFvJWT was carried out at room temperature and the labelling efficiency monitored at 15, 30, 60, 90 and 120 minutes. The protein concentration was 14.1 μM and consequently the radiochemical yield was compared to that of the J591scFvJWT radiolabelling experiment at 14.1μM when heated to 37^oC. Figure 4-11 demonstrates that performing the $[^{99m}Tc(CO)_3]^+$ radiolabelling at room temperature does not affect the efficiency but avoids the problem of precipitation. This experiment was performed with higher activity than the comparative radiolabelling studies and a specific activity of 5 MBq/μg was obtained for the $[^{99m}Tc(CO)_3$-J591scFvJWT$]^+$ protein conjugate after 60 minutes reaction time.

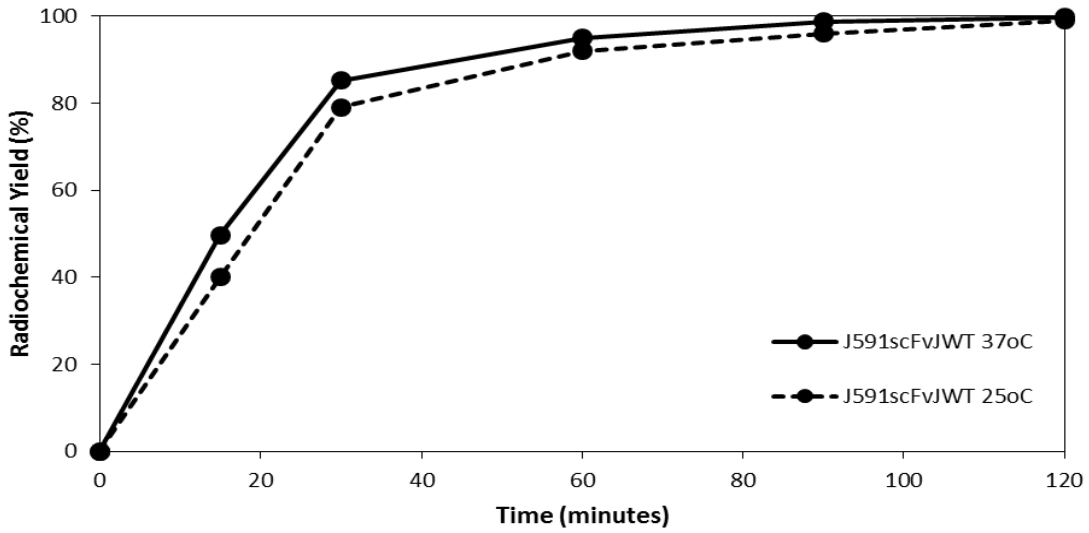

Figure 4-11. Comparison between the radiolabelling efficiency of J591scFvJWT at 37°C and 25°C. The protein concentration for both experiments was 14.1 μM.

4.4.7 Serum Stability of $[^{99m}Tc(CO)3\text{-}J591scFvJWT]^+$

Stability of the $[^{99m}Tc(CO)_3]^+$ radiolabelled J591scFvJWT upon incubation in human serum was analysed by ITLC-SA and SDS-PAGE. The ITLC-SA method has previously been used in analysing the radiolabelling efficiencies of the J591scFvJWT through comparisons between the percentage of $[^{99m}Tc(CO)_3]^+$ labelled J591scFvJWT and the unbound $[^{99m}Tc(CO)_3]^+$ and unreduced $^{99m}TcO_4^-$. Once developed in the citrate buffer mobile phase, the unbound $[^{99m}Tc(CO)_3]^+$ complex and unreduced $^{99m}TcO_4^-$ move to the solvent front with an $R_f = 0$. The $[^{99m}Tc(CO)_3]^+$ radiolabelled J591scFvJWT remains at the baseline with an $R_f=0$. The same principles apply when analysing the serum stability and it is possible to observe whether the $[^{99m}Tc(CO)_3]^+$ is dissociated and released as free $[^{99m}Tc(CO)_3]^+$. According to Figure 4-12, results from the serum stability demonstrate that there is no loss of radiolabel from the $[^{99m}Tc(CO)_3]^+$-J591scFvJWT conjugate over a 4 hour period at 37°C. The radiochemical integrity remains at 99.8% throughout.

It must be taken into consideration that the $[^{99m}Tc(CO)_3]^+$ can coordinate to serum proteins. Similarly to the $[^{99m}Tc(CO)_3]^+$-J591scFvJWT conjugate, the serum proteins remain at the baseline of the ITLC-SA paper once developed in 0.1 M citrate buffer at a pH 5.

Consequently, any radiolabelled serum proteins present in the sample will be recorded at the baseline in the same position as the radiolabelled J591scFvJWT, $R_f = 0$.

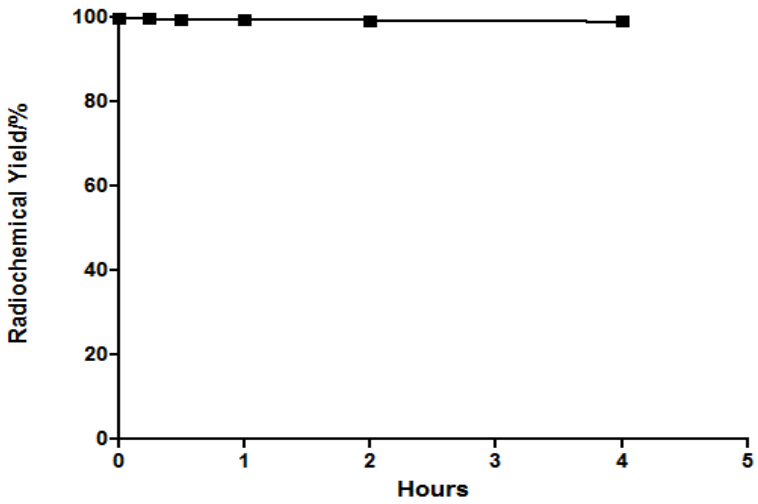

Figure 4-12. ITLC-SA results for the stability of the $[^{99m}Tc(CO)_3]^+$-J591scFvJWT conjugate in serum for 4 hrs at 37°C. The radiochemical purity remains at 98.9%.

To discriminate between the serum protein-bound and J591scFvJWT-bound radioactivity, SDS-PAGE was carried out on all the samples collected at the 0, 15, 30, 60, 120 and 240 minute time points. In addition control samples were included on the SDS-PAGE as references for the individual components: $[^{99m}Tc(CO)_3]^+$, serum proteins and J591scFvJWT. The control samples were $[^{99m}Tc(CO)_3]^+$ only, $[^{99m}Tc(CO)_3]^+$-serum protein conjugate and $[^{99m}Tc(CO)_3]^+$-J591scFvJWT conjugate. The results of the SDS-PAGE can be seen in Figure 4-13 with the Coomassie staining image on the left (A) and autoradiograph on the right (B).

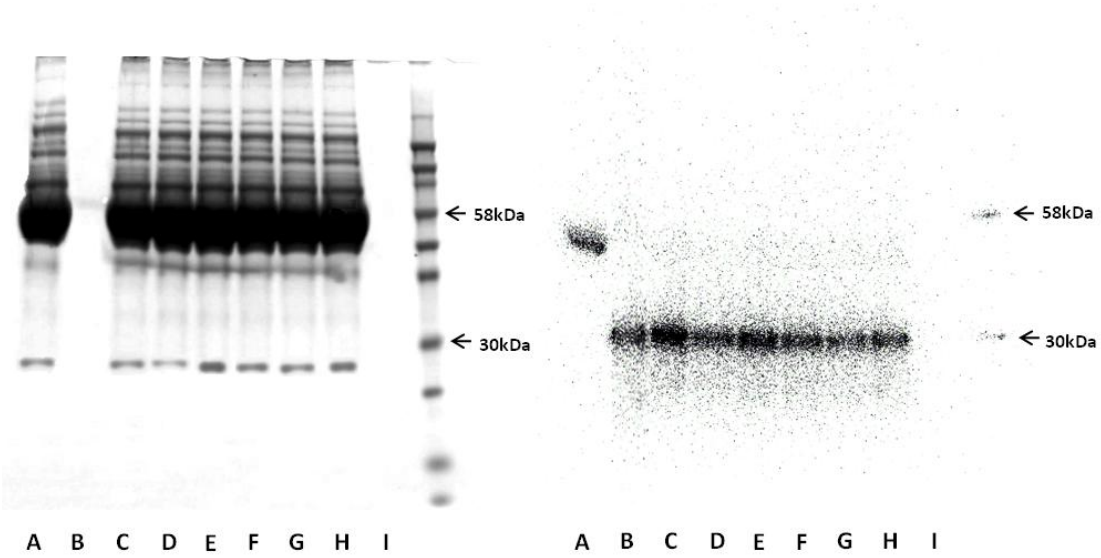

A = Serum Proteins + $[^{99m}Tc(CO)_3]^+$

B = J591(scFv)LRRRLAHHHHHH-Tc^{99m}

C = J591(scFv)-Tc^{99m} & Serum at 0 min

D = J591(scFv)-Tc^{99m} & Serum at 15 min

E = J591(scFv)-Tc^{99m} & Serum at 30 min

F = J591(scFv)-Tc^{99m} & Serum at 60 min

G = J591(scFv)-Tc^{99m} & Serum at 120 min

H = J591(scFv)-Tc^{99m} & Serum at 240 min

I = $[^{99m}Tc(CO)_3]^+$

Figure 4-13. SDS-PAGE Coomassie staining (A) and autoradiograph (B) for the serum stability analysis of J591scFvJWT for 4 hours at 37°C.

Lanes C-H in the autoradiograph confirm the presence of the radiolabelled J591scFvJWT as single black bands at 28 kDa corresponding to the monomeric protein. Row A is a control and in the autoradiograph the black band corresponds to $[^{99m}Tc(CO)_3]^+$ conjugated to serum proteins. In row I, it is not possible to observe any radioactivity. This is understandable as the sample loaded in this row was $[^{99m}Tc(CO)_3]^+$ which is small and highly charged. It is very likely that it has travelled to the end of the NuPAGE gel and is no longer registered on the SDS-PAGE. The corresponding Coomassie blue stained image (Figure 4-13, A), identifies the location of the serum proteins within the serum containing samples. Once the serum proteins have been visualised it is possible to confirm that the serum proteins are not conjugated to $[^{99m}Tc(CO)_3]^+$ as they do not appear as black bands in the autoradiograph. There is a slight decrease in radioactivity in the bands corresponding to the J591scFvJWT-$[^{99m}Tc(CO)_3]^+$-serum samples from 15 minutes to 120 minutes. Due to the extremely low

concentrations of J591scFvJWT protein, it is not possible to observe the protein in the SDS-PAGE gel .

To conclude, once radiolabelled, J591scFvJWT is radiochemically stable in serum for at least 4 hours at 37^{o}C. The other four proteins (J591scFv, huJ591scFv, 6C7.1 and 6C7.1-Cys) have previously been analysed for serum stability by Dr Florian Kampmeier and they demonstrate an identical behaviour.

4.4.8 Cell Binding Assay of [^{99m}Tc(CO)$_3$-J591scFvJWT]$^+$ and [^{99m}Tc(CO)$_3$-huJ591scFv]$^+$

Results from the preliminary cell binding assay of [^{99m}Tc(CO)$_3$-J591scFvJWT]$^+$ and [^{99m}Tc(CO)$_3$-huJ591scFv]$^+$ are shown in Figure 4-14. Although the results appear subject to high standard deviation and poor adherence to a smooth curve, competitive binding studies between the ^{99m}Tc using labelled and unlabelled J591scFvJWT protein confirmed specific binding to the PSMA positive cells. A KD of 4 nM and 3.2 nM was observed for huJ591 and J591scFvJWT respectively which implies that the affinity of the proteins for the target PSMA is very similar in both proteins. However, J591scFvJWT demonstrated a relatively high level of non-specific binding to both the DU145 control cells and DU145-PSMA cells. A repeat of this study was precluded by the low amount of available protein and lack of time to prepare additional batches.

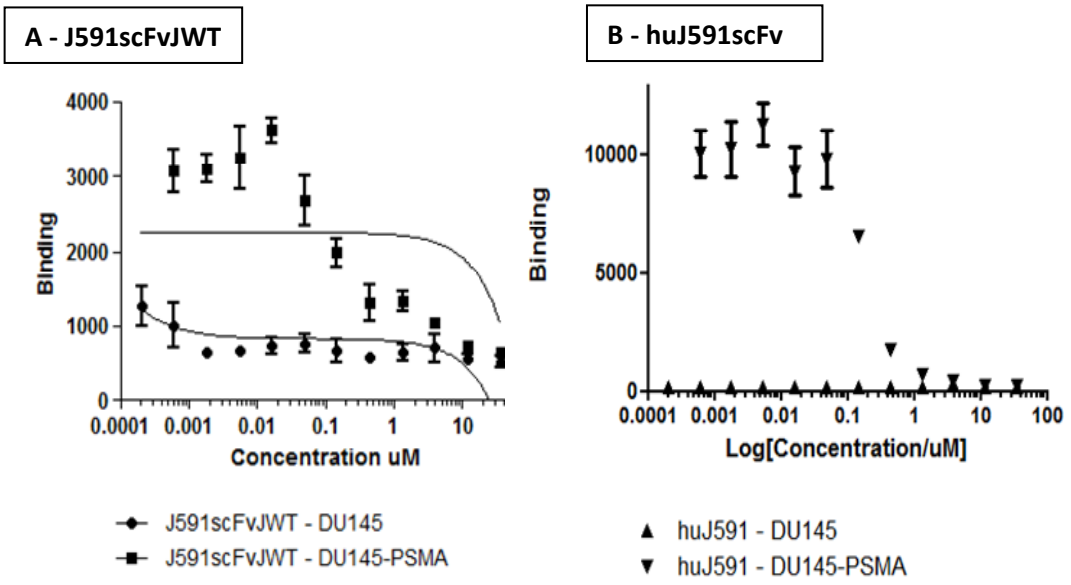

Figure 4-14. Cell binding competition assay using DU145 and DU145 PSMA positive cells. Competition is between 1nM $[^{99m}Tc(CO)_3]^+$ labelled protein and the unlabelled protein as a cold competitior. **A)** J591scFvJWT protein, **B)** huJ591scFv protein.

4.1.5 DISCUSSION & CONCLUSION

This research is primarily focused on the influence of the amino acids that surround the $(His)_6$ Tag on its labelling efficiency with $[^{99m}Tc(CO)_3]^+$. JWT Tag was identified as a labelling sequence (pI = 12.1) that demonstrated one of the highest labelling efficiencies towards $[^{99m}Tc(CO)_3]^+$ according to the His-Tagged CelluspotTM peptide array experiment. In this instance the labelling sequence is defined as the 13 amino acids at the C-terminal of the protein, including the $(His)_6$-Tag and another 7 amino acids. For the JWT and JWT-Cys proteins 13 amino acids at the C-terminal have been specifically engineered into the protein for the purpose of radiolabelling with $[^{99m}Tc(CO)_3]^+$. The control proteins have been expressed to only contain the $(His)_6$ Tag as the labelling sequence and the 7 amino acids surrounding the Tag are either part of the antibody framework or are a cloning artefact coding for the NotI restriction site. Previous studies have demonstrated that the influence of the surrounding amino acids is important when analysing the labelling efficiencies of the proteins. Therefore for the purpose of these experiments the amino acids surrounding the

$(His)_6$-Tag were included as part of the labelling sequence and contributed towards the local calculated pI of that sequence.

The low protein production yields suggest that production of the proteins in HEK293T cells was hindered to varying extents by the presence of the JWT and JWT-CYS labelling sequences. For example, while J591Cdia had an average yield of 4-6 mg/L of purified protein from culture supernatant, a protein with an almost identical primary amino acid composition, J591diaJWT-Cys, gave yields of 1.5-2 mg/L of culture supernatant. The difference between the two diabodies was in the labelling sequence in which the 3 consecutive Ala residues in the J591Cdia had been substituted with 3 Arg in the J591diaJWT-Cys. Expression yields for the other JWT Tagged proteins, J591diaJWT and J591scFvJWT, were comparably low giving 1.5-2 mg of purified protein per litre of culture supernatant. Although these observations are preliminary it appears that there is a tendency that the high positive charged density at the C-terminal due to the 3 consecutive Arg residues results in a decrease in protein expression or secretion, or introduces problem that diminish yield during purification.

In addition in SDS-PAGE analysis J591diaJWT-Cys and J591diaJWT behaved unexpectedly in comparison to other $(His)_6$-Tagged diabodies such as the J591Cdia. All diabodies were produced according to the same methodology and the difference between the diabodies is entirely restricted to the amino acids surrounding the $(His)_6$-Tag. Neither of the JWT-Cysor JWT tagged diabodies appeared as a single band at the appropriate molecular weight. J591diaJWT-Cys demonstrated a preferential formation of the monomer with a double band appearing at 28 kDa for 90-95% of the protein composition. Due to the free Cys residue at the C-terminal it is expected to form a covalent dimer which would not be destroyed when the samples are heated with SDS loading buffer, and should appear as a dimer at 54 kDa. It is possible that the presence of the highly positive charged region may restrict the formation of the covalent dimer. The rigidity and positivity of the Arg residues in the labelling sequence could be sterically or electrostatically hindering the Arg sequences of the partner protein, inhibiting their ability to form a diabody. Furthermore, two distinct bands very close together were detected for both J591diaJWT-Cys and J591diaJWT at 28kDa suggesting misfolding had occurred as a result of the positive charge from the 3 consecutive Arg residues. The two bands in the monomer region imply that 2 different protein structures have been produced and there is a potential that they may not be

structurally compatible to form the diabody. This would help provide an explanation as to why the Cys containing diabody does not appear as a covalent dimer.

Unlike the JWT-CYS or JWT tagged J591 diabodies, J591scFvJWT was successfully produced and expressed to yield a monomer with one structure that, once purified, demonstrated greater than 95% purity. Its behaviour according to SDS-PAGE was identical to that of the J591scFv and the other scFv control proteins. Other than restrictions to the expression of the J591scFvJWT protein, the highly positively charged labelling sequence did not appear to have a negative impact on the folding or structure of the J591 scFv. Consequently from the results of the SDS-PAGE it was concluded that J591scFvJWT should be used for these comparative radiolabelling studies as it gave the best results in terms of its expression and purification. There was a single band present in the purified sample that corresponded to the monomer of 28 kDa which contributed towards 90-95% of the protein solution. The J591scFvJWT protein was concentrated to 1.3 mg/ml, a suitable concentration for use in the comparative studies. The J591diaJWT and J591diaJWT-Cys were not pursued any further due to the problems with the folding.

All control proteins were successfully expressed and purified to > 95% purity and a single band was detected at the expected MW for each scFv by SDS-PAGE and Western blot. Once purified all control scFv proteins were concentrated to a minimum of 0.9 mg/ml. The variation in scFv control proteins gave a reasonable range of comparator proteins for the binding ability of J591scFvJWT to the $[^{99m}Tc(CO)_3]^+$ complex. J591scFv is perhaps the most comparable protein in that it has an identical amino acid composition other than in the labelling sequence. The labelling sequence of the J591scFv control has an Arg and Lys residue 6 and 7 amino acids away from the $(His)_6$ Tag, KRLAAALEHHHHHH. Despite having a pI < 9.5 for the labelling sequence, a single Arg in close proximity to the $(His)_6$ Tag has shown a positive influence on the labelling efficiencies in the studies described in chapter 3.3. Therefore J591scFv may demonstrate improved labelling efficiencies in comparison to most generic $(His)_6$ tagged proteins. The humanised J591 scFv control has a labelling sequence containing no Arg residues but instead it has a Lys residue which is 6 amino acids away from the $(His)_6$ Tag. Lys is also positively charged, however due to the lower pka of the Lys side chain its basicity is not comparable to that of Arg and, in chapter 3.3a positive impact on the labelling efficiencies is only demonstrated when at least 2 Lys residues are present in the sequence. 6C7.1scFv and 6C7.1-CscFvys controls provide a comparison in

which there are no Arg residues or any other positively charged amino acids in the labelling sequence. In addition, 6C7.1scFv and 6C7.1-CscFv are fragments that were not expressed from the same antibody as J591 and did not have similar amino acid compositions. The diversity in protein structures and labelling sequences within the control group is important to fully analyse any improvements in labelling efficiencies as a result of the Arg/$(His)_6$ Tag.

On the surface it appears as though the Arg/$(His)_6$ Tag hinders the production of antibody fragments from the evidence provided with the J591 scFvs and diabodies. It is not yet clear whether this is due to problems with expression, secretion or purification. It is important to take into consideration that only 2 different types of Arg/$(His)_6$ Tags, JWT and JWT-CYS, have been used and they have only been engineered into J591 scFv and diabody fragments, proteins that share the Vh/Vl domain interface and thus exhibit similar folding properties. Other proteins with a highly positive charged labelling sequence may behave differently. It would be very interesting to engineer the Arg/$(His)_6$ Tag sequence into a variety of different proteins and observe their behaviour during expression and folding. Furthermore, from the His-Tagged CelluspotTM array, sequences with a pI >9.5 demonstrated a superior labelling efficiency. To obtain a pI > 9.5 sequences can include a minimum of 2 Arg residues or even 3 Lys residues which would reduce the high charge density and the rigidity associated with the Arg residues. The use of different Arg/$(His)_6$ Tag or Lys/$(His)_6$ Tag labelling sequences could potentially have a different effect on protein folding and also its expression. It would be interesting to further investigate the balance between the number of Arg or Lys residues in the labelling sequence required to give a high labelling efficiency, good protein expression and correct protein folding. Despite the possible negative impact of poly-arginine sequences on protein production and folding, radiolabelling studies were conducted on the group of proteins designed to improve Tc-^{99m} labelling.

When engineered at the C-terminal of the scFv fragment, the JWT tag appears to retain the superior labelling efficiency observed on the Celluspot array, compared to the scFv controls that have labelling sequences with a pI < 9.5 and do not contain multiple Arg residues. J591scFvJWT at the highest concentration (28.2 μM), reached the threshold radiochemical yield of 95% within 30 minutes which for J591scFv and huJ591scFv was not achievable until 90 minutes. Theoretically, this would mean that in the $[^{99m}Tc(CO)_3]^+$ labelling of a protein for clinical or pre-clinical use, an JWT Tagged protein at 28.2μM would be prepared in 30

minutes whereas it would take another 60 minutes for the non-Arg containing proteins to be sufficiently labelled.

Interestingly, J591scFv had a slightly higher labelling efficiency than the other control proteins. The data presented in Chapter 3.3 allows us to suggest that this is most probably due to the Arg residue 6 amino acids away from the His-Tag. The array experiments show that even a single Arg clearly has a positive impact on the labelling efficiency of the His-Tag and the number of Arg residues included in the Tag is proportional to an increase in labelling efficiency. Despite the Arg residue present in close proximity to the $(His)_6$ tag of the J591scFv, the labelling sequence does not have a pI > 9.5. An increase in positively charged residues would contribute towards an overall positive charge on the peptide sequence at ambient pH and theoretically a higher affinity for the $[^{99m}Tc(CO)_3]^+$. Explanations to account for the positively charged amino acids having such a strong influence on the coordination of $[^{99m}Tc(CO)_3]^+$ to the His-Tag and substantially increases labelling efficiency are discussed in Chapter 5.

To conclude, the results from the radiolabelling experiments clearly illustrate that the J591scFvJWT with its Arg/$(His)_6$ Tag provides a number of notable advantages in terms of its efficiency in conjugating with $[^{99m}Tc(CO)_3]^+$ and as compared to comparators with non-Arg containing labelling sequences. The efficiency of the JWT Tag is so high that useful radiochemical yields for the labelled protein, greater than 95%, can be achieved using concentrations of the protein at the time of conjugation as low as 7μM. In addition, high levels of conjugation can also be seen using only short periods of incubation times and this rapid labelling provides considerable practical advantages. Radiochemical yields of 95% were demonstrated after less than a 60 minute incubation period for 28.2 μM and 14.1 μM protein concentrations whereas for the non-Arg containing $(His)_6$ Tag a 95% radiochemical yield was only achieved at 28.2 μM after a 90 minute incubation period. Finally, the radiolabelling of J591scFvJWT can be carried out at room temperature and demonstrates an equal efficiency to heating to 37°C. In summary, an JWT Tag improves $[^{99m}Tc(CO)_3]^+$ protein labelling to the extent that lower protein concentrations, shorter incubation times and lower temperatures can be used to achieve higher levels of radiochemical yields and specific activity, with a greater likelihood of avoiding the necessity of a post-labelling purification step. These advantages have significant utility in clinical, diagnostic and research settings.

The Arg/$(His)_6$ Tagged J591scFv demonstrates a stability in serum that is equivalent to that of other $(His)_6$ Tagged proteins and is consequently suitable for in vivo experiments. To further evaluate the suitability of the Arg/$(His)_6$ Tag as a standardised labelling mechanism for site-specific chelation of $[^{99m}Tc(CO)_3]^+$, in vitro and in vivo studies must be performed to ensure that the high positively charged region does not affect the bioactivity of the protein towards the target. For J591scFvJWT that is the affinity of the protein towards the PSMA receptor, and its non-specific binding to cells.

In terms of the biological function of the J591scFvJWT protein, it is not possible to reach an accurate conclusion based on the results obtained in the cell binding assay. This experiment was only performed once and many errors can occur during binding competition assays that can significantly influence the results obtained. J591scFvJWT did demonstrate specific binding to the PSMA positive cells. In addition, J591scFvJWT also demonstrated unspecific binding to the control DU145 cells that did not express PSMA as well as non-specific binding to the PSMA-expressing cells. However, binding of the ^{99m}Tc-labelled J591scFvJWT and huJ591 to the PSMA positive cells was observed at very similar concentrations of unlabelled protein competitor. This implies that the affinity of J591scFvJWT and huJ591 for the PSMA target are similar. A cell binding assay should be repeated in the short term to further investigate these results and provide more reliable data.

The main purpose of the protein production was to incorporate an Arg/$(His)_6$ labelling sequence, identified in Chapter 3 as demonstrating exceptional $[^{99m}Tc(CO)_3]^+$ binding, into a protein and evaluate its ability to improve the labelling efficiency of that protein with $[^{99m}Tc(CO)_3]^+$. Controls were used to compare the improvement in radiolabelling efficiency as a consequence of the Arg containing labelling sequence. Although the radiolabelling is dramatically enhanced by the new tag, other aspects of protein behaviour may be adversely affected due to the presence of the high positively charged density e.g. production, purification, folding properties and non-specific binding. It may be a compromise to use a sequence with fewer Arg, 2 Arg, or a combination of Arg and Lys to give better protein behaviour while retaining the advantages of labelling efficiency.

Further experimentation should be considered which uses proteins with labelling sequences that include negatively charged amino acids such as Glu and Asp. It was noted

that Glu and Asp were detrimental to the labelling efficiency of His-Tags with $[^{99m}Tc(CO)_3]^+$ (Chapter 3.3) and therefore this should be investigated in the context of protein labelling.

REFERENCES

1. Elgamal, A. A., Holmes, E. H., Su, S. L., Tino, W. T., Simmons, S. J., Peterson, M., Greene, T. G., Boynton, A. L., and Murphy, G. P. (2000) Prostate-specific membrane antigen (PSMA): current benefits and future value, *Semin Surg Oncol 18*, 10-16.
2. Smart, C. R. (1997) The results of prostate carcinoma screening in the U.S. as reflected in the surveillance, epidemiology, and end results program, *Cancer 80*, 1835-1844.
3. Sweat, S. D., Pacelli, A., Murphy, G. P., and Bostwick, D. G. (1998) Prostate-specific membrane antigen expression is greatest in prostate adenocarcinoma and lymph node metastases, *Urology 52*, 637-640.
4. Bostwick, D. G., Pacelli, A., Blute, M., Roche, P., and Murphy, G. P. (1998) Prostate specific membrane antigen expression in prostatic intraepithelial neoplasia and adenocarcinoma: a study of 184 cases, *Cancer 82*, 2256-2261.
5. Wright, G. L., Jr., Haley, C., Beckett, M. L., and Schellhammer, P. F. (1995) Expression of prostate-specific membrane antigen in normal, benign, and malignant prostate tissues, *Urol Oncol 1*, 18-28.
6. Han, M., and Partin, A. W. (2001) Current Clinical Applications of the In-capromab Pendetide Scan (ProstaScint(R) Scan, Cyt-356), *Rev Urol 3*, 165-171.
7. Horoszewicz, J. S., Kawinski, E., and Murphy, G. P. (1987) Monoclonal antibodies to a new antigenic marker in epithelial prostatic cells and serum of prostatic cancer patients, *Anticancer Res 7*, 927-935.
8. Wynant, G. E., Murphy, G. P., Horoszewicz, J. S., Neal, C. E., Collier, B. D., Mitchell, E., Purnell, G., Tyson, I., Heal, A., Abdel-Nabi, H., and et al. (1991) Immunoscintigraphy of prostatic cancer: preliminary results with 111In-labeled monoclonal antibody 7E11-C5.3 (CYT-356), *Prostate 18*, 229-241.
9. Sacha, P., Zamecnik, J., Barinka, C., Hlouchova, K., Vicha, A., Mlcochova, P., Hilgert, I., Eckschlager, T., and Konvalinka, J. (2007) Expression of glutamate carboxypeptidase II in human brain, *Neuroscience 144*, 1361-1372.
10. Chang, S. S., Reuter, V. E., Heston, W. D., Bander, N. H., Grauer, L. S., and Gaudin, P. B. (1999) Five different anti-prostate-specific membrane antigen (PSMA) antibodies confirm PSMA expression in tumor-associated neovasculature, *Cancer Res 59*, 3192-3198.
11. Hinkle, G. H., Burgers, J. K., Neal, C. E., Texter, J. H., Kahn, D., Williams, R. D., Maguire, R., Rogers, B., Olsen, J. O., and Badalament, R. A. (1998) Multicenter radioimmunoscintigraphic evaluation of patients with prostate carcinoma using indium-111 capromab pendetide, *Cancer 83*, 739-747.
12. Murphy, G. P., Greene, T. G., Tino, W. T., Boynton, A. L., and Holmes, E. H. (1998) Isolation and characterization of monoclonal antibodies specific for the extracellular domain of prostate specific membrane antigen, *J Urol 160*, 2396-2401.
13. Elsasser-Beile, U., Wolf, P., Gierschner, D., Buhler, P., Schultze-Seemann, W., and Wetterauer, U. (2006) A new generation of monoclonal and recombinant

antibodies against cell-adherent prostate specific membrane antigen for diagnostic and therapeutic targeting of prostate cancer, *Prostate 66*, 1359-1370.
14. Morris, M. J., Pandit-Taskar, N., Divgi, C. R., Bender, S., O'Donoghue, J. A., Nacca, A., Smith-Jones, P., Schwartz, L., Slovin, S., Finn, R., Larson, S., and Scher, H. I. (2007) Phase I evaluation of J591 as a vascular targeting agent in progressive solid tumors, *Clin Cancer Res 13*, 2707-2713.
15. Morris, M. J., Divgi, C. R., Pandit-Taskar, N., Batraki, M., Warren, N., Nacca, A., Smith-Jones, P., Schwartz, L., Kelly, W. K., Slovin, S., Solit, D., Halpern, J., Delacruz, A., Curley, T., Finn, R., O'Donoghue J, A., Livingston, P., Larson, S., and Scher, H. I. (2005) Pilot trial of unlabeled and indium-111-labeled anti-prostate-specific membrane antigen antibody J591 for castrate metastatic prostate cancer, *Clin Cancer Res 11*, 7454-7461.
16. Pandit-Taskar, N., O'Donoghue, J. A., Morris, M. J., Wills, E. A., Schwartz, L. H., Gonen, M., Scher, H. I., Larson, S. M., and Divgi, C. R. (2008) Antibody mass escalation study in patients with castration-resistant prostate cancer using 111In-J591: lesion detectability and dosimetric projections for 90Y radioimmunotherapy, *J Nucl Med 49*, 1066-1074.
17. Bander, N. H., Trabulsi, E. J., Kostakoglu, L., Yao, D., Vallabhajosula, S., Smith-Jones, P., Joyce, M. A., Milowsky, M., Nanus, D. M., and Goldsmith, S. J. (2003) Targeting metastatic prostate cancer with radiolabeled monoclonal antibody J591 to the extracellular domain of prostate specific membrane antigen, *J Urol 170*, 1717-1721.
18. Holland, J. P., Divilov, V., Bander, N. H., Smith-Jones, P. M., Larson, S. M., and Lewis, J. S. (2010) 89Zr-DFO-J591 for immunoPET of prostate-specific membrane antigen expression in vivo, *J Nucl Med 51*, 1293-1300.
19. Evans, M. J., Smith-Jones, P. M., Wongvipat, J., Navarro, V., Kim, S., Bander, N. H., Larson, S. M., and Sawyers, C. L. (2011) Noninvasive measurement of androgen receptor signaling with a positron-emitting radiopharmaceutical that targets prostate-specific membrane antigen, *Proc Natl Acad Sci U S A 108*, 9578-9582.
20. Williams, L. E., Wu, A. M., Yazaki, P. J., Liu, A., Raubitschek, A. A., Shively, J. E., and Wong, J. Y. (2001) Numerical selection of optimal tumor imaging agents with application to engineered antibodies, *Cancer Biother Radiopharm 16*, 25-35.
21. Olafsen, T., Sirk, S. J., Olma, S., Shen, C. K., and Wu, A. M. (2012) ImmunoPET using engineered antibody fragments: fluorine-18 labeled diabodies for same-day imaging, *Tumour Biol 33*, 669-677.
22. Li, L., Crow, D., Turatti, F., Bading, J. R., Anderson, A. L., Poku, E., Yazaki, P. J., Carmichael, J., Leong, D., Wheatcroft, D., Raubitschek, A. A., Hudson, P. J., Colcher, D., and Shively, J. E. (2011) Site-specific conjugation of monodispersed DOTA-PEGn to a thiolated diabody reveals the effect of increasing peg size on kidney clearance and tumor uptake with improved 64-copper PET imaging, *Bioconjug Chem 22*, 709-716.
23. Wu, A. M., and Olafsen, T. (2008) Antibodies for molecular imaging of cancer, *Cancer J 14*, 191-197.
24. Vegt, E., de Jong, M., Wetzels, J. F., Masereeuw, R., Melis, M., Oyen, W. J., Gotthardt, M., and Boerman, O. C. (2010) Renal toxicity of radiolabeled peptides and antibody fragments: mechanisms, impact on radionuclide therapy, and strategies for prevention, *J Nucl Med 51*, 1049-1058.
25. Tsai, S. W., Li, L., Williams, L. E., Anderson, A. L., Raubitschek, A. A., and Shively, J. E. (2001) Metabolism and renal clearance of 111In-labeled DOTA-conjugated antibody fragments, *Bioconjug Chem 12*, 264-270.

26. Ahmad, Z. A., Yeap, S. K., Ali, A. M., Ho, W. Y., Alitheen, N. B., and Hamid, M. (2012) scFv antibody: principles and clinical application, *Clin Dev Immunol 2012*, 980250.
27. Todorovska, A., Roovers, R. C., Dolezal, O., Kortt, A. A., Hoogenboom, H. R., and Hudson, P. J. (2001) Design and application of diabodies, triabodies and tetrabodies for cancer targeting, *J Immunol Methods 248*, 47-66.
28. Schneider, D. W., Heitner, T., Alicke, B., Light, D. R., McLean, K., Satozawa, N., Parry, G., Yoo, J., Lewis, J. S., and Parry, R. (2009) In vivo biodistribution, PET imaging, and tumor accumulation of 86Y- and 111In-antimindin/RG-1, engineered antibody fragments in LNCaP tumor-bearing nude mice, *J Nucl Med 50*, 435-443.
29. McCabe, K. E., Liu, B., Marks, J. D., Tomlinson, J. S., Wu, H., and Wu, A. M. (2012) An engineered cysteine-modified diabody for imaging activated leukocyte cell adhesion molecule (ALCAM)-positive tumors, *Mol Imaging Biol 14*, 336-347.
30. Girgis, M. D., Kenanova, V., Olafsen, T., McCabe, K. E., Wu, A. M., and Tomlinson, J. S. (2011) Anti-CA19-9 diabody as a PET imaging probe for pancreas cancer, *J Surg Res 170*, 169-178.
31. Sundaresan, G., Yazaki, P. J., Shively, J. E., Finn, R. D., Larson, S. M., Raubitschek, A. A., Williams, L. E., Chatziioannou, A. F., Gambhir, S. S., and Wu, A. M. (2003) 124I-labeled engineered anti-CEA minibodies and diabodies allow high-contrast, antigen-specific small-animal PET imaging of xenografts in athymic mice, *J Nucl Med 44*, 1962-1969.
32. Verhaar, M. J., Keep, P. A., Hawkins, R. E., Robson, L., Casey, J. L., Pedley, B., Boden, J. A., Begent, R. H., and Chester, K. A. (1996) Technetium-^{99m} radiolabeling using a phage-derived single-chain Fv with a C-terminal cysteine, *J Nucl Med 37*, 868-872.
33. Pietersz, G. A., Patrick, M. R., and Chester, K. A. (1998) Preclinical characterization and in vivo imaging studies of an engineered recombinant technetium-^{99m}-labeled metallothionein-containing anti-carcinoembryonic antigen single-chain antibody, *J Nucl Med 39*, 47-56.
34. Adams, G. P., Schier, R., McCall, A. M., Crawford, R. S., Wolf, E. J., Weiner, L. M., and Marks, J. D. (1998) Prolonged in vivo tumour retention of a human diabody targeting the extracellular domain of human HER2/neu, *Br J Cancer 77*, 1405-1412.
35. Tavare, R., Torres Martin De Rosales, R., Blower, P. J., and Mullen, G. E. (2009) Efficient site-specific radiolabeling of a modified C2A domain of synaptotagmin I with $[^{99m}Tc(CO)_3]^+$: a new radiopharmaceutical for imaging cell death, *Bioconjug Chem 20*, 2071-2081.
36. Strebe, N., Guse, A., Schungel, M., Schirrmann, T., Hafner, M., Jostock, T., Hust, M., Muller, W., and Dubel, S. (2009) Functional knockdown of VCAM-1 at the posttranslational level with ER retained antibodies, *J Immunol Methods 341*, 30-40.
37. Mees, G., Dierckx, R., Mertens, K., Vermeire, S., Van Steenkiste, M., Reutelingsperger, C., D'Asseler, Y., Peremans, K., Van Damme, N., and Van de Wiele, C. (2012) ^{99m}Tc-labeled tricarbonyl his-CNA35 as an imaging agent for the detection of tumor vasculature, *J Nucl Med 53*, 464-471.
38. BerndoR_ff, D., Borkowski, S., Moosmayer, D., Viti, F., Muller-Tiemann, B., Sieger, S., Friebe, M., Hilger, C. S., Zardi, L., Neri, D., and Dinkelborg, L. M. (2006) Imaging of tumor angiogenesis using ^{99m}Tc-labeled human recombinant anti-ED-B fibronectin antibody fragments, *J Nucl Med 47*, 1707-1716.
39. Bidlingmaier, S., He, J., Wang, Y., An, F., Feng, J., Barbone, D., Gao, D., Franc, B., Broaddus, V. C., and Liu, B. (2009) Identification of MCAM/CD146 as the target antigen of a human monoclonal antibody that recognizes both epithelioid and sarcomatoid types of mesothelioma, *Cancer Res 69*, 1570-1577.

40. Chen, W. J., Yen, C. L., Lo, S. T., Chen, K. T., and Lo, J. M. (2008) Direct ^{99m} Tc labeling of Herceptin (trastuzumab) by ^{99m} Tc(I) tricarbonyl ion, *Appl Radiat Isot 66*, 340-345.
41. Tait, J. F., Smith, C., and Gibson, D. F. (2002) Development of annexin V mutants suitable for labeling with Tc(i)-carbonyl complex, *Bioconjug Chem 13*, 1119-1123.
42. Virna Cortez-Retamozo, T. L., Vicky Caveliers, Lea Olive Tchoute Gainkam, Sophie Hernot, Ann Packeu, Filip De Vos, Chris Vanhove, Serge Muyldermans, Patrick De Baetselier, Hilde Revets. (2008) ^{99m}Tc-Labeled Nanobodies: A New Type of Targeted Probes for Imaging Antigen Expression, *Current Radiopharmaceuticals 1*, 37-41.
43. Tolmachev, V., Hofstrom, C., Malmberg, J., Ahlgren, S., Hosseinimehr, S. J., Sandstrom, M., Abrahmsen, L., Orlova, A., and Graslund, T. (2010) HEHEHE-tagged affibody molecule may be purified by IMAC, is conveniently labeled with [(9)(9)(m)Tc(CO)(3)](+), and shows improved biodistribution with reduced hepatic radioactivity accumulation, *Bioconjug Chem 21*, 2013-2022.
44. Kampmeier, F., Williams, J., Maher, J., Mullen, G. E., and Blower, P. J. A Tc^{99m}-labelled diabody friagment mAb J591 for SPECT imaging of prostate specific membrane antigen (PSMA), *Unpublished*.
45. Maher, J., Brentjens, R. J., Gunset, G., Riviere, I., and Sadelain, M. (2002) Human T-lymphocyte cytotoxicity and proliferation directed by a single chimeric TCRzeta /CD28 receptor, *Nat Biotechnol 20*, 70-75.

CHAPTER FIVE

Reasons Behind the High Labelling Efficiency of the Arg/$(His)_6$-Tag

5. Why do Positively Charged $(His)_6$-Tag Sequences Demonstrate Superior Labelling Efficiencies?

5.1 INTRODUCTION

5.1.1 Aim and Objective

Results from the His-Tagged CelluspotTM peptide array (Chapter 3.3) and the radiolabelling of the proteins (Chapter 4) established that positively charged $(His)_6$-Tag sequences demonstrate superior labelling efficiencies for $[^{99m}Tc(CO)_3]^+$ in PBS buffer. It is unclear why positively charged residues, namely Arg, have such a strong influence on the $(His)_6$-Tag coordination. The following hypotheses may be suggested:

i) Arg in addition to the His residues binds to the $[M(CO)_3]^+$ core

ii) Arg affects the pKa of the peptide NH backbone

iii) Arg affects the pKa of nearby His residues

iv) Arg attracts a negatively charged metal synthon

v) A phosphate bridge is formed between Arg and the $[M(CO)_3]^+$ complex

Hypothesis i) is highly unlikely as an explanation of the results; it is hard to see how the Arg side chain could coordinate directly to the metal except at extremely high pH. In an attempt to investigate these hypotheses, particularly hypotheses iv) and v), to account for the positive impact of Arg residues on the labelling efficiency of His sequences, preliminary studies were carried out, using electrophoresis, on the charge behaviour of $[^{99m}Tc(CO)_3]^+$ in various buffers at different pHs. The buffers used were the same as for the His-Tagged CelluspotTM array experiments (Chapter 3), that is PBS at pH 7.4, citrate at pH 5.1, Tris-HCl at pH 8.8 and Tris-HCl at pH 7.4. Optimising labelling conditions previously identified PBS at pH 7.4 as the buffer that gave the highest labelling efficiencies. It was only in PBS buffer that the Arg sequences labelled at a greater efficiency. This suggests that the phenomenon involves not only the amino acid sequence but the buffer. It is also unreasonable not to consider the nature of the $^{99m}Tc(CO)_3$ speciation, which may also be influenced by the buffer, in the labelling solution in this

discussion. Preliminary ^{31}P NMR spectroscopic experiments were performed with the aim of investigating the relationship between phosphate, and $[^{99m}Tc(CO)_3]^+$ using the analogous non-radioactive $[Re(CO)_3]^+$ complex as a model.

5.1.2 Charge Behaviour of $[^{99m}Tc(CO)_3]^+$

The organometallic aqua-ion $[^{99m}Tc(CO)_3(H_2O)_3]^+$ has been prepared by the reduction of $^{99m}TcO_4^-$ and the oxidation state of ^{99m}Tc is reduced from +VII to +1.(*1*) In the literature, labelling with ^{99m}Tc-tricarbonyl is always presumed to involve a complex with a single positive charge, reported as $[^{99m}Tc(CO)_3(H_2O)_3]^+$ where ^{99m}Tc is in its +1 oxidation state and all ligands are neutral (*2-5*) (see Chapter 1.2 for further details). When designing the His-Tagged CelluspotTM array this was taken into consideration and it was predicted that multiple negatively charged amino acids, Glu or Asp, surrounding the His residues may have a positive impact on the labelling. An electrostatic interaction could form between the supposed positively charged $[^{99m}Tc(CO)_3]^+$ complex and the area of high negatively charged density surrounding the His residues, leading to an increased effective concentration of Tc in the vicinity of the His-Tag and hence to more rapid labelling. However, opposing results were observed from the His-Tagged CelluspotTM array experiments and confirmed by the subsequent J591 protein radiolabelling. Positively charged amino acids surrounding the His residues demonstrated significantly higher labelling efficiencies and substitution with negatively charged amino acids was detrimental towards the coordination. To address this apparent anomaly, electrophoresis was performed in order to analyse the charge behaviour of the $[^{99m}Tc(CO)_3]^+$ in various buffers.

Electrophoresis is the process by which samples can be characterised according to their charge and size. Its principle is that the charged particles of a sample will migrate in an applied electrical field with the positively charged molecules migrating towards the cathode and the negatively charged molecules migrating towards the anode. Electrophoresis was therefore used to determine whether the assumption that the ^{99m}Tc in the tricarbonyl synthon is positively charged is valid under various buffer conditions.

As a positively charged complex $[^{99m}Tc(CO)_3(H_2O)_3]^+$ would be expected to migrate towards the cathode. However, it is known that the H_2O ligands coordinated to the ^{99m}Tc core are

extremely labile towards substitution. This has been demonstrated by the easy exchange of H_2O with ligands from biomolecules such as His amino acids or nucleophiles in serum proteins.(*6-7*) In addition, Re or ^{99m}Tc-tricarbonyl cores have been functionalised with nitrogen- or phosphorus-containing bidentate and tridentate chelators through substitutions of the H_2O molecules.(*8*) In particular, sp^2 nitrogens of imidazoles, phosphines, carboxylic acids and thio-functionalised molecules have proven to coordinate efficiently to the tricarbonyl core.(*1, 6, 8-9*) Recrystallisation of $[Re(CO)_3(H_2O)_3]^+$ from polar organic solvents such as methanol and acetonitrile provides complexes in which the labile H_2O ligands have been substituted for MeOH or CH_3CN yielding $[Re(CO)_3(MeOH)_2Br]$ and $[Re(CO)_3(CH_3CN)_2Br]$ respectively.(*9*)

During the preparation of $[^{99m}Tc(CO)_3(H_2O)_3]^+$ from the Isolink kits there are several steps involving molecules that could potentially displace the coordinating H_2O molecules from the ^{99m}Tc core. The pH of the $[^{99m}Tc(CO)_3(H_2O)]$+ post carbonylation is neutralised with a proportionally large volume of 1M HCl; 170 μl of 1M HCl added to approximately 350 μl of $[^{99m}Tc(CO)_3]^+$ in saline. When radiolabelling the biomolecule the $[^{99m}Tc(CO)_3]^+$ is substantially diluted in a buffer, namely PBS, which contains 0.012M phosphate ions and 0.140M Cl^- ions. It is possible that the Cl^-, or phosphate ions, PO_4^{3-}, HPO_4^{2-} or $H_2PO_4^-$, displace the H_2O ligands and coordinate to the ^{99m}Tc core. In these situations neutral H_2O molecules would have been replaced with anionic ligands resulting in a change to the overall charge of the $[^{99m}Tc(CO)_3]^+$ complex. It is possible for up to three anionic molecules to substitute for the H_2O ligands which for Cl^- for example would give a Re-Tricarbonyl complex with a maximum overall charge of -2. Phosphate ions have the potential to coordinate as monodentate, bidentate or possibly even tridentate ligands. In figure 5-1 equations demonstrate some of the possible ligand substitutions that can occur between the H_2O ligands and anionic molecules. In this figure, Cl^- and HPO_4^{2-} have been used as examples of anionic ligands.

A: Cl^- Substitution

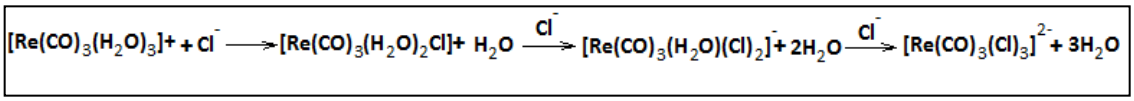

B: Phosphate Ion (HPO_4^{2-}) Substitution.

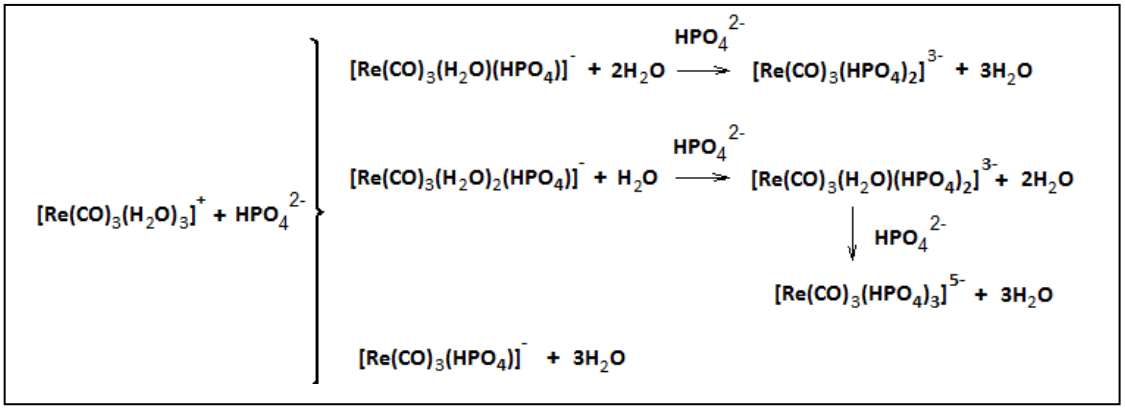

Figure 5-1. Equations demonstrating H_2O ligand substitution by anions. **A)** Substitution with Cl^- ion. **B)** Substitution with the HPO_4^{2-} phosphate ion.

Another factor of consideration is the protic equilibria formed between H_2O and the $[M(CO)_3(H_2O)_3]Br$ complex.(*10-11*) It has been reported by Egli et al, that the H_2O molecules of $[Re(CO)_3(H_2O)_3]Br$ can lose a H^+ to produce a coordinated OH^- ligand. This results in the loss of the positive charge from the $[MCO)_3]^+$ complex as a neutral ligand is replaced by a negative ligand producing complexes such as $[Re(CO)_3(H_2O)_2(OH)]$ where the overall charge will be neutral or negative. (Figure 5-2)

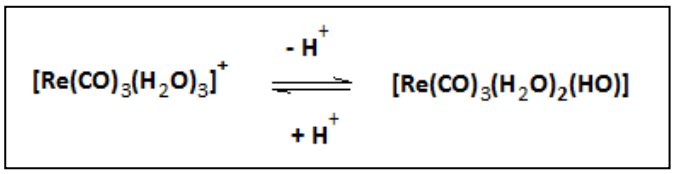

Figure 5-2. An equation representing protic equilibria between H_2O and the $[Re(CO)_3(H_2O)_3]Br$ complex. A H^+ is lost forming the monohydroxide ligand.(*10-11*)

Results from the His-Tagged CelluspotTM array suggest that PBS may be involved in the coordination between His, Arg and $[^{99m}Tc(CO)_3]^+$. It is well established that the guanidinium side chain of Arg can participate in both an electrostatic interaction and hydrogen bond with phosphate ion (*12-13*) (Figure 5-3). In addition, it has also been suggested (above) that the $[M(CO_3)]^+$ core can bind to phosphate groups. This could be achieved by the formation of a coordination bond between the metal centre and the oxygen functionality of the phosphate ions or hydrogen bonds between the H_2O ligands of $[^{99m}Tc(CO)_3)(H_2O)_3]^+$ and the phosphate.(*14*) PBS buffer contains 0.012 mmol of phosphate ions, which is in large molar excess compared with the amount of $[^{99m}Tc(CO)_3]^+$ and Arg amino acids present in the PBS buffered labelling solution. Consequently, it is possible that the phosphate from the PBS acts via a bridging mechanism between the Arg residues and $[^{99m}Tc(CO)_3]^+$ complex. To investigate this prospect, preliminary studies were performed using ^{31}P NMR spectroscopy on the interaction between $[Re(CO)_3]^+$ and a phosphate solution.

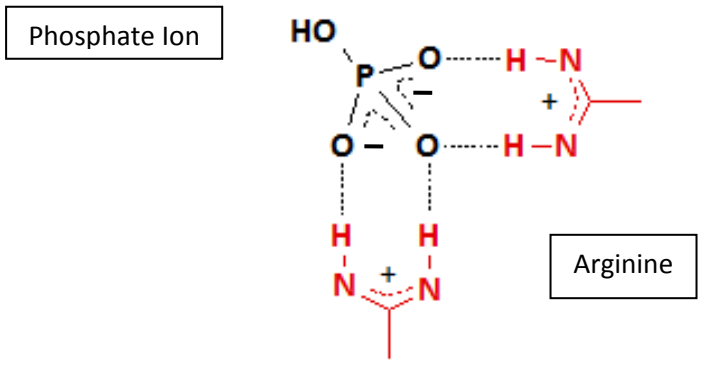

Figure 5-3. A diagram representing the interaction between the guanidinium side chain of Arg (red) and the phosphate anion (black).(*12*)

This chapter described experiments to characterise features of the $[^{99m}Tc(CO)_3]^+$ synthon - specifically its charge and its interaction with phosphate - that might affect its interaction with the peptide sequences in different buffers using electrophoresis and ^{31}P NMR spectroscopy.

5.2 MATERIALS

Electrophoresis was performed using a cellulose acetate gel electrophoresis system (30 x 32 cm) (Scie-Plas) with cellulose acetate strips obtained from Sigma Aldrich. All reagents were purchased from Sigma Aldrich, Dorset, UK unless otherwise specified and deionised H_2O was used for buffer preparation. For the synthesis of $[Re(CO)_3]^+$, $[Re(CO)_5]Br$ was obtained from Strem Chemicals Inc., Cambridge, UK. $^{99m}TcO_4^-$ and ^{99m}Tc-sestamibi were kindly provided by Guy's and St Thomas' Radiopharmacy, Guy's Hospital, London and the $^{99m}TcO_4^-$ converted to $[^{99m}Tc(CO)_3(OH_2)_3]^+$ using the Isolink kit as previously described (Chapter 2). Phosphor imaging was performed using the Cyclone storage phosphor system and OptiQuant image analysis software both from Perkin-Elmer Instruments, Cambridge, UK. ^{31}P NMR spectra were acquired on a Bruker 400MHz Avance III spectrometer (Bruker, Ettlingen, Germany) and analysed using Bruker's Topspin 5.1 software.

5.3 METHODS

5.3.1 $^{99m}TcO_4^-$, ^{99m}Tc-Sestamibi and $[^{99m}Tc(CO)_3]^+$ Electrophoresis

Electrophoresis was performed on the $^{99m}TcO_4^-$, ^{99m}Tc-Sestamibi and $^{99m}Tc(CO)_3]^+$ complexes. Both $^{99m}TcO_4^-$ and ^{99m}Tc-sestamibi were used as comparative markers for $[^{99m}Tc(CO)_3]^+$ as they are well established as, respectively, negatively and positively charged complexes. $^{99m}TcO_4^-$ would be expected to migrate towards the anode and ^{99m}Tc-sestamibi would be expected to migrate towards the cathode in the electrophoresis chamber. The structure of $^{99m}TcO_4^-$, ^{99m}Tc-sestamibi and the supposed structure of $[^{99m}Tc(CO)_3(H_2O)_3]^+$ complexes are shown in figure 5-4, image A, B and C respectively.

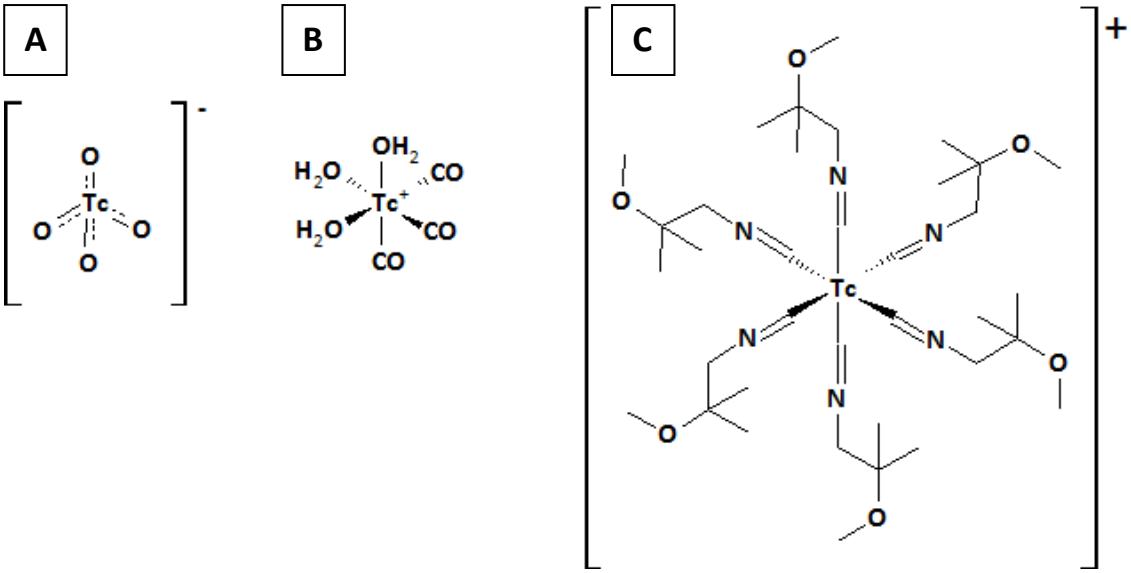

Figure 5-4. Structure of: **A)** $^{99m}TcO_4^-$, **B)** $[^{99m}Tc(CO)_3(H2O)_3]^+$ and **C)** ^{99m}Tc-Sestamibi

$[^{99m}Tc(CO)_3]^+$ was prepared using a standard Isolink kit and quality control carried out with glass backed silica TLC plates (Merck, UK) and a mobile phase of 1% HCl in methanol. 4-5 MBq of the $^{99m}TcO_4^-$, ^{99m}Tc-Sestamibi and $[^{99m}Tc(CO)_3]^+$ complexes were diluted in 100 µl of the buffer used in the electrophoresis tank and 0.5 µl of the samples were spotted onto the middle of the cellulose acetate strips. The strips were placed in the electrophoresis chamber with the radioactive spot positioned on the central partition which was equidistant from the anode and the cathode. 0.01 M PBS, 0.05 M Tris-HCl (pH 8.8), 0.05 M Tris-HCl (pH 7.4) or 0.1 M citrate (pH 5.1) buffers were used to fill the chamber and a power pack connected. A constant current of 4 mA was applied for 1 hour or 2 hours before the cellulose acetate strips were removed for imaging. Prior to imaging, a radioactive marker was used to represent the position of the complexes before the electrical field was applied and to show which side the anode was positioned during the experiment. This provided a visual reference in the phosphor imager. Exposure of the strips to the phosphor film occurred for 2-3 mins. All experiments were repeated 3 times.

5.3.2 ^{31}P NMR Spectroscopy of a $[Re(CO)_3]^+$ Containing Phosphate Solution.

Rhenium tricarbonyl (fac-$[(H_2O)_3Re(CO)_3]Br$) was prepared and characterised as previously reported in Chapter 2.(*9*) A 0.1 M phosphate buffer at pH 7.4 was prepared and used to

dissolve the $Re(CO)_3(H_2O)_3]Br$ to give 4 solutions with a 0.5 mM, 1 mM, 2 mM and 5 mM concentration of $[Re(CO)_3]^+$. 10% D_2O was added to all samples so that the deuterium signal can be used as a reference for the other NMR signals. ^{31}P NMR spectroscopy was performed on the samples after dissolving the $[Re(CO)_3]^+$ in phosphate buffer at RT and then heating the samples for 30 mins at 37^oC. As a control an NMR of phosphate buffer was also acquired at RT and after heating at 37^oC for 30mins. The spectra were acquired on the NMR spectrometer with ^1H decoupling operating at a frequency of 161.7 MHz for the ^{31}P nucleus. 512 scans were obtained per spectrum and all data processed using Bruker's Topspin 5.1 software.

5.4 RESULTS

5.4.1 Electrophoresis to Asses the Charge Behaviour of $[^{99m}Tc(CO)_3]^+$

Electrophoresis was performed on the $^{99m}TcO_4^-$, ^{99m}Tc-sestamibi and $[^{99m}Tc(CO)_3]^+$ in PBS (pH 7.4), Tris-HCl (pH 7.4 and 8.8) and citrate buffer pH 5.1. The results can be seen in figure 5-5 after a 1 hr applied electrical field. $^{99m}TcO_4^-$ and ^{99m}Tc-sestamibi in all buffers performed as expected and migrated towards the anode and cathode respectively.

$[^{99m}Tc(CO)_3]^+$ behaved differently depending on the buffer in which it is incubated. In PBS at pH 7.5 it migrated as an anion towards the anode in a similar way to $^{99m}TcO_4^-$. The extent of the migration towards the anode increased for the $[^{99m}Tc(CO)_3]^+$ in citrate buffer at pH 5.1. $[^{99m}Tc(CO)_3]^+$ behaves similarly in the Tris-HCl buffer at both pH 7.4 and pH 8.8 and migrates the same distance towards the cathode which demonstrates that it is positively charged. Its migration towards the cathode was less than that of the ^{99m}Tc sestamibi complex.

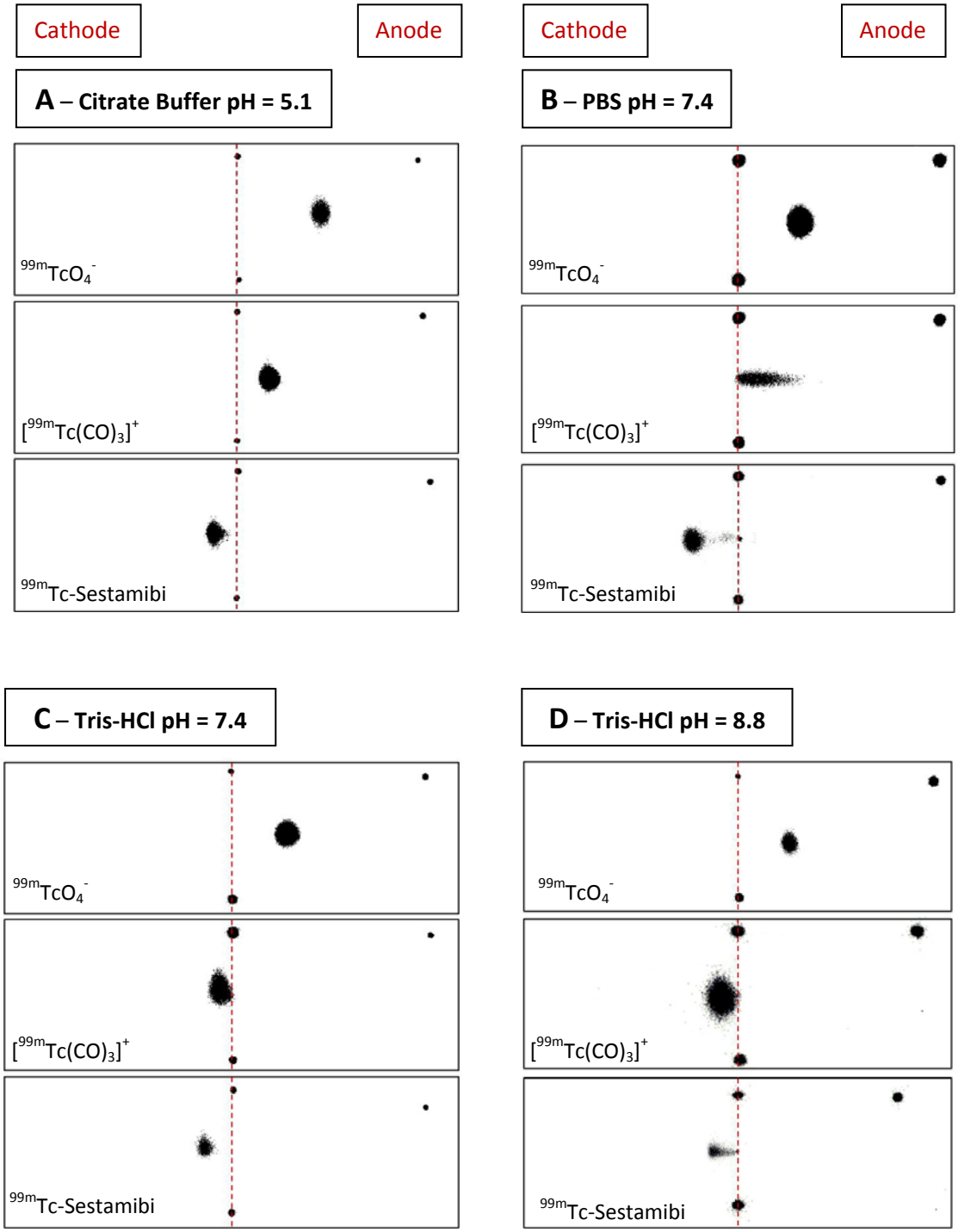

Figure 5-5. Images obtained from the electrophoresis of $^{99m}TcO_4^-$, ^{99m}Tc-Sestamibi and $[^{99m}Tc(CO)_3]^+$ in various buffers after 1 hr in a 4 mA applied electrical field. The two black spots joined by a red dashed line in the middle represent the starting point of the radioactive complexes before the applied electrical field and the black spot in the top right hand corner indicates the position of the anode during the experiment. Electrophoresis was performed in different buffers: **A)** Citrate Buffer at pH 5.1, **B)** PBS at pH 7.4, **C)** Tris-HCl Buffer at pH 7.4 and **D)** Tris-HCl Buffer at pH 8.8

5.4.2 ^{31}P NMR Spectroscopy on a $[Re(CO)_3]^+$ Containing Phosphate Solution.

The ^{31}P NMR spectroscopic data acquired for the different concentrations of $[Re(CO)_3]^+$ in a phosphate buffered solution can be seen in figure 5-6. Stack plot A represents the results for the experiment after incubation at RT for 30 mins and stack plot B the results after heating the samples for 30 mins at 37^{o}C. NMR A in each stackplot is the control 0.1 M phosphate buffer containing no $[Re(CO)_3]^+$. The effect of increasing in $[Re(CO)_3]^+$ concentration from 0.5 mM to 1 mM, 2 mM and 5 mM can be seen in NMR B-E respectively. The peak at δ = 2 ppm, relative to the deuterium signal from the solvent, represents the phosphate and this does not shift in the presence of $[Re(CO)_3]^+$. Upon addition of $[Re(CO)_3]^+$ new ^{31}P-NMR signals appeared between δ = 4-8 pm. At the 5mM concentration of $[Re(CO)_3]^+$, 7 new ^{31}P-NMR peaks can be detected (Figure 5-6A, NMR E). Furthermore, their signal intensity increases with the concentration of $[Re(CO)_3]^+$. This evidence suggests that $[Re(CO)_3]^+$ is influencing the environment of the phosphate and the formation of the new peaks could correspond to the binding of $[Re(CO)_3]^+$ to phosphate. The multiple new peaks imply that many different environments are formed between $[Re(CO)_3]^+$ and phosphate and on the NMR timescale these environments are not rapidly interchangeable. After heating the $[Re(CO)_3]$-phosphate buffered solutions, the ^{31}P NMR spectrum remained largely unchanged (Figure 5-6B, NMR A-E). Two new ^{31}P-NMR signals appeared in the spectrum at 5mM concentration of $[Re(CO)_3]^+$. This indicates that an additional two environments have been formed in the interaction between phosphate and $[Re(CO)_3]^+$ at a 5mM concentration of $[Re(CO)_3]^+$.

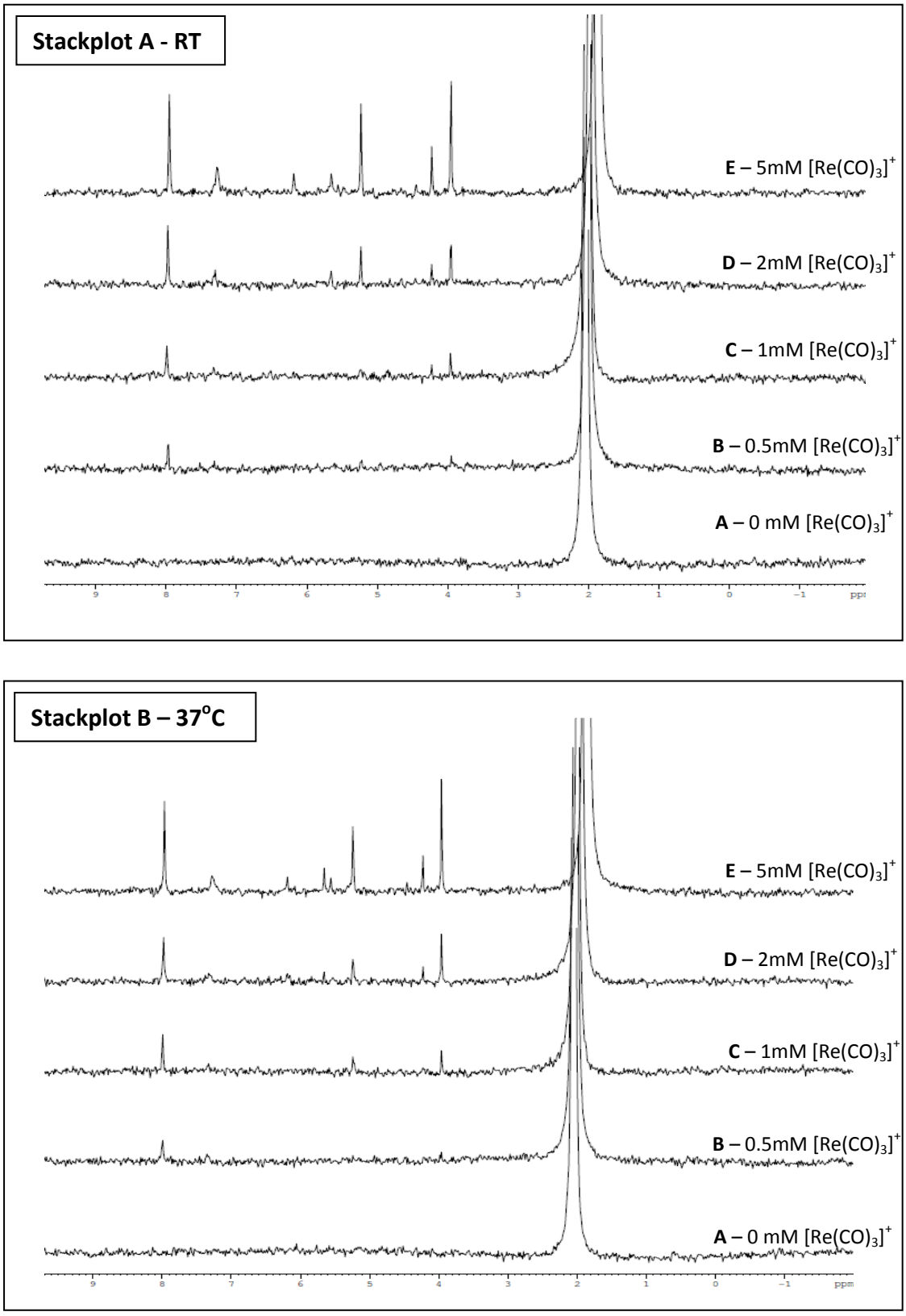

Figure 5-6. ^{31}P NMR Spectra of increasing concentrations of $[Re(CO)_3]^+$ in a 100 mM phosphate buffered solution at pH 7.4. **Stackplot A)** Spectra obtained after incubation at RT. **Stackplot B)** Spectra obtained after 30mins incubation at 37°C.

Further analysis was performed between the ^{31}P NMR spectra obtained after the addition of 0mM and 5mM $[Re(CO)_3]^+$. It was revealed that the fraction of phosphate changed by addition of 5mM $[Re(CO)_3]^+$ was approximately 4-5%. 5 mM $[Re(CO)_3]^+$ was added to a 100 mM solution of phosphate buffer which meant that essentially all the $[Re(CO)_3]^+$ was somehow associated with the phosphate. No change was observed after heating the 5 mM $[Re(CO)_3]^+$ in phosphate buffer to 37^{o}C. Figure 5-7 reveals the full scale spectra of 5 mM $[Re(CO)_3]^+$ and 0 mM $[Re(CO)_3]^+$ in phosphate buffer. It is not possible to observe any of the new peaks formed when the full scale spectra is in view. A closer look at the main peak representing phosphate (δ = 2ppm) in figure 5-8 reveals that there is a very slight shift downfield and broadening of the phosphate peak after addition of 5 mM $[Re(CO)_3]^+$. This suggests that may be some exchange between the $[Re(CO)_3]^+$ bound and free phosphates. The formation of multiple new peaks in the ^{31}P NMR spectra and a slight shift and broadening of the peak that represents phosphate after addition of $[Re(CO)_3]^+$, provides evidence which strongly implies that $[Re(CO)_3]^+$ does coordinate to phosphate.

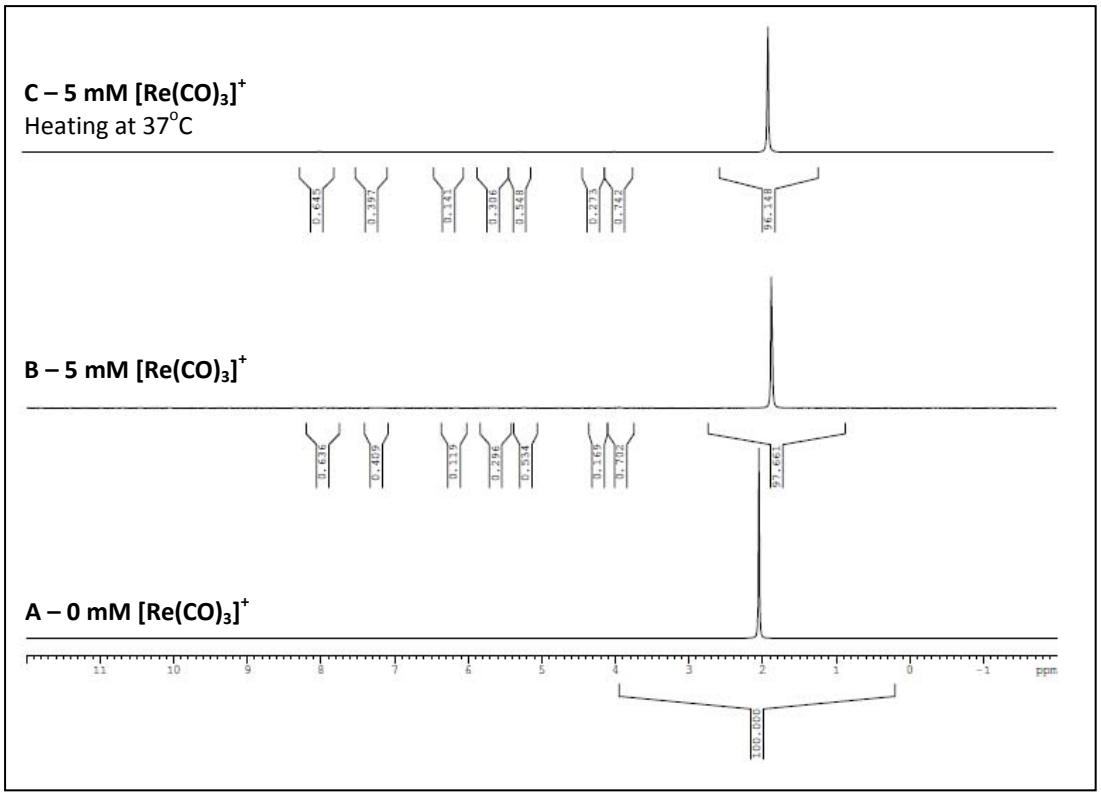

Figure 5-7. Full scale ^{31}P NMR spectra of $[Re(CO)_3]^+$ in a 100mM phosphate buffer. **A)** phosphate buffer with 0mM $[Re(CO)_3]^+$. **B)** Phosphate buffer after the addition of 5mM $[Re(CO)_3]^+$ and incubation at RT. **C)** Phosphate buffer after the addition of 5mM $[Re(CO)_3]^+$ and incubation at 37°C.

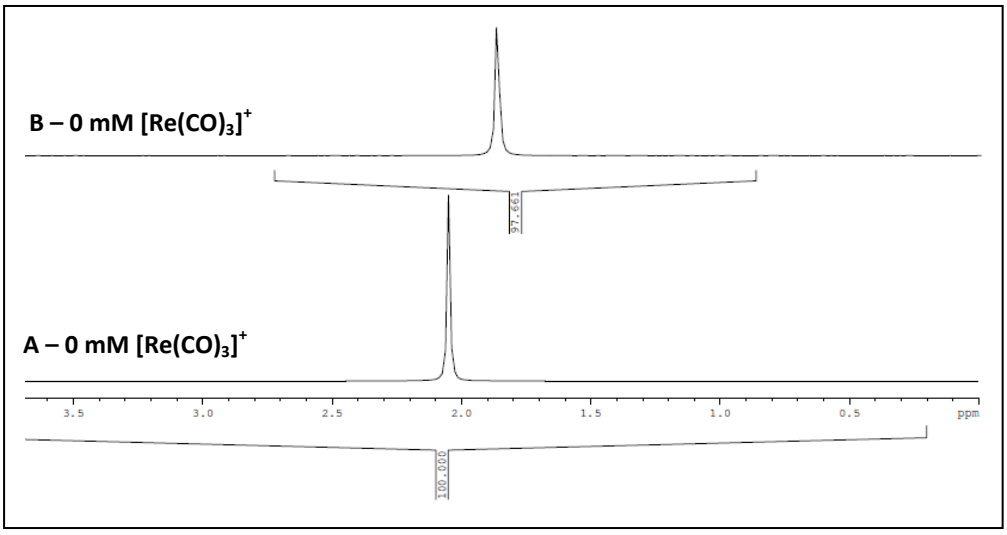

Figure 5-8. Enlarged ^{31}P NMR spectra of the peak that represents the phosphate buffer at approximately δ = 2ppm. Spectra has been enlarged between 0-4ppm. **A)** phosphate buffer with 0mM $[Re(CO)_3]^+$. **B)** Phosphate buffer after the addition of 5mM $[Re(CO)_3]^+$

5.5 DISCUSSION & CONCLUSION

In Chapter 3 and 4, preferential coordination of $[^{99m}Tc(CO)_3]^+$ was demonstrated by the positively charged peptide sequences in PBS buffer. Electrophoresis shows that in PBS buffer $[^{99m}Tc(CO)_3]^+$ behaves as an anion. Consequently it is possible that an electrostatic interaction between the $[^{99m}Tc(CO)_3]$ species and Arg occurs which brings the $[^{99m}Tc(CO)_3]^+$ complex into the vicinity of the His residues and coordination is more accessible and rapid. The Arg would be acting as a catalyst accelerating the coordination between His and $[^{99m}Tc(CO)_3]^+$ by increasing the effective local concentration of the metal complex. This is further supported by the behaviour of $[^{99m}Tc(CO)_3]^+$ in Tris-HCl buffer. Electrophoresis revealed that $[^{99m}Tc(CO)_3]$ species has a positive charge in Tris-HCl buffer which would hinder the formation of an electrostatic interaction with the positively charged Arg residues. Radiolabelling the His-Tagged array in Tris-HCl, confirms that no superior labelling efficiencies were observed for the positively charged sequences. (see Chapter 3.3). However, if electrostatic effect was important, then in Tris-HCl buffer at pH 8.8 and 7.4, labelling of the negative charged Glu/Asp rich sequences should have a higher labelling efficiency than all other sequences. This did not occur suggesting the electrostatic interaction between Arg and the negatively charged metal synthon, $[M(CO)_3]^+$ is not a major consideration.

The negatively charged behaviour of the $[^{99m}Tc(CO)_3]$ species in PBS buffer, according to electrophoresis, is most probably due to exchange of the labile H_2O molecules with anionic ligands e.g. PO_4^{3-} from PBS buffer (0.012 M) and Cl^- from PBS buffer (0.140 M). One possibility is a substitution with excess phosphate anions present in the PBS buffer. This could be studied by ^{31}P NMR spectroscopy but the concentration of Tc in the ^{99m}Tc solution is too low to measure effects on NMR. Therefore, as a model the ^{31}P NMR spectroscopic experiments were performed with the rhenium analogue, with $[Re(CO)_3]^+$ concentrations that were approximately 100 x less concentrated than the phosphate ions. ^{31}P NMR spectroscopy reveals that in the presence of $[Re(CO)_3]^+$ the environment of a fraction of the phosphate changes and new peaks appear suggesting that phosphate is binding to the $[Re(CO)_3]^+$. The electrophoresis and NMR data are consistent with the formation of a negatively charged phosphate complex of the metal tricarbonyl fragment. This might have the effect of either electrostatically attracting the $[M(CO)_3]^+$ complexes to Arg, or forming a hydrogen bonded salt bridge between the two ions. Both could have the effect of increasing the local concentration of the metal tricarbonyl

near to the His-tag, providing a mechanism by which the combination of local arginine residues and phosphate enhance the rate of labelling.

A purely electrostatic mechanism seems less than likely when analysing the electrophoresis results. Citrate also forms an anionic $[^{99m}Tc(CO)_3]^+$ complex but does not enhance labelling of Arg rich sequences; and Tris buffer forms a cationic complex yet this does not increase the labelling efficiency of the Glu/Asp rich sequences. Consequently a phosphate bridge between Arg and $[M(CO)_3]^+$ seems to be more likely.

$[^{99m}Tc(CO)_3]^+$ has a different charge distribution in all three buffers; PBS, Tris and Citrate buffer. This is probably accounted for by the coordination of each buffer to $[^{99m}Tc(CO)_3]^+$ and the influence they have on the charge of the Tc complex. Looking at the structure of Tris and Citrate it is apparent as to why the $[^{99m}Tc(CO)_3]^+$ in Tris-HCl forms a positively charged complex whereas a negatively charged complex is produced in citrate buffer (Figure 5-7). It is likely that Tris coordinates to $[^{99m}Tc(CO)_3]^+$ via its amine functionality producing a positively charged complex and citrate coordinates via its carboxylate anions forming a negatively charged complex. A schematic representation of the buffers coordinating to $[^{99m}Tc(CO)_3]^+$ can be seen in figure 5-9.

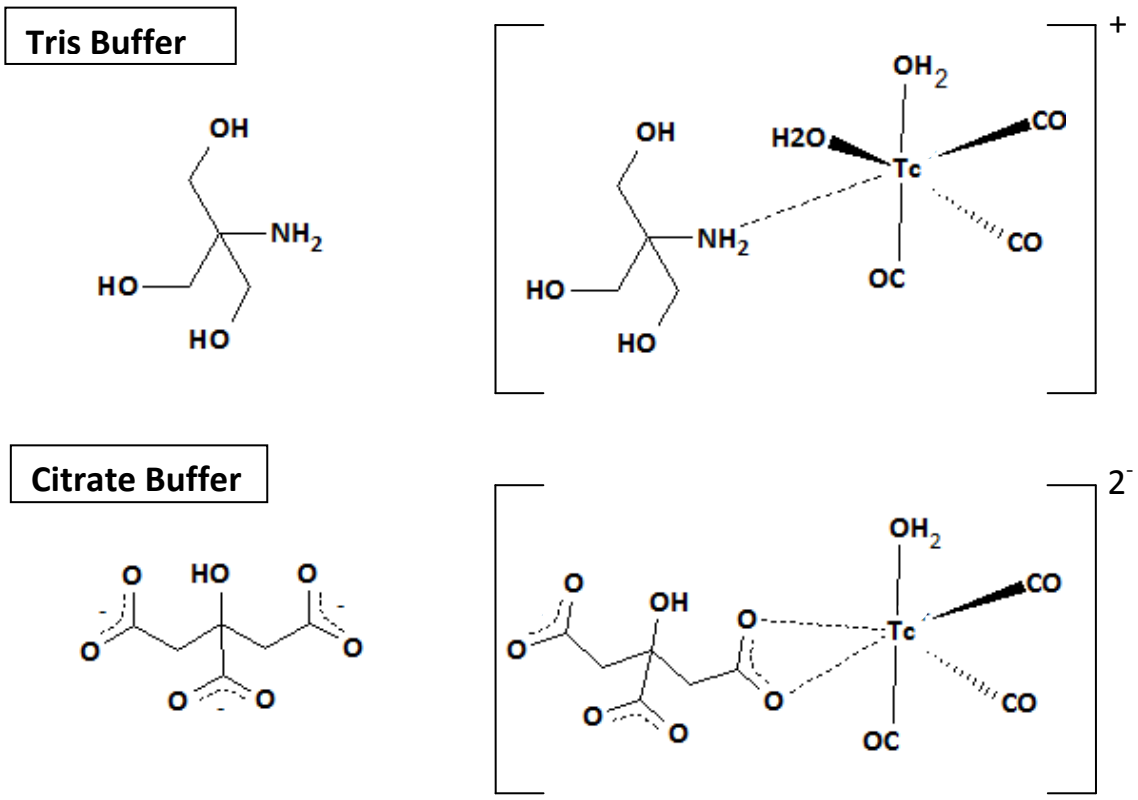

Figure 5-9. Schematic diagrams of Tris and Citrate and the proposed coordination of the complexes to $[^{99m}Tc(CO)_3]^+$.

Other ^{99m}Tc or Re metal cores such as MO^{3+} have demonstrated significantly improved binding to peptide sequences containing Arg residues.(*15*) MO^{3+} complexes are particularly effective at coordinating sequences that comprise of a cysteine thiol and three sequential anionic, deprotonated amide nitrogens of the peptide backbone. It was found that the $^{99m}TcO^{3+}$ binding was enhanced by the presence of a series of Arg residues. This suggests that the Arg residues due to their positive charge can create an environment in which the nitrogens of the amide backbone are more readily deprotonated. Coordination of the amide backbone has been demonstrated for metals including high oxidation states of Tc such $^{99m}TcO^{3+}$, and Cu(III) and it could be another possibility as to why the Arg containing peptides demonstrate a higher labelling efficiency.(*15-17*)

The electrophoresis and NMR experiments performed only provide preliminary data and a firm conclusion cannot be made with regards to the role of the Arg or phosphate in coordinating $[M(CO)_3]^+$ complexes. It would be interesting to further investigate the relationship between Arg, $[M(CO)_3]^+$ and phosphate buffer. High field ^1H NMR spectroscopy on $[Re(CO_3]^+$ conjugated

peptide sequences could be performed to identify which particular amino acids coordinate to the $[Re(CO)_3]^+$ core. Kinetic NMR spectroscopic studies depending on phosphate concentration could also be carried out to identify whether phosphate is involved in binding between Arg and $[M(CO)_3]^+$. It may also be able to distinguish whether it is a permanent bond formation between Arg and $[M(CO)_3]^+$ or an initial catalytic interaction before coordination to the His residues occurs. Thorough mass spectrometry analysis may be able to confirm whether the phosphate does coordinate to the $[M(CO)_3]^+$ complexes.

To conclude, data in chapter 3 shows that the combination of phosphate and Arg residues cause higher labelling efficiencies. Electrophoresis has provided evidence that $[^{99m}Tc(CO)_3]^+$ does not behave as a positively charged complex in PBS buffer. NMR data show that the presence of $[Re(CO)_3]^+$ leads to new phosphate-species, most likely due to substitution of coordinated water by phosphate which leads to an overall negatively charged phosphate complex. It is likely to be this species that interacts favourably with the arginine- and lysine-rich labelling sequences.

REFERENCES

1. Waibel, R., Alberto, R., Willuda, J., Finnern, R., Schibli, R., Stichelberger, A., Egli, A., Abram, U., Mach, J. P., Pluckthun, A., and Schubiger, P. A. (1999) Stable one-step technetium-99m labeling of His-tagged recombinant proteins with a novel Tc(I)-carbonyl complex, *Nat Biotechnol 17*, 897-901.
2. Chen, W. J., Yen, C. L., Lo, S. T., Chen, K. T., and Lo, J. M. (2008) Direct 99m Tc labeling of Herceptin (trastuzumab) by 99m Tc(I) tricarbonyl ion, *Appl Radiat Isot 66*, 340-345.
3. Chen, Y. L., Wu, C. C., Lin, Y. C., Pan, Y. H., Lee, T. W., and Lo, J. M. (2009) 99mTc(I)-tricarbonyl Labeled Histidine-tagged Annexin V for Apoptosis Imaging., *ICBME 2008, Proceedings 23*, 1393-1396.
4. Tavare, R., Torres Martin De Rosales, R., Blower, P. J., and Mullen, G. E. (2009) Efficient site-specific radiolabeling of a modified C2A domain of synaptotagmin I with [99mTc(CO)3]+: a new radiopharmaceutical for imaging cell death, *Bioconjug Chem 20*, 2071-2081.
5. Egli, A., Alberto, R., Tannahill, L., Schibli, R., Abram, U., Schaffland, A., Waibel, R., Tourwe, D., Jeannin, L., Iterbeke, K., and Schubiger, P. A. (1999) Organometallic 99mTc-aquaion labels peptide to an unprecedented high specific activity, *J Nucl Med 40*, 1913-1917.
6. Roger Alberto, R. S., Andre Egli, August P. Schubiger. (1998) A Novel Organometallic Aqua Complex of Technetium for the Labeling of Biomolecules: Synthesis of $[^{99m}Tc(OH_2)_3(CO)_3]^+$ from $[^{99m}TcO_4]^-$ in Aqueous Solution and Its Reaction with a Bifunctional Ligand, *J. Am. Chem. Soc. 120*, 7987-7988.

7. Zamora, P. O., and Rhodes, B. A. (1992) Imidazoles as well as thiolates in proteins bind technetium-99m, *Bioconjug Chem 3*, 493-498.
8. Schibli, R., and Schubiger, P. A. (2002) Current use and future potential of organometallic radiopharmaceuticals, *Eur J Nucl Med Mol Imaging 29*, 1529-1542.
9. Lazarova, N., James, S., Babich, J., and Zubieta, J. (2004) A convenient synthesis, chemical characterization and reactivity of [Re(CO)(3)(H2O)(3)]Br: the crystal and molecular structure of [Re(CO)(3)(CH3CN)(2)Br], *Inorg Chem Commun 7*, 1023-1026.
10. Salignac, B., Grundler, P. V., Cayemittes, S., Frey, U., Scopelliti, R., Merbach, A. E., Hedinger, R., Hegetschweiler, K., Alberto, R., Prinz, U., Raabe, G., Kolle, U., and Hall, S. (2003) Reactivity of the organometallic fac-[(CO)3ReI(H2O)3]+ aquaion. Kinetic and thermodynamic properties of H2O substitution, *Inorg Chem 42*, 3516-3526.
11. Egli, A., Hegetschweiler, K., Alberto, R., aBRAM, U., Schibli, R., Hedinger, R., Gramlich, V., Kissner, R., and Schubiger, P. A. (1997) Hydrolysis of the Organometallic Aqua Ion fac-Triaquatricarbonylrhenium(I). Mechanism, pKa, and Formation Constants of the Polynuclear Hydrolysis Products, *Organometallics 16*, 1833-1840.
12. Woods, A. S., and Ferre, S. (2005) Amazing stability of the arginine-phosphate electrostatic interaction, *J Proteome Res 4*, 1397-1402.
13. Su, Y., Doherty, T., Waring, A. J., Ruchala, P., and Hong, M. (2009) Roles of arginine and lysine residues in the translocation of a cell-penetrating peptide from (13)C, (31)P, and (19)F solid-state NMR, *Biochemistry 48*, 4587-4595.
14. Torres Martin de Rosales, R., Finucane, C., Mather, S. J., and Blower, P. J. (2009) Bifunctional bisphosphonate complexes for the diagnosis and therapy of bone metastases, *Chem Commun (Camb)*, 4847-4849.
15. Le Clainche, L., LeCoq, A., Zinn-Justin, S., Thai, R., Masella, M., Cuniasse, P. . (2010) Cysteine-Free Technetium (Tc) or Rhenium (Re) Chelating Peptide Tags and Their Use, In *France:* , p WO2010/076654
16. Rivillas-Acevedo, L., Maciel-Baron, L., Garcia, J. E., Juaristi, E., and Quintanar, L. (2013) Insertion of beta-alanine in model peptides for copper binding to His96 and His111 of the human prion protein, *J Inorg Biochem 126*, 104-110.
17. Liu, S., and Edwards, D. S. (1999) 99mTc-Labeled Small Peptides as Diagnostic Radiopharmaceuticals, *Chem Rev 99*, 2235-2268.

CHAPTER SIX

Radiolabelling with $[^{188}Re(CO)_3]^+$

6. Preliminary $[Re(CO)_3]^+$ Labelling of the His-Tagged CelluspotTM Peptide Array

6.1 INTRODUCTION

6.1.1 Aims & Objectives

So far, all radiolabelling of the His-Tagged CelluspotTM peptide array has been reported with $[^{99m}Tc(CO)_3]^+$. For many imaging applications ^{99m}Tc is preferred however, its periodic congener rhenium can be used as an isostructural therapeutic analogue by virtue of the availability of its beta-emitting radioisotopes, ^{186}Re and ^{188}Re. The aim in this chapter is to distinguish which characteristics of a peptide sequence are beneficial or detrimental towards the coordination of $[^{188}Re(CO)_3]^+$ complexes. This was achieved with a preliminary study, radiolabelling the His-Tagged CelluspotTM array with $[^{188}Re(CO)_3]^+$. Particular emphasis will be focused on whether similar preferences for labelling sequences with multiple positively charged amino acids is also observed when substituting ^{99m}Tc with $^{186/188}Re$. Another objective is to investigate whether the $[Re(CO)_3$-peptide$]^+$ complexes are stable in human serum for a sufficient period of time to allow the therapeutic dose to be supplied to the site of action.

6.2 The $[^{188}Re(CO)_3]^+$ Complex

^{188}Re has favourable attributes for therapeutic applications: medium-short half life, $t_{1/2}$ = 18 hrs, β-emission 2.12 MeV, γ-photons 155keV (15%) and it is readily available from a generator as $^{188}ReO_4^-$. Most ^{188}Re labelling techniques are based on the known precursors and complexes previously formed and characterised with ^{99m}Tc due to the similar chemistry demonstrated by both metals.(*1-2*) ^{188}Re requires harsher conditions than ^{99m}Tc to be reduced to its +1 oxidation state required for $[^{188}Re(CO)_3]^+$ and it also has a higher tendency to reoxidise in comparison to the technetium analogues.(*3-5*) Non-radioactive $[^{185/187}Re(CO)_3]^+$ complexes have often been used for the labelling of His amino acids for characterisation and modelling purposes.(*6-10*) A convenient synthesis for $^{188}Re(CO)_3]^+$ has

been identified by Schibli *et al*. and consequently the radiolabelling of His-Tagged sequences with $[^{188}Re(CO)_3]^+$ is more easily facilitated.(*4*)

6.2 MATERIALS

$Na[^{188}ReO_4]$ was eluted in physiological saline at pH 7.4 from a 7.4 GBq $^{188}W/^{188}Re$ generator purchased from ITG Isotope Technologies (Garching GmbH, Germany). Unless otherwise specified all reagents and solvents were obtained from Sigma-Aldrich, the solvents were all HPLC grade and sterile water was used for buffer preparation. CO gas was provided by CK Gas (Hampshire, UK). Purification of $[^{188}Re(CO)_3]^+$ was performed using a two column system, OnGuard II Ag Dionex, $1cm^3$ (Dionex, California, USA) and SAX Varian Bond Elut, 100 mg, (Agilent, UK) followed by filtration using hydrophilic 13 mm PTFE 0.22 um filter (Millipore Millex IC). TLC studies used silica gel 60 F254 glass plates (2.5 x 7 cm, Merck Millipore, Germany) and analysis carried out with a Mini-ScanTM TLC Scanner with a FC3600 detector (Lablogic, UK). CelluspotTM arrays were provided by Intavis Bioanalytical Instruments AG (Germany). Images of the CelluspotTM array were taken using a Cyclone Storage Phosphor system and OptiQuant image analysis software (Perkin-Elmer, USA). For stability assay, human plasma was purchased (human male AB plasma) from Sigma-Aldrich (UK).

6.3 METHODS

6.3.1 Synthesis and Purification of $[^{188}Re(CO)_3]^+$

$[^{188}Re(CO)_3]^+$ was synthesised according to previously published methods.(*4, 11*) 3 mg of $BH_3{\bullet}NH_3$ (ammonia borane) was added to a 10 ml rubber-sealed vial and flushed with CO gas at a low flow rate for 15 mins. To the vial 1 ml of $^{188}ReO_4^-$ (38 MBq) in saline was added followed by 6 μl of 85% H_3PO_4 using a 20 mL syringe. The syringe was left inserted into the vial in order to allow for volume expansion as a result of H_2 generation (approximately 10 mL). The vial was heated for 15 mins at 60°C and then cooled to RT. A TLC analysis was performed on the crude $[^{188}Re(CO)_3]^+$. 2 μl of the crude solution was spotted onto the glass

backed silica gel TLC and developed in a 1% HCl in MeOH solvent phase. With this method $[^{188}Re(CO)_3]^+$ appears as a broad peak with R_f = 0.2-0.6, $^{188}ReO_2$ colloids remain at the baseline with Rf = 0 and $^{188}ReO_4^-$ migrates to the solvent front and has Rf = 0.9. The radiochemical purity for the reduction of $^{188}ReO_4^-$ to $[^{188}Re(CO)_3]^+$ was 82%.

A purification method was carried out to remove $[^{188}Re(CO)_3]^+$ from any unreduced $^{188}ReO_4^-$ and other by-products such as $^{188}ReO_2$ colloids. At a flow rate of approximately 5 ml/min the crude solution was passed through a two column system comprising an Ag cation exchange column (OnGuard II Ag Dionex, 1 cm^3) followed by an anion exchange column (SAX Varian Bond Elut, 100 mg). Both columns were pre-prepared according to the manufacturer's instructions and dried with air before use. The collected $[^{188}Re(CO)_3]^+$ fraction was filtered using a hydrophilic 13 mm PTFE 0.22 um filter and analysed by TLC using the same system as discussed before. The radiochemical yield of $[^{188}Re(CO)_3]^+$ was 61% and the radiochemical purity > 99%. Once synthesised, $[^{188}Re(CO)_3]^+$ was used quickly to avoid re-oxidisation.

6.3.2 $[^{188}Re(CO)_3]^+$ Radiolabelling of His-Tagged CelluspotTM Array

2 MBq in 0.5 ml was added to two Falcon tubes and diluted up to 50 ml with pre-heated PBS at 37^oC with a physiological pH of 7.4. The His-Tagged CelluspotTM array was fully immersed in the Falcon tube and shaken at 37^oC for 15 mins. After 15 mins the array was removed from the $[^{188}Re(CO)_3]^+$ buffered solution and washed for 3 seconds in 50 ml of non-radioactive PBS to wash off any unbound $[^{188}Re(CO)_3]^+$ from the array surface. The array was carefully padded dry with filter paper and the filter paper monitored. Only minimal activity was recorded on the filter paper (10 cps from a distance of 0.2 m). The CelluspotTM array was exposed to the phosphor film for 4 mins and the film placed in the phosphor imager to generate an image. Re-immersion of the array in the original $[^{188}Re(CO)_3]^+$ buffered solution was carried out for another 15 mins to give a total incubation time of 30mins. The process of washing and imaging was repeated to obtain results at a total incubation time of 30 mins, 60 mins and 120 mins.

6.3.3 Serum stability of the $[^{188}Re(CO)_3]^+$ Labelled His-Tagged CelluspotTM Array

After 120 mins incubation time in $[^{188}Re(CO)_3]^+$ solution, the CelluspotTM array was placed in 50 ml of a human serum:PBS solution at a 1:1 v/v ratio at 37^oC. Images of the CelluspotTM array were obtained after 1 hr, 12 hr and 48 hr incubation in the human serum:PBS solution. To account for radioactive decay the plate was exposed to the phosphor film for 15 mins and 30 mins after incubation at 1 hr, 2 hrs and 48 hrs respectively.

The stability analysis of the $[^{188}Re(CO)_3$-peptide]+ conjugates was performed as previously discussed in Chapter 3.3 for the $[^{99m}Tc(CO)_3$-peptide]+ conjugates. The DLU for each peptide after washing in human serum was compared with the DLU of each peptide at the end of the 120 mins radiolabelling period. This effectively converts the yields at the start of the stability analysis to 100%. The stability was reported as remaining %Bound $[^{188}Re(CO)_3]^+$.

6.3.3 Data analysis of the $[^{188}Re(CO)_3]^+$ Labelled His-Tagged CelluspotTM Array

As previously mentioned in Chapter 3.1 and 3.3, image procession was done using the Opti-quant programme. A grid was placed around the CelluspotTM image and DLU values were recorded for each peptide sequence. DLU is an arbitrary value that is associated with the radiochemical yield of the peptide sequences. Graphs were produced that compared the radiochemical yield (DLU value) of all sequences. The 384 peptide sequences were categorised according to specific categories and these are summarised in Chapter 3.2.

6.4 RESULTS

6.4.1 $[^{188}Re(CO)_3]^+$ Radiolabelling of the His-Tagged CelluspotTM Array

Similarly to the images seen post $[^{99m}Tc(CO)_3]^+$ labelling of the His-Tagged CelluspotTM array, Chapter 3.1 and 3.3, the phosphor imager had sufficient resolution to be able to detect the individually bound peptide sequences. $[^{188}Re(CO)_3]^+$ labelled peptides appear as black spots on the area surface and the intensity of the black spot generates a DLU value

which corresponds to the labelling efficiency of the peptide. The images generated from the radiolabelling of the His-Tagged CelluspotTM array are shown in figure 6-1, with $[^{188}Re(CO)_3]^+$ labelling on the left hand side and the equivalent $[^{99m}Tc(CO)_3]^+$ labelling on the right hand side as a comparison. Images A, B, C and D represent the radiolabelling after 15, 30, 60 and 120 mins total incubation time respectively. Visually it is possible to see that after 15 mins incubation time, the preferential coordination of $[^{99m}Tc(CO)_3]^+$ to specific sequences is mirrored in the coordination pattern of $[^{188}Re(CO)_3]^+$. Consequently it can already be interpreted that peptides with multiple positively charged amino acids also demonstrate a superior labelling efficiency for $[^{188}Re(CO)_3]^+$. Unlike $[^{99m}Tc(CO)_3]^+$, an increase in radiochemical yield over time for all sequences was not observed when radiolabelling with $[^{188}Re(CO)_3]^+$. The intensity of black spots representing the sequences coordinated to $[Re(CO)_3]^+$ after 15 mins increases over time, but the majority of the other peptides remain unbound or demonstrate a low labelling efficiency for $[^{188}Re(CO)_3]^+$ throughout the experiment. For $[^{99m}Tc(CO)_3]^+$ the radiochemical yield of the sequences increases so that by 120 mins most peptides appear as a black spot on the array surface.

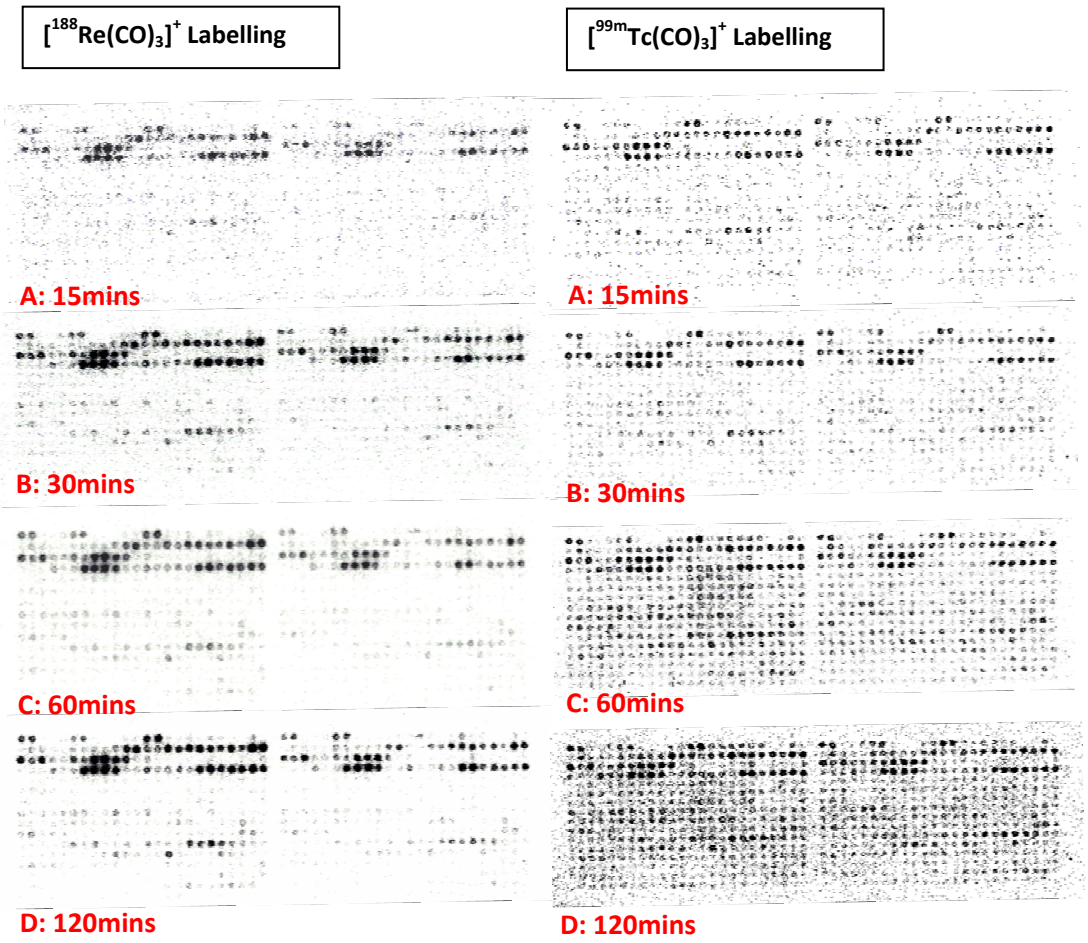

Figure 6-1. Phosphor images of the $[^{188}Re(CO)_3]^+$ (**left hand side**) and $[^{99m}Tc(CO)_3]^+$ (**right hand side**) labelling of the His-Tagged CelluspotTM peptide array. **A)** Image after 15 mins total incubation time, **B)** Image after 30 mins total incubation time, **C)** Image after 60 mins total incubation time and **D)** Image after 120 mins total incubation time.

Plotting the radiochemical yield of each peptide sequence reveals that the sequences in the "Positively Charged Amino Acids → Arg, Lys" (purple) category demonstrate a significantly higher labelling efficiency than all other peptides (Figure 6-2). This preferential labelling can be seen after 15, 30, 60 and 120 mins incubation time with $[^{188}Re(CO)_3]^+$, figure 6-2 graph A-D. As a reminder, in the "Positively Charged Amino Acids → Arg, Lys" category all amino acids have at least 2 Lys or Arg residues with a maximum of 4 Arg or 4 Lys. In figure 6-2, the graphs demonstrate that unless the peptide contains multiple positively charged amino acids surrounding the His-Tag, then a low radiochemical yield was detected. As a result it is confirmed that $[^{188}Re(CO)_3]^+$ labelling is parallel to that of $[^{99m}Tc(CO)_3]^+$ and the same

preferences for coordination to sequences with a high pI due to multiple Arg or Lys residues is observed.

The extent of the positive charge influence on labelling is highlighted in the two categories "Proline" (red) and "Catalytic Sequences" (lime green). Within these categories it is possible to see some individual sequences with a superior radiochemical yield in comparison to all other sequences in that category. These sequences all contain at least 2 Arg residues. For example in the "Catalytic Sequences" category of the 8 peptides only two contain multiple Arg residues, GRCRGHHHHHH and RCRGHHHHHHGRCR, and these are the two that show a preferential coordination to $[^{188}Re(CO)_3]^+$ throughout the 120 mins labelling experiment. For $[^{188}Re(CO)_3]^+$ and $[^{99m}Tc(CO)_3]^+$ coordination, the sequence that demonstrates the highest labelling efficiency is CLRRRLAHHHHHH.

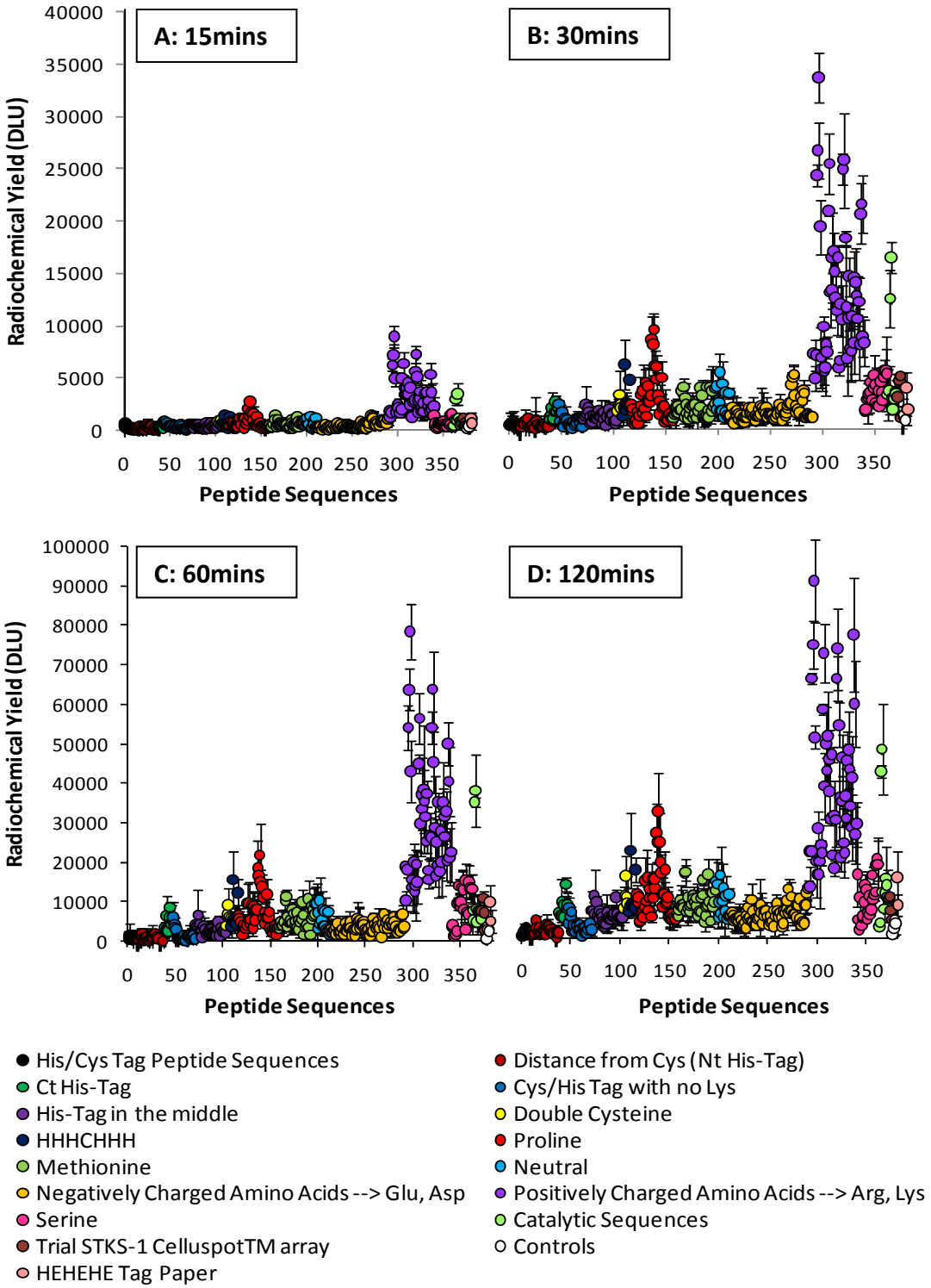

Figure 6-2. Radiochemical yield of all 384 peptides on the His-Tagged CelluspotTM peptide array post radiolabelling with $[^{188}Re(CO)_3]^+$ in PBS at pH 7.4. Results and standard deviations are calculated based on 2 sets of data. Peptides are categorised according to the characteristic features of the amino acids that surround the His residues and the arrangement of these amino acids in relation to the His residues. The categories are listed in the legend and a description is provided in Chapter 3.2. **A)** after 15 mins incubation, **B)** after 30 mins incubation, **C)** after 60 mins incubation and **D)** after 120 mins incubation.

6.4.2 Serum Stability of the $[^{188}Re(CO)_3]^+$ Labelled His-Tagged CelluspotTM Array

The stability of the $[^{188}Re(CO)_3]^+$ conjugated peptides on the array was assessed in human serum after complete immersion of the array for 1 hr, 12 hrs and 48 hrs. The results after 48 hrs incubation can be seen in figure 6-3 and are reported as the remaining %Bound $[^{188}Re(CO)_3]^+$. All His-Tag peptides remained bound to $[^{188}Re(CO)_3]^+$ in the range of 77-116%. The values for %Bound $[^{188}Re(CO)_3]^+$ that fluctuate from 100% are likely to be due to experimental error. Had the peptides been unstable in human serum after 48 hrs exposure a low %Bound $[^{188}Re(CO)_3]^+$ would have been observed. For the 4 control peptides, 2 spots with no sequences and the non-His containing sequences, the remaining %[Bound $^{188}Re(CO)_3]^+$ was less than 35% which means that they are not stable in human serum.

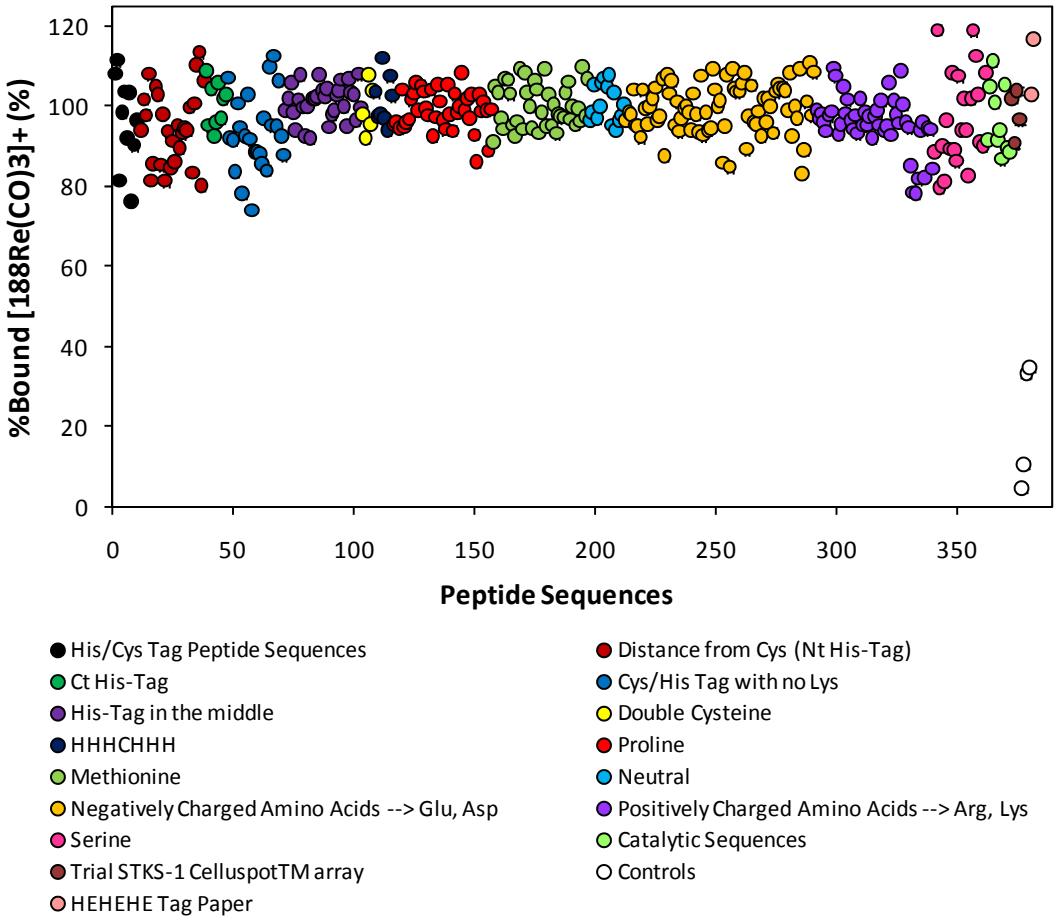

Figure 6-3. The calculated %Bound $[^{188}Re(CO)_3]^+$ for all peptide sequences after exposure to human serum for 48 hrs. The data has been presented according to the categories previously established based on the characteristics of the peptide sequences.

6.5 DISCUSSION & CONCLUSION

Preliminary studies to evaluate whether $[^{188}Re(CO)_3]^+$ behaves analogously to $[^{99m}Tc(CO)_3]^+$ in labelling the His-Tagged CelluspotTM array have been carried out. It has been revealed that His-Tagged peptide sequences containing multiple positively charged amino acids also demonstrated a preferential coordination to $[^{188}Re(CO)_3]^+$ in comparison to all other sequences on the CelluspotTM array. It can be deduced from this observation that peptide sequences with a high pI, due to the presence of multiple Arg or Lys residues, will demonstrate efficient labelling with $[^{188}Re(CO)_3]^+$. In addition, the $[^{188}Re(CO)_3]$-peptide$]^+$ conjugates were stable in human serum for up to 48 hrs and are therefore suitable for pre-clinical and clinical applications. Consequently, the JWT-Tag, LRRRLAHHHHHH, engineered at the C-terminal of the J591scFv protein in chapter 4, can also be used for labelling with $[^{188}Re(CO)_3]^+$ and the Tc and Re complexes behave highly analogously. Theoretically this will provide a method of delivering a therapeutic dose of β radiation to the site of action, which for J591scFv is prostate cancer.

It must be taken into consideration that the experiment was only performed using one CelluspotTM array and the labelling of peptides with $[^{188}Re(CO)_3]^+$ has not been investigated in solution. It is not possible to conclude whether the results observed for the peptides on solid phase correlate with the $[^{188}Re(CO)_3]^+$ labelling of the peptides in solution. The $[^{188}Re(CO)_3]^+$ radiolabelling of Arg/His-Tagged peptides should be carried out in solution before any definitive conclusions are made, although it is expected that the analogy will be maintained as it was for the ^{99m}Tc complexes. It will be interesting to further examine the radiolabelling of proteins with $[^{188}Re(CO)_3]^+$ via the Arg/His-Tag method and hence the possible use of a $[^{188}Re(CO)_3$-protein$]^+$ conjugate as a therapeutic radiopharmaceutical.

REFERENCES

1. Ferro-Flores, G., Pimentel-Gonzalez, G., Gonzalez-Zavala, M. A., Arteaga de Murphy, C., Melendez-Alafort, L., Tendilla, J. I., and Croft, B. Y. (1999) Preparation,

biodistribution, and dosimetry of ^{188}Re-labeled MoAb ior cea1 and its F(ab')2 fragments by avidin-biotin strategy, *Nucl Med Biol 26*, 57-62.

2. Karacay, H., McBride, W. J., Griffiths, G. L., Sharkey, R. M., Barbet, J., Hansen, H. J., and Goldenberg, D. M. (2000) Experimental pretargeting studies of cancer with a humanized anti-CEA x murine anti-[In-DTPA] bispecific antibody construct and a (^{99m})Tc-/(^{188})Re-labeled peptide, *Bioconjug Chem 11*, 842-854.
3. Prakash, S., Went, M. J., and Blower, P. J. (1996) Cyclic and acyclic polyamines as chelators of rhenium-^{186} and rhenium-^{188} for therapeutic use, *Nucl Med Biol 23*, 543-549.
4. Schibli, R., Schwarzbach, R., Alberto, R., Ortner, K., Schmalle, H., Dumas, C., Egli, A., and Schubiger, P. A. (2002) Steps toward high specific activity labeling of biomolecules for therapeutic application: preparation of precursor [(^{188})Re(H(2)O)(3)(CO)(3)](+) and synthesis of tailor-made bifunctional ligand systems, *Bioconjug Chem 13*, 750-756.
5. Mullen, G. E., Blower, P. J., Price, D. J., Powell, A. K., Howard, M. J., and Went, M. J. (2000) Trithiacyclononane as a ligand for potential technetium and rhenium radiopharmaceuticals: synthesis of [M(9S3)(SC2H4SC2H4S)][BF4] (M = 99Tc, Re, ^{188}Re) via C-S bond cleavage, *Inorg Chem 39*, 4093-4098.
6. Tavare, R., Torres Martin De Rosales, R., Blower, P. J., and Mullen, G. E. (2009) Efficient site-specific radiolabeling of a modified C2A domain of synaptotagmin I with [^{99m}Tc(CO)$_3$]$^+$: a new radiopharmaceutical for imaging cell death, *Bioconjug Chem 20*, 2071-2081.
7. Tavare, R., Williams, J., Howland, K., Blower, P. J., and Mullen, G. E. (2012) [Re(CO)(3)](+) labelling of a novel cysteine/hexahistidine tag: insights into binding mode by liquid chromatography-mass spectrometry, *J Inorg Biochem 114*, 2$_4^-$27.
8. Zobi, F., and Spingler, B. (2012) Post-protein-binding reactivity and modifications of the fac-[Re(CO)$_3$]$^+$ core, *Inorg Chem 51*, 1210-1212.
9. Salignac, B., Grundler, P. V., Cayemittes, S., Frey, U., Scopelliti, R., Merbach, A. E., Hedinger, R., Hegetschweiler, K., Alberto, R., Prinz, U., Raabe, G., Kolle, U., and Hall, S. (2003) Reactivity of the organometallic fac-[(CO)3ReI(H2O)$_3$]$^+$ aquaion. Kinetic and thermodynamic properties of H2O substitution, *Inorg Chem 42*, 3516-3526.
10. Binkley, S. L., Ziegler, C. J., Herrick, R. S., and Rowlett, R. S. (2010) Specific derivatization of lysozyme in aqueous solution with Re(CO)3(H2O)3(+), *Chem Commun (Camb) 46*, 1203-1205.
11. Torres Martin de Rosales, R., Finucane, C., Foster, J., Mather, S. J., and Blower, P. J. (2010) ^{188}Re(CO)3-dipicolylamine-alendronate: a new bisphosphonate conjugate for the radiotherapy of bone metastases, *Bioconjug Chem 21*, 811-815.

CHAPTER SEVEN

Conclusion & Summary

7. Conclusion & Future

The purpose of this thesis was to improve upon the currently available site-specific protein labelling methods in an attempt to satisfy the requirements for an optimal biomolecular conjugate as discussed in Chapter 1.1. Focus was on the development of the $(His)_6$-Tag as a method of site-specific labelling with $[M(CO)_3]^+$ complexes, where M = ^{99m}Tc or $[Re(CO)_3]^+$. This was achieved through the optimisation of a His-Tagged proteogenic amino acid sequence using the characteristic features of the amino acids surrounding the His residues to influence its coordination to $[M(CO)_3]^+$ complexes.

A high throughput screening methodology was established using Celluspot™ peptide arrays that provided an efficient methodology for the analysis of multiple peptide sequences as suitable tags for coordination of $[M(CO)_3]^+$. It provided a straightforward method in which labelling conditions such as pH, temperature and buffer could also be assessed. Radiolabelling a specifically designed His-Tagged peptide library (His-Tagged Celluspot™ array) with $[^{99m}Tc(CO)_3]^+$ and $[^{188}Re(CO)_3]^+$ was able to provide extensive information with regards to which characteristics provided a positive or negative impact on the labelling efficiency.

A summary of the main outcomes post radiolabelling of the His-Tagged Celluspot™ array with $[^{99m}Tc(CO)_3]^+$ can be seen below:

1. A good correlation was observed between the radiolabelling of the peptides in solution and on solid phase which confirms the suitability and reliability of the His-Tagged Celluspot™ array.
2. Multiple positively charged amino acids significantly improved labelling efficiency of the His-containing sequences.
3. Multiple negatively charged amino acids were detrimental towards the labelling efficiency.
4. Sequences with a pI > 9.5, due to the presence of positively charged amino acids, demonstrated an improved labelling efficiency.

5. A minimum of 2 Arg residues or 3 Lys residues are required to give the most efficient labelling efficiency and to provide a sufficient amount of positive charge on the sequence to yield a pI > 9.5.
6. Sequences in which Arg is positioned separating the His residues is not a favourable arrangement in terms of labelling efficiency e.g. RRRXXHHHHHH > XXXXRHRHRHR
7. Labelling efficiency increases with the number of His residues included in the sequence e.g. HHHHHH > HHHH> HXHXHX > HXHX > HXXH.
8. Cys does contribute towards improving the labelling efficiency but it is not the most influential factor and in the presence of Arg residue it does not make a significant difference to the radiochemical yield.
9. Met can replace Cys, to avoid disulfide bond formation, and the radiochemical yields of the sequences are comparable.
10. No labelling occurs unless a His residue is present in the sequence.
11. Labelling at pH 7.4 in PBS buffer was considerably more favourable than at pH 5.5 in citrate buffer and at pH 8.8 or 7.4 in Tris-HCl buffer.
12. The $[^{99m}Tc(CO)_3]^+$ conjugates are stable in PBS buffer and human serum for at least 24 hours.
13. The $[^{99m}Tc(CO)_3]^+$ conjugates are stable in a 1000-fold excess molar solution of Cys and His residues for 3 hrs consecutively.
14. CLRRRLAHHHHHH was identified as the sequence with the highest labelling efficiency in comparison to all other sequences on the array. It demonstrated an 8 fold increase in radiochemical yield in comparison to the best His-Tagged sequences often used in the literature.
15. ^{188}Re demonstrates the same sequence preferences as ^{99m}Tc.

An Arg containing His-Tagged sequence, LRRRLAHHHHHH (JWT-Tag), was successfully engineered at the C-terminal of the J591scFv protein and illustrated a number of notable advantages in terms of its efficiency in conjugating $[^{99m}Tc(CO)_3]^+$ as compared to comparators with non-Arg labelling sequences. Labelling efficiency for the JWT Tag was so high that greater than 95% radiochemical yield was achieved after 1 hour labelling at a protein concentration as low as 7μM. Other non-Arg conatinign sequences required a 4 fold increase in protein concentration before a 95% radiochemical yield was obtained. Clearly the superior affinity of the Arg/$(His)_6$-Tag sequences for $[^{99m}Tc(CO)_3]^+$ is translational to a protein context. The $[^{99m}Tc(CO)_3$-J591scFvJWT$]^+$ protein was kinetically stable in human

serum and can theoretically be used in pre-clinical and clinical applications. This would then provide a method of improving $[^{99m}Tc(CO)_3]^+$ protein labelling to the extent that lower protein concentrations, shorter incubation times and lower temperatures can be used to achieve higher levels of radiochemical yields and specific activity, with a greater likelihood of avoiding the necessity of a post-labelling purification step. These advantages have significant utility in clinical, diagnostic and research settings.

In the short term, further experimentation should be performed using the J591scFvJWT protein and other proteins containing sequences of comparable labelling efficacy. Evaluation of the Arg/(His)6 Tag as a standardised labelling mechanism for site-specific chelation of $[^{99m}Tc(CO)_3]^+$ requires thorough in vitro and in vivo analysis to ensure that the highly positively charged region does not affect the bioactivity of the protein towards the target. This can be performed for the J591scFvJWT protein as in vivo models have already been established with PSMA positive tumours. Labelling efficiency with negatively charged His-Tagged sequences was not as promising however these Glu and Asp containing sequences should also be investigated in a protein labelling context. In addition it will also be interesting to engineer the JWT tag into other protein sequences and assess their labelling abilities and biological function for different targets. Ultimately, it would be desirable if the JWT Tag could be incorporated into libraries of trial recombinant proteins for the large scale evaluation of their suitability as radiopharmaceuticals.

There were some suggestions presented as to why the positively charged His-Tagged sequences demonstrated a high labelling efficiency for $[^{99m}Tc(CO)_3]^+$. Some of these include:

1. $[M(CO)_3(H_2O)_3]^+$ is negatively charged due to ligand substitution of the H_2O molecules for anions within the labelling solution.
2. A hydrogen bonded phosphate bridge can form between $[M(CO)_3]^+$ and the Arg residues.
3. The Arg reduces the pka of the amide backbone.
4. Arg in addition to His binds to the $[M(CO)_3]^+$ core.

It has not been possible to reach a definitive conclusion and further analysis should be performed in an attempt to identify the coordination between an $Arg/(His)_6$ sequence and $[M(CO)_3]^+$. Ideally NMR structural analysis should be performed in an attempt to discover to which exact molecules does $[M(CO)_3]^+$ coordinate. In addition other studies could involve

ESI-MS and MSMS on the Arg/$(His)_6$-Tag peptide conjugate or the Arg/$(His)_6$-Tagged-protein conjugate.

Finally, perhaps one of the most important features of this thesis is the development of a high throughput screening methodology. The simplicity of the His-Tagged Celluspot™ array in combination with its ability to analyse multiple sequences simultaneously, provides an excellent platform from which the coordination of other radioisotopes to amino acids can be investigated. $[^{188}Re(CO)_3]^+$, a radioisotope complex analogous to $[^{99m}Tc(CO)_3]^+$, demonstrate an ability to coordinate to the peptides on the His-Tagged Celluspot™ array. From the labelling experiment it was possible to identify that $[^{188}Re(CO)_3]^+$ had similar preferences to $[^{99m}Tc(CO)_3]^+$ in terms of its coordination to positively charged His-Tagged sequences. Further studies with $[^{188}Re(CO)_3]^+$ are desirable as ^{188}Re is a high energy beta emitter which would provide an opportunity for the use of a JWT-Tagged protein as a therapeutic option.

There are other radioisotopes that can be bound effectively by sequences of amino acids. Of these, the MO^{3+} and MN^{2+} cores are prime examples where M also equals ^{99m}Tc or $^{186/188}Re$ and the metal is in a +5 oxidation state. MO^{3+} is particular effective in the context of amino acid sequences containing a cysteine thiol. The coordinating atoms are believed to be comprised of typically the thiolate sulphur and three sequential anionic, deprotonated amide nitrogens of the peptide backbone.(*4-5*) Others have found that binding of $^{99m}TcO^{3+}$ to peptides is enhanced by the presence of a series of Arg residues.(*6*) Many of the sequences present on the His-Tagged Celluspot™ peptide array contain thiolate sulfur functionalities in combination with anionic amino acids and Arg residues. Labelling the sequences on the His-Tagged array may identify a sequence with greater affinity than has previously been observed. Another possibility is to design a new Celluspot™ array with specific specifications for radiolabelling with the MO3+ complex.

Furthermore, with regards to protein or peptide labelling, Lys and Cys are two amino acids that are often utilised as methods of conjugating chelators to a protein sequence due to the favourable reactivity of their side chains. For example chelators with sulfonyl chloride, isocyanate, isothiocyanate or activated ester functionality are often used to target Lys residues whereas disulfide exchange, alkylation and Michael addition reactions are more common for targeting Cys residues in a protein.(*7-8*) Problems associated with this method

are often related to the lack of site specificity with the chelator conjugations.(*9*) The His-Tagged Celluspot^{TM} array contains many sequences with Lys and Cys residues surrounded by different neighbouring amino acids and experiments can be designed to assess the reactivity of the Lys and Cys within these environments. Incubation of the arrays in a solution containing a radiolabelled chelator with a functionality suitable for targeting Lys or Cys residues, may identify a Lys or Cys that demonstrates a particularly high reactivity towards the chelator. Engineering a Lys or Cys within this environment into a protein structure may facilitate site-specific labelling.

In summary, the His-Tag method of site-specific labelling has been optimised. Multiple positively charged amino acids such as Arg or Lys in combination with a $(His)_6$-Tag appears to be the optimal labelling sequence for $[M(CO)_3]^+$ where M= ^{99m}Tc or ^{188}Re, the $[M(CO)_3]^+$ conjugated Arg/$(His)_6$-Tag is stable in human serum and the labelling ability is translatable to a protein labelling context. There is now a strong possibility that the Arg/$(His)_6$-Tag labelling methodology can be used for the high throughput screening of recombinant protein libraries to efficiently assess their suitability as a molecular imaging agent. This would significant advances in molecular imaging.

.